AICTE Sponsored
Online International Conference on

ADVANCEMENTS IN STRUCTURAL ENGINEERING

ASE'2023

EDITORS

V. R. Panchal • Nirpex A. Patel

V. R. Panchal · Nirpex A. Patel
Editors

Proceedings of ASE'2023

Advancements in Structural Engineering

August 2023

ISBN: 978-81-932056-2-4

CHARUSAT

Charotar University of Science and Technology (CHARUSAT) is a premier private university located in Gujarat, India. It is awarded 'Grade A+' by National Assessment and Accreditation Council (NAAC), Bangalore. CHARUSAT has been accorded status of Center of Excellence (CoE) by the Government of Gujarat.

CHARUSAT offers various programs, viz., UG, PG, Doctoral, Post-Doctoral, Diploma, Value-added and Executive Development Programs under the tutelage of 9 Institutes, 7 Faculties, and various Centers/Cells. The programs are offered in the allied disciplines of Technology & Engineering, Pharmacy, Computer Applications, Management Studies, Applied Sciences, Nursing, Physiotherapy, Humanities, and other Paramedical Sciences.

CSPIT

Chandubhai S. Patel Institute of Technology (CSPIT) is the first Institute established in the year 2000 at Education Campus, Changa (now CHARUSAT). The Institute is managed through a think tank of academicians, scientists, engineers, and professionals from various parts of the world. Starting with 240 seats with four bachelor's degree engineering programs, the institute now has a total intake of 600 seats in 8 programs of bachelor's degree and 72 seats of post graduate degree program.

Department of Civil Engineering

The Branch of Civil Engineering was introduced in the Year 2008. It has made significant progress in the last five years and is now recognized as one of the major engineering departments of the institute.

The department started developing strong links with industries and academic institutions like NITs, IITs, etc. Apart from high quality teaching at UG level, department is actively involved in Basic and Applied Research. It offers B.Tech., M.Tech (Structural Engineering) and Ph.D. programs.

The department has a NABL accredited Environmental Engineering Laboratory, which is recognized as a Schedule - I Environment Auditor by Gujarat Pollution Control Board (GPCB), Gandhinagar. It also has NABL accredited Concrete Technology Laboratory and Geotechnical Engineering Laboratory. Apart from this, the department has various laboratories including a state-of-the-art Structural Analysis Laboratory with sophisticated structural models.

The Department actively promotes curriculum development activities by upgrading existing courses, developing new courses, and preparing resource materials for teaching. It undertakes industrial consultancy work as a part of its interaction with renowned industries and organizes Seminars / Symposia for professional interaction. The Department contributes to the interdisciplinary academic and research activities of the institute.

Advancements in Structural Engineering (ASE'2023)

An online International Conference on Advancements in Structural Engineering (ASE'2023) is organized by M. S. Patel Department of Civil Engineering of Chandubhai S. Patel Institute of Technology, a constituent institute of CHARUSAT.

The mission of the ASE'2023 Conference is to provide a forum for exchange of ideas concerning current developments in Structural Engineering. The conference invites researchers from around the world (from academia, research institutions and industries) to contribute results of their work and participate in a conference, addressing the most recent trends and developments in their areas of expertise.

The ASE'2023 is to be held online. The conference offers a great opportunity to bring together professors, engineers, scientists, researchers, and scholars in the area of Structural Engineering.

The conference will open opportunities for academicians, leading engineering researchers and industrial professionals to exchange their knowledge in the field of Structural Engineering. Participants will get the valuable benefits of hearing researchers, executives and practicing industry engineers describing their challenges, experiences, and solutions.

Themes

- Concrete Materials and Reinforced Concrete Structures
- Steel Materials and Steel Structures
- Composite Structures and Composite Materials
- Structural Rehabilitation, Retrofitting and Strengthening
- Earthquake, Wind and Fire Engineering
- Theories and Methods of Structural Analysis
- Advanced Simulation and Computational Studies in Structural Engineering
- Ground Improvement Techniques
- Sustainable Materials and Innovative Structures
- Seismic Evaluation and Mitigation Techniques
- Advanced Concrete Technology
- Vibration Control Techniques for Structures
- Earthquake Studies Using GIS/GPS/SAR/ Remote Sensing
- Structural Health Monitoring
- Soil-Structure Interaction
- Machine Learning and Artificial Intelligence for Structural Engineering
- Soil Liquefaction
- Advanced Composite Materials and Composite Structures

Preface

Structural engineering is a field of paramount importance as it forms the backbone of infrastructure development worldwide. With rapid urbanization and technological advancements, it becomes essential to explore novel ideas, sustainable practices, and resilient solutions for structural challenges. An AICTE partially sponsored International Conference on Advancements in Structural Engineering (ASE'2023) was held during June 22-23, 2023 to facilitate interdisciplinary collaboration and foster an environment where ideas converged to tackle real-world engineering problems effectively.

This conference marked a significant milestone in the field of structural engineering, as it provided a unique platform for researchers, academicians, industry professionals, and students to come together and discuss the latest advancements and innovations.

ASE'2023 was conducted in an online mode over two days and received an overwhelming response from delegates around the globe. The papers presented covered current and future technologies, experimental investigations and research findings in the areas related to the conference themes. The deliberations of the conference helped achieve the purpose of dissemination and passing on the innovative methodologies and practices in place globally.

The proceedings of the Conference are published for the benefit of a wider audience.

On behalf of the organizing committee, we would like to express our gratitude to each of advisory committee members, reviewers, keynote speakers and the contributors of research for their constant support and efforts at making the conference a grand success.

The support and guidance of our esteemed academic leaders have been instrumental in bringing this conference to fruition. We extend our appreciation to Dr. Trushit Upadhyaya, Principal, CSPIT and Dr. Vijay Chaudhary, Dean, Faculty of Technology and Engineering (FTE), CHARUSAT for their support and encouragement in organizing the conference.

We express our gratitude to Dr. R. V. Upadhyay, Honorable Provost, CHARUSAT, whose guidance has been instrumental in fostering an environment conducive to research and innovation.

We would also like to thank the entire team of faculty members and non-teaching staff of the Civil Engineering Department for their untiring support for the smooth conduct of the conference.

We would especially like to thank the authors of the papers and the participants for making the conference a success.

Wishing you all very best and looking forward to the next edition of the conference.

Mr. Nirpex A. Patel
Co-Coordinator, ASE'2023

Dr. V. R. Panchal
Coordinator, ASE'2023

Contents

ESTIMATING IN SITU COMPRESSIVE STRENGTH OF ECO-FRIENDLY PERVIOUS CONCRETE USING NON DESTRUCTIVE TESTS

Bharti Tekwani[1] and Dr. Archana Bohra Gupta[2]

[1] PhD Research Scholar, Department of Structural Engineering, M.B.M. Engineering college, MBM University, Jodhpur, Rajasthan, India
[2] Professor, Department of Structural Engineering, M.B.M. Engineering college, MBM University, Jodhpur, Rajasthan, India

[1] bharti.tekwani148@gmail.com
[2] archanabohragupta@gmail.com

Abstract. Correlation data of conventional concrete using destructive test and Non-Destructive Techniques (NDT) are abundantly available. Estimation of strength of conventional concrete using Rebound Number (RHN) and Ultra-Sonic Pulse Velocity (U) values has been widely discussed and appropriate models have also been suggested for correlations between the outcomes of NDT and DT and insitu compressive strength (*CS*). Predicted models suggested by researchers for conventional concrete cannot be suitably applied for non-conventional concretes like high performance concrete, fiber reinforced concrete, pervious concrete (*PC*) etc. in most cases. However, with more and more use of non-conventional concretes, there is an ardent requirement to develop correlations equations to determine insitu compressive strengths of such concretes from non-destructive test values. Though researchers are gradually progressing to non-conventional concrete for determining its strength and mechanical properties using NDT techniques, yet correlation models for pervious concrete are not suggested. In this study, correlation equations between compressive strength and non-destructive test values viz. Rebound Number (RHN) and Ultra-Sonic Pulse Velocity (U) have been derived for pervious concrete. Statistical regression analysis results obtained in this study concluded that the correlation equations formed for compressive strengths up to 20 MPa give strongest correlation between *CS* and both RHN and U taken together (R^2 = 0.927) so strongly recommended, good correlation with coefficient of determination (R^2) as 0.909 between *CS* and RHN so recommended to be used, but weak correlation between *CS* and U values (R^2 = 0.6215) hence is not recommended to be used to find out insitu *CS* of pervious concrete. In this case, in situ compressive strength using combined RHN and U values shows strongest correlation.

Keywords: correlation equations, pervious concrete, rebound hammer, UPV.

1 Introduction

Pervious Concrete is hydraulic gravel cement concrete with appropriate proportion of interconnected void which allows water to drain through it [2]. Pervious concrete is reliable tool for storm water management which allows water to pass through its matrix. Since it is highly porous it reduces surface runoff water during heavy rainfall. The yearly approximate precipitation in India recorded 4000 billion cubic meter including snowfall.

ISBN: 978-81-932056-2-4

Only ten percent of storm water is used as ground water recharge in India according to master plan for recharge the ground water artificially announced in 2020.

Pervious concrete contribute many categories of (LEED^{TM} 2009) such as sustainable sites (heat island effect); water efficiency (runoff water management); raw material and resource management (supplementary cementitious material, locally available and regional material); innovation design such as ready mix concrete plant [17] .

Pervious concrete can also provide as 'drain' beneath the hydraulic structure. Pervious concrete with fly ash extensively use for construction of tennis court in Europe; in wall building construction to reduce noise from traffic also use as heat exchanger floor to reduce greenhouse effect [24] and established in enhancing acoustic noise absorption [2] therefore various mix design procedures for applications of pervious concrete such as road pavements, green buildings, sustainable structure etc. have been developed [4].

2 Review of Literature

2.1 Properties of Pervious Concrete

Properties of *PC* may vary with binder content, water cement proportion, compaction effort, gradation of aggregate, mixture proportion and quality of local material. Pervious concrete is also called 'No fines concrete' [21]. The strength and permeability (K) are inverse result in pervious concrete sample. If we increase the percentage of fines to achieve strength, its K will decrease, replacing sand by admixture so that both strength and K can be achieved [6]. Experimental testing to determine permeability (K) and optimum water/cement (w/c) on pervious concrete was started by Meininager RC [23]. Falling head method and tomography technique used to measure K and pore net of pervious concrete [28]. The K values have also been calculated along with compressive strength of pervious concrete for varying aggregate sizes such as 9.375mm and 18.75mm by taking three different batches of aggregate cement ratio and conclusion was that smaller size of aggregate justify both compressive strength and K and advocated the use of 'Constant Head Permeameter' to determine K [1, 6]. However, a control mix can provide maximum compressive strength (*CS*) and optimum K rate for strength up to 30 MPa and K between 57.8 and 299.5 in/hr. at controlled W/C 0.35 [3].

CS of pervious concrete however may increase by addition of admixtures (i.e., pozzolan silica fume, GGBS etc.). Silica fume obtained as waste product of silicon industrial production has high amount of silicic acid. The tiny particles have larger surface area it is used as additional cementitious material to increase density (ρ) and strength of cement. The abundant availability of silicic acid (up to 90%) improves the property of calcium silicate hydrated (CSH) gel and form pozzolana CSH gel. This optimizes the bonding between cement binders and aggregate [18]. GGBS is off-white colored by product of iron, obtained from blast furnace. Portland slag cement can be replaced by GGBS up to 70% of total weight as per IS 455:1989. Typical chemical compositions and physical properties of GGBS described in [33]. It is traditionally used in sustainable construction and green house buildings because it entails less carbon emission. The embodied energy and carbon emission (CO_2) count reduced by 51% and 34% respectively using 50% GGBS as cementitious material in pervious concrete [7].

ISBN: 978-81-932056-2-4

Comparative and cost-effective studies have been done between the compressive strength results obtained from normal concrete and trial mix by using silica fumes, fly ash and GGBS as pozzolona admixture. The results showed cost reduction up to 60% in trial mix than normal mix [30]. The variation of percentage silica fume added in pervious concrete affects *CS* and K of pervious concrete, Optimum dosage of silica fume is 10-15% of cement for maximum *CS* and K [29].

A sustainable pervious concrete casted by using recycled coarse aggregate, GGBS and polypropylene fibers computed *CS* 23.11 N/mm^2, spilt tensile strength of 5.17 N/mm^2 and K=32.3 mm/sec [5,25]. The increment in *CS*, split tensile strength, flexural strength (M), coefficient of K and young's modulus (E) for pervious concrete were respectively observed as 12%, 16.4%, 54.63%, 5.66% and 55.55% by partially replacing cement with both GGBS and cellulose fibers as compared to plain previous concrete tested at 28 days [8]. Experimental results described optimum amount (10%) substitutions of cement by fly ash to achieve highest compressive strength [24]. Silica fume and GGBS usage improves compressive strength of pervious concrete by 10%-20%, tested for pavements used to deal airplanes having gross weight less than 40 tons [32]. Geo polymer pervious concrete has also been tested successfully using GGBS [20]. Replacement of cement by 12% silica fume helps achieve optimum compressive and flexural strength and is recommended for durability of freeze and thaw action on pervious concrete construction [18]. Correlations were developed between the torque, spindle speed, permeability, and unit weight verses void ratio for different mixes of pervious concrete made with partial cement replacement with pozzolan polypropylene fiber and light weight building substituent [35].

The correlation equations were developed between compressive strength and total percentage voids for 0, 10% and 20% substitution of cement by coal ash. Results also showed that the optimum *CS* was obtained for 10% replacement of cement by coal ash [26].

The correlation "Eqs. (1), (2), (3) and (4)" were developed for pervious concrete of grade up to 10 MPa for calculating *CS*, σ_T, M and P respectively from coarse aggregate size x, by results obtained using destructive tests [14].

$$y = 16.64x^{-0.29}, R^2 = 0.991 \quad (1)$$

$$y = 12.31x^{-0.63}, R^2 = 0.864 \quad (2)$$

$$y = 4.517x^{-0.41}, R^2 = 0.739 \quad (3)$$

$$y = 11.56e^{-0.02x}, R^2 = 0.820 \quad (4)$$

y =Compressive Strength (*CS*) in "Eq. (1)", Tensile Strength (σ_T) in "Eq. (2)", Flexural Strength (M)in "Eq. (3)", Porosity (P) in "Eq. (4)" and x is aggregate size in mm [14].

Different correlation "Eqs. (5), (6), (7) and (8)" for pervious concrete strength up to 10-20 MPa was developed for calculating Porosity (P), density (DE), permeability (K),

ISBN: 978-81-932056-2-4

compressive strength (σ_c), tensile strength (σ_T) respectively from paste-aggregate ratio (p/Ag) and UPV values [22].

$$P = 105.576 + 11.586.\frac{P}{Ag} - 0.022308.UPV \quad (5)$$

$$DE = 413.28 - 457.86.\frac{p}{Ag} + 0.45534.UPV \quad (6)$$

$$K = 65.842 + 10.089\frac{p}{Ag} - 0.01677.UPV \quad (7)$$

$$\sigma_c = -18.56 + 6.418.\frac{p}{Ag} + 0.006297.UPV \quad (8)$$

$$\sigma_T = -9.4966 - 3.237.\frac{p}{Ag} + 0.003354.UPV \quad (9)$$

3 Destructive and Non-Destructive Tests and Data Extraction

3.1 Ingredients and Mix Proportioning Range of Pervious Concrete

- Aggregates: Angular crushed aggregate of size 6mm, 10mm and 20mm and specific gravity (G) 2.67 from Kakani quarry, Jodhpur, Rajasthan were used.
- Cement: 53 grade ordinary Portland cement (OPC), having G = 3.15 [37]
- Fine Aggregate (Sand): Natural sand of zone two procured from local market, having G=2.46, was used [38]
- Silica Fume: TamCem micro silica having dry bulk density (ρ) of 500-700 kg/m^3 and G= 2.27 was used to partially replace (0% to 20%) cement.
- Admixture: Admixture fulfilling the requirements of ASTM C494/ C494M was selected. Conplast SP 500 of dosage 1% of cementitious material has been used in this study.

All the necessary constituents were mixed in certain amount to achieve desire permeability and strength without segregation in structure. In the experimental program, total 90 specimens of size 150 mm ×150 mm ×150 mm was casted by using pozzolana (silica fume) in different proportions respectively. Total six sets of mixing proportion of pervious concrete had been prepared. Data range and mix proportioning range are shown in Table 1.

Table 1. Mix Proportioning Data Range per cubic meter of Pervious Concrete

Materials	Mix proportioning range Selected
Silica Fume	0% to20%

ISBN: 978-81-932056-2-4

Coarse aggregate (20-60 mm)	1538 kg/m^3 to 1440kg/m^3
w/c ratio	0.34 to 0.31
Aggregate: Cement	4.33 to 3.7 to 1
Fine: Coarse aggregate	0 to 1.1

3.2 Data Extraction

After removing the casted samples from moulds, specimens were placed under water tanks with temperature maintained at 28ºC to 30ºC for wet curing for 28 days so that specimens could get enough moisture to achieve good strength. After 28 days, non-destructive (i.e., Schmidt rebound hammer (RHN) test [11] and ultrasonic pulse velocity (U) test [10]) tests were carried out and results were noted for all cube specimens "Fig.1 (a), (b)". When all the required non-destructive tests were accomplished, the cubes were destructively tested for compressive strength "Fig. 1(c)".

Schmidt rebound hammer test was carried out for each cube with an average of 6 readings each on top, bottom, and side face. Similarly, average of three UPV readings in Km/sec (direct and semi direct) were taken. *CS* was the average value for 3 cubes tested on compression testing machine (CTM).

(a) (b) (c)

Fig. 1. (a) Performing Schmidt Rebound Hammer Test on cubes, (b) Performing Ultrasonic Pulse Velocity Test on cubes and (c) Performing Compressive Strength Test on cubes

The data set included 540 records. Table 2 shows the range of dataset obtained for statistical regression using curve fitting method in excel software.

Table 2. Test Data Range

Parameters	Min	Max	Mean	Standard Deviation
Rebound Numbe(RN)	7	19	14.70	3.43
UPV Km/sec	2.99	4.5	3.651	0.473
Compressive strength (CS) (rounded off) N/mm^2	5	20	16.25	3.1

ISBN: 978-81-932056-2-4

4 Results

The predictive correlation equations have been derived from the above experimental work using Statistical Curve Fitting method. “Eq. (10)” shows the correlation between *CS* and rebound number (RHN), “Eq. (11)” shows the correlation between *CS* and U and “Eq. (12)” represents the correlation between *CS*, RHN and U values. “Eqs. (10), (11) and (12)” are derived for pervious concrete 0% to 20% substitution of cement by silica fume.

$$CS = 7.50e^{0.055RHN}, R^2 = 0.894 \quad (10)$$

$$CS = 4.76e^{0.331U}, R^2 = 0.624 \quad (11)$$

$$CS = 0.820 + 0.715\,RHN + 1.54U, R^2 = 0.928 \quad (12)$$

The predictive values of *CS* from statistical regression curve fitting method “Eq. (10), (11) and (12)” were compared with actual observed values in laboratory. Error evaluations by computing root mean square error (RMSE), mean absolute percentage error (MAPE) and variance (VAR) are conducted as per “Eqs. (16), (17) and (18)” and results are shown in Table 3.

$$RMSE = \sqrt{\frac{1}{N}\sum_{i=1}^{n}(P_i - O_i)^2} \quad (16)$$

$$MAPE = \frac{1}{N}\left[\sum_{i=1}^{n}\left\{\frac{|O_i - P_i|}{O_i}\right\} \times 100\right] \quad (17)$$

$$VAR = \left[1 - \frac{var(O_i - P_i)}{varO_i}\right] \times 100 \quad (18)$$

Where P is predicted value of compressive strength obtained using “Eqs. (10), (11), (12)” O is observed value of compressive strength obtained by destructive testing and N is total number of observations made.

Table 3. Performance Evaluation of the Proposed Regression Equations

Errors	Equations		
	10	**11**	**12**
RMSE	0.338	3.44	1.190
MAPE	0.07	0.104	0.09
VAR	90.9%	63.15%	92.7%

The values of CS evaluated using statistical regression (Fig. 2.) from “Eqs. (10), (11) and (12)” are compared with observed values of compressive strength obtained by destructive tests performed in laboratory. It is observed that the correlation between CS and RHN “Eq. (10)” shows strong correlation ($R^2 = 0.909$), correlation between CS and U “Eq. (11)” shows weak correlation ($R^2 = 0.6315$) and correlation between CS and combined RHN and U “Eq. (11)” shows strongest correlation ($R^2 = 0.927$). Fig. 2.

ISBN: 978-81-932056-2-4

shows the comparison of predicted CS values obtained using "Eqs. (10), (11) & (12)" respectively with observed CS values obtained from destructive tests.

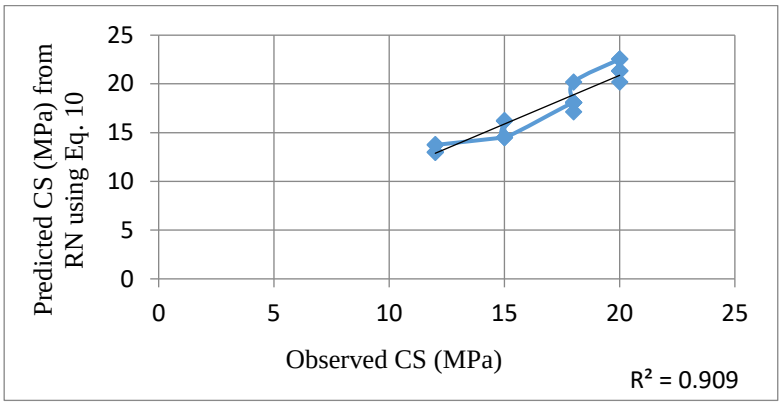

(a)

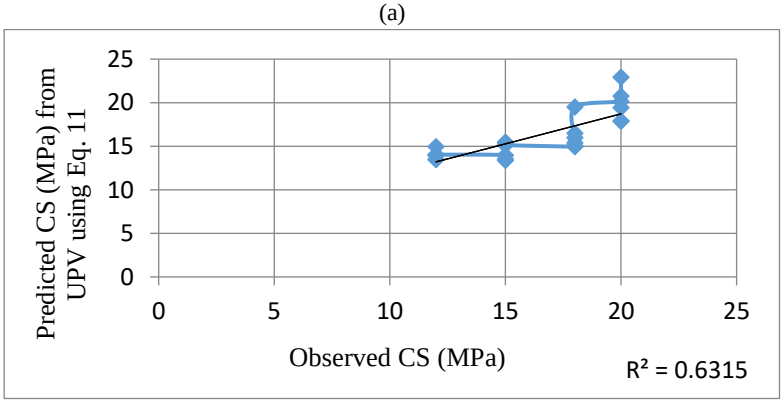

(b)

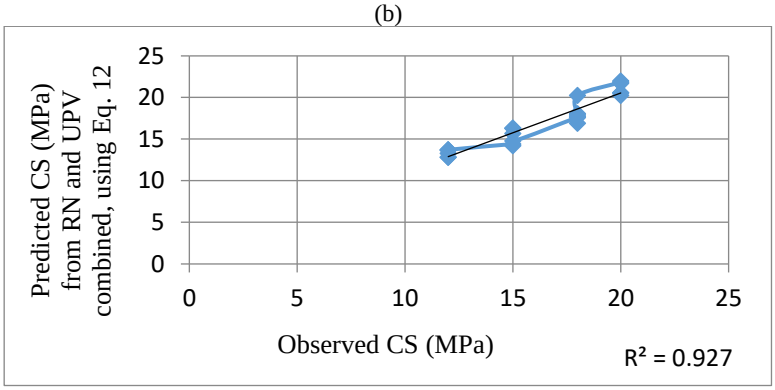

(c)

Fig. 2. (a), (b) and (c) presenting comparison of predicted CS values with observed CS values using Eqs. (10), (11) & (12) respectively

5 Conclusions

- Exponential correlation equations have been developed between in situ

ISBN: 978-81-932056-2-4

compressive strength and non- destructive testing values using only one non-destructive test technique, either RHN or U "Eqs. (10), (11)" and also using combined RHN and U values "Eq. (12)" for pervious concrete.

- Correlation equation between compressive strength of pervious concrete and RHN values show strong correlation ($R^2 = 0.909$). The RMSE and MAPE values are also less. Hence, this correlation can be effectively used for determining in situ CS of pervious concrete.

- Correlation equation between CS of pervious concrete and U values show weak correlation ($R^2 = 0.6315$). RMSE value is also very high (3.44). Hence, this correlation is not recommended to be used for determining in situ CS of pervious concrete.

- Correlation equation between CS and both RHN and U values combined show strongest correlation ($R^2 = 0.927$). RMSE value is less (1.19) while MAPE value is negligible. Hence, this correlation is also recommended to be used for computation of in situ CS of pervious concrete.

- Other machine learning techniques such as Fuzzy logic, ANN, ANFIS etc. can be used to check whether better correlation is obtained between compressive strength and U values.

References

1. Ajamu, S.O., Jimah, A.A. and Oluremi, J.R. Evaluation of Structural Performance of Pervious Concrete in Construction. International Journal of Engineering and Technology May (2012) vol.2 No 5.

2. American Concrete Institute (ACI 522R-10) Report on Pervious Concrete, chapter 6-Pervious Concrete Mixing Proportioning. (2010) Farmington Hills, MI, USA.

3. Ayyappan, A., Dinesh kumar, D., Sangeetha, G., Roshini, S., Sivasangari, M. Experimental study on Pervious Concrete. International Journal of Scientific Development and Research (IJSDR), (2018) ISSN: 2455-2631, vol.3, Issue 3.

4. Balaji, M.H., Amarnaath, M.R., Kavin, R.N., Pradeep, S.J. Design of Ecofriendly Pervious Concrete. International Journal of Civil Engineering and Technology (IJCIET), (2015) vol.6 pp. 22-26.

5. Chandrashekar, V.C. et al. Effect on the Engineering Properties of Pervious concrete by Partial Replacement of Cement with GGBS. GRD Journal of Engineering, (2018) vol. 3, Issue 3.

6. Crounch, L.K, Smith, N., Walker, A.C., Dunn, T.R., and Sparkman, A. Determining Pervious PCC Permeability with a simple Triaxial Flexible-wall Constant Head Permeameter. TRB 85th Annual Meeting Compendium of paper, (2006) 18 pp.

ISBN: 978-81-932056-2-4

7. El-Hassan, H. and Kianmehr, P. Sustainability Assessment and Physical Characterization of Pervious Concrete Pavement made with GGBS. MATEC Web Conference 120, 07001 (2017).

8. Ganesh, K.M., Vara Prasad, A.S.S., Viswa Harish, P.S., Subrahmanyam, A. Study of Mechanical Properties of Pervious Concrete as a Pavement Material by Partial Replacement of GGBS in Cement with Addition of Cellulose Fiber. International Journal of Engineering and Technology 219-223 (2018).

9. Humdulay, H. N., John, R.J. Pervious Concrete: Step towards Green Concreting. International Journal of Scientific & Engineering Research (2015).

10. Indian standard code for Hardened Concrete – Methods of Test, part 5 Non-Destructive testing of concrete, Section 1 ultrasonic pulse velocity Test" IS 516 (part 5 /sec 1): (2018), Bureau of Indian Standard (BIS).

11. Indian standard code for Hardened Concrete – Methods of Test, part 5 Non-Destructive testing of concrete, Section 4 Rebound Hammer Test IS 516 (part 5 /sec 4): (2020), Bureau of Indian Standard (BIS).

12. Indian standard code for Portland Slag Cement- Specification (Fourth Revision), (IS 455:1989).

13. Indian standard code Method of Tests for Strength of Concrete, (IS 516:1959).

14. Joshaghani, A., Ramezanianpour, A.A., Jaberizadeh, M. Mechanical Characteristic of Pervious concrete considering Gradation and Size of Course Aggregates. Research Journal of Environmental and Earth Science (2014) ISSN: 2041-0484.

15. Karthik Navada, R., Mittun, B.M., Marathe, S. Pervious Concrete for Transportation Application. International Research Journal of Engineering and Technology (2018) vol.5, Issue 5.

16. Kashyap, H. and Singh Rana, A. Studying the Effect of Silica Fumes on Mechanical Properties of Pervious Concrete. International Journal of Engineering Research Technology (2019).

17. LEED™ 2009 LEED Reference Guide for Green Building Designing and Construction with Global ACPs (2009).

18. Liu, H., Luo, G., Wang, L., Wang, W., Li, W., Gong, Y. Laboratory Evaluation of Eco Friendly Pervious Concrete Pavement Material Containing Silica Fume. Applied Science (2019), 9, 73.

19. Liu, T., Wang, Z., Zou, D., Zhou, A., Du, J. Strength enhancement of recycled aggregate pervious concrete using a cement paste redistribution method. Construction and Building Material, 'Elsevier' (2019).

20. Malayali, A.B., Chokkalingam, R.B., Hari Krishanan, T., Nagaselvam, P. Effect of Molar Content on GGBS Based Geopolymer Pervious Concrete. IOP Conference series: Material Science and Engineering (2020) 879 012128.

ISBN: 978-81-932056-2-4

21. Malhotra, V.M. No- Fines Concrete- Its Properties and Application. ACI Journal, Proceedings (1976) V.73, No.11, Nov., pp. 628-644.

22. Martins Filho, S.T., Bosquesi, E.M., Fabro, J.R., Pieralisi, R. Characteristics of Pervious Concrete Focusing on Nondestructive testing. IBRACON Structure and Material Journal (2020) vol. 13, number 3 pp. 483-500.

23. Meininager, R.C. No Fines Pervious Concrete for Paving, Concrete International (1988) V.10, Aug., PP 20-27.

24. Mishra, S. and Jena, A. Effect of Fly Ash on Pervious Concrete. International Journal of Engineering Technology and Applied Science (2018), vol.6, Issue 5.

25. Mohan Raj, R., Chinnasamy, M., Thenmozhi, S. Experimental Studies on Performance of Pervious Concrete Using Recycled Aggregate and GGBS. International Journal of Multidisciplinary Science and Technology (2017) vol.2, Issue 4.

26. Muthaiyan, U.M. and Thirumalai, S. Studies on Properties of Pervious Fly ash- Cement Concrete as a Pavement Material. Cogent Engineering, Civil & Environmental Engineering (2017). https://www.tandfonline.com/loi/oaen20

27. Nash't, I.H., A'bour, S.H. and Sadoon, A.A. Finding a unified relationship between Crushing Strength of Concrete and nondestructive test. www.ndt.net-3rd MENDT – Middle East Nondestructive Testing Conference & Exhibition-27-30 Nov (2005) Bahrain, Manama.

28. Neithenalath, N. Development and Characterization of Acoustically efficient Cementitious Materials. PhD thesis, Purdue University, West Lafayette, IN, (2004), pp. 269.

29. Raghwani, J.R., Shah, D., Bhavsar, J.K. Performance Assessment of Pervious Concrete using Silica Fume. Journal of Civil Engineering and Environment (2016) vol.3 pp.269-273.

30. Ramkumar, T.D., Rajkumar, S., Rajesh, V., Ramkumar, R. Cost Analysis and Comparison of Urban Road with Permeable Pavements. International Journal of Creative Research Thoughts (IJCRT) (2018).

31. Sir, B.S. and Setiana, S.M. Pavement Design using Environmental Pervious Concrete. IOP Conference series, Material Science and Engineering (2020).

32. Sugajanarthan, G., Arivumangai, A. Study on Behavior of Porous Concrete with Silica Fume and GGBS (for Airport Runway purpose). International Journal of Research Publication and Review (2021), vol.2 number 12, pp. 628-632.

33. Suresh, D. and Nagaraju, K. Ground Granulated Blast Slag (GGBS) In Concrete- A Review. IOSR journal of Mechanical and Civil Engineering (2015) vol. 12, Issue 4, Ver. VI, PP 72-82.

34. Swaminathen A.N., Saravana kumar, N. Experimental Studies on Strength Properties of Pervious Concrete. International Research Journal of Engineering Technology (2016).

35. Tank, C.-W.; Cheng, C.K., Ean, L.-W. Mix Design and Engineering Properties of Fiber Reinforced Pervious Light Weight Concrete. Applied science (2022).

ISBN: 978-81-932056-2-4

36. Zeeshan, M. A Study on Compressive strength of Pervious Concrete. Master's thesis. CECOS University (2020).

37. IS 12269-1987 Ordinary Portland Cement 53 Grade Specification.

38. IS 383:2016 Coarse and Fine aggregate Specifications.

ISBN: 978-81-932056-2-4

SEISMIC ANALYSIS OF CONVENTIONAL, DIAGONAL, AND CROSS-BRACING ELEVATED WATER TANK FOR SEISMIC ZONES III AND IV

Chukesh Singh[1] and Dr. A. K. Dwivedi[2]

[1] M. Tech Scholar, University Department, Rajasthan Technical University, Kota, Rajasthan
[2] Professor, University Department, Rajasthan Technical University, Kota, Rajasthan, India

[1] chukeshsingh2014@gmail.com
[2] akdwivedi@rtu.ac.in

Abstract. The water tanks are used to store the water and distribute it through the public water distribution systems. The water tanks built at a certain height are called overhead water tanks (OWT) or elevated water tanks (EWT). The elevated water tank contains a big mass concentrated at the top and thin supporting structures. It is particularly sensitive to earthquake-related horizontal pressures. The supporting systems are either designed or improperly chosen, and the elevated water tanks across the world collapsed or sustained significant damage as a result of the earthquake. For safe design, several researchers and designers have used different structural systems and materials to make the EWT stable under earthquake conditions. The purpose of the present research is to analyze the conventional, diagonal, and cross-bracing, elevated intze water tanks for different seismic zones. For that purpose, conventional, diagonal, and cross-bracing elevated intze tanks have been analyzed and compared in terms of lateral displacement and base shear. The present study also demonstrates the impact of full and empty EWT conditions for zone III and IV. The comparison of lateral displacement and base shear reveals that the cross-braced EWT has performed better than conventional, elevated water tanks.

Keywords: Intze Tank, Conventional, Diagonal Bracing, Cross Bracing, Lateral Displacement, Base Shear.

1 Introduction

Water is necessary for people and other forms of life. an elevated tank is a big storage container designed to retain various types of liquid at a specific height in order to maintain proper pressure. Liquid tanks are used in industries to store chemicals, petroleum products, and water in public water distribution systems. Industrial liquid tanks may hold very poisonous and combustible substances, and their contents must not be lost during the earthquake. The design of a water tank in a certain location determines adequate water distribution. There are several methods for storing liquids, including subterranean, ground supported, raised, and so on. Elevated tanks do not require constant pump operation since the pressure is maintained by gravity, which does not affect the distribution system. Elevated storage tanks are commonly utilized for water storage. The strategic location of the tank can equalize water pressures in the distribution system. The pressure of the water pouring from an elevated tank is determined by the depth of the water in the tank. Elevated storage tanks are utilized in situations where ground storage tanks cannot be created owing to a lack of adequate natural elevation and when standpipes are serviced from a well through a windmill or other powered

ISBN: 978-81-932056-2-4

pumps. Elevated tanks may service a huge population as well as a small group of homes. Elevated water tanks are a key and important construction, and damage to these structures during earthquakes can jeopardize drinking water supplies, cause failure to prevent big fires, and result in significant economic loss. As a result, water tanks are critical for public utilities. In comparison to typical buildings, liquid storage tanks have limited ductility and energy absorption capability. As a result, the seismic safety of liquid storage tanks is critical.

2 Literature Review

Jayadeep K. S. et al. (2022) studied the seismic response on an elevated water tank [1]. The objective of this research was to analyze the seismic response of an elevated water tank while taking into reference the sloshing effect and assessing behavior. For this research, the authors considered the influence of soil-structure interaction for seismic zone II and III. According to the results, the time period (0.262 sec.), displacement (2.9mm), total Base Shear (28.91kn.), and Base moment (185. 77kn.m) was found higher in the case of the tank being full than empty.

Diwakar Yadav and Vinayak Mishra (2021) carried out a study on elevated water tank (EWT) design and seismic study in various earthquake profiles [2]. The objective of this research was to the performance of an elevated-water tank under different loading circumstances during earthquakes. Seismic design factors such as shear strength, base moment, and tank displacement were analyzed in seismic zones II, III, IV, and V under empty and full situations. The researchers found that the Intze tank having a conical bottom and another spherical bottom, reduces stresses in the ring beams. In a full tank condition, the lateral force is larger than in an empty tank, and the base shear is proportional to the zone factor.

Sheetal Mohan Tarwatkar and Niraj Bias (2021) analyzed the seismic behavior of elevated RCC water tanks having different h/d ratios and shapes [3]. The purpose of this work was required to construct an earthquake-resistant construction for elevated water tanks, as well as to research the h/d ratio and various tank shapes. As per the outcomes of the research, the nodal displacement increases as such zone factor, h/d ratio, and base shear increase from zone II to zone V. The circular shape of the elevated water tank is more resistant than the rectangular design (against seismic waves).

Tejaswini R and Mamatha A (2020) analyzed the EWT [4]. The goal of the reported research was to build an economical structure using the limit state approach rather than the working stress method and analysis was carried out for the empty tank, and full tank condition, with linear dynamic analysis utilizing ETABS Software. The researchers found that the area of steel utilized in the Limit State method was higher than in the working stress method and the critical reaction of raised water tanks may not always occur under the same conditions as described above; it may also vary depending on earthquake characteristics.

Vangaveti Sai Santhosh et al (2020) This study examined the seismic behavior of overhead water tanks using Indian, American, and British codal provisions [5]. The purpose of this study was dynamic response spectrum analysis was used to analyze the

ISBN: 978-81-932056-2-4

seismic behavior of RCC overhead tanks in seismic zone iii under IS 1893: 2002. The study draws the conclusion that in comparison to the other two standards, ACI is more affordable and the codal clauses are ranked in order of economic worth as ACI, IS, and BS.

3 Design Parameters for EWT and Methodology

Providing a safe working environment for the water tank is the responsibility of staging, an essential component of the overhead tank structure. A set of horizontal or inclined braces are placed at intermediate levels between vertical columns to shorten the effective length of the column, forming staging. In addition, it might function as a circular hollow shaft supporting a shear wall rather than a column and bracing. The staging is divided into two categories based on structure: Shell Staging and Column-Brace Staging. Column-Brace Staging is further divided into three categories: 1) Conventional Staging, 2) Diagonal Staging, and 3) Cross Staging, all these Column-Brace Staging are used for present research.

Table 1. Design Parameter for Tank Design

Tank Volume	900 m^3	Size of Top Beam	0.2 x 0.3 m
Staging Height	16 m	Width Of Balcony Beam	1.3m
No. of Column	8 No.	Depth of Balcony Beam	0.4m
Internal Diameter of Cylindrical Portion (D)	15 m	Depth of Balcony Beam	0.15 m
Height of Cylindrical Portion (H)	3.7 m	Size of Main Ring Beam	0.25 x 0.6 m
Free Board	0.3 m	Diameter of Column	0.5 m
Height of Conical Dome (h)	2.7 m	Size of Periphery Bracing	0.25 x 0.40 m
Bottom Diameter of Conical (d)	9.1 m	Size of Diagonal And X-Bracing	0.23 x 0.3 m
Rise of Bottom Dome	1.8 m	The thickness of the Top Dome	0.15 m
The radius of the Curvature of the Bottom Dome	6.6 m	The thickness of the Cylindrical Wall	0.20 m
Rise of Top Dome	2 m	The thickness of the Conical and Bottom Dome	0.25 m
The radius of the Curvature of the Top Dome	15.1 m		

ISBN: 978-81-932056-2-4

The literature study demonstrates that several researchers have used different geometrical criteria for designing the EWT. The authors have performed analysis for zone II and III. In addition, a few researchers have used different types of bracing for zone II and III. However, the impact of the different types of bracing has not been carried out for zone IV and compared with zone III. The literature study reveals that lateral displacement and base shear are the most important structural properties of any elevated water tank. These structural properties have not been compared and analyzed for elevated water tanks having diagonal and cross staging, designed for zone III and IV. A live model is used to compare various parameters in order to determine the optimal staging method for the Intze water tank. The tank is estimated to hold 900kL and be supported by 8 columns, each of which may stage 5 stories, depending on the type. In order to draw a conclusion, this article investigates conventional, diagonal, and cross-bracing forms of staging. the empty and full water tank situation is included for analysis. As a result, STAAD Pro connect addition software has examined a total of 18 distinct models.

4 Analysis and Results

The results obtained for conventional, diagonal, and cross-braced EWT has been analyzed and discussed below.

Table 2. Base shear for Zone III

Types of Bracing	Base Shear (kN.)	
	Empty Tank	Full Tank
Conventional	366.06	598.84
Diagonal	723.6	1623.82
Cross	772.38	2028.19

Table 2 shows that the conventional intze tank has achieved the base shear of 366.06 KN. (in empty tank condition) and 598.84 KN. (in full tank condition) as per IS code 1893-2005. Also, Table 2 demonstrates that the intze tank with cross bracing (mentioned by "X") has achieved high base shear than the intze tank with diagonal bracing, i.e., 772.38 KN. (for an empty tank) and 2028.19 KN. (for full tank condition).

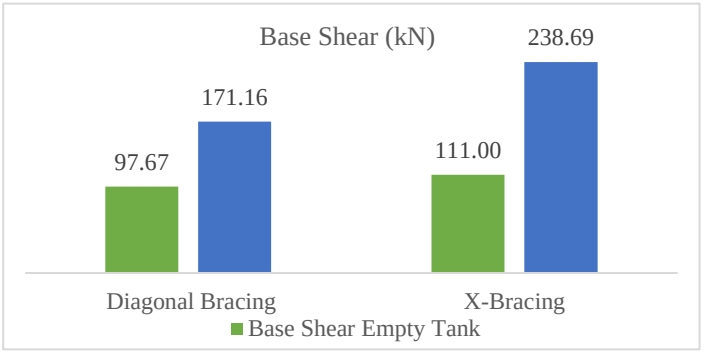

Fig. 1. Illustrates the percentage variation base shear for zone III

ISBN: 978-81-932056-2-4

Fig. 1 illustrates that (i) the intze tank with diagonal bracing has attained 97.67% (in empty tank condition) and 171.16% (in full tank condition) more base shear than the conventional intze tank; (ii) the intze tank with X-bracing has achieved 111.00% in empty tank conditions and 238.69% in full tank condition more base shear than conventional intze tank.

Table 3 shows that the conventional intze tank has achieved a base shear of 548.79 KN. (in empty tank condition) and 896.9 KN. (in full tank condition) as per IS code 1893-2005. Also, Table 3 demonstrates that the intze tank with cross bracing (mentioned by "X") has achieved high base shear than the intze tank with diagonal bracing, i.e., 1158.84 KN. (for an empty tank) and 3042.8 KN. (for full tank condition).

Table 3. Base shear for Zone IV

Types of Bracing	Base Shear (kN.)	
	Empty Tank	Full Tank
Conventional	548.79	896.9
Diagonal	1085.66	2435.03
Cross	1158.84	3042.8

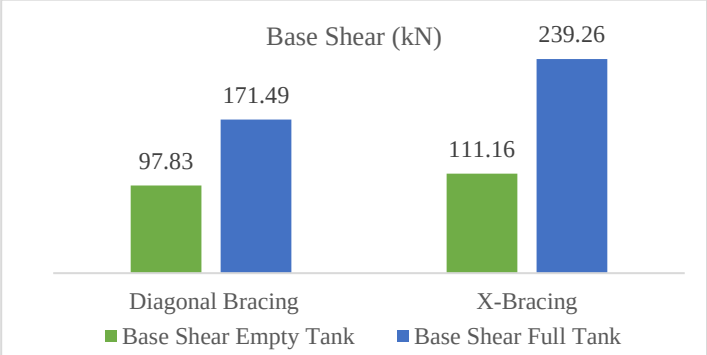

Fig. 2. Illustrates the percentage variation base shear for zone IV

Fig. 2 illustrates that (i) the intze tank with diagonal bracing has attained 97.83% (in empty tank condition) and 171.49% (in full tank condition) more base shear than the conventional intze tank; (ii) the intze tank with X-bracing has achieved 111.16% in empty tank conditions and 239.26% in full tank condition more base shear than conventional intze tank.

ISBN: 978-81-932056-2-4

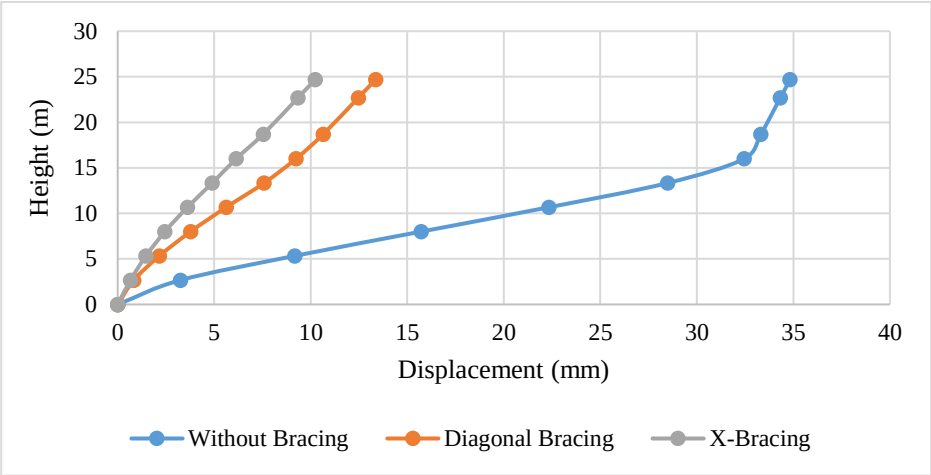

Fig. 3. Illustrate lateral displacement for soft soil in empty condition, zone III

Fig. 3 illustrates that the conventional intze tank has attained 34.831mm lateral displacement at the top of the tank. furthermore, it can be seen that 70.62% for X-bracing and 61.63% for diagonal bracing, present in Fig. 3 for empty tank condition in zone III.

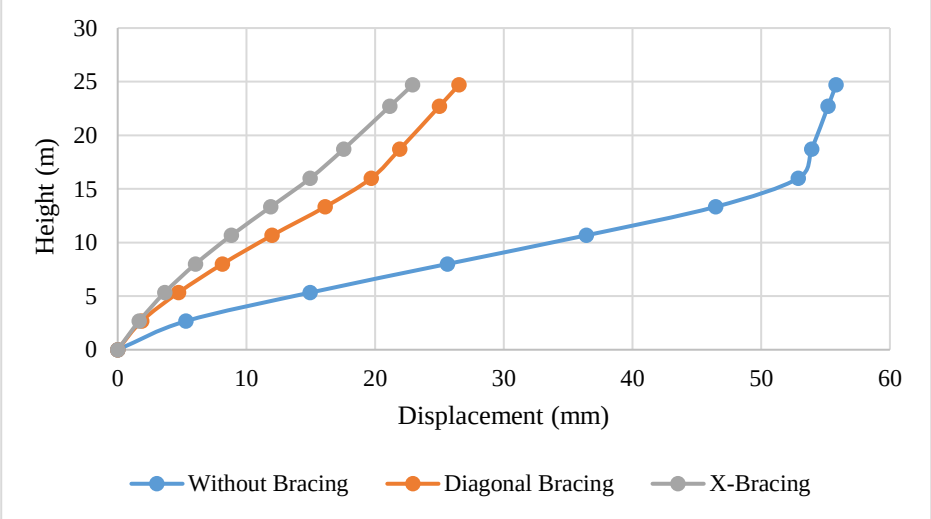

Fig. 4. Illustrate lateral displacement for soft soil in full condition, zone III

Fig. 4 illustrates that the conventional intze tank has attained 55.819mm lateral displacement at the top of the tank. furthermore, it can be seen that 58.93% for X-bracing and 52.49% for diagonal bracing, are present in Fig. 4 for full tank condition in zone III.

ISBN: 978-81-932056-2-4

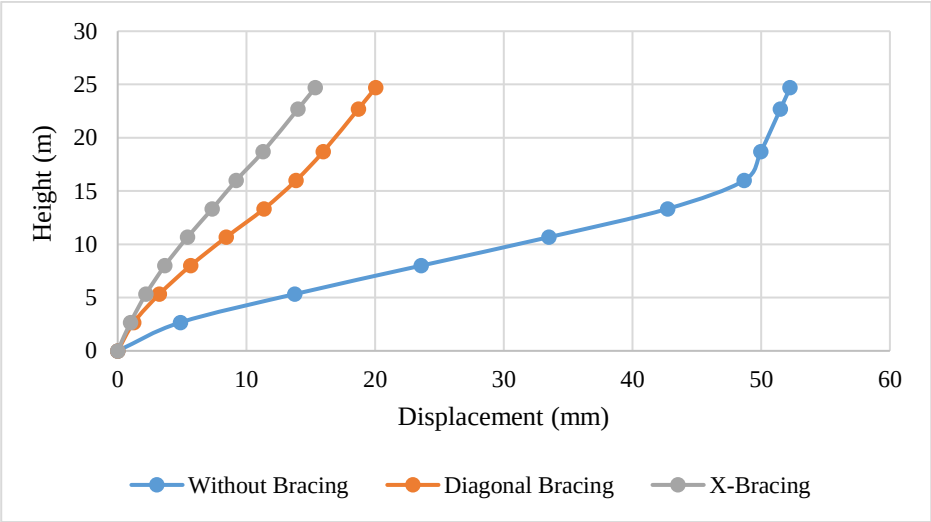

Fig. 5. Illustrate lateral displacement for soft soil in empty condition, zone IV

Fig. 5 illustrates that the conventional intze tank has attained 52.247mm lateral displacement at the top of the tank. furthermore, it can be seen that 70.61% for X-bracing and 61.63% of diagonal bracing, are present in Fig. 5 for empty tank condition in zone IV.

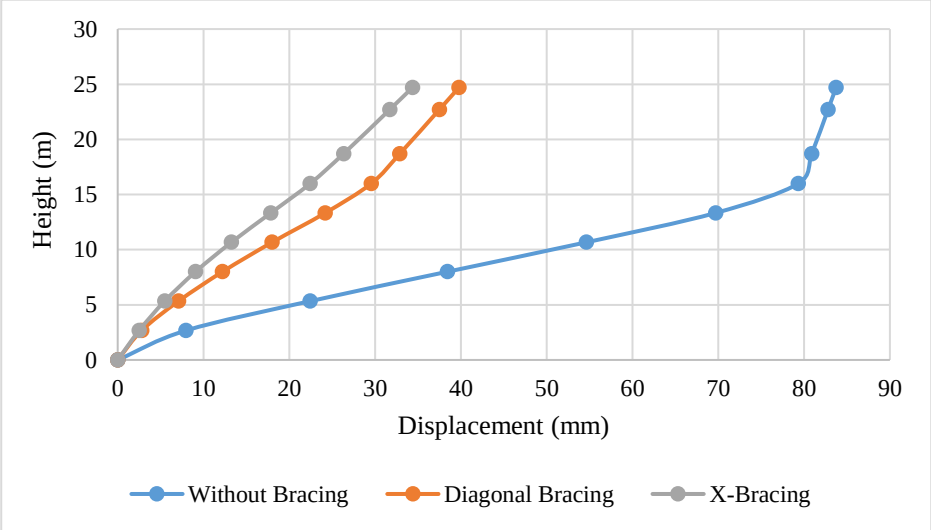

Fig. 6. Illustrate lateral displacement for soft soil in full condition, zone IV

Fig. 6 illustrates that the conventional intze tank has attained 83.728mm lateral displacement at the top of the tank. furthermore, it can be seen that 58.97% for X-bracing and 52.49% for diagonal bracing, are present in Fig. 6 for full tank condition in zone IV.

ISBN: 978-81-932056-2-4

5 Conclusions

From the analysis and comparison of different elevated intze tanks, the following conclusions are drawn,

- The conventional elevated intze tank has attained maximum lateral displacement in Zone IV than Zone III. It has also been observed that cross-braced elevated intze tank has achieved less lateral displacement than conventional elevated intze tank.
- The higher lateral displacement, when it is filled with water than empty elevated intze tanks in both earthquake zones.
- It has also been observed that a conventional elevated intze tank has less base shear than diagonal-braced and cross-braced elevated intze tanks in each earthquake zone.
- The comparison of the base shear of the cross-braced intze tank with the conventional and diagonal-braced elevated intze tank reveals that the cross-braced intze tank has higher base shear in filled and empty conditions for both zones.
- The results obtained in the full tank condition demonstrate that water increases the base shear of the elevated intze tank (for all cases) and has less lateral displacement.

References

1. Jayadeep K. S, Thejaswini R.M, and L. Govindaraju, 2022. A Study on The Seismic Response of Elevated Water Tank. International Research Journal of Engineering and Technology, 09(03), pp. 833-841.
2. Y adav D. and Mishra V., 2021. Elevated Water Tank Design and Seismic Study in Various Zones. International Research Journal of Engineering and Technology, 08(10), pp. 588-595.
3. Tarwatkar S.M. and Bias N.,2021. Seismic Behaviour of Elevated RCC Water Tank Having Different H/D Ratio and Shape. International Journal of Engineering Research & Technology, 10(08), pp. 236-237.
4. Tejaswini, M., 2020. Design and Analysis of Elevated Water Tank. International Research Journal of Engineering and Technology, 07(08), pp. 3083-3088.
5. Santhosh, V.S., Sethy, S.K. and Shankar, A.N., 2020. Seismic Analysis of Overhead Water Tank Using Indian, American, and British Codal Provisions. International Research Journal of Engineering and Technology, 07(05), pp. 480-490.
6. Singh, A. and Gupta, S., 2019. Analysis of INTZE water tank supported on RC shaft. Int J Res Appl Sci Eng Technol, 7, pp.1032-1037.
7. Gujar S. and Sayyed S., 2019. Review on Seismic Analysis of Elevated Water Tank with Different Staging Configuration. International Journal of Engineering Research & Technology, 8(12), pp. 735-736.

ISBN: 978-81-932056-2-4

8. Tokhi, A. and Arora, S., 2019. Seismic analysis and comparison of overhead intze water tank, circular water tank, and rectangular water tank and response spectrum analysis.B Technology, 10(3), pp.2519-2527.

9. Aakhunji A. M. A. and Vanpariya K.L., 2019. Analysis of Intze Type Water Tank with Different Staging System & its Optimal Design. Emerging Research and Innovations in Civil Engineering, pp. 234-240.

10. Bansode, P.A. and Datye, V.P., 2018. Seismic analysis of elevated water tank with different staging configurations. MAT Journal of geotechnical studies, 3(1), pp. 1-5.

ISBN: 978-81-932056-2-4

NONLINEAR STATIC ANALYSIS AND DESIGN OF INNOVATIVE HYBRID COUPLED SHEAR WALL FOR G+4 AND G+6 STOREY BUILDINGS

Finhasali Navsariwala[1], Dr. N. K. Solanki[2] and Variya Sagar[3]

[1] PhD Research Scholar, Department of Applied Mechanics and Structural Engineering, Faculty of Technology & Engineering, The Maharaja Sayajirao University of Baroda, India – 390002
[2] Associate Professor, Department of Applied Mechanics and Structural Engineering, Faculty of Technology & Engineering, The Maharaja Sayajirao University of Baroda, India – 390002
[3] PG Student, Department of Applied Mechanics and Structural Engineering, Faculty of Technology & Engineering, The Maharaja Sayajirao University of Baroda, India – 390002

[1] finhasali.n-appmech@msubaroda.ac.in
[2] nksolanki-appmech@msubaroda.ac.in
[3] sagarvariya12vsg@gmail.com

Abstract. Modern construction techniques provide various solutions for earthquake resistance in building. Many researches emphasize on the importance of shear wall to resist lateral forces. From past studies it is found that coupled shear wall is an effective lateral load resisting system which offers higher resistance against lateral force compared to single shear wall and also incorporates the architectural demands. However, there is a need to enhance this study looking to present construction feasibility. Hybrid building system is an effective solution for this purpose. Coupled shear wall innovation combined with hybrid building system is presented.

Innovative Hybrid Coupled Shear Wall (IHCSW) system is made up of a Reinforced Concrete shear wall tied to steel column by replaceable steel link." Proportion of resisting moment taken by side columns, termed as coupling ratio (CR), turns out to be an influencing parameter for effectiveness of this system.

In this work, seismic load resisting mechanism of IHCSW system is studied by adopting suitable analysis and design method for various configuration of buildings such as G+4 and G+6 storey building having IHCSW system. Effect of CR on IHCSW system is studied by analyzing and designing structures for various coupling ratios. Nonlinear static (pushover) analysis is performed, using analysis software ETABS2017.

Result shows that the dimensions of shear wall and length of steel link are significant parameters for effective working of IHCSW system. Pushover analysis shows that building shows decent ductile behavior if CR is considered under critical limit. Overall study shows that IHCSW system is a worthy alternative to conventional single shear wall and coupled shear wall system and is effective in resisting lateral loads in the building.

Keywords: Inno-Hyco, Pushover Analysis, Coupled Shear Wall, Coupling Ratio, Hybrid Structures.

ISBN: 978-81-932056-2-4

1 Introduction

A "Hybrid Structure" is a structure made with the use of two or more materials/elements, where each material/element can be used to explore its own capacity. Many constructions cohabit two different structural forms, such as ductile structural walls and reinforced concrete ductile frames. A structure is referred to as a hybrid structure when the combined contribution of structural walls and frames provides lateral force resistance.

The advantages of the individual parts may be combined in a hybrid system. When needed, especially in the building's upper levels, it offers a sizable quantity of energy dissipation. On the other hand, because to the frame's considerable stiffness, it is possible to get good storey drift during earthquakes., (Sheriff El-Tawil et al. (2002) [1] (Sheriff El-Tawil et al. (2010)) [2].

2 Structural Systems

2.1 Conventional Hybrid Coupled Shear Wall

When two RC shear walls gets connected by a coupling beam made up of steel, coupling is said to be attained by inserting steel coupling beams, also known as links, in the wall, then the system is named “Hybrid Coupled Shear Wall system (HCSW)”.

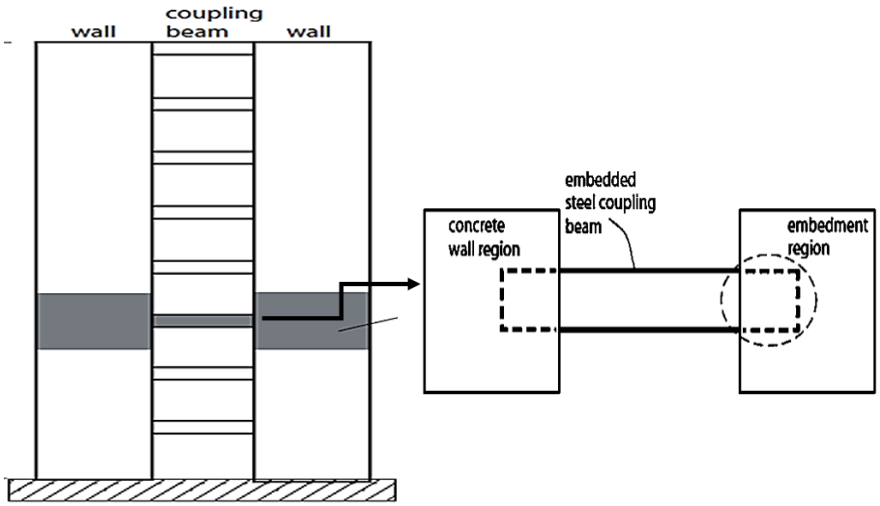

Fig. 1. Conventional Hybrid Coupled Shear Wall

Under moderate to high seismic loads, conventional HCSW systems exhibit the necessary balance of stiffness, strength, and ductility. However, these currently existing hybrid systems could have significant disadvantages, like the necessity for pricey foundations, expensive detailing, and extremely challenging restoration tasks. So, in order to improve this shear wall and steel links combination, a system termed innovative HCSW is discussed in the research project of INNO-HYCO [3].

ISBN: 978-81-932056-2-4

2.2 Innovative Hybrid Coupled Shear Wall

In Inno-HYCO Shear Wall (IHCSW), the side columns are exposed to bending moments and links are a replaceable element and to ensure that only shear force is transmitted, the steel coupling or link beam connections to the side columns are pinned.

While the RC shear wall transfers nearly all of the shear force during a seismic load, the overturning moments are combinedly taken by the two side steel columns with the virtue of an axial compression and tension couple formed instead of by the wall alone.

Because we provide links as a repeating component, the elastic field should either hold the RC wall in place or only slightly harm it, and only the dissipative steel links should be connected to the wall.

If only the connection steel pieces are damaged, the structure becomes easy to repair. It will be clear that the suggested hybrid system works well as a seismic-resistant component if a significant number of links yield. The response of IHCSW structure is mainly influence by the coupling. Coupling is action by which amount of lateral force transfer to shear wall and side column by means of coupling beam. RC shear wall, side column and link element are design according to the force taken by individual element and that is mainly influence by the Coupling Ratio (CR).

Total overturning moment taken by two columns (Mc) divided by the total moment that is moment in the column Mc + overturning moment Mw in RC wall is named Coupling ratio CR.

Therefore, it is noteworthy to study the behaviour of IHCSW under various CR and its influence in overall design of the structure which leads to one of the key purposes of the research which is to attain the optimum CR value and to understand the lateral load mechanism of the overall system. Paulay (1969) [4],

Lower CR selection is undesirable as a high CR indicates a reduction in the wall's moment demands, while large ductility of the coupling beam which leads to uneconomical design. Hence, the selection of CR is an effective parameter for design and the range of CR suggested in the work of Sheriff El-Tawil et al. (2010) [2] was 35%-45%.

In the work of T. Bogdan et al. (2013) [5], it was shown that raising the wall over-strength has benefits since it postpones reinforcement yielding, wall failure, and achieving the ultimate strain in the concrete, enhancing the lateral load capacity as well as ductility of the IHCSW system. Given that there will be fewer reinforcements, the design should be based on how to best use the wall aspect ratio, possibly staying within recommended ranges, ratio H/lw should be less than equal to 10.

As an outcome of researches by Andrea Dall' Asta et al. (2015) [3], Zona et al. (2016) [6], Zona et al. (2017) [7], Das et al. (2018) [8], the European and extra European codes were reviewed to understand and provide guidance regarding the hybrid building system and also studied various existing solutions and have proposed IHCSW system and

ISBN: 978-81-932056-2-4

presented design guideline and detailed design formula and steps for the IHCSW system according to Euro code.

2.3 Resisting Mechanism and Coupling Ratio of IHCSW

Although the two side steel columns' axial compression-tension couple rather than the wall's individual flexural action is what mostly resists the overturning moments, the RC shear wall absorbs nearly entire lateral shear force caused by seismic load. (Daneshvar and Karamodin (2020))[9]

The SF and BM generated by Lateral loads in the IHCSW system are as highlighted in fig. 2. These lateral loads are supposedly only applied to the RC wall, which means that only the RC wall is connected to the floors of the frame resisting gravity. Since the tensile and compressive forces in the links are negligible in this case, their impact on the design can be disregarded. Ceccolini et al. (2023) [10].

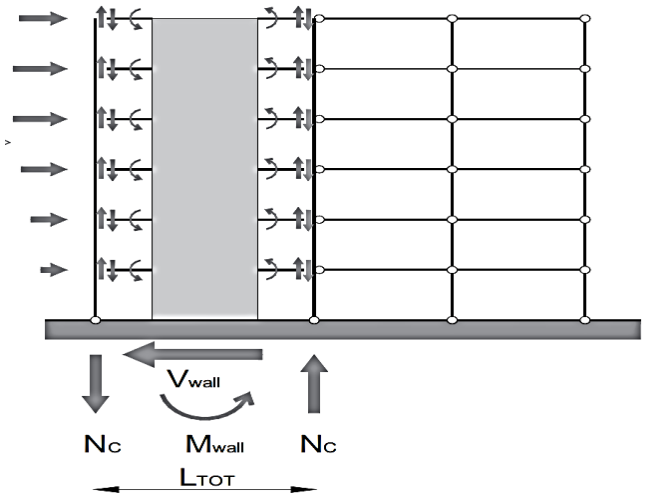

Fig. 2. Resisting mechanism of IHCSW

The axial force N_C is calculated by combining the shear forces in the links, at the base of the column, as the total length between two column L_{TOT} act as a lever arm and generates the overturning moment M_C taken by two columns.

Coupling Ratio (CR) can be given as,

$$\frac{Mc}{Mc + Mw} \quad (1)$$

The CR permits customising the relative characters of RC and steel element in the mechanism of resisting seismic load since it calculates the influence offered by the coupling action.

ISBN: 978-81-932056-2-4

2.4 Steel Links Design.

Design steps of the dissipative steel links are described in the work of Andrea Dall'Asta et al. (2015) [3].

Lateral load causes the shear force in the link $V_{link,i}$ (refer fig. 3). N_C and Vlinki can be related as:

$$N_C = \sum_{i=1}^{n} V_{link,i} \quad (2)$$

Therefore,

$$M_c = L_{tot}\, N_C \quad (3)$$

Where, L_{tot} = Length of IHCSW system which includes twice the length of steel link and the length of RC shear wall.

$$M_C = (l_W + 2l_{link}) \sum_{i=1}^{n} V_{link,i} \quad (4)$$

From the CR formula, moment in column M_c can be given as

$$M_C = \frac{CR}{1-CR} M_W \quad (5)$$

N_C for a particular CR can be given as

$$N_C = \frac{Mc}{Ltot} = \frac{CR}{1-CR} \frac{Mw}{Ltot} \quad (6)$$

$$N_C = \frac{CR}{1-CR} \frac{Mu}{L_{tot}\, \gamma w} \quad (7)$$

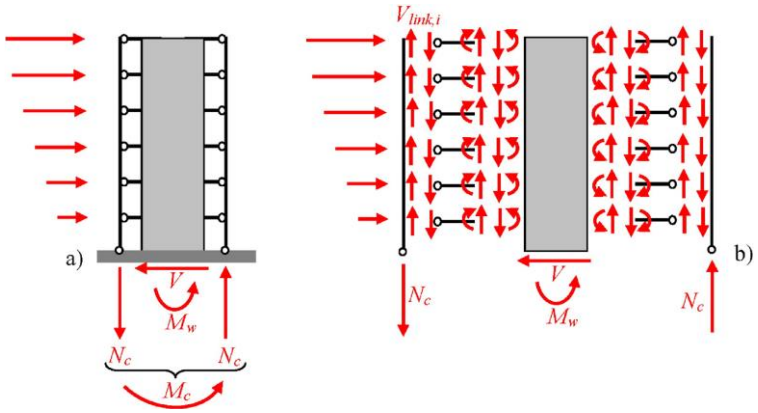

Fig. 3. Force resisting mechanism under lateral load in link beams

Where; Mu is the Factored bending moment at the shear wall base

ISBN: 978-81-932056-2-4

γ_w = Partial safety factor

Distribution of N_C, on the steel links, is done as the shear forces $V_{link,i}$ which is obtained as:

$$V_{link,i} = \psi \frac{Nc}{N_{link}} \quad (8)$$

$$V_{link,i} = \psi \frac{1}{N_{link}} \frac{CR}{1-CR} \frac{M_u}{L_{tot}\, \gamma w} \quad (9)$$

$$V_{link,i} = \psi \frac{1}{N_{link}} \times \frac{CR}{1-CR} \times \frac{Mu}{(L_w + 2\, L_{link})\gamma w} \quad (10)$$

Where; ψ = vertical shear link distribution factor.

In order to estimate the shear stress in each link, two distributions are proposed.

1. Uniform distribution: The axial stress at the base of the column is spread along the height of the structure by assigning the same rate of total shear to each link and the distribution factor is assumed as one.

2. Non uniform distribution: the axial force is not distributed equally to each floor, but the shear rate to the link is derived by the following function of storey level Z_i chosen:

$\Psi = 2CR \leq 1.6$ when $Z_i \leq H/2$. (11)

$\psi = 2(1\text{-}CR) > 0.4$ when $Z_i > H/2$. (12)

Link's Bending moment is found as:

$$M_{link,i} = V_{link,i}.\, l_{link} \quad (13)$$

After calculating SF and BM in each link beam, Link beam design is carried out.

There are no proper guidelines for the design of steel link beam in Indian standards IS 800:2007 [11], therefore Eurocode specification are followed for link beam design.

According to Eurocode 8 part I [12] and Eurocode 4. EN 1994-1-2 [13] the design resistance of link in shear and bending are calculated by;

$$V_{p,link} = \frac{fy}{\sqrt{3}}\, t_w\, (h - t_f). \quad (14)$$

$$M_{p,link} = f_y\, b\, t_f\, (h - t_f). \quad (15)$$

Where,

ISBN: 978-81-932056-2-4

f_y = nominal yield stress of steel.

t_w =thickness of web

h = depth of section.

b = width of flange

t_f = thickness of flange

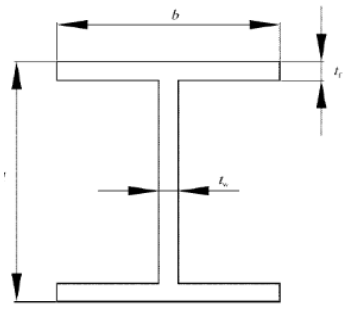

Fig. 4. Definition of symbols for I-section links

The classification of Seismic links into three categories is done depending on the plastic mechanism formed:

- Short links- in which energy gets dissipated essentially by yielding in shear;
- Long link- in which energy gets dissipated essentially by yielding in bending;
- Intermediate link – in which the bending and shear together contribute in plastic mechanism.

The link's type is found according to their link length as follows:

Table 1. Classification of Link

Long links	Intermediate links	Short links
$e > e_l$	$e_s < e < e_l$	$e<e_s$

Where, e is the link length considered.

$$e_l = 1.5\ M_{p,link}/V_{p,link}$$

$$e_s = 0.8\ M_{p,link}/V_{p,link}$$

ISBN: 978-81-932056-2-4

2.5 Design of side column.

Shear forces from the steel links are carried by the two columns. Design axial force is factored according to the euation:

$$N_{cd} = 1.1\gamma_{ov} \sum_{i=1}^{n} V_{link,i} \quad (16)$$

By taking γ_{ov} = 1.25, for the column's cross section and the connection's geometry, it should be thought about whether to include distance between the column's axis and the interconnection that transfers the SF from the link to the column. Afterward, it is possible to ascertain column's BM.

2.6 RC Shear Wall Design.

Assuming that the wall alone can resist the entire base shear, an suitable boundary against non-ductile failure of the shear wall should be permitted; whereas the influence of the two side columns is minimal as a result of which it is disregarded in this process.

After calculating the shear force and base moment acting at the shear wall design is carried out as specified in IS1893:2016 [14], IS456:2000 [15] and IS 13920:2016 [16]. Reinforcement is provided according to the specifications given in these codes for the vertical, horizontal, and confined reinforcement.

2.7 Proposed designing procedure for IHCSW.

The steps of the proposed design process are as follows:

1. Define the building configuration and various parameters such as height of the building, length and width of each bay, etc.

2. Definition of wall geometry such as width of wall b_W, height H_W from this length of wall l_W is carried out from relation H_W/l_W =10.

3. Design and detail the shear wall in order to make the most of the shear wall flexural capacity.

4. Design of the resisting mechanism formed by coupled dissipative steel links by changing only the value of CR.

5. Design of the side columns.

IHCSW system then is subjected to nonlinear static pushover analysis, after designing every element to find the optimum CR.

ISBN: 978-81-932056-2-4

3 Analysis and Design

In the present study the modeling of IHCSW system using ETABS 2017 for various building configurations. Designing of the shear wall is carried out for each configuration. Design of the coupling steel link beam and column design is presented for different values of CR for G+4 and G+6 storey building.

3.1 Design Input Parameters for G+4 and G+6 Buildings

Following design parameters are considered in the study.

1. Plan Dimension = 5 bays @ 3.5 m c/c in both directions.
2. Typical Storey height = 3 m
3. Dimension of building = 17.5m x 17.5m
4. Grade of concrete = M30
5. Steel section grade = Fe250
6. Reinforcement grade = Fe415
7. Slab thickness =120 mm
8. Dead load per unit area of the floor, including finishes = 4 kN/m^2
9. Live load = 2 kN/m^2 (on every floor)

   = 1 kN/m^2 (on terrace)
10. Location = Surat
11. Seismic zone = III
12. Response Reduction Factor, R = 5
13. Type of soil = Medium
14. Importance factor, Z=1
15. Earthquake load = As per IS 1893:2016
16. Height of shear wall H_W = 15 m for G+4 Building

    21 m for G+6 Building

ISBN: 978-81-932056-2-4

17. Width of shear wall = H_W /10 =1.5 m for G+4 Building

    2.1 m for G+6 Building

18. Thickness of shear wall t_W = 300 mm for G+4 and G+6 Building

19. Length of link = 1 m for G+4 Building

    0.7 m for G+6 Building

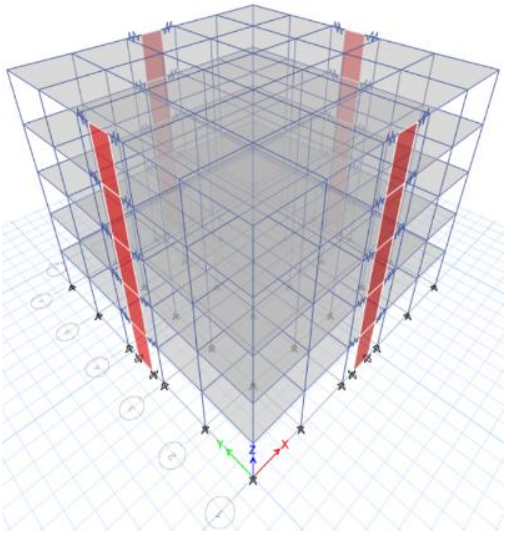

Fig. 5. 3D view of G+4 storey building

Design parameters of dissipative steel link and side column for CR value of 30%, 40%, 50%, 60%, and 70% is as shown in Tables 2 and 3 for G+4 and G+6 buildings.

Table 2 Design steel link properties for G+4 model for various CR.

CR	0.3	0.4	0.5	0.6	0.7
Shear demand V_{link} (kN)	48.059	74.75	112.137	168.206	261.654
Moment demand M_{link} (kN.m)	48.059	74.75	112.137	168.206	261.654
Link section	ISLB275	ISLB300	ISLB325	ISLB400	ISLB500
Yield shear $V_{p,link}$ (kN)	245.91	281.028	318.46	447.446	645.229
Yield moment $M_{p,link}$ (kN.m)	81.98	102.436	127.419	199.80	308.303
e (m)	1	1	1	1	1
e_s (m)	0.26	0.291	0.32	0.35	0.38
e_l (m)	0.50	0.546	0.6	0.66	0.716
Link classification	Long	Long	Long	Long	Long

ISBN: 978-81-932056-2-4

Table 3 Design steel link properties for G+6 model for various CR

CR	0.3	0.4	0.5	0.6	0.7
Shear demand V_{link} (kN)	71.372	111.023	166.535	249.803	388.583
Moment demand M_{link} (kN.m)	48.059	77.716	116.575	174.860	272.01
Link section	ISLB250	ISLB300	ISLB325	ISLB400	ISLB500
Yield shear $V_{p,link}$ (kN)	212.891	281.028	318.46	447.446	645.229
Yield moment $M_{p,link}$ (kN.m)	61.961	102.436	127.419	199.80	308.303
e (m)	0.7	0.7	0.7	0.7	0.7
e_s (m)	0.23	0.291	0.32	0.35	0.38
e_l (m)	0.43	0.546	0.6	0.66	0.716
Link classification	Long	Long	Long	Long	Intermediate

4 Results and Discussions

Nonlinear static analysis by increasing lateral loads until collapse is considered. After performing the pushover analysis, the curves recording the base shear vs. displacement measured is plotted for every considered value of CR.

A typical pushover curve for G+4 building with CR 30% is shown in Fig. 6 and four key events are noticed:

1. The very first yielding noticed in steel links is marked with ▬
2. All links yielded is marked with ▲
3. Instance when first Hinge is developed in shear wall is shown by ⬭
4. Collapse of the structure is depicted by ✖

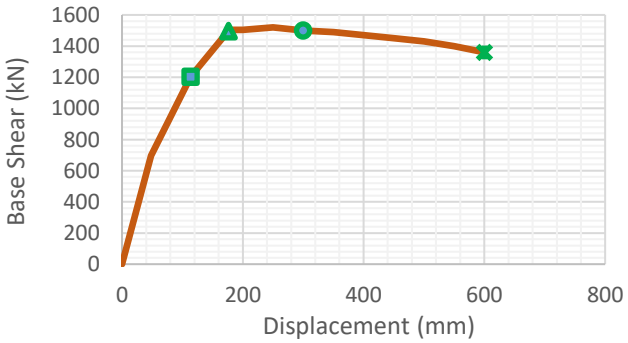

Fig. 6. Pushover Curve of G+4 building with CR 30%

ISBN: 978-81-932056-2-4

Base Shear values for various CR values for G+4 and G+6 Buildings are shown in Fig. 7 and 8.

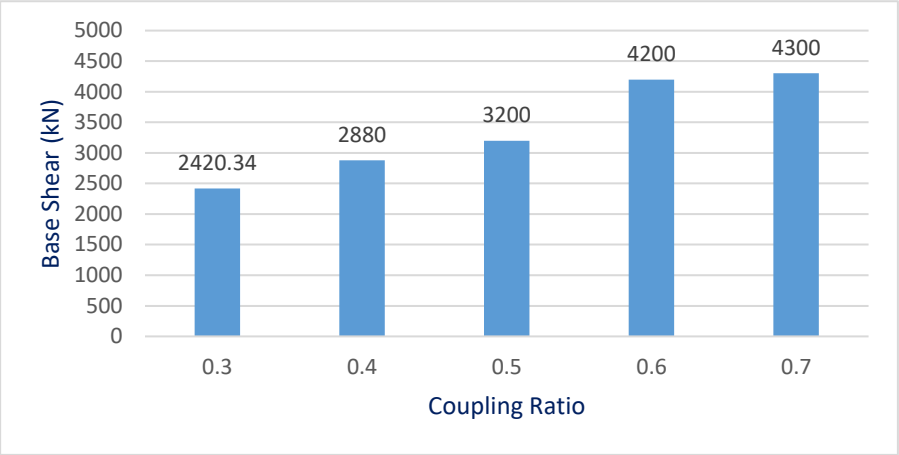

Fig. 7. Base Shear values for different CR values for G+4 Building

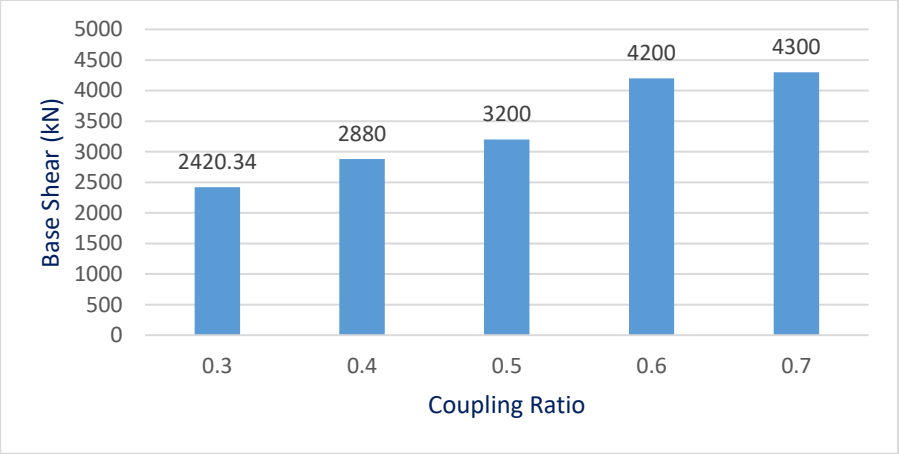

Fig. 8. Base Shear values for different CR values for G+6 Building

Stages of Development of hinge in various members for G+4 Building with CR 30% are displayed from Fig. 9 to 11.

ISBN: 978-81-932056-2-4

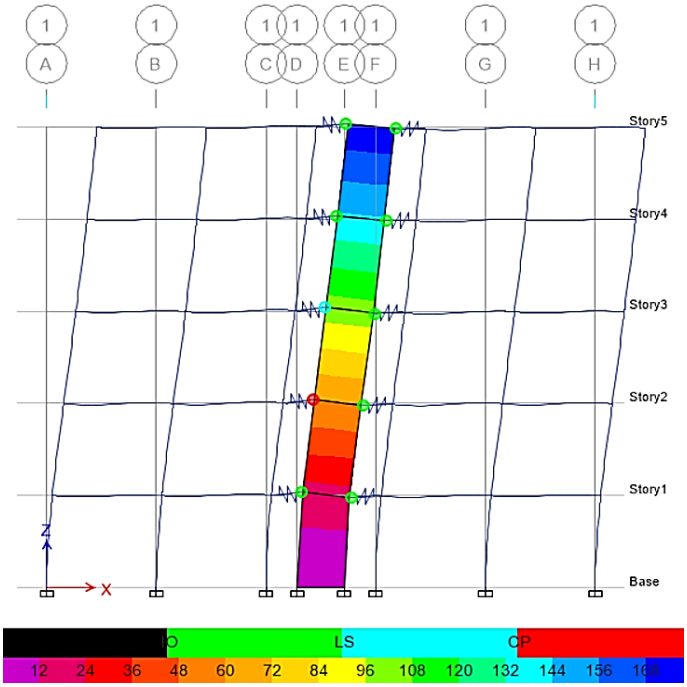

Fig. 9. Yielding of the first link

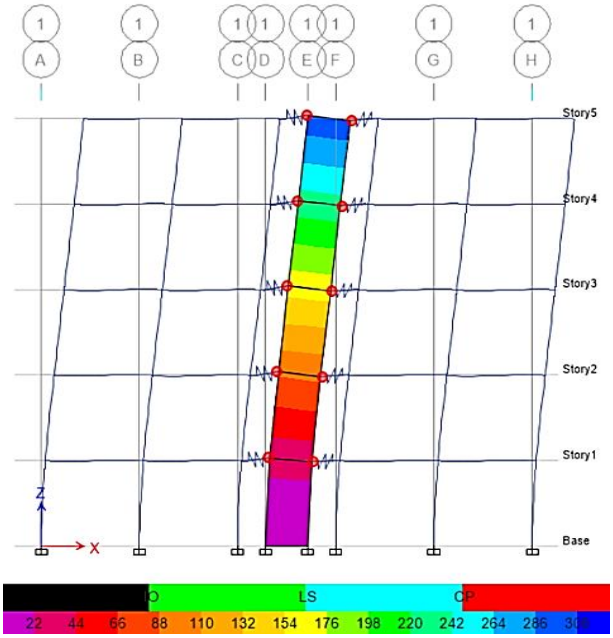

Fig. 10. All links are yielded

ISBN: 978-81-932056-2-4

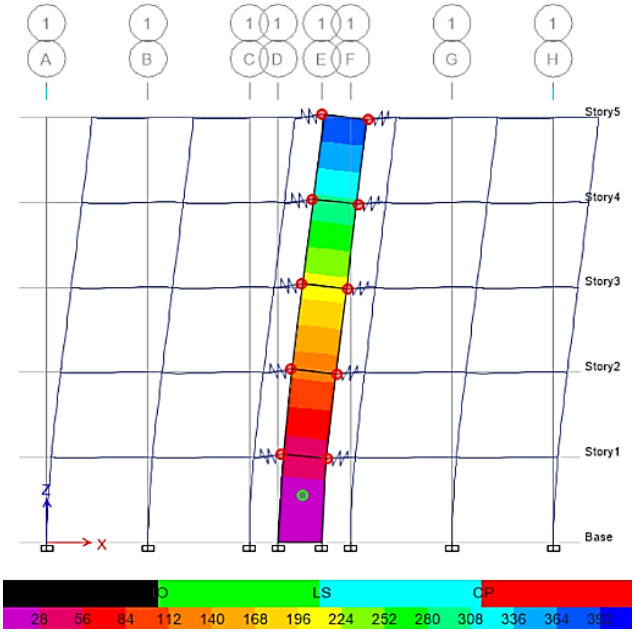

Fig. 11. Formation of hinges in wall

From all the pushover curves it is noticed that the first yielding always occurs in the links whereas the shear wall is in the elastic range (see Fig. 9).

Formation of hinge is observed initially at the base of the wall and yielding in all the links are observed before the collapse of the IHCSW system.

It is also seen that the behavior of the IHCSW systems significantly varies according to the design carried out considering different CR.

Likewise, the lateral load carrying capacity of the structure shows a rise with an increase in CR. The rate of increase is initially gentle when CR is 30%, 40% and 50%, and becomes steep while reaching 70%.

5 Conclusions

Following are the important deductions from the analysis:

- Since a fixed shear wall has been assumed for all CR values that correspond to one building configuration, the bending moment at the base is consistent in all cases, which confirms that the side column is responsible for the additional couple.

- It can be concluded that the height of the shear wall taken into account and the given link length are important factors in how well IHCSW performs.

- For both the building configurations, a similar trend is detected that first yielding

ISBN: 978-81-932056-2-4

occurs in the link then the state of the building where there is yielding of all the links and then the hinges are formed in wall for a particular value of CR. This confirms the design objective of the IHCSW that shear wall remains in the elastic state and link fails so that the concept of replaceable link is beneficial.

- However, models with higher CR value do not exhibit the same pattern. It is found that the formation of hinges in shear wall occurs prior to the yielding of seismic links for the models having value of CR above 50% and so the critical limits of the CR can be considered as 50%.

- Since, for the greater value of CR, peak value of base shear is more which means the resistance offered by the system is more. Also, as CR is more, the section required becomes heavy which escalates the steel requirement, thus achieving higher lateral capacity is less appealing. Hence, higher value of CR is not recommended for the design to fulfill the objective of the lateral load mechanism.

- It is determined that the value below 50% gives the optimized design and from the perspective of economy and safety, the value of CR as 40% is recommended from the study.

References

1. El-tawil, S., Asce, M., Kuenzli, C. M. & Hassan, M. Pushover of Hybrid Coupled Walls . I : Design and Modeling. **128**, 1272–1281 (2002).

2. Sheriff El-Tawil et al. Seismic Design of Hybrid Coupled Wall Systems: State of the Art. *J. Struct. Eng.* **136**, 755–769 (2010).

3. Zona, A. et al. *Innovative hybrid and structural solutions fo Innovative hybrid and composite steel-concrete structural solutions for building in seismic arear*. (2015). doi:10.2777/85404.

4. Paulay, T. The coupling of shear walls. *Univ. Canterbury, Christchurch, New Zeal.* **1**, (1969).

5. Bogdan, T. *et al.* Design and performance of steel - Concrete hybrid coupled shear walls in seismic conditions. *ECCOMAS Themat. Conf. - COMPDYN 2013 4th Int. Conf. Comput. Methods Struct. Dyn. Earthq. Eng. Proc. - An IACM Spec. Interes. Conf.* 2404–2421 (2013) doi:10.7712/120113.4674.c1295.

6. Zona, A., Degée, H., Leoni, G. & Dall'Asta, A. Ductile design of innovative steel and concrete hybrid coupled walls. Journal of Constructional Steel Research 117, 204–213 (2016).

7. Zona, A., Leoni, G. & Dall'Asta, A. 11.18: Seismic analysis of innovative hybrid steel concrete coupled walls. Ce/Papers 1, 2985–2992 (2017).

8. Das, R., Zona, A., Vandoren, B. & Degée, H. Optimizing the coupling ratio of seismic resistant HCW systems with shear links. Journal of Constructional Steel Research. **147**, 393–407 (2018).

9. Daneshvar, M. H. & Karamodin, A. Investigating the behavior factor of coupled concrete

ISBN: 978-81-932056-2-4

shear walls with steel coupling beam. *Sci. Iran.* **27**, 2189–2197 (2020).

10. Ceccolini, N. *et al.* Preliminary analyses of an innovative solution for reducing seismic damage in steel-concrete hybrid-coupled walls. *Procedia Struct. Integr.* **44**, 450–455 (2023).

11. IS 800 (2007): General construction in steel-code of practice, Bureau of Indian Standards, New Delhi.

12. Eurocode 8. EN 1998-1, Design of structures for earthquake resistance, part-1: General rules, seismic actions and rules for buildings. European Committee for Standardization (CEN), Brussels, 2004.

13. Eurocode 4. EN 1994-1-2, Design of composite steel and concrete structures part 1-2: General rules – Structural fire design. European Committee for Standardization (CEN), Brussels, 2005.

14. I.S. 1893 (2016): Indian standard criteria for earthquake resistant design of structures part 1: General provisions and buildings. Bureau of Indian Standards, New Delhi.

15. IS 456 (2000): Indian standard plain and reinforced-concrete code of practice. Bureau of Indian Standards, New Delhi.

16. IS 13920 (2016): Indian standard ductile detailing of reinforced concrete structures subjected to seismic forces-code of practice (incorporating amendment nos. 1 and 2). Bureau of Indian Standards, New Delhi.

ISBN: 978-81-932056-2-4

DESIGN AIDS FOR BUILT-UP I SECTION COLD FORMED STEEL COMPRESSION MEMBERS

Renushree Ambatwar[1], Chetan Rokade[2], Shraddha Shinde[3], Tanya Singh[4], Shankar Suthar[5] and Ankit Asher[6]

[1,2,3,4,5] UG Students, Department of Civil Engineering, Sardar Patel College of Engineering, Mumbai- 400058
[6] Assistant Professor, Department of Civil Engineering, Sardar Patel College of Engineering, Mumbai- 400058

[1] c1910049@spce.ac.in
[2] c1910050@spce.ac.in
[3] c1910058@spce.ac.in
[4] c1910063@spce.ac.in
[5] c1910062@spce.ac.in
[6] ankit.asher@spce.ac.in

Abstract. With the increasing demand for rapid construction and prefabricated structures, the demand for cold-formed steel is on the rise. The availability of design charts for structural members greatly reduces designers' efforts in the design and gives a better idea in checking the designs made by other engineers too. This paper provides an aid for cold formed structural sections having lipped channel profile connected with back to back configuration subjected to axial compression. By the help of spreadsheets, graphs are prepared between effective length and axial load capacity.

Keywords: Cold Formed members, compression members, effective length, effective width of section, axial load.

1 Introduction

In civil engineering, cost is a major factor affecting the design and construction of a structure, therefore, cold formed steel structures are used as they provide cost effective design. The increase of utilization of cold formed steel structures is due to its high strength/weight ratio, fabrication ease, wide range of sections available and the designers can also customize the sections as per their need, making the designs more economical than hot rolled steel, mainly for short span applications. The cold-rolled steel sections can, however, be made from strip steel with the yield stresses (MPa) of 210, 240, 300, etc. Cold formed steel sections are made by mainly two methods, namely, press braking and rolling. The steel sheets of width 1.0 to 1.25 m are fed into a sequence of roll forms. The number of pairs of rolls (also known as stages) varies from 5 to 15 depending on how intricate the cross-sectional geometry is. Press-braking is a different method of shaping, although it can only be used for short lengths (up to 6 m) and for reasonably straightforward designs. The strips are passed through dies to get the desired shape. The steel sections are classified in four categories, namely plastic, compact, semi-compact and slender sections. Cold formed steel sections are mostly classified under slender sections, which buckle before it reaches yield stress.

ISBN: 978-81-932056-2-4

1.1 Gross Area and Effective Area

As cold formed steel sections are mostly classified under slender sections, they are prone to local buckling before reaching yield stress, hence the gross cross-sectional area cannot be used for design calculations. The area that can be used to calculate the resistance against stress is less than the actual area of cross section hence, only effective area can be used for the design calculations. The effective width of the cross-section changes with respect to different boundary conditions the member is subjected to at both ends.

Cold formed steel sections commonly used in structural framing are Channels (C-sections), Z- sections, angles, hat sections. For more stability, built up sections are used by spot welding two individual simple sections. Cold formed steel elements are either stiffened or unstiffened. A stiffened element is one that has webs supporting it along both of its longitudinal edges. Unstiffened elements are those that are only supported along one longitudinal edge, leaving the other parallel edge free to move in any direction.

2 Design Procedure

In the development of design aids, the assumptions used are as follows:

1. Built-up I section is made up of a double channel section connecting back-to-back with spot weld and with no gap between the elements connected.
2. All the charts have been drawn by considering the effective span of the compression members.
3. In a stiffened flat plate element, the ineffective area is assumed to be lying in the center of the width for axially loaded compression members.
4. In an unstiffened flat plate element, the ineffective area is assumed to be lying on the unstiffened end of the element for axially loaded compression members.
5. The yield stress considered for computations is 240 N/mm^2
6. The modulus of elasticity (E) is taken as 2.05 x 10^5 N/mm^2
7. Partial factor of safety =1.1

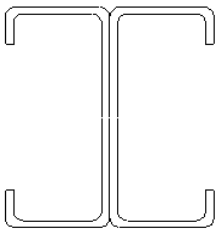

Fig. 1. Cross section used for developing the design aids

ISBN: 978-81-932056-2-4

2.1 Determination of Compressive Strength of Member

1. Note down relevant properties of section and calculate properties of built-up section like area and moment of inertia then find minimum radius of gyration r_{min}. Then, determine flat width of elements (i.e. of flange, web and lip).

2. Next step is to determine effective width of elements (i.e. of flange, web and lip), for that first step is to calculate the stiffness factor (k) for all elements as per code provision (BS 5950-5:1998). For stiffened elements if 'k' value comes less than 4 then take k = 4, or else take the respective calculated value of 'k'. And for unstiffened elements take k = 0.43.

3. Find local buckling stress, f_{cr}.

4. Find the value of the parameter,

5. $\left(\frac{Yield\ strength\ of\ steel\ (f_y)}{(\text{Local buckling stress}\ (f_{cr}))\ *(Partial\ safety\ factor(\lambda_{mo}))}\right)$, if it is greater than 0.123 then, effective width will be calculated as per the formula, if not then the effective width will be equal to flat width.

6. Calculate the effective area of the section by deducting the effective area from the gross area.

7. Determine the short strut resistance, Pd,c for that effective area.

8. Check the section against limiting slenderness.

9. Determine Perry coefficient ($\bar{\eta}$), ϕ and minimum elastic flexural buckling load (Pe). Then with the help of these values calculate axial buckling resistance, P_d .

10. Now the compression capacity of the section will be the minimum of value P_d and $P_{d,c}$.

2.2 Section Selection Procedure for Design Using the Developed Charts Shown in Fig. 2 To 6.

Step 1: Determine Axial load acting and calculate the effective span of the column according to the provided support conditions.

Step 2: Select a graph containing the effective span and Axial load.

Step 3: Plot the point on the graph selected with abscissa as effective span and ordinate as axial load.

Step 4: If the point lies on any of the curves on the chart, then that respective curve of the section is selected for designing. If not, then, the curve of the section lying above the point is to be selected for designing.

ISBN: 978-81-932056-2-4

Step 5: Add the thickness (0.04 mm) to the selected section for the protective galvanized coating for designing.

For example, if a compression member of effective length 3m has a cross section of double channel sections 100x100x25x4 (h x b x c x t), h= height of web, b= width of flange, c= width of lip, t= thickness of the member, as shown in figure 6, the capacity under pure axial compression will be 450kN.

3 Results

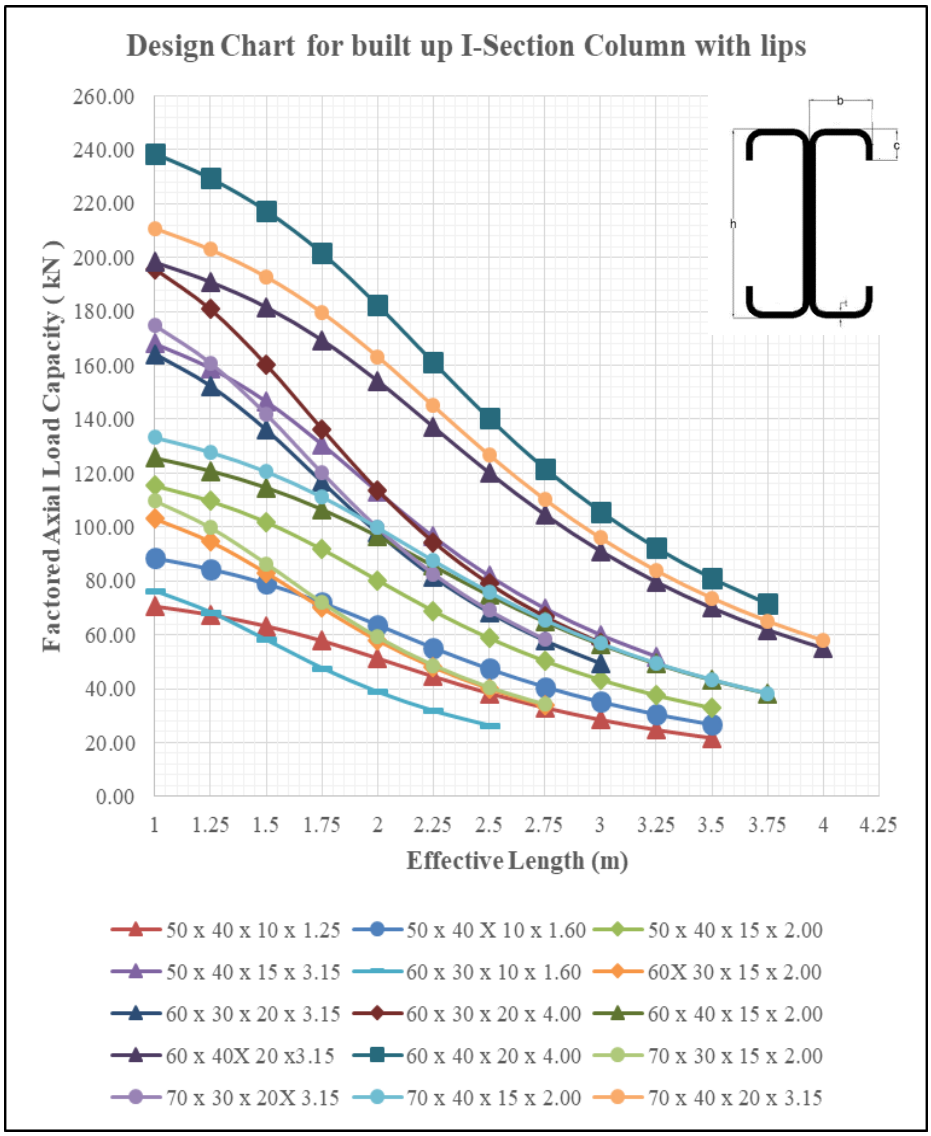

Fig. 2. Factored Axial Load Capacity Vs Effective Span of I-section made with Double Rectangle Channels with Lip Sections

ISBN: 978-81-932056-2-4

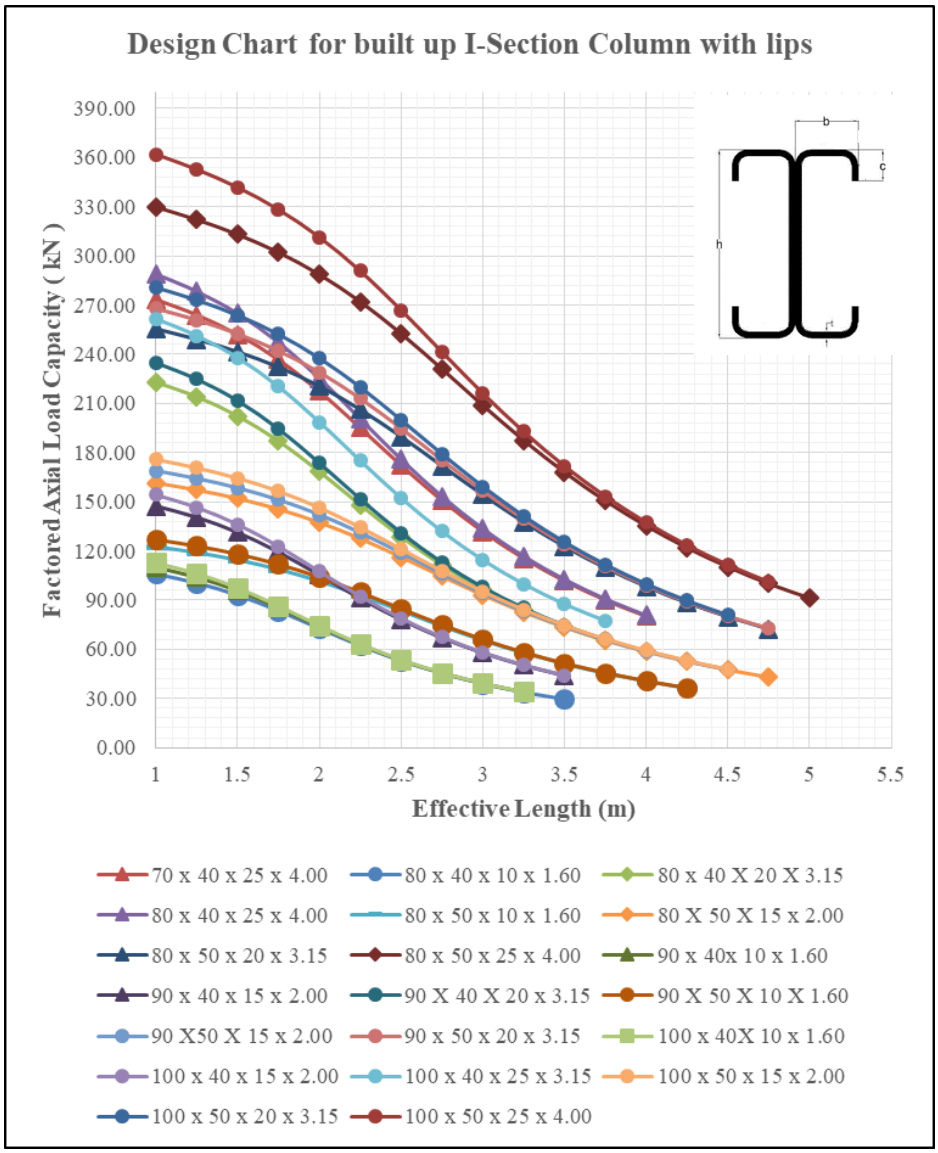

Fig. 3. Factored Axial Load Capacity Vs Effective Span of I-section made with Double Rectangle Channels with Lip Sections

ISBN: 978-81-932056-2-4

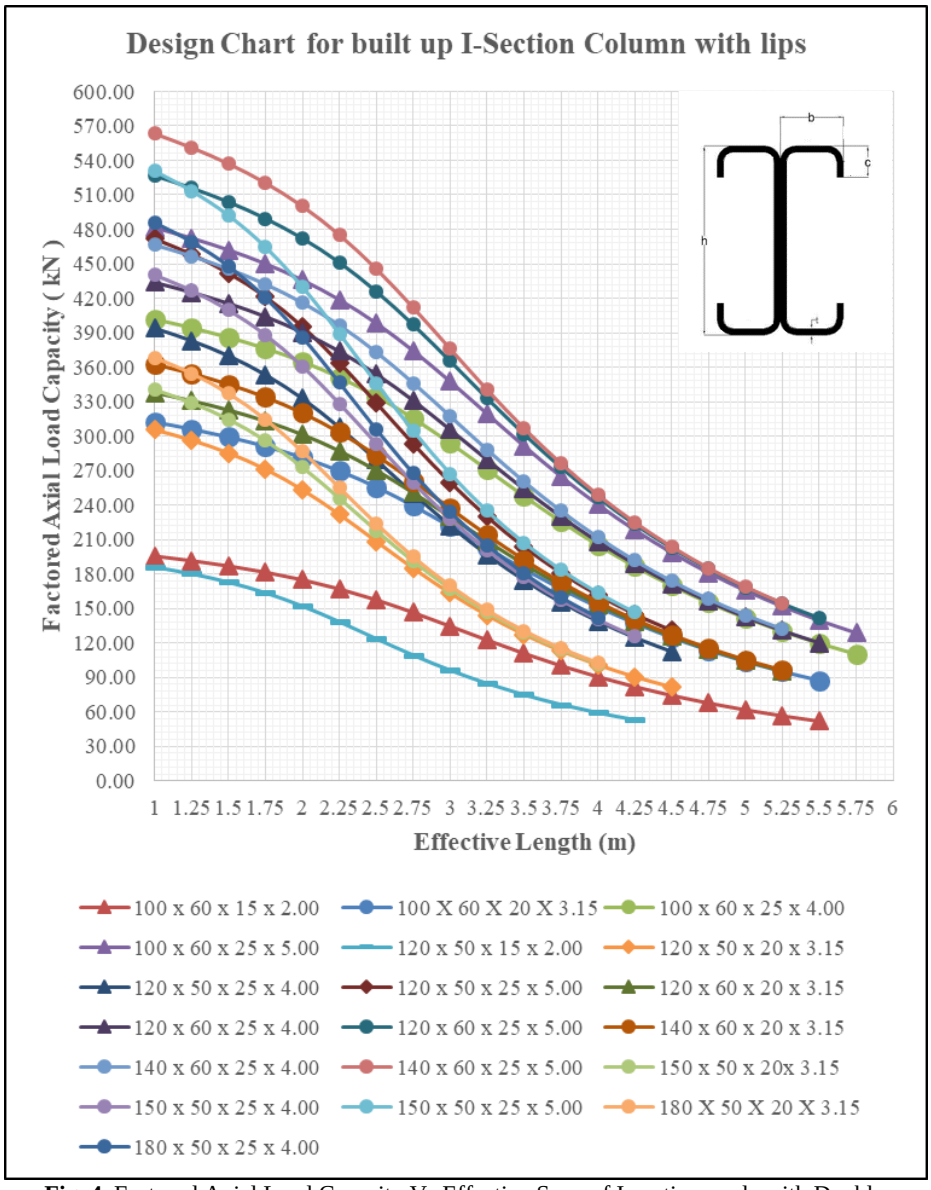

Fig. 4. Factored Axial Load Capacity Vs Effective Span of I-section made with Double Rectangle Channels with Lip Sections

ISBN: 978-81-932056-2-4

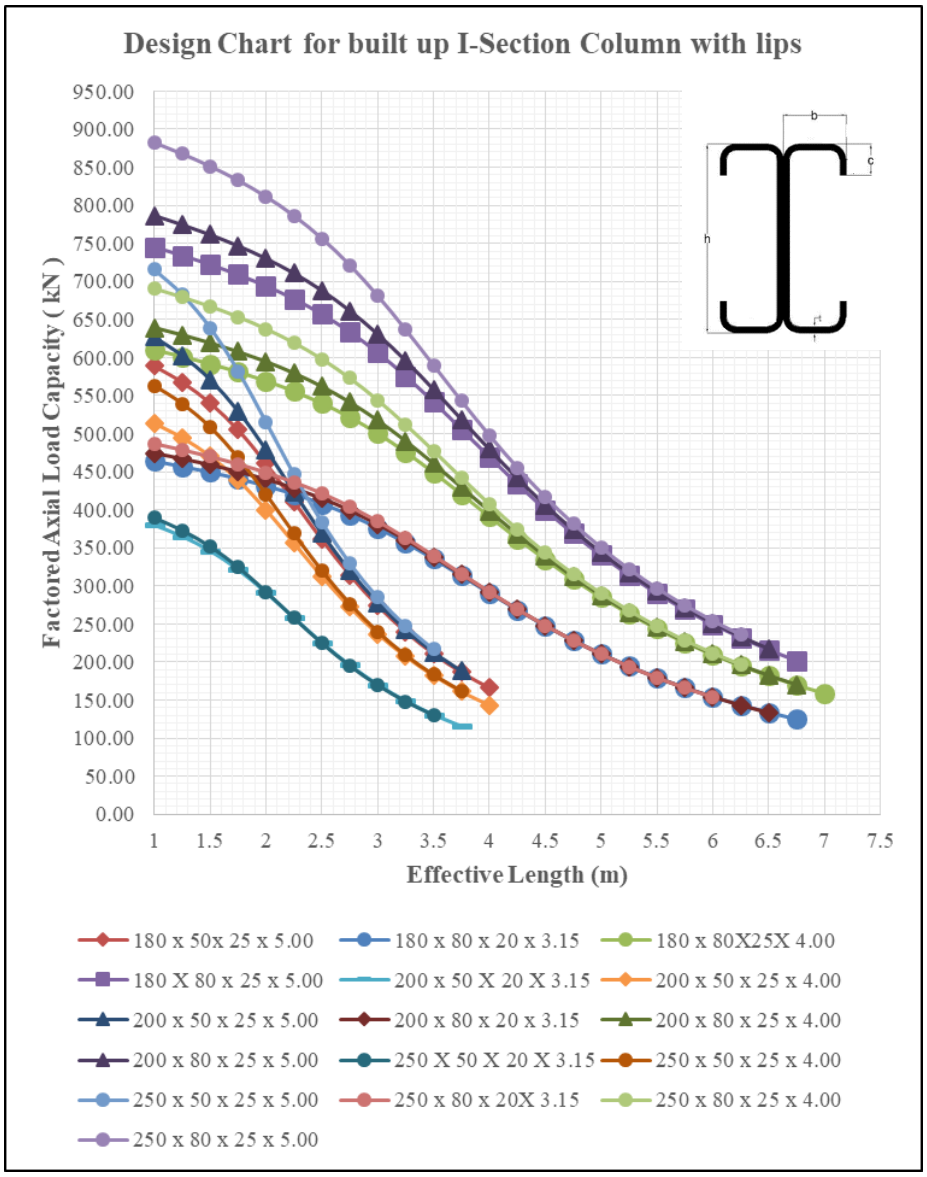

Fig. 5. Factored Axial Load Capacity Vs Effective Span of I-section made with Double Rectangle Channels with Lip Sections

ISBN: 978-81-932056-2-4

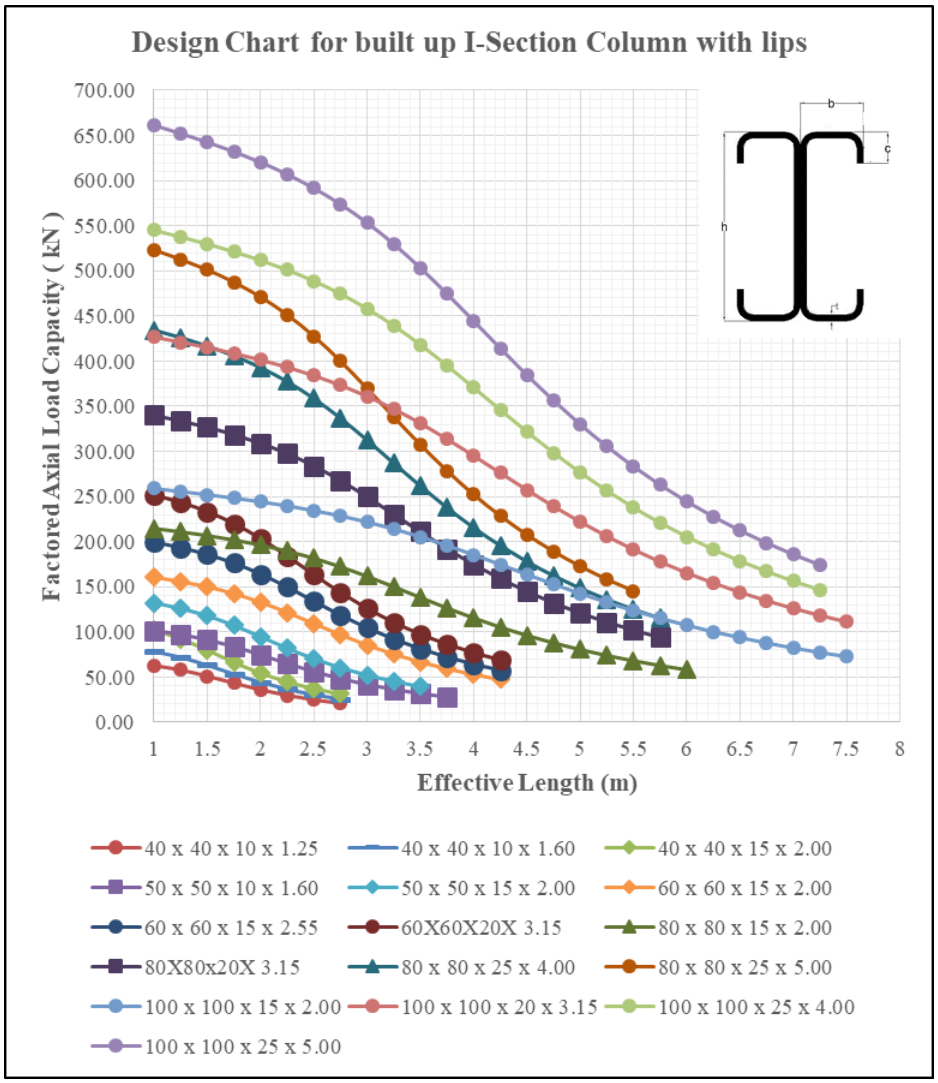

Fig. 6. Factored Axial Load Capacity Vs Effective Span of I-section made with Double Square Channels with Lip Sections

ISBN: 978-81-932056-2-4

4 Conclusion

The charts prepared for built up I-section columns will make it easy for structural engineers to design compression members made up of cold formed steel built-up I section. The methodology to use these charts has also been mentioned. It shall be noted that the charts are applicable for cold formed steel having $f_y = 240$ N/mm^2 only. These charts are also useful in designing as some of the design software do not design built-up cold formed steel sections.

5 Future Scope

Similar to the design charts prepared above, charts can be prepared:

- For Z section, hat section, hollow sections and single C sections can be prepared.
- For tension members can be prepared for easier calculations.
- For flexural members in a similar manner.
- For built-up I section made of channel sections without lips connected back-to-back can be possible.
- For higher grade of steel sections.

References

1. M.L. Gambhir, Fundamentals of Structural Steel Design. McGraw Hill Education (India) Private Limited, New Delhi (2013).
2. Prof. Ravindra Bhimarao Kulkarni, Vikas Arjun Patil: Design Aids of Flexural members and Beam-Column based on Limit State Method. In: International Journal of Scientific and Engineering Research, Volume: 02, Issue: 10. India (2011).
3. British Standard Code BS 5950-5 (1998), Structural use of steelwork in building -Part 5-Code of practice for design of cold formed thin gauge sections.
4. IS:811 (1987), Specification for Cold Formed Light Gauge Structural Steel Sections (Second Revision).

ISBN: 978-81-932056-2-4

PERFORMANCE OF OUTRIGGERS AND FRICTION DAMPERS IN HIGH RISE STRUCTURE USING RESPONSE SPECTRUM ANALYSIS

Shriya Mehendale[1], Keerti Rangnekar[2], Adarsh Jasiwal[3], Rewati Gaikwad[4], Yash Dhalkari[5], Dr. A.A. Bage[6] and Ankit Asher[7]

[12,3,4,5] UG students, Department of Civil Engineering, Sardar Patel College of Engineering, Andheri, Mumbai, India
[6] Associate Professor, Sardar Patel College of Engineering, Andheri, Mumbai, India
[7] Assistant Professor, Sardar Patel College of Engineering, Andheri, Mumbai, India

[1] c1910034@spce.ac.in
[2] keerti331@gmail.com
[3] c1910018@spce.ac.in
[4] c1910012@spce.ac.in
[5] c1910008@spce.ac.in
[6] a_bage@spce.ac.in
[7] ankit.asher@spce.ac.in

Abstract. With the ever-increasing population, rise in the standard of living, and limited availability of free lands in cities thereof, structures are growing vertically. Thus, there is a need to construct high-rise buildings while keeping the design approach sustainable. A building is subjected to lateral loads, such as wind and earthquake loads, in plus the gravity loads. In recent times, the use of outriggers and dampers has increased to make the tall and narrow buildings resistant to lateral loads in an efficient and effective way. This paper deals with a two-way symmetric, 90 m (30 storeys) tall RCC high-rise building having shear walls at the center. A damped outrigger system is used, comprising friction dampers and x-braced truss as outriggers, four models were modelled and analyzed on ETABS using Response Spectrum Method.

Keywords: High-rise structure, Friction Damper, Outrigger, Response Spectrum Analysis, Shear wall, ETABS.

1 Introduction

It is known that lateral loads such as wind and earthquake loads are very important when designing a building. Buildings have been developing vertically in cities due to a lack of available land, which presents a challenge to structural engineers in terms of finding an effective and economical solution. This has given impetus to the engineers to search for various lateral load-resisting systems. Solutions like outriggers, dampers, etc. have been found. They are even used in combination like- damped-outrigger systems. Outrigger and friction dampers have both been the subject of several research, but neither a comparison of the two nor a study of them in combination had been done. According to IS 16700 (Part 1)-2017 a 50m to 250 m tall building is a high-rise [4]. This study compares the performance (effect) of outrigger and friction dampers on a 90m tall, two-way symmetric RCC building comprising of shear walls at the center. Four models were made for comparing the performance of outrigger, friction damper and their combination by using Response Spectrum Analysis on ETABS. The plan area is

ISBN: 978-81-932056-2-4

25m x 25m with columns placed at 5m intervals. Throughout the storeys beams, columns, walls and slabs of the same size and grade of concrete are provided.

2 Literature Review

There is a vast body of literature on the subjects discussed. P.M.B. Kiran Nanduri, B. Suresh, and MD. Ihetesam Hussain determine the ideal position of the outrigger system for high-rise reinforced concrete buildings under wind and seismic stress. In light of the 90-meter-high RCC skyscraper, they described how to use outriggers and belt trusses that were put in various locations. The analysis method used for the study was dynamic. They concluded that the outrigger should be placed at the halfway point of the building's height [1].

According to a study by Jain Shubham and Mohd Adnan on seismic friction dampers for a rectangular building, the lateral displacement and base shear value without a damper are higher than the two with one, and the value of storey drift with a damper is higher than storey drift without one for EQX and EQY [2].

Majd Armali, Hala Damerji, Jaafar Hallal, and Mahmoud Fakih have investigated the effectiveness of friction dampers on the seismic response of high-rise buildings compared to shear wall systems. A shear wall system is used in the first of two plans with irregular shapes, while a frame system with friction dampers at each level and on alternating frames is used in the second. At the base of both models are fixed supports. They concluded that this positioning of friction dampers was successful for that specific earthquake excitation after doing a dynamic time history study [3].

Sameer J Suthar, Radhey Shyam Jangid have designed tuned liquid sloshing dampers using non-linear constraint optimization for tall buildings. Due to liquid sloshing damper, the top floor peak acceleration value is minimized, and constraint is kept on the depth of liquid sloshing dampers due to practical considerations. This type of damper used for light weight high rise building subjected to wind load dominantly [4].

3 Modelling

All four of the models below have been designed in ETABS software for comparative performance analysis.

1.Without Outrigger and Friction Dampers (Model 1)

2.With Outrigger (Model 2)

3.With Friction Damper (Model 3)

4.With Outrigger System and Friction Damper (Model 4)

ISBN: 978-81-932056-2-4

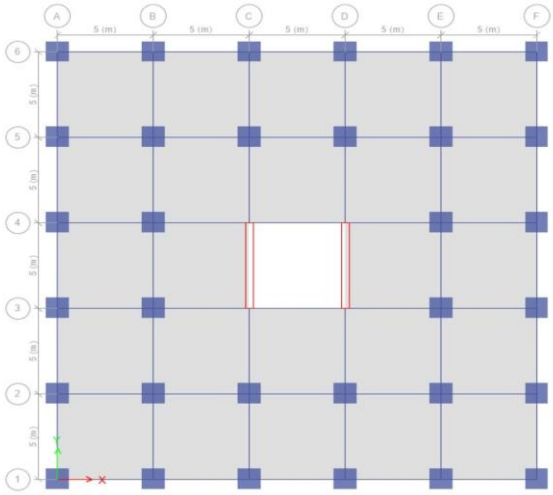

Fig. 1. Plan view

The plan shown in Fig. 1 is applicable to all models. The usable area for the plan in is 96% and the service area is 4%.

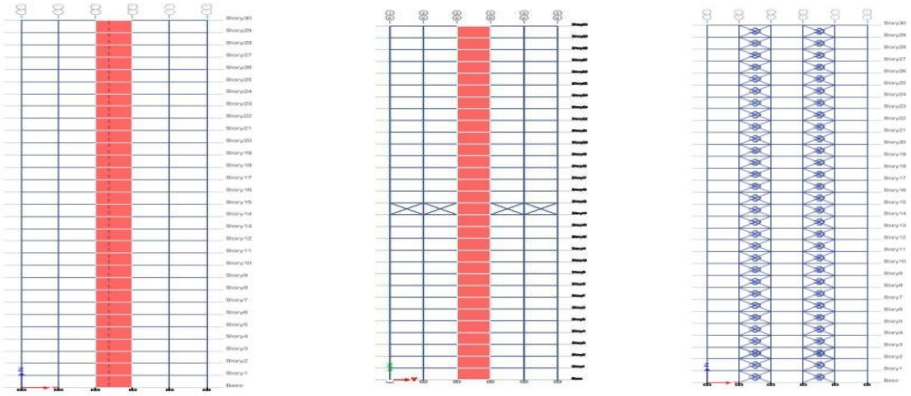

(a) (b) (c)

Fig. 2. Elevations for (a) Model 1, (b) Model 2 and (c) Model 3

This configuration was finalized after checking for torsional irregularity and lateral storey irregularity. In Model 4 friction damper is provided on the outer frames as shown in Fig. 2(c) and outriggers on the inner frames as shown in Fig. 2(b).

The structure is intended to serve as a commercial building. It is located in Seismic Zone III, and has soil type-I. A uniform concrete grade of M40 has been used for all members of the structure. The main reinforcement of grade Fe 500 is used for all main reinforcements and in shear reinforcement (for beams and columns). Slabs have a depth

ISBN: 978-81-932056-2-4

of 150mm. All the beams are sized 350mm x 700mm, columns 1200mm x 1200mm. The shear wall is 400mm thick.

Outrigger trusses of an ISMB 500 section (steel grade Fe 250) in X-bracing is provided on mid story (from 14^{th} floor to 15^{th} floor i.e., 3m height). The trusses span along the sections (C, D and 3,4) Re (Fig.1) mid frame sections in a (+) shape.

Friction Dampers have been provided on all stories in alternate frames in the form of link connection as cross bracing with the link type defined as exponential in ETABS. The weight of the damper is taken to be 0.225kN. Effective stiffness of 20,000kN/m and Effective damping of 4,000kN-s/m have been considered.

According to IS 875:2015 Part III [9], Dynamic analysis is carried out when the building's minimum lateral dimension exceeds its minimum height ratio of 5.

For our project H/B= 90/25 = 3.6 < 5

Hence, Dynamic Analysis of wind is not considered.

Appropriate stiffness modifiers have been applied to beam, column, and shear wall as per IS 16700-2017 [5]. Load combinations for strength and serviceability are considered. Having defined Response Spectrum function, the models have been analyzed to study and compare the parameters i.e., time period, maximum storey displacement, maximum storey drift, maximum storey stiffness and base shear of the four models.

4 Result

The comparison is done between four models as mentioned above with identical dimensions, plan, and properties under similar loading conditions. The models were analyzed on ETABS software. The parameters used for comparison are as follows:

4.1 Modal Parameters

To find out if the structure has any lateral story irregularities or torsional irregularities, we investigate the modal mass participation ratios. We cite the following clauses from IS 1893 (Part 1): 2016 [6]. Clause 7.7.5.2 of IS 1893 states that there is a minimum number of modes to be taken into account, resulting in modal masses added together being to equal at least 90% of the seismic weight. Torsional irregularity (clause 7.1): A structure is free of torsional irregularity if the period of the principal torsional mode of oscillation (which is the third mode) is shorter than the periods of the first two translational modes.

ISBN: 978-81-932056-2-4

Table 1. Modal Parameters

Case	Mode	Period sec	UX	UY	RZ	SumRZ
Model without Outrigger and Friction Damper						
Modal	1	4.055	0.7672	0	7.58E-06	7.58E-06
Modal	2	3.526	0	0.7426	2.24E-06	9.82E-06
Modal	3	3.186	7.37E-06	2.11E-06	0.7755	0.7755
Model with Outrigger						
Modal	1	3.838	0.7835	0	1.31E-05	1.31E-05
Modal	2	3.208	0	0.7634	0.0002	0.0002
Modal	3	3.166	1.32E-05	0.0002	0.7774	0.7776
Model with Friction Damper						
Modal	1	3.853	0.7668	2.31E-05	0.0003	0.0003
Modal	2	3.368	2.45E-05	0.744	6.33E-06	0.0003
Modal	3	2.924	0.0003	6.71E-06	0.7759	0.7763
Model with Outrigger and Friction Damper						
Modal	1	3.662	0.7819	1.73E-05	0.0004	0.0004
Modal	2	3.086	1.92E-05	0.764	3.08E-05	0.0004
Modal	3	2.912	0.0004	3.16E-05	0.7773	0.7777

Lateral storey irregularity (Table 6): If the first three modes have contributed more than 65 percent of the mass participation, which is vital for structures in seismic zone III, the structure won't have lateral storey irregularity.

As seen in Table 1, the above clauses are satisfied indicating that modelling for all models is appropriate. In all 4 models, the first mode is the primary x-direction translational mode, the second mode is involved in the y-direction, and the third mode is torsional with the maximum Rz Value.

4.2 Maximum Storey Displacement

The maximum storey displacement was identified to be at the 30th storey; however, Models 2 and 4's outriggers caused a modest reduction on the 15th storey. According to IS 1893-2016 [6], under seismic loading, the maximum storey displacement at the top should be limited to H/250, where H is the height of the building. IS 456-2000 [7] gives specific limits for maximum storey displacement, including H/500 for transient wind load.

- (H/500) = (90000/500) = 180 mm.
- (H/250) = (90000/250) = 360 mm.

ISBN: 978-81-932056-2-4

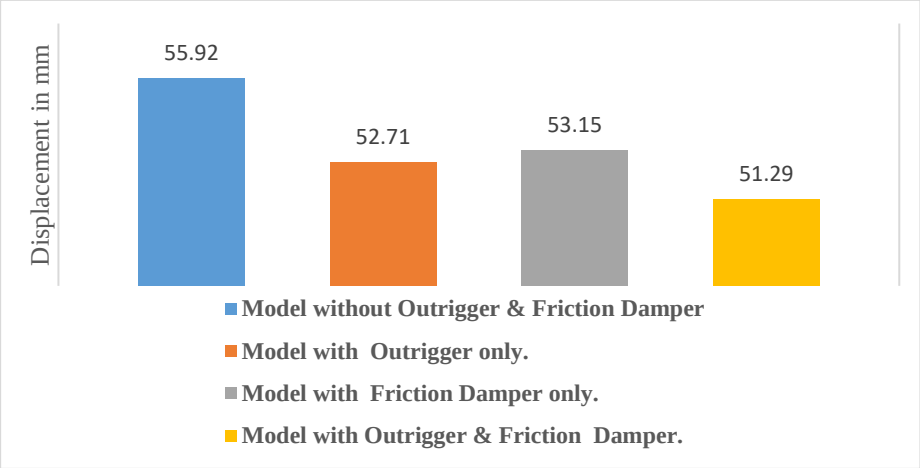

Fig. 3. Maximum Displacement for All Models

As seen in Fig. 3, the maximum displacement values of all models are less than deflection limits calculated above. The Model 4 has the lowest maximum displacement.

4.3 Maximum Storey Drift

As stated in IS 1893-2016 [6] clause 7.11.1.1, under the influence of design base shear (V_b), storey drift in any storey must be limited to 0.004 times storey height, with partial safety factors for all loads as 1. Floor-to-floor height is 3.0 m for all models; hence the maximum allowable storey drift is 0.004 * 3 = 0.012. As can be seen from the Table 2, all models meet this requirement, which states that the drift must be smaller than 0.012 (Fig. 4). Where the outrigger is positioned, the drift has decreased. Table 2 shows that Model 3 has the lowest response for maximum storey drift in x-direction and that Model 4 has the lowest maximum drift in y-direction.

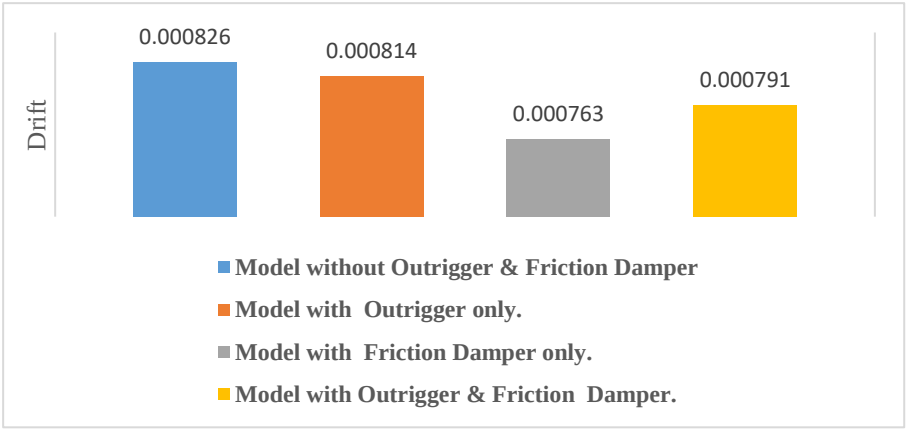

Fig. 4. Maximum Drift for All Models

ISBN: 978-81-932056-2-4

4.4 Maximum Storey Stiffness

It is observed that the storey stiffness is the highest at the bottom most storey.

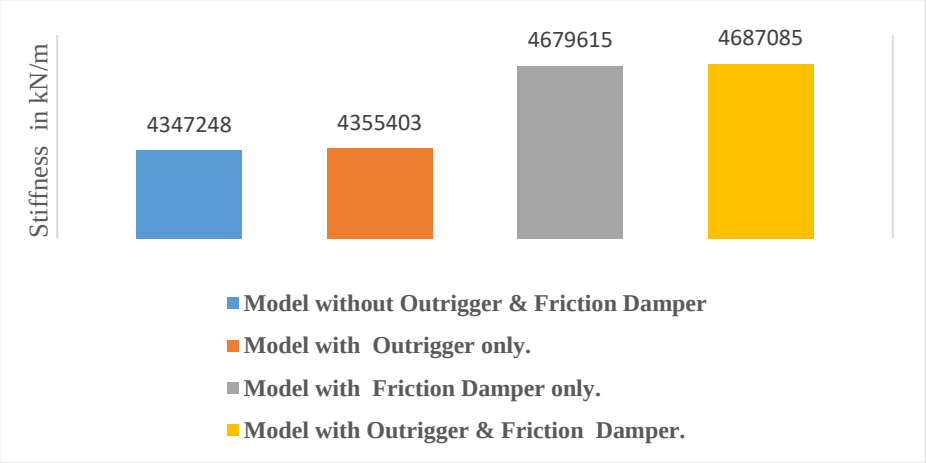

Fig. 5. Maximum Stiffness for All Models

It is seen from Fig. 5, that Model 4 has the maximum stiffness value.

4.5 Base Shear

There was a small variation in the graph where outrigger, friction damper and their combination are provided. However, from Fig. 6, that Model 4 has the lowest base shear among the 4 models for minimum base shear.

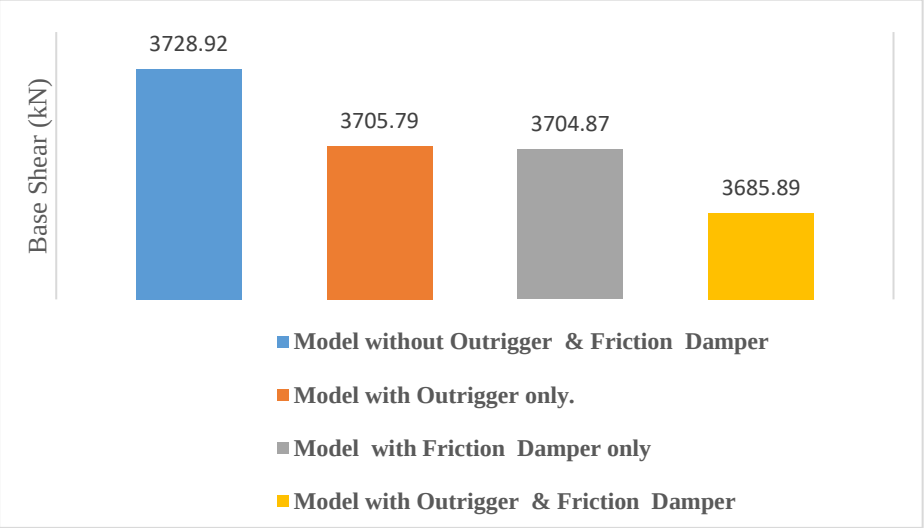

Fig. 6. Base Shear for All Models

ISBN: 978-81-932056-2-4

Table 2. Summary

Display Types	Load Cases	Model w/o Outrigger & Friction Damper	Model with Outrigger only	Model with Friction Damper	Model with Outrigger & Friction damper
Maximum Displacement (mm)	EQ_X	55.92	52.71	53.15	51.29
	EQ_Y	46.42	42.24	43.31	40.13
Maximum Drift	EQ_X	0.000826	0.000814	0.000763	0.000791
	EQ_Y	0.000687	0.000648	0.000623	0.000615
Maximum Stiffness (kN/m)	EQ_X	4347248	4355403	4679615	4687085
	EQ_Y	7316943	7465820	7766987	7898631
Base Shear (kN)	EQ_X	3728.92	3705.79	3704.87	3685.89
	EQ_Y	3645.19	3614.78	3631.52	3605.98

5 Conclusions

The model with integrated outrigger and friction damper provides relatively the best structural performance among all models, according to the factors that were taken into account and a comparison of the values of Models 2, 3, and 4 with those of Model 1.

- Model 4 reduces the maximum storey displacement by 8.28% when compared to Model 1. This reduction is maximum among all other models where the reduction ranges from 4.95%- 5.74% (Fig. 3).

- For storey drift, Model 2 shows minor reduction in comparison to Model 3 and Model 4. Storey drift reduces by 7.63% and 4.24% for Model 3 and Model 4 respectively whereas it reduces by only 1.45% for Model 2 (Fig. 4).

- Stiffness hardly increases for Model 2, by 7.65% for Model 3 and by 7.82% for Model 4. This means the stiffness of combined model is maximum (Fig. 5).

- Model 4 shows minimum base shear. Combination of outrigger and friction damper helps to reduce the Shear forces experienced by each storey of the building during an earthquake (Fig. 6).

- By comparing the time periods of the models, model 4 has the least time period which implies maximum stiffness among models (Table 1).

6 Future Scope

- This research paper is restricted objective to comparing the effect of outrigger vis-à-vis friction dampers. The structural framing system can be further optimized by modifying the position of shear walls and size of columns.

ISBN: 978-81-932056-2-4

- We have considered Friction Dampers for improving the structural performance but other type of damper such as tuned mass damper can also be used to verify if it can provide more damping effect for the outrigger structural system.

- The method selected for dynamic analysis is Response Spectrum analysis, in future projects, Time history analysis can also be used.

- In our research, soil – structure interactions have not been taken into consideration, this can be taken into consideration in the future.

References

1. Shubham Jain and Mohd Adnan, Structural Analysis of Seismic Friction Dampers, International Research Journal of Engineering and Technology (2019).

2. P.M. B Raj Kiran Nanduri, B.Suresh and MD.Ihetesam Hussain, Optimum position of Outrigger system for High-Rise Reinforced Concrete Buildings Under Wind and Earthquake loading, American Journal of Engineering Research (2013).

3. Majd Armali, Hala Damerji, Jaafar Hallal and Mahmoud Fakih, Effectiveness of friction dampers on the seismic behavior of high-rise building VS shear wall system (2019).

4. Sameer J Suthar, Radhey Shyam Jangid, Design of tuned liquid sloshing dampers using nonlinear constraint optimization for a cross-wind response control of benchmark tall building.

5. IS 16700-2017: Criteria for structural safety of tall concrete buildings

6. IS 1893 (Part 1)-2016: Criteria for Earthquake resistant design of structures

7. IS 456-2000: Plain and Reinforced Concrete- Code of practice

8. IS 800-2007: General Construction in Steel.

9. IS 875 (Part 3)-2015: Design Loads (other than Earthquake) for Buildings and Structures- Code of practice

ISBN: 978-81-932056-2-4

ASSESSMENT OF WIND LOAD FOR CONJOINED BUILDINGS

Mit R. Patel[1] and Dr. Paresh V. Patel[2]

[1]Post Graduate Student, Institute of Technology, Nirma University, Ahmedabad.
[2]Professor, Department of Civil Engineering, Institute of Technology, Nirma University, Ahmedabad.

[1]21mclc12@nirmauni.ac.in
[2]paresh.patel@nirmauni.ac.in

Abstract. Generally, tall buildings are constructed as an isolated structure. Few tall buildings are conjoined. But number of conjoined tall buildings will rise in the future. As the height of buildings increases, lateral load also increases caused by wind or earthquake. Wind load assessment for isolated buildings has already been defined by various standards, but it is very difficult for conjoined buildings. Three approaches are presented in this paper to evaluate wind-induced response on conjoined tall buildings. First approach utilizes specifications of IS 875(Part 3):2015. Second approach considers Tokyo Polytechnique University (TPU) Database. While third approach is based on recently published research article. The wind interference effect and its evaluation based on three approaches are explained in this paper. IS 875 suggests the multiplication factor according to the interfering zone. TPU Database presents the contour map of local wind pressure coefficients for principal buildings depending on various parameters. The comparison of results obtained from force measurement and pressure measurement is presented in the research article for wind pressure assessment. Four separate buildings with 0.66 times plan dimension of isolated building are joined together at the top by a rigid link structure to form the conjoined building. Two rows of four separate buildings with two buildings in each row are arranged in tandem. Each isolated building is having plan dimensions of 30 m × 30 m. The evaluation of the wind load on conjoined buildings using these three approaches is compared. Principal buildings experience increased wind loads according to IS 875, whereas principal buildings experience negative drag according to the TPU database and research article.

Keywords. Tall building, Conjoined structural system, Wind load, Interference condition, Tandem arrangement.

1 Introduction

Tall buildings are becoming more prominent these days because of rapid urbanization, scarcity of land, and increasing land costs. With the increase in the building's height, the design of structural elements is governed by the lateral loads in tall buildings. To resist the lateral load, many interior and exterior structural system are developed over a period. One of exterior structural systems for tall buildings is a conjoined structural system. Conjoined structural systems are created by linking two or more separate buildings at various levels along tall building heights.

Undoubtedly, one of the most important design considerations is behaviour of a conjoined tower subjected to wind. Conjoined towers face more challenging wind-related problems than single towers. When designing conjoined buildings, it is essential

ISBN: 978-81-932056-2-4

to assess the wind forces for the safety and stability of the structure. Wind loads are dynamic forces that act on a building, and their magnitude and direction vary depending on various factors such as building height, shape, and orientation, as well as local wind conditions.

The wind-related problems for conjoined structures are more complex than those for a single structure. Typically, wind loads on isolated tall buildings are assessed using standards and guidelines for structural design. The wind load criteria that are used in codes and standards are typically derived from model tests carried out in a boundary layer wind tunnel on an isolated building. However, many research studies have shown that because of the presence of other structures, the wind loads on a building that is interfered with by nearby structures may be very different from those on a similar building that is isolated. To assess wind loads for conjoined buildings, either computer simulation or wind tunnel testing is carried out. These processes involve defining wind characteristics based on the design wind speed, exposure category, and other relevant parameters as per the building code.

Based on a variety of geometric, structural, and wind criteria, the existing interfering structures may result in increment or decrement of wind loads on a principal building [1]. Wind load is influenced by several variables, including building size, section shape, location in relation to one another, wind velocity, number of structure adjacent to one another, and upstream terrain conditions [2]. The interference effect is a term used to describe a very complicated phenomenon that needs to be properly evaluated in addition to the total wind loads. The assessment of wind loads for conjoined buildings also involves considering the interaction between the buildings. This interaction can affect the local wind flow patterns. Therefore, it is necessary to carefully model the buildings and the surrounding environment to accurately predict the wind loads and ensure the safety of the structure.

This paper summarizes three different approaches to evaluate wind induce response of conjoined buildings. The occurrence of interference effects in the wind condition are described in depth by IS 875, the TPU database and the research articles. The assessment on wind load on conjoined structure using three approaches is illustrated in this paper.

2 Problem formulation

In the conjoined building, four isolated buildings with a spacing of 0.66 times plan dimension are connected using a rigid link structure at the top. Four isolated buildings are arranged in two rows, with two buildings in each row in a tandem arrangement as shown in Fig. 1

ISBN: 978-81-932056-2-4

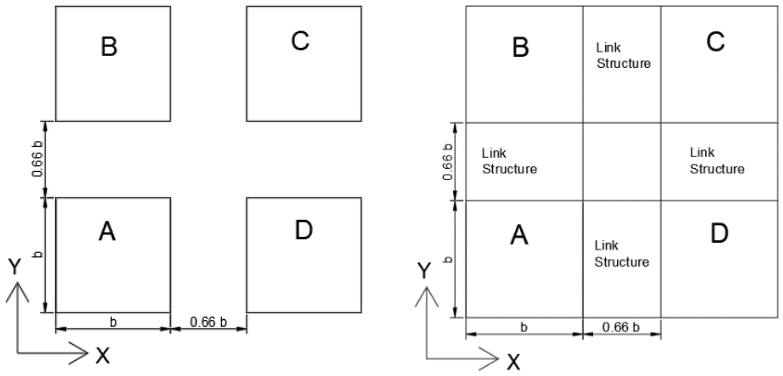

(a) (b)

Fig. 1. (a) Four separate buildings (b) Four buildings connected by link structure.

Conjoined structure made up of four independent buildings with identical plan dimensions. Wind load will act on A and B buildings similar to isolated buildings when conjoined buildings are subjected to wind force in the X direction. However, C and D buildings will experience an interference effect. Similarly, for wind in Y direction, A and D buildings act as isolated buildings while B and C buildings will face interference effects. For wind acting in X-direction, C and D are principal buildings while, A and B are interfering buildings. For wind in Y-direction B and C are principal buildings, while A and D are interfering buildings. Thus, it is necessary to determine the interference impact on the principal building in both directions. The height (H) of all buildings is the same. At top the buildings are connected by rigid link structure.

3 Various Approaches for Assessment of Wind Load

Following three approaches are presented in this paper to evaluate wind load on conjoined buildings:

(1) IS 875 (Part III): 2015

(2) Tokyo Polytechnique University (TPU) Database

(3) Research article published recently

Wind load is calculated for conjoined building as per these approaches and the most relevant approach is recommended. These approaches are explained in the following subsections.

3.1 IS 875 (Part 3): 2015 [1]

For the design of flexible buildings, the dynamic wind effects need to be considered, and their parts are described in clause 9.1 of IS 875 (Part 3):2015 [1]. Clause 8 gives a preliminary explanation about wind interference effects. It can be used to understand the assessment of wind load for conjoined buildings. Wind interference is the result of

ISBN: 978-81-932056-2-4

a change in the wind's characteristics based on an obstruction in the flow of the wind due to an object or a structure. The wind pressures are typically increased if such a wind hits another structure, while there may also be some shielding between two structures that are quite close to one another. The interference-related wind forces and pressures can only be determined by thorough wind tunnel and CFD research because the actual occurrence is too complex to allow for generalization.

For preliminary design, some guidance can be offered, though. A wind interference factor (IF), which should be multiplied by the design wind forces or pressures, has been developed to take the effect of wind interference into account.

Various zones of interference are shown in Fig. 2 based on research on tall rectangular buildings. For a preliminary estimation of the wind loads under interference from interfering building of the identical height or greater located at various zones Z1 to Z4 is shown in Fig. 2, For wind loads equivalent to an isolated building, the interference factor (IF) must be considered as a multiplier.

Table 1. Multiplication Factor for interference zones

Zone	Z1	Z2	Z3	Z4
IF	1.35	1.25	1.15	1.07

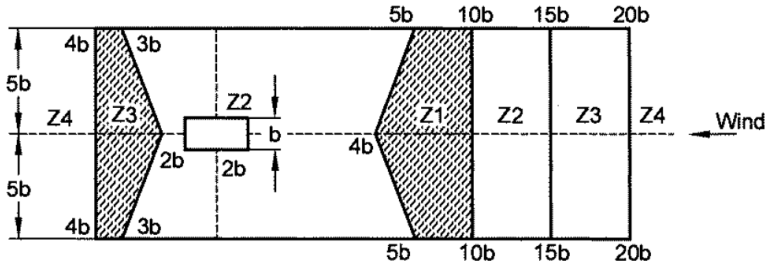

Z1 - Zone of high interference
Z2 - Zone of moderate interference
Z3 - Zone of low interference
Z4 - Zone of insignificant interference

Fig. 2. Tall rectangular buildings with interference zones that are the same height or higher [1]

In present conjoined building, the distance of 0.66 times plan dimension between individual buildings is considered placed in a tandem arrangement. Due to close spacing between the buildings, shielding effect will be produced. Shielding effect is not properly explained in IS:875 (Part III). Because of this, it is necessary to explore other approaches based on wind tunnel testing or computer simulation.

3.2 TPU Database [3]

As part of a Research Fellow of the Japan Society, Tokyo Polytechnic University developed an aerodynamic database relating to interference caused by the wind. This study aims to offer test data for a wind tunnel on a local wind pressure of high rise building under the interference of structural designer. It included contours of a statistical value of a local wind pressure coefficient and graph of area average wind pressure coefficient. Two buildings made up the experimental model under consideration: the

ISBN: 978-81-932056-2-4

principal building, which is the pressure model, and the interfering building, which is the other model. There are five different interfering building types taken into consideration, each with a different height but sharing the same cross section as the principal structure. All interfering structures are positioned with 37 different configurations upstream of the principal structure with their on-face normal to the principal structure as shown in Fig. 3.

Configuration of the principal building and interfering building is kept as mentioned in section 2. The considered model's breadth, depth, and height were 70, 70, and 280 respectively. In this database, several S/b ratios are considered for the understanding of the wind interference effect. Where S is the clear distance between two adjacent buildings in the tandem direction of wind load and b is plan dimension of individual building. In Fig. 3, number 34 indicates the location of the interfering building where S/b ratio is 0.5. It is the nearest case for our required data where the S/b ratio is 0.66.

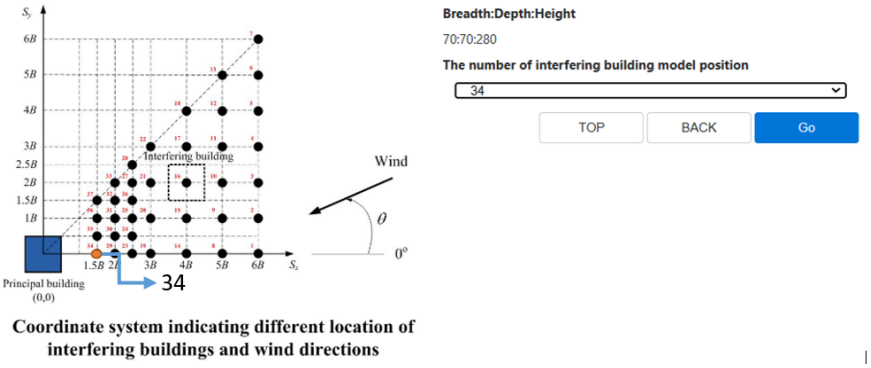

Fig. 3. Placement of the building that is interfering with the principal building

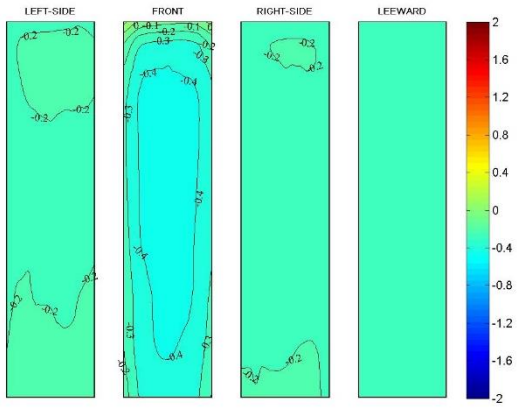

Fig. 4. Contour map of local wind pressure coefficients for principal buildings

ISBN: 978-81-932056-2-4

For the case of S/b =0.5, the wind pressure coefficient's contours for the principal building are displayed in Fig. 4. In these contours, coefficient of the wind pressure for -0.4 for the front face means negative drag force generated. When the S/b ratio increases negative drag force decreases. When a building is experiencing negative drag force then wind load-induced deflection will be in the opposite direction of the wind load. It indicates that the overall wind load will be less as compared to that in isolated conditions.

3.3 Research Article (IIT Roorkee) [2]

The analysis of wind load on rectangular-shaped tall buildings under interference conditions is reported in the research article released in 2022. The position of principal building is kept constant whereas the distance between the mentioned two buildings is adjusted by shifting the interfering building in a tandem arrangement. For varying interfering building height two types of independent measurements are taken which are pressure measurement and force measurement. According to the results of a force measurement s and interference effect decrease as the spacing and height of the interfering building both increase. Nevertheless, it is conclusive by pressure contours when the interfering building has less distance from the windward face of the principal building the wind pressure decreases. Evident from pressure contours when the interfering building is close to the main building, the wind pressure force on the windward face decreases.

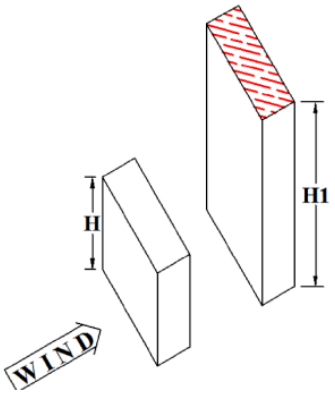

Fig. 5. Experimental setup's isometric view and plan view [b = 100 mm, H_1 = 500 mm].

The principal building in the research article has a rectangular cross-section, a height of 100 m and plan dimension of 60 m × 20 m. Building models are created using a 1:200 geometric scale. In the direction of the wind load, a principal building and an interfering model are displayed in tandem, with H1 standing for the principal building's height and H for the interference buildings' height, as shown in Fig. 5.

In this investigation, H1/H ratios of 0.2, 0.4, 0.6, 0.8, and 1 were taken into consideration, along with different S/b ratios of 0.25, 0.5, 0.75, 1.0, …. and 30. However, for the present study, H1/H = 1 with S/b= 0.5 to 4 is appropriate to evaluate

ISBN: 978-81-932056-2-4

the wind load for the connected structure. In Table 2, the outcomes of force measurement and pressure measurement for H1/H=1 are compared.

Table 2. Comparison result from force and pressure measurements

	Force measurement	**Pressure measurement**
Isolated	10.03	9.47
S/b = 0.0	-3.15	-2.14
S/b = 0.5	-3.26	-3.71
S/b = 1.0	-3.29	-3.69
S/b = 2.0	-2.88	-2.96
S/b = 3.0	-1.78	-2.08
S/b = 4.0	-0.92	-0.80

As per In Table 2, the outcomes of force measurement and pressure measurement for H1/H=1 are compared.

Table 2, negative drag was observed for closely spaced structures. Moreover, for both force and pressure measurement data, negative drag force decreases as the S/b ratio of experimental models increases. It is the similar to the TPU database. IS:875 (Part-III) recommends the shielding effect on the closely spaced structures.

4 Dynamic Wind Load on Isolated Buildings as per IS 875 (Part 3):2015

According to clause 9.1 of IS 875 (Part 3): 2015, buildings and closed structures with height-to-minimum lateral dimension ratios greater than or equal to 5.0, or with natural frequencies in the first mode less than or equal to 1.0 Hz, must be assessed for the effects of dynamic wind. In its gust factor-based dynamic wind load analysis, according to the gust factor method of IS 875 (Part 3):2015, the following steps illustrate the evaluation of along and across wind response.

The Design Peak Along Wind Load $F_{z,along}$ from the equation given in clause 10.2 of IS 875 (Part 3): 2015.

$$F_{z,along} = C_{f_{(z)}} A_{e_{(z)}} \overline{pd_{(z)}} G \ (1)$$

Where,

A_z = The building's effective frontal area at height z,

$\overline{P_d}$ = Mean design wind pressure for each hour,

$C_{f,z}$ = the area-corresponding of the building's drag coefficient A_z,

G = Gust Factor.

ISBN: 978-81-932056-2-4

Load $F_{\text{z,across}}$ as per the equation given in clause 10.3 of IS 875 (Part 3): 2015.

$$F_{z,across} = \left(\frac{3Mc}{h^2}\right)\left(\frac{z}{h}\right) \text{ (2)}$$

Where.

M_c = the peak base bending moment across the wind design,

h = height of the building,

z = distance above the ground.

5 Dynamic Wind Load on Conjoined Buildings

As mentioned in section 56, in conjoined buildings, the spacing between two buildings is 0.66 times plan dimensions and arranged in a tandem arrangement. Evaluation of dynamic wind load on conjoined buildings varies with different approaches. For interfering buildings, dynamic wind along and across wind response is calculated as per Eq. 1 & 2 respectively.

As per IS 875 (Part 3), if the spacing between interfering buildings and principal buildings is up to 4b then the multiplication factor is calculated as per zone 2 as shown in Fig. 2. Dynamic wind load on conjoined buildings is calculated as per the following equation.

Along wind response for principal buildings,

$$F_{z,along} = 1.25\, C_{f_{(z)}} A_{e_{(z)}} \overline{pd_{(z)}} G \text{ (3)}$$

Across wind response for the principal building,

$$F_{z,across} = 1.25 \left(\frac{3Mc}{h^2}\right)\left(\frac{z}{h}\right) \text{ (4)}$$

As per the TPU database, if two buildings are placed very closely in tandem manner then principal buildings may experience negative drag when subjected to wind load. So, principal buildings will deflect opposite to wind direction. As per Fig. 4. wind pressure coefficient of the front face of the principal building will be -0.4 for 0.5b spacing of two buildings in a tandem arrangement which is nearest to condition of present study. Thus, wind load on principal buildings would be calculated as per the following equation.

Along wind response for principal buildings,

$$F_{z,along} = -0.4\, C_{f_{(z)}} A_{e_{(z)}} \overline{pd_{(z)}} G \text{ (5)}$$

Across wind response for principal buildings,

ISBN: 978-81-932056-2-4

$$F_{z,across} = -0.4 \left(\frac{3Mc}{h^2}\right)\left(\frac{z}{h}\right) \text{ (6)}$$

The approach based on research article as described in section 3.3 is similar to the TPU database. As per this approach, if the spacing between two buildings in tandem direction is increased then the shielding effect will be decreased as mentioned in Table 2. The outcomes of force measurement and pressure measurement for H1/H=1 are compared in Table 2.

Along wind response for principal buildings,

$$F_{z,along} = -0.39\, C_{f_{(z)}} A_{e_{(z)}} \overline{pd_{(z)}} G \text{ (7)}$$

Across wind response for principal buildings,

$$F_{z,across} = -0.39 \left(\frac{3Mc}{h^2}\right)\left(\frac{z}{h}\right) \text{ (8)}$$

6 Illustrative Example

Three approaches discussed above for evaluation of wind loading on conjoined building are illustrated with an example. In the 30 storey conjoined buildings, each isolated building is considered to have a dimension of 30m × 30m with 3.6 storey height. Four isolated buildings with a spacing of 20 m are connected using a rigid link structure at the top. For wind load estimation, location is considered as Ahmedabad. Basic wind speed, probability factor k_1, topography factor k_3, importance factor k_4, and terrain category are considered as 39 m/s, 1, 1, 1, and 2 respectively.

According to Eq. 1 and 2, along and across wind-induced response on interfering structures is calculated. According to IS 875, the TPU Database, and a research article, the principal buildings along wind response is calculated using Eq. 3, 5, and 6, and across wind response is determined using Eq. 4, 5, and 7, respectively. Wind load for conjoined building is evaluated using three approaches as mentioned above. Table 3 presents comparison of wind load at each storey. Storey shear due to dynamic wind load on conjoined buildings as per these three approaches is shown in Fig. 6

Table 3. Comparison of Wind forces (in kN) on conjoined buildings by three approaches

Storey	IS code	TPU Database	Research Article
30	243.77	243.77	243.77
29	485.14	485.14	485.14
28	482.63	482.63	482.63
27	702.78	363.41	365.47
26	918.93	245.05	249.13
25	911.99	243.20	247.25
24	904.75	241.27	245.29
23	897.22	239.26	243.25
22	889.38	237.17	241.12
21	881.23	234.99	238.91

ISBN: 978-81-932056-2-4

20	872.75	232.73	236.61
19	863.93	230.38	234.22
18	854.74	227.93	231.73
17	845.15	225.37	229.13
16	835.11	222.70	226.41
15	824.57	219.89	223.55
14	813.47	216.92	220.54
13	801.71	213.79	217.35
12	789.19	210.45	213.96
11	775.77	206.87	210.32
10	761.27	203.01	206.39
9	745.44	198.78	202.10
8	727.96	194.12	197.36
7	708.36	188.90	192.04
6	685.97	182.92	185.97
5	659.73	175.93	178.86
4	627.89	167.44	170.23
3	587.19	156.58	159.19
2	530.43	141.45	143.80
1	217.68	58.05	59.01

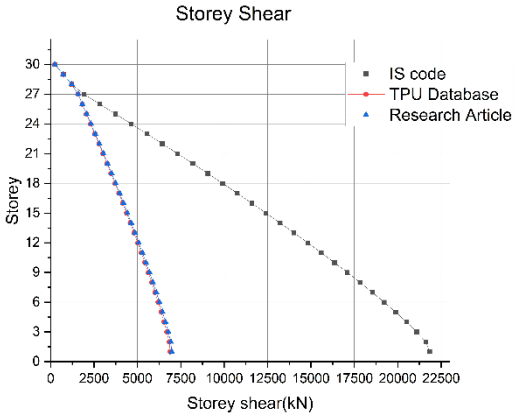

Fig. 6. Storey shear of dynamic wind load of conjoined buildings

7 Conclusions

IS 875 (Part III):2015, TPU Database and recently published research article are used to evaluate dynamic wind loads on conjoined tall buildings. An example of 30 storey building is considered to illustrate application of three approaches. IS:875(Part III) specifies the interfering effect for preliminary design purposes. IS:875 (Part III) overestimates wind loads on conjoined tall buildings resulting into uneconomical design.

The approaches based on TPU Database and Research article for evaluation of dynamic wind loading on conjoined tall building result into identical results. As per both these

ISBN: 978-81-932056-2-4

approaches, negative drag will occur on a principal building if interfering buildings are near to the principal building, and with the increase in S/b ratio negative drag will decrease. According to TPU Database and Research article, wind load acting on principal buildings is -0.4 and -0.39 times that of wind load on interfering buildings. Alternatively, the ratio of wind load on the interfering building and principal building is 10: -4.

References

1. IS 875 (Part 3) :2015, "Design Loads (Other than Earthquake) for Buildings and Structures - Code of Practice," vol. 875, no. April, 2015.

2. Chauhan B. S., Chakrabarti A., and Ahuja A. K., "Study of wind loads on rectangular plan tall building under interference condition," Structures, vol. 43, no. June, pp. 105–130, 2022, doi: 10.1016/j.istruc.2022.06.041.

3. "TOKYO POLYTECHNIC UNIVERSITY : New Frontier of Education and Research in Wind Engineering." http://wind.arch.t-kougei.ac.jp/system/eng/contents/code/tpu (accessed May 31, 2023).

4. Gu M. and Xie Z. N., "Interference effects of two and three super-tall buildings under wind action," Acta Mech. Sin. Xuebao, vol. 27, no. 5, pp. 687–696, 2011, doi: 10.1007/s10409-011-0498-9.

5. Moon K.S., "Structural performance of superframed conjoined towers," Struct. Des. Tall Spec. Build., vol. 30, no. 10, pp. 1–14, 2021, doi: 10.1002/tal.1857.

6. Song J. and Tse K. T., "Dynamic characteristics of wind-excited linked twin buildings based on a 3-dimensional analytical model," Engineering Structures, vol. 79. pp. 169–181, 2014, doi: 10.1016/j.engstruct.2014.08.015.

7. Qin W. feng, Shi J. Yang, Yang X., Xie J., and Zuo S., "Characteristics of wind loads on Twin-Tower structure in comparison with single tower," Eng. Struct., vol. 251, no. PA, p. 112780, 2022, doi: 10.1016/j.engstruct.2021.112780.

8. Kim B., Tse K. T., and Tamura Y. "POD analysis for aerodynamic characteristics of tall linked buildings." J. wind Eng. 2018.

ISBN: 978-81-932056-2-4

BEHAVIOUR OF CONCRETE WITH THE ADDITION OF NANO SILICA, FLY ASH AND WASTE FOUNDRY SAND

Rabikanta Chanam[1] and Balwinder Lallotra[2]

[1,2] Chandigarh University, Department of Civil Engineering, Mohali, Punjab, India

[1] rabikantachanam27@gmail.com
[2] balwinder.e9116@cumail.in

Abstract. Nano science and technology is a rapidly evolving ground of substances science and engineering research that lays groundwork in the development of fresh technological substances. Almost 2000000 tons of waste foundry sand is processed annually in India. This paper examines the behaviour of nano silica (NS) as well as fly ash (FA) as a fractional alternative of cement and waste foundry sand (WFS) as a fractional substitute of fine aggregate in concrete. The amount of fly ash is kept constant as 10% as a fractional substitute of cement. The optimum amount of waste foundry sand is determined as 20% by checking at 10%,15%,20%and 25% as a fractional substitute of fine aggregate. This proportions of fly ash (10%) and waste foundry sand (20%) are not varied for all the different mixes and the amount of nano silica is varied as 1%,2%,3% and 4%. The different concrete properties are determined using different laboratory test and is compared to a normal control mix (M 30). It is detected that the accumulating nano silica enhances the mechanical and durability properties of the concrete. The mix with 2% nano silica, fly ash 10% and waste foundry sand 20% is found out to be the optimum mix. The microstructure of the mix is analysed using scanning electron microscopy (SEM) test. After the test outcomes it can be concluded that the use of nano silica, fly ash and waste foundry sand does not only help in waste disposal reduction but also in producing quality concrete.

Keywords: Nano-silica, Fly ash, Waste foundry sand, Mechanical properties, Microstructure.

1 Introduction

Concrete, whose main composition is of cement, is widely used on the planet and is considered as the most trustworthy construction substances accessible to man [1]. The primary component of concrete, cement, has recently come under fire for emitting carbon dioxide during production [2]. The production of cement ranges from 3.0 to 3.6 Gt per year, and it has been observed that for every one kilogram of cement manufactured, 0.5-0.9 kg of CO_2 emissions are produced [3]. The construction part is the world's 3rd major CO_2 discharging institution [4]. Even if cement has good mechanical properties, it cannot keep up with the demand of durability. So, need of new materials which can improve the durability performance is a much-required solution [6]. Numerous research has been doing to reduce the cement industry's impact on greenhouse gas emissions. [8] through either increasing the productivity of the cement producing process or [9] partly using SCMs, that substitute regular cement. FA, GGBS, natural pozzolans, and SF are a few of the SCMs that have been studied [10]. The most promising areas of study that may significantly advance cement-based materials'

ISBN: 978-81-932056-2-4

performance, production, and mixture design is nanotechnology, according to experts [11]. The potential for producing different types of NS with greater specific surface areas and actions than traditional SF is assured with recent advances in nanotechnology [12]. Various measures have been used by investigators from around the world to identify the issue, along with pozzolanic reactions of cement utilizing cementitious materials, chemical responses of the end-product Calcium hydroxide to form excess calcium silica hydrate materials, and hole filling processes utilising cementitious materials. [13]. In addition to the hole stuffing impact of nano silica in concrete and other researched or formed nano materials like NS, NA, nano titania, nano zirconia, nano Fe2O3, and so on, putting NS advances the possibility of the reaction with CH, arriving in a stronger bearing configuration of cement: calcium silica hydrate [14].

Enhancing the properties of the plastic as well as hardened substance is the goal of using ultra-fine cementitious admixtures like nano silica in cementitious systems. Silica particles with a size between a micron and a nanometer fill the spaces between cement grains to create a filler effect. Higher packing density minimises the demand for water in the mixture while simultaneously increasing strength by reducing capillary porosity with the proper composition. In addition to this addition-induced physical effect, nano-silica shows considerably higher pozzolanic reactivity than SF. Therefore, it is crucial to consider both effects when creating ultra-high-performance concrete [6].

Around the world, the ferrous and nonferrous metal casting industries generate millions of tonnes of waste. Every year, roughly 2000000 tonnes of WFS are generated in India [15]. WFS has been utilised effectively as a land filler substance for several decades. However, due to the rapid increase in disposal costs, the practice of WFS for layering land is developing a challenge. To make the WFS more widely available, research is being conducted on its potential extensive application as a temporary substitute for fine aggregate [16]. This study is concerned on demonstrating the blend of NS on the nature of concrete when used as a cement additive or partial substitute.

2 Experimental Program

2.1 Materials Used

Of all the cement that has been established, Ordinary Portland Cement (OPC) is one of the commonly utilised cements. Several examinations were executed to discover the nature of OPC (43 Grade) which was utilized for the different mixes and it followed to IS8112 2013. The nano silica utilised is in powder form ranging between 30-50 nm in size as well as specific surface area ranging from 200-600 m^2/g. Usual rough sand having 4.75 mm largest particle size was utilised after testing in accordance to IS 383 1970. The coarse aggregate with largest size 12.5 mm was utilised. Fly ash utilised in this study was purchased from nature and greens company. The specific gravity of the FA is 2.09 g/cm^3. WFS was collected manually from Boparai metals private limited. WFS were utilised as a fractional substitute of fine aggregate. Table 1 shows the specifications of NS. The properties of WFS are given in Table 2.

ISBN: 978-81-932056-2-4

Table 1. Specifications of nano silica.

Description	Values
Particles Size	30-50nm
Colour	White
Purity	>99.5%
Atomic Weight	60.08 g/mol
Morphology	Spherical

Table 2. Properties of waste foundry sand.

Parameters	Value
Specific gravity	2.18
Water absorption (%)	0.42
Fineness modulus	1.89
Moisture content (%)	0.11
Materials finer than 75μ (%)	8
Clay lumps (%)	0.8

2.2 Mix Design

IS: 10262-2019 was utilised to create a mix design for concrete to get a typical compressive strength (CS) of 30 N/mm^2 (mostly used for everyday uses), and the mix percentage is prepared. In this investigation, six distinct mix was prepared. One is a normal mix, and the remaining are concrete mix made by replacing cement and fine aggregate. Cement is replaced by 10% fly ash for all other mixes except the normal mix and the amount of nano silica is varied for the four different mixes by 1%,2%,3% and 4% by weight of cement. The optimum amount of WFS is found to be 20% by testing at 10%,15%,20% and 25% of fine aggregate replacement in the normal mix. So fine aggregate is replaced by WFS as 20% by weight of fine aggregate. The various mix designations are shown in Table 3.

Table 3. Different types of mix.

Mix	Cement (%)	Fly Ash (%)	Nano Silica (%)
NS0	90	10	0
NS1	89	10	1
NS2	88	10	2
NS3	87	10	3
NS4	86	10	4

2.3 Test Performed

The fresh state property is determined by performing workability test using slump cone test. Fresh concrete has different percentage of nano silica 1%,2%,3% and 4% is tested for workability using slump cone test in accordance to IS:1199-1959. The CS, STS and FS was conducted as per the specification given in Indian Standards (IS 516 1959) (IS 5816 1999) after curing the concrete for 7,28 and 56 days. The density and WA were obtained by using specifications as given in ASTM C 642 2006. In every test conducted a total of 3 same preparations was made and the average value is recorded. To observe

ISBN: 978-81-932056-2-4

the microstructure, scanning electron microscopy (SEM) was done in the mix which is obtained as optimum. Ultrasonic Pulse Velocity (UPV) test were performed on every cube and the average value is considered.

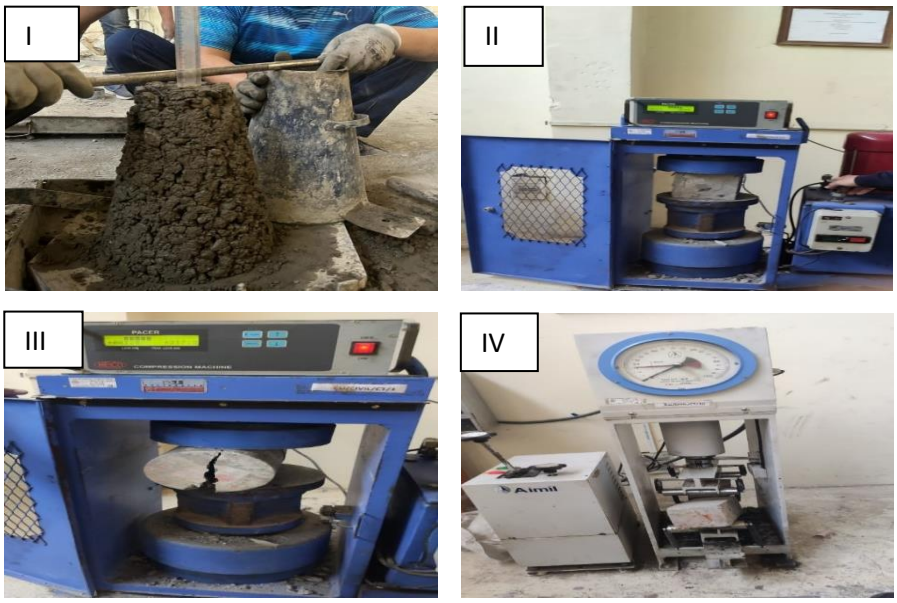

Fig. 1. I) Slump cone test, II) Compressive test, III) Split tensile test, IV) Flexural test.

3 Results of an Experimental Work

3.1 Workability

The comparison of the different mixes is shown in Fig. 2. The findings of the test on concrete with various NS (%) levels reveal that the NS (%) is what caused the slump value of the mixes to decrease. Because NS attracts some of the mixing water, workability has decreased with the rise in NS. Unsaturated bonds are present in NS due to its large surface area which leads to attraction of water. The establishment of a chemical connection between H_2O and these NS is caused by the silanol groups (SiOH) that result from the attractive contact of NS and water molecules. The amount of water needed to increase the liquidity of the mix is thereby drastically reduced [24].

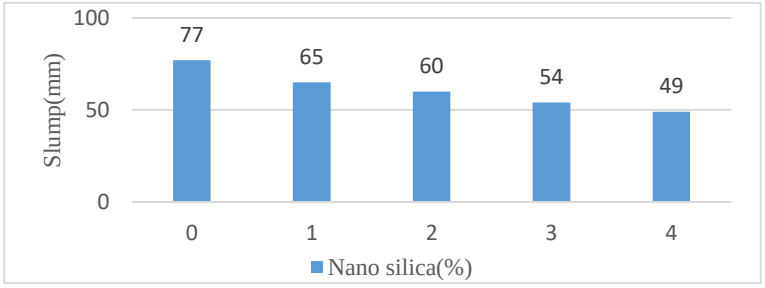

Fig. 2. Result of slump test of different proportion of nano silica.

ISBN: 978-81-932056-2-4

3.2 Compressive Strength (CS)

The CS of a concrete piece is obtained by testing hardened concrete. The size of cubes is 150mm × 150 mm × 150 mm are casted for all the proportion and is cured for a period of 7, 28 and 56 days. Then the samples are tested in CTM and the average value is recorded and considered as the CS of the mix. The use of a minor quantity of nano silica increases the CS considerably because it functions as a catalyst to enhance pozzolanic reaction. Owing to its high specific surface area, nano silica is extremely reactive, producing calcium silica hydrate gel as a result of reaction with calcium hydroxide.

Increasing the nano silica dosage reduces concrete CS as nano silica particles have a strong propensity to agglomerate because of their extreme surface energy. After too many nanomaterials are introduced to the mixture, they aren't evenly distributed in the cement paste, developing in feeble zones in the concrete because of accumulation. Fig 3 shows that concrete containing nano silica attains an earlier 7 days CS in comparison to the normal concrete. This might be the effect of the enhanced pozzolanic behaviour of NS.2%NS has the maximum compressive strength after which there is a decline in the strength (3% and 4%). The large concentration of minute NS particles in concrete causes more agglomerated sites and voids, which reduces strength at high NS dosage.

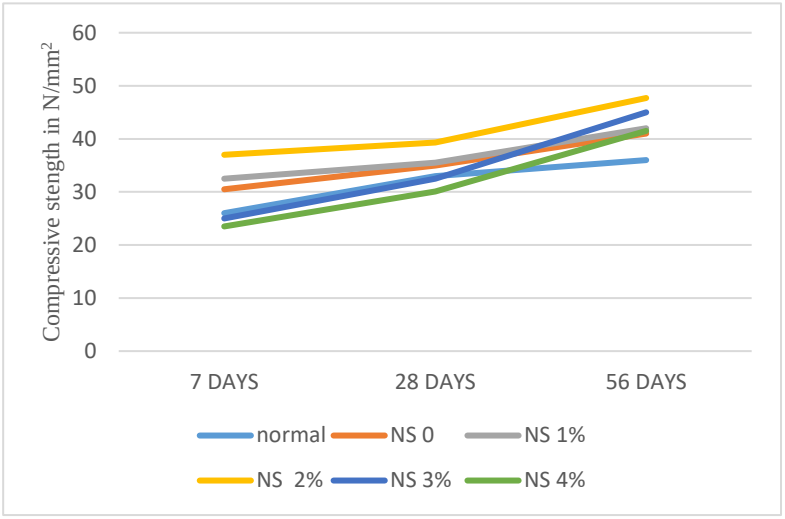

Fig. 3. Compressive strength at different curing stages.

3.3 Split Tensile Strength (STS)

Cylinders having size150mm×300mm each of all the mix are casted and cured in the water container. Fig 4 demonstrated the change in STS. As we can see from the figure the STS of the concrete containing nano silica gradually increases upto2% and slightly decreases after that. The greater STS for nano silica mixes might be credited to the additional binding property of finely divided nano silica because of the increased pozzolanic reaction and improved cement paste-aggregate interface, which increased bond strength.

ISBN: 978-81-932056-2-4

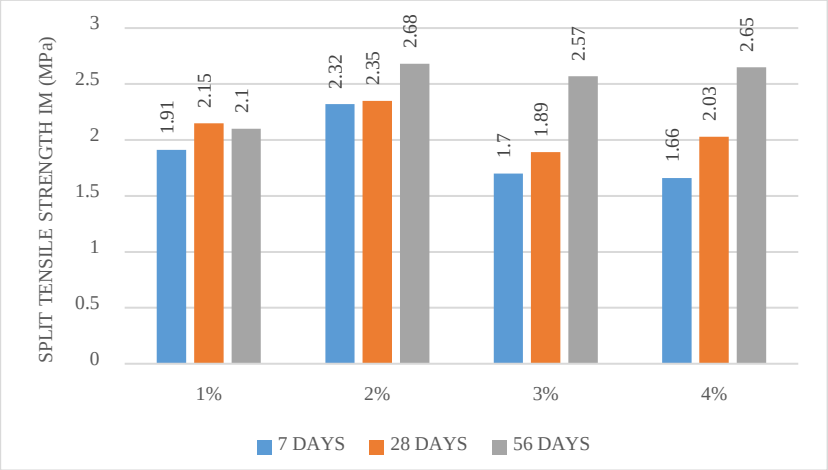

Fig. 4. Split tensile strength at different curing days.

3.4 Flexural strength (FS) test

Beam mould of size 100mm ×100mm ×500mm were casted and then cured inside the water and then tested. Fig 5 shows the FS of the difference in the FS of the different mix. The strength gradually increases till 2% and then it gradually diminishes as the quantity of NS increases. Flexural strength tests revealed that, owing to its filler and pozzolanic properties, NS can enhance the physical properties.

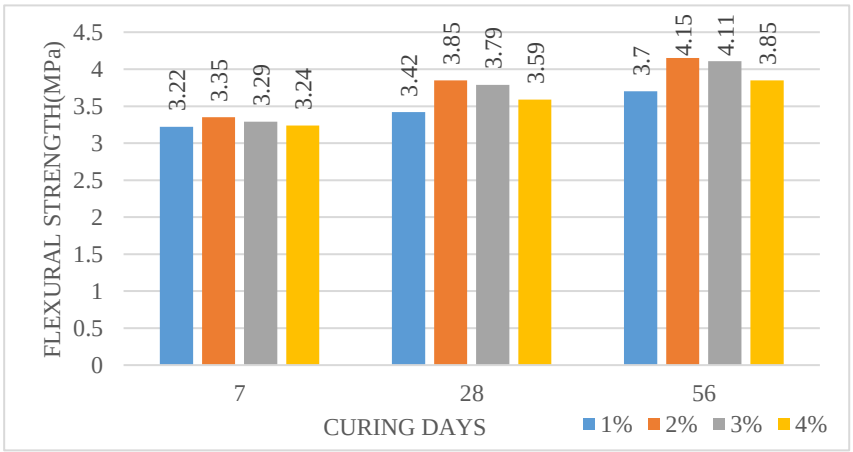

Fig. 5. Flexural strength of concrete

3.5 Water Absorption and Density

The variation in water absorption (WA) of the different percentage of NS is revealed in fig 6 below. It is detected that adding of NS decrease the water absorption. With the growth in the amount of NS the quantity of WA decreases. This decrease in WA is because the presence of NS diminishes the number of holes in concrete; so, the water-

ISBN: 978-81-932056-2-4

absorbing amount of mixes reduces. Fig7 depicts variation in density by different concentration of NS. It is realized that the density of the mix with 0% NS is 2350Kg/m3 which then shifts to 2426.67 Kg/m3 with the inclusion of 2% NS. This shows that the accumulation of NS in the mix is denser than the mix without NS.

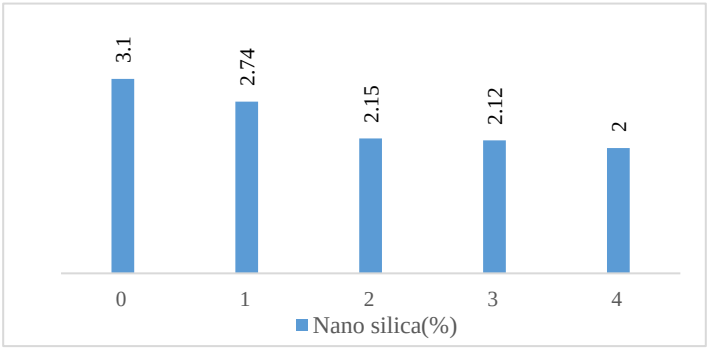

Fig. 6. Water absorption.

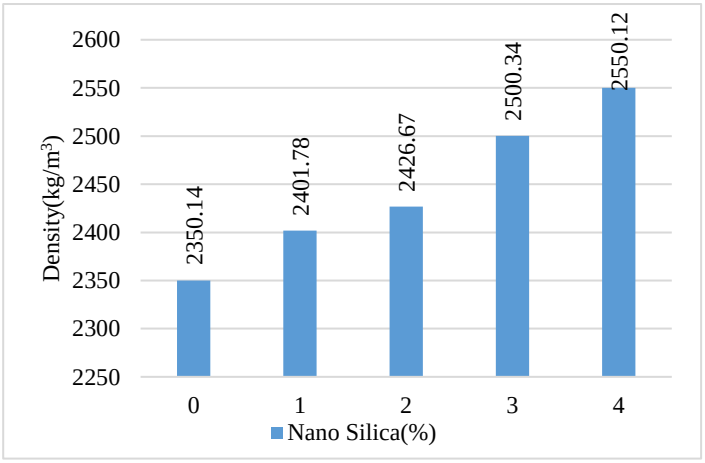

Fig. 7. Wet Density.

3.6 Non-Destructive Parameter

The Ultrasonic Pulse Velocity (UPV) with varying concentration of Nano silica (NS) is shown in fig 8. It is detected that the UPV value varies from good to excellent with the accumulation of NS (as per IS 13311 part 1:1992). NDT are typically used to forecast the value of samples without physically disintegrating them. From the investigation, the presence of NS resulted in a significant improvement in UPV, indicating an improvement in concrete quality.

ISBN: 978-81-932056-2-4

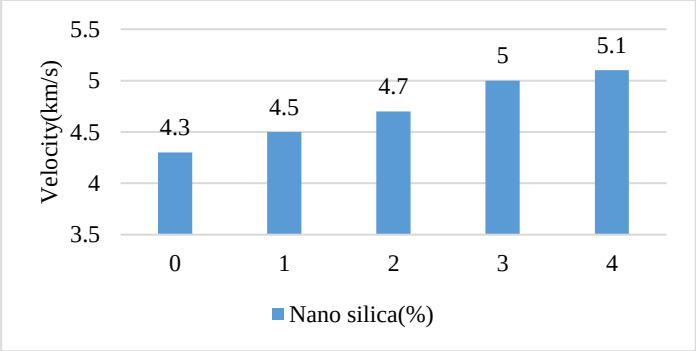

Fig. 8. UPV values.

3.7 Microstructure

SEM analysis of the concrete mixed with NS revealed a decline in voids, indicating improved presentation of the concrete as depicted in fig 9 below. While comparing to control concrete, concrete with NS has a compact and homogeneous microstructure . With the presence of NS, the microstructure remained denser. According to the findings, NS successfully reduces the amount of portlandite, resulting in a narrow microstructure of the ITZ among aggregate and pastes .

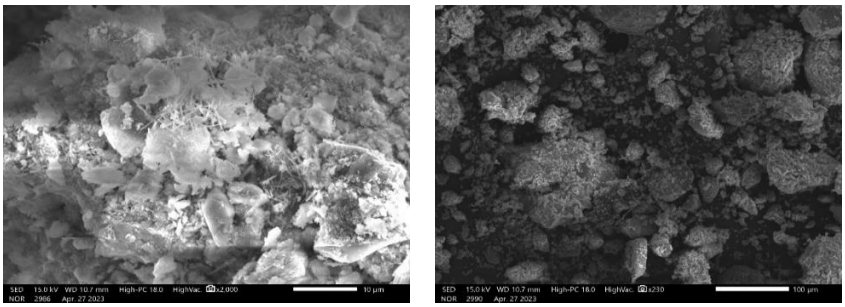

Fig. 9. SEM image of nano silica added concrete

4 Conclusions

- The workability decreases as nano silica concentration rises.
- Compressive strength is higher as the amount of nano silica increases.
- The microstructure of concrete is enhanced with nano silica in the mix.
- Durability also enhances with the usage of nano silica.
- Generally, Mechanical properties, microstructures and quality of concrete are enhanced when nano-silica is added.

ISBN: 978-81-932056-2-4

References

1. Fayomi, G. U., Mini, S. E., Fayomi, O. S. I., & Ayoola, A. A. (2019, September). Perspectives on environmental CO2 emission and energy factor in Cement Industry. In *IOP Conference Series: Earth and Environmental Science* (Vol. 331, No. 1, p. 012035). IOP Publishing.

2. Du, H., Du, S., & Liu, X. (2014). Durability performances of concrete with nano-silica. *Construction and building materials*, *73*, 705-712.

3. Maheswaran, S., Bhuvaneshwari, B., Palani, G. S., Nagesh, R., & Kalaiselvam, S. (2013). An overview on the influence of nano silica in concrete and a research initiative. *Research Journal of Recent Sciences, ISSN*, *2277*, 2502.

4. Barbhuiya, G.H., Moiz, M.A., Hasan, S.D., & Zaheer, M.M. (2020). Effects of the nano silica addition on cement concrete: A review. *Materials Today: Proceedings*, *32*, 560-566.

5. Said, A. M., Zeidan, M. S., Bassuoni, M. T., & Tian, Y. (2012). Properties of concrete incorporating nano-silica. *Construction and building materials*, *36*, 838-844.

6. Yu, R., Spiesz, P., & Brouwers, H. J. H. (2014). Effect of nano-silica on the hydration and microstructure development of Ultra High-Performance Concrete (UHPC) with a low binder amount. *Construction and Building Materials*, *65*, 140-150.

7. Ghafari, E., Costa, H., Júlio, E., Portugal, A., & Durães, L. (2014). The effect of nano silica addition on flowability, strength and transport properties of ultra high-performance concrete. *Materials & Design*, *59*, 1-9.

8. Çevik, A., Alzeebaree, R., Humur, G., Niş, A., & Gülşan, M. E. (2018). Effect of nano-silica on the chemical durability and mechanical performance of fly ash based geopolymer concrete. *Ceramics International*, *44*(11), 12253-12264.

9. Singh, L. P., Karade, S. R., Bhattacharyya, S. K., Yousuf, M. M., & Ahalawat, S. (2013). Beneficial role of nanosilica in Cement based materials–A review. *Construction and building materials*, *47*, 1069-1077.

10. Aladdin M. Sharkawi, Metwally A. Abd-Elaty, Omar H. Khalifa (2018) Synergistic influence of micro-nano silica mixture on durability performance of cementious materials, Construction and Building Materials 164 (2018) 579–588.

11. Mukharjee, B. B., & Barai, S. V. (2020). Influence of incorporation of colloidal nano-silica on behaviour of concrete. *Iranian Journal of Science and Technology, Transactions of Civil Engineering*, *44*, 657-668.

12. Zhang, P., Sha, D., Li, Q., Zhao, S., & Ling, Y. (2021). Effect of nano silica particles on impact resistance and durability of concrete containing coal fly ash. *Nanomaterials*, *11*(5), 1296.

13. Avudaiappan, S., Prakatanoju, S., Amran, M., Aepuru, R., Saavedra Flores, E. I., Das, R., ... & Vatin, N. (2021). Experimental investigation and image processing to predict the properties of concrete with the addition of nano silica and rice husk ash. *Crystals*, *11*(10), 1230.

ISBN: 978-81-932056-2-4

14. Zahedi, M., Ramezanianpour, A. A., & Ramezanianpour, A. M. (2015). Evaluation of the mechanical properties and durability of cement mortars containing nanosilica and rice husk ash under chloride ion penetration. *Construction and Building Materials*, *78*, 354-361.

15. Singh, G., & Siddique, R. (2012). Effect of waste foundry sand (WFS) as partial replacement of sand on the strength, ultrasonic pulse velocity and permeability of concrete. *Construction and building materials*, *26*(1), 416-422.

16. Shah, H., Lee, C. C., Zamzuri, M., & Vijayan, V. (2022). Colloidal Nanosilica Effect on the Properties and Durability of Coir Reinforced Cement Brick. *Advances in Materials Science and Engineering*, *2022*.

17. Anjusha R, B. S. (2014). Influence of nano silica on the properties of ternary blended concrete. *International Journal of Scientific & Engineering Research*, *5*(7), 2229-5518.

18. Kumar, S., Kumar, A., & Kujur, J. (2019). Influence of nanosilica on mechanical and durability properties of concrete. *Proceedings of the Institution of Civil Engineers-Structures and Buildings*, *172*(11), 781-788.

19. Alhawat, M., Ashour, A., & El-Khoja, A. (2019, August). Influence of using different surface areas of nano silica on concrete properties. In *AIP Conference Proceedings* (Vol. 2146, No. 1, p. 020007). AIP Publishing LLC.

20. Varghese, L., Rao, V. V. L. K., & Parameswaran, L. (2019). Nanosilica-added concrete: strength and its correlation with time-dependent properties. *Proceedings of the Institution of Civil Engineers-Construction Materials*, *172*(2), 85-94.

21. Sobolev, K., & Gutiérrez, M. F. (2005). How nanotechnology can change the concrete world. *American Ceramic Society Bulletin*, *84*(10), 14.

22. Oner, A. D. N. A. N., Akyuz, S., & Yildiz, R. (2005). An experimental study on strength development of concrete containing fly ash and optimum usage of fly ash in concrete. *Cement and Concrete Research*, *35*(6), 1165-1171.

23. Li, W., Huang, Z., Cao, F., Sun, Z., & Shah, S. P. (2015). Effects of nano-silica and nano-limestone on flowability and mechanical properties of ultra-high-performance concrete matrix. *Construction and Building Materials*, *95*, 366-374.

24. Senff, L., Labrincha, J. A., Ferreira, V. M., Hotza, D., & Repette, W. L. (2009). Effect of nano-silica on rheology and fresh properties of cement pastes and mortars. *Construction and Building Materials*, *23*(7), 2487-2491.

25. Bureau of Indian Standards. Indian Standards IS: 1199-1959, Methods of Sampling and Analysis of Concrete; Bureau of Indian Standards: New Delhi, India, 1959.

26. Bureau of Indian Standards. Indian Standards IS: 516-1959, Method of Tests for Strength of Concrete; Bureau of Indian Standards: New Delhi, India, 2004.

27. Bureau of Indian Standards. Indian Standards IS: 5816-1999, Method of Tests for Splitting Tensile Strength of Concrete; Bureau of Indian Standards: New Delhi, India, 1999.

ISBN: 978-81-932056-2-4

28. Bureau of Indian Standards IS: 1331 (1992) Indian standard non-destructive testing of concrete: method of test: Part 1 ultrasonic pulse velocity. Bureau of Indian Standards, New Delhi.

29. IS: 383 (1970) Indian standard specification for coarse and fine aggregates from natural sources for concrete. Bureau of Indian Standards, New Delhi.

30. IS:456 (2000) Indian standard plain and reinforced concrete code of practice. Bureau of Indian Standards, New Delhi.

31. IS:8112 (1989) Indian standard specification 43 grade ordinary Portland cement specification. Bureau of Indian Standards, New Delhi.

32. ASTM C642-06 (2006) Standard test method for density, absorption, and voids in hardened concrete. ASTM International, West Conshohocken

ISBN: 978-81-932056-2-4

EXPERIMENTAL STUDY ON THE PARTIAL REPLACEMENT OF NANO ZIRCONIA AND RICE HUSK ASH (RHA) IN MORTAR

Thounaojam Yaiphasana[1] and Er Ankit Mahajan[2]

[1,2] Chandigarh University, Department of Civil Engineering, Mohali, Punjab, India, 140413

[1]thouyaipha178@gmail.com
[2]ankitmahajan.civil@cumail.in

Abstract. This paper investigates the effect of using zirconia powder and RHA as a partial replacement for cement and sand, on mechanical properties and water absorption of mortar. The rice manufacturing industry produces a large amount of RHA waste, which is an ecologically beneficial pozzolanic substance and low-cost. Cement Mortar is mixed with a 1:3 cement/sand ratio, with nano zirconia as a replacement for cement in different content (1%, 2%, 3%, 4%, and 5% by the weight of cement) and RHA as a replacement for fine aggregate in various amounts (10%, 20%, 30%, 40%, 50%, 60%, and 70% by the weight of fine aggregate). The mechanical properties and water absorption tests were done after curing for 7, 14, and 28 days. The replacement, of cement with zirconia at 3% has a strength of 9.7 MPa, 11.30 MPa, and 36.27 MPa, and sand with rice husk ash at 50% has a strength of 22.64 MPa, 26.29 MPa, and 30.78 MPa at 7, 14, and 28 days respectively, showed a better effect on mechanical properties than the other sample. The result revealed replacement of combined zirconia and RHA has shown better properties on the mechanical characteristics of mortar. The highest compressive and tensile strength value in 28 days is 51.16 MPa and 20.93Mpa for replacement mortar.

Keywords: zirconia, RHA, compressive and tensile strength, Water absorption, SEM.

1 Introduction

Mortar mostly consists of sand, water, and cement. Ordinary Portland Cement (OPC) plays a main character like the binder in mortar. Mortar with sand or cement replacement of mineral and fine particles is known as modified mortar [1]. Mortar is a main factor used in construction, at this time requirement for mortar is very high or increases in construction sites because the world population increasing day by day and increasing the construction of schools, residential buildings, office buildings, etc [2]. The cement manufacturer is producing around 7.5% of global greenhouse gas emissions (GHGE) and production of GHGE is rising by the day, Cement demand is high on construction sites across the world. [3,4]. River sand is an important resource as a filler in the production of tiles, glass, mortar, ceramics, concrete, and other products [5,6]. Globally, the building industry utilizes around 40% of river sand, equal to approximately 10 billion tonnes per year [7]. Overuse of river sand has a serious effect on the ecosystem, economy, and society [8]. Zirconia is a nonreactive ceramic material that has many varieties of uses due to its exceptional mixture of mechanical properties and physical, chemicals, including high strength, high chemical stability, and resistance to corrosion by acid, salt water, etc. This has been shown by the finding that increasing

ISBN: 978-81-932056-2-4

the percentage of zirconia, reduces the workability of the mortar [9]. Rice mills process large amounts of rice husk is an agro waste. It has been used by several nations, primarily Sri Lanka, as a significant biomass source to produce fuel and energy source for the creation of electricity [10]. In the past 20 years, Sri Lanka has increased its yearly rice production to almost 4.6 million metric tonnes, producing 0.89 million tonnes of waste rice husk waste [11]. Normally, rice husks are discarded in free spaces, damaging water, and using a large amount of land while doing little good for the environment [12]. The most popular method of getting rid of rice husks is open burning, which generates a lot of rice husks ash waste in rural areas and causes air pollution, heart disease, and airborne disease. This rice husks ash waste management cannot be regarded as an entirely clean production [14,15]. As a result, the aim of this study was to partially replace cement with zirconia and sand with RHA, and investigate the effect such as mechanical strength, and water absorption.

➢ Materials

1.1 Cement

In the current study (OPC) of 43 grade was used and bought from JK supper cement company of Kharar Punjab follows ASTM C150 standards should be presented.

Table 1. Properties of OPC cement

Material	Al_2O_3	MgO	CaO	Fe_2O_3	SiO_2
Cement %	5.2	6.51	53.41	3.62	21.76
Material	K_2O	SO_3	Na_2O	Loss on ignition	
Cement %	0.96	3.8	0.17	3.27	

1.2 Fine Aggregate / Sand

Fine aggregate is easily available in Kharar River sand with particles passing through a 4.75mm sieve.

1.3 Nano Zirconia Powder (ZrO_2)

Nano zirconia with a size of 30-50nm was acquired from Nano Research Lab, Jamshedpur, Jharkhand / India as received, it has been used.

Table 2. Physical properties of zirconia powder

Name of product	Nano zirconia powder
Purity	99.55
Color	White
Specific surface	40-45m^2/g
Ture Density	5.89 g/cm^3
Atomic Weight	123.218 g/mol
Melt point	2715^{0}C
Boiling Point	4300^{0}C

ISBN: 978-81-932056-2-4

Table 3. Chemical properties of zirconia powder

ZrO_2	Al	Fe	Pb
99.5%	<0.06%	<0.02%	<0.02%

1.4 Rice Husk Ash (RHA)

Rice husk should be burned at 600 to 700 in the furnace for a minimum of 2 hours to form rice husk ash (RHA).

Table 4. Chemical properties of RHA (Specific Gravity - 2.14)

Al_2O_2	SiO_2	Fe_2O_3	SO_3	CaO	Na_2O
0.21	89.7	0.11	0.85	2.21	0.81

2 Mix Design

Mortar is mixed with a 1:3 cement/sand ratio. The mortar was a mixture of cement, river sand, zirconia powder, rice husk ash, and water. Firstly, sand and rice husk are mixed properly for a few minutes again cement and zirconia powder are added and then are mixed all together for a few minutes. It is levelling and then water is added and again mix properly for 3-5 minutes to form mortar. The prepared mortar is collected by trowel and wet mortar is filled in the moulds (cube and briquette), compacting of mortar was done by using a vibrating machine and levelling by trowel. On the next day of casting, all the moulds will be removed from the mortar and put inside the water for curing. All the samples are curing for 7. 14, and 28 days as required as shown in Fig. 1.

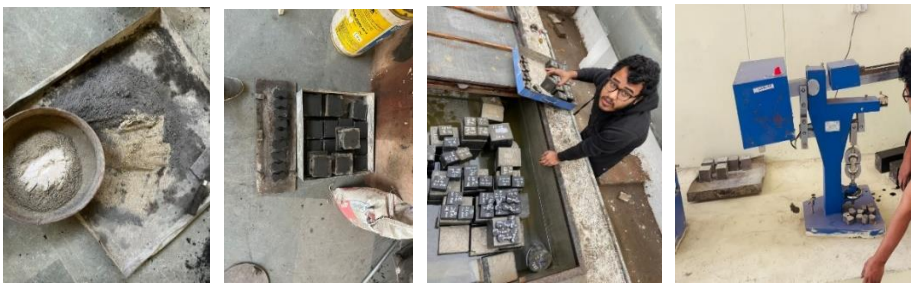

(a) (b) (c) (d)

Fig. 1. (a) mixing, (b) casting, (c) curing, (d) tensile strength.

3 Experimental Work

3.1 Compressive Test

Compressive strength tests were performed on the cube mortar sample. The compressive strength must be calculated, by taking three cubic samples on average at 7, 14, and 28 days after curing.

ISBN: 978-81-932056-2-4

3.2 Tensile Test

Tensile strength tests were performed on mortar briquette test specimens. The tensile strength of mortar must be calculated, by taking an average of six briquette samples at 7,14, and 28 days.

3.3 Water Absorptions

The water absorption of cement mortar was tested in accordance with ASTM C642-13. Weighing the cubes was used for calculating water absorption. Three cubes of cement mortar were tested for water absorption after 7, 14, and 28 days of curing. (step 1) All the sample was 24 hours oven-dried at 100-1050C. (step 2) All the sample was submerged inside the water tank for 24 hours. Measuring all the sample weights for both steps 1 and 2. The below calculation is applied to find the water absorption. In this calculation, the mass value was taking an average of three cubes for each mix design.

$$\text{Water absorption (\%)} = \frac{D_2 - D_1}{D_1} \times 100 \quad (1)$$

Where D1 = weight of the mortar in oven dries for 24 hours.

D2 = weight of the mortar that was submerged in water for 24 hours.

3.4 Density Test

The mortar cubes were removed from the water container after curing. A weighing balance was used to determine each cube's weight to calculate the density of the mortar cube. The density test of each cube was calculated using this equation.

$$\text{Density } (\rho) = \frac{weight\ of\ mortar\ cube}{volume\ of\ mortar\ cube} (\text{kg/m}^3) \quad (2)$$

3.5 SEM Test

After the 28-day curing and the mechanical test was finished, SEM test was conducted to examine the internal structure of the breaking mortar sample. This test is conducted at Scanning Electron Microscope Laboratory University Center for Research & Development (UCRD) Chandigarh University.

4 Results of an Experimental Work

4.1 Compressive Strength Test

Fig. 2 shows to finding the optimum compressive strength for the presence of zirconia in the mortar with different percentages. The results of samples obtained after curing at 7, 14, and 28 days were examined. It was found that zirconia mortar increases compressive strength up to 3% replacement. The compressive strength decreases after 3% of zirconia replacements. The 3% replacement has an optimum level for zirconia.

ISBN: 978-81-932056-2-4

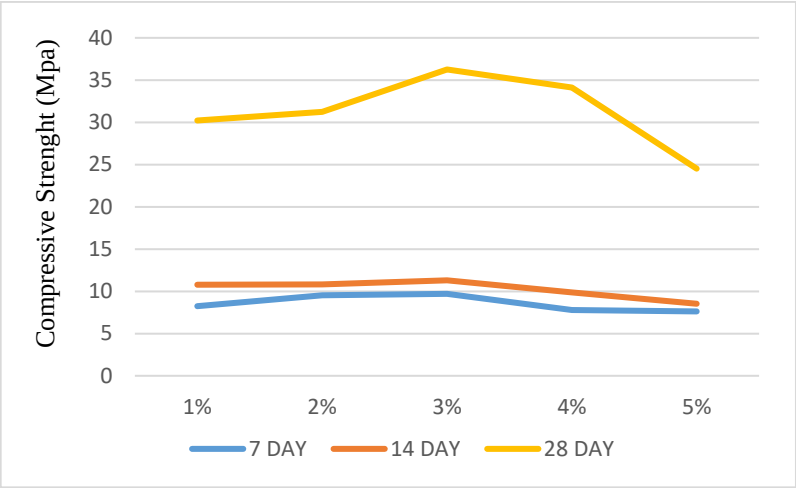

Fig. 2. Compressive strength of zirconia.

Fig. 3 shows to finding the optimum compressive strength for the presence of RHA in the mortar with different percentages. RHA mortar is found to increase strength up to 50% replacement. After 50% RHA replacements, the compressive strength decreases. The 50% replacement has an optimum level of RHA. As a result, the higher percent of RHA replacement in mortar is increasing the water required in the mortar. Moreover, the large specific surface area of RHA reduces workability as the replacement level to rises. while more water was required to maintain workability.

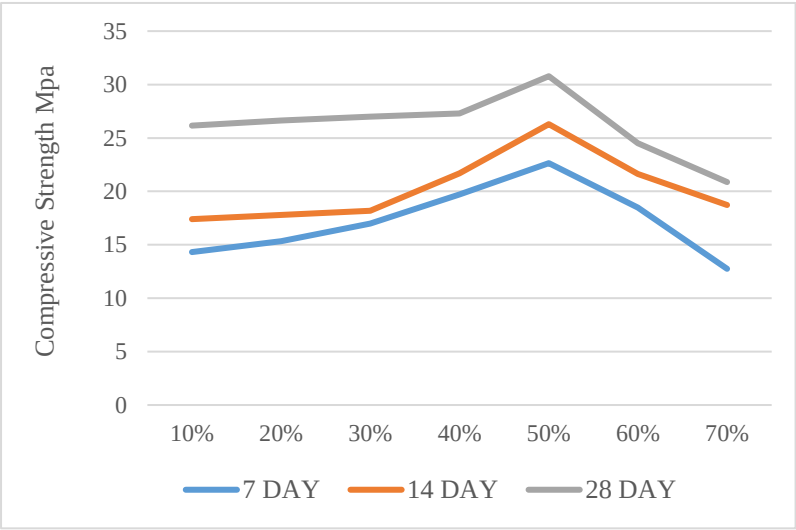

Fig. 3. Compressive strength of RHA.

Fig. 4 shows the comparing compressive strength of normal mortar and combine replacement at the optimum level of zirconia 3% and RHA 50% mortar for 7, 14, and

ISBN: 978-81-932056-2-4

28 days. The replacement mortar has higher compressive strength as compared to the normal mortar sample.

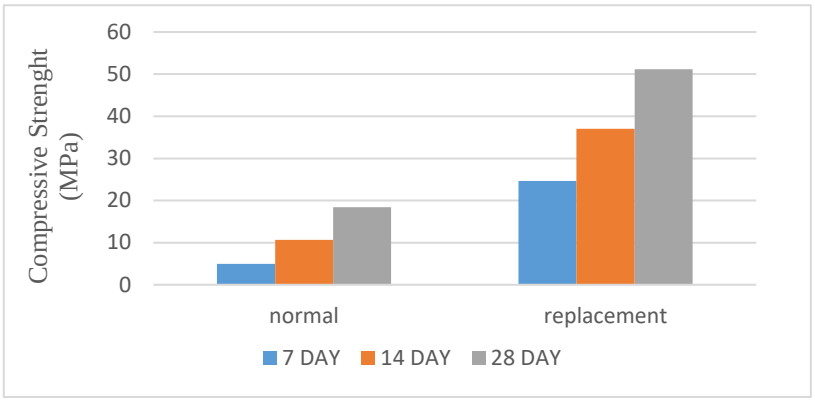

Fig. 4. Compressive strength of normal and replacement mortar.

4.2 Tensile Strength Test

Fig. 5 shows the result of tensile strength for normal mortar and replacement with combined zirconia nanoparticles and RHA in cement and sand in mortar for 7, 14, and 28 days. The replacement mortar of zirconia and RHA at their optimum level (3% and 50%) respectively. The tensile strength of replacement mortar has higher strength as compared to normal mortar sample.

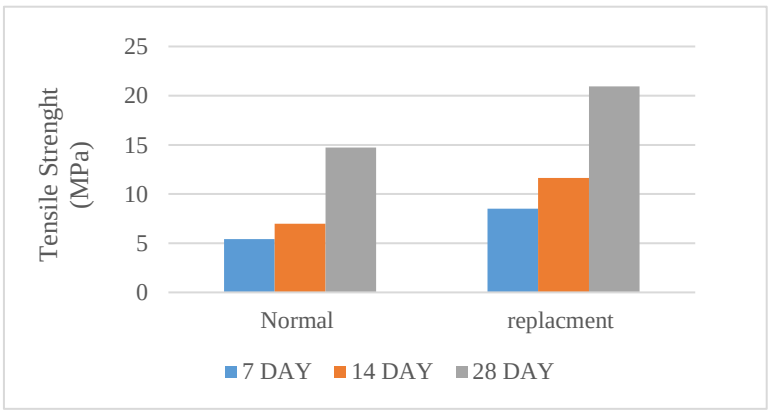

Fig. 5. Tensile strength of normal and replacement mortar.

4.3 Water Absorption

The results of water absorption were shown in Fig. 6 for normal mortar and combined replacement mortar at the optimum level of zirconia 3% and RHA 50% for 7, 14, and 28 days.

ISBN: 978-81-932056-2-4

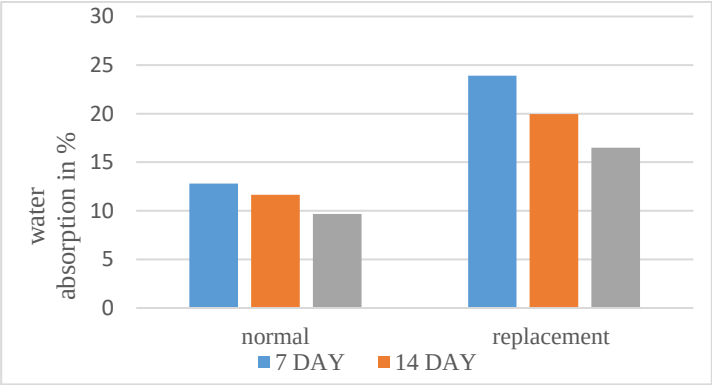

Fig. 6. Water absorption of normal and replacement mortar.

The above figure shows the water absorption in % of the normal mortar and replacement mortar. The water absorption% for normal mortar and replacement mortar is highest at 7 days, the value of water absorption will automatically down with the curing days increase. Replacement mortar has a higher water absorption rate than the normal mortar sample, since RHA is present in the replacement mortar. RHA has a high tendency for water absorption.

4.4 Density Test

The results of a Density test were shown in Fig. 7 for normal mortar, combine zirconia nanoparticles, and RHA replacement of cement and sand in mortar, for 7, 14, and 28 days.

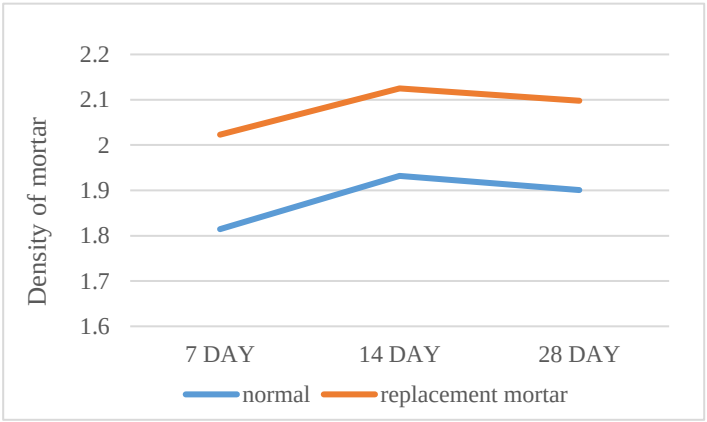

Fig. 7. Density of normal and replacement mortar.

The above figure shows the density of mortar in % of the normal mortar and replacement mortar. The value of density mortar for normal mortar and replacement mortar is higher at 14 days while that of 7 days and 28 days. The replacement mortar has a higher density than the normal mortar sample.

ISBN: 978-81-932056-2-4

4.5 SEM Test

Scanning analyses of mortars such as replacement of RHA, ZrO_2, and combinations of (RHA and ZrO_2) have been performed for the highest-strength mortar sample. The picture showed the equivalent micrograph of the surface at various magnifications of 200x - 2000x, with oscillations of roughly 10 - 100 µm visible. To conduct the analysis, the sample has been coated with gold coating (construction materials are non-conductivity), which provides improved image clearance during analysis.

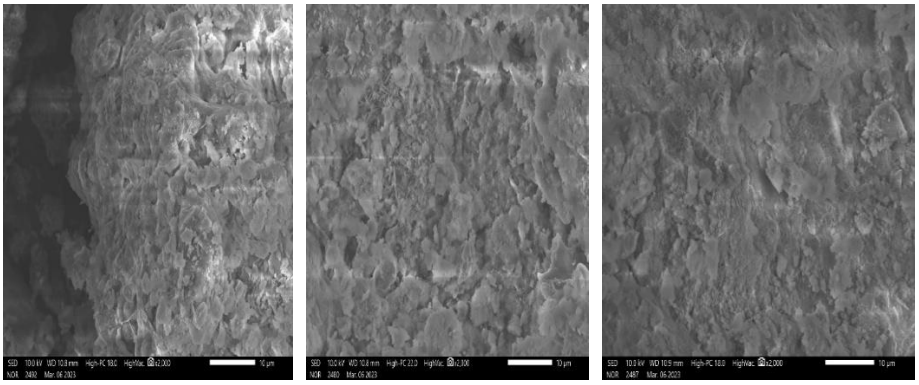

(a) (b) (c)

Fig. 8. SEM images: (a) Zirconia x2000, (b) RHA x2000, and (c) Combine x2000.

In the Fig. 8, the SEM analysis consists of (a) ZrO_2 x2000, (b) RHA x2000, and (c) Combined optimum strength for both ZrO_2 and RHA with a magnification of x2000. In Fig. 8 (a) with the magnification of x2000 showing the formation of a crystal may be observed in the interface zone between the specimen's edges and center. While the micrograph clearly shows the large portlandite crystals with a size of 10 µm. Fig. 8 (b) shows the microstructure of RHA, the high number of voids (holes) produce during cement hydration. It can be seen in the image that the crystal dispersed between the specimen and the area with interlaced crystals is in the form of a little needle matching to the crystal. Fig. 8 (c) shows the contribution of ZrO_2 nanoparticles, the amount of compaction may be related to the effect of their high surface of favored nucleation sites as the product formed by cement hydration production. The combination of ZrO_2 and RHA in mortar where the void or hole are not visible or observed, although the changes of porosity, as shown by a significant degree of compaction found between the aggregate and the cleft region in the direction of creating flat surfaces.

5 Conclusions

The use of RHA as a replace for sand in mortar gives benefits to our environment as the agricultural waste is reduced, and minimizes the use of river sand, therefore economical to the construction site. While the use of nano zirconia powder is a non-reactive ceramic material that has a vast range of uses on account of improved mechanical and physical characteristics, including as high strength and chemical stability, and resistance to corrosion by acid, salt water, etc. This study's conclusion is as follows:

ISBN: 978-81-932056-2-4

- The replacement of cement with 3% zirconia powder gets the highest strength at 28 days as compared to the other percentage of zirconia. And for the replacement of sand with 50% rice husk ash had more strength as compared to the other percentage of rice husk ash at 28 days.

- While comparing the mechanical characteristics of normal mortar and combined (3% ZrO_2 and 50% RHA) replacement mortar, it is found that combined replacement mortar has higher compressive and tensile strength for 7, 14, and 28 days than normal mortar.

- For water absorption of normal and combined replacement mortar, the combined mortar has higher absorption properties than normal mortar. The water absorption result shows that at 7 days has the highest, then slowly decreases up to 28 days.

- The result for density shows that from 7 to 14 days there is a gradual increase in density and then from 14 to 28 days it is generally decreasing for both the normal and replacement mortar. The combined replacement mortar has a higher density than the normal mortar.

References

1. Yaşar, E., Erdoğan, Y., & Kılıç, A. Effect of limestone aggregate type and water–cement ratio on concrete strength. *Materials letters*, *58*(5), 772-777. (2004).

2. Gastaldini, A. L. G., Da Silva, M. P., Zamberlan, F. B., & Neto, C. M. Total shrinkage, chloride penetration, and compressive strength of concretes that contain clear-colored rice husk ash. *Construction and Building Materials*, *54*, 369-377. (2014).

3. Hossain, M. M., Karim, M. R., Hasan, M., Hossain, M. K., & Zain, M. F. M. Durability of mortar and concrete made up of pozzolans as a partial replacement of cement: A review. *Construction and building materials*, *116*, 128-140. (2016).

4. Alex, J., Dhanalakshmi, J., & Ambedkar, B. Experimental investigation on rice husk ash as cement replacement on concrete production. *Construction and Building Materials*, *127*, 353-362. (2016).

5. Xu, W., Lo, T. Y., & Memon, S. A. Microstructure, and reactivity of rice husk ash. *Construction and Building Materials*, *29*, 541-547. (2012).

6. Cordeiro, G. C., Toledo Filho, R. D., & de Moraes Rego Fairbairn, E. Use of ultrafine rice husk ash with high-carbon content as pozzolan in high-performance concrete. *Materials and structures*, *42*, 983-992. (2009).

7. Al-Khalaf, M. N., & Yousif, H. A. Use of rice husk ash in concrete. *International Journal of Cement Composites and Lightweight Concrete*, *6*(4), 241-248. (1984).

8. Norhasri, M. M., Hamidah, M. S., & Fadzil, A. M. Applications of using nano material in concrete: A review. *Construction and Building Materials*, *133*, 91-97. (2017).

ISBN: 978-81-932056-2-4

9. Rashad, A. M. Effects of ZnO2, ZrO2, Cu2O3, CuO, CaCO3, SF, FA, cement and geothermal silica waste nanoparticles on properties of cementitious materials–A short guide for Civil Engineer. *Construction and Building Materials*, *48*, 1120-1133. (2013).

10. Ganesan, K., Rajagopal, K., & Thangavel, K. Rice husk ash blended cement: Assessment of optimal level of replacement for strength and permeability properties of concrete. *Construction and building materials*, *22*(8), 1675-1683. (2008).

11. El-Dakroury, A., & Gasser, M. S. Rice husk ash (RHA) as cement admixture for immobilization of liquid radioactive waste at different temperatures. *Journal of nuclear materials*, *381*(3), 271-277. (2008).

12. Chao-Lung, H., Le Anh-Tuan, B., & Chun-Tsun, C. Effect of rice husk ash on the strength and durability characteristics of concrete. *Construction and building materials*, *25*(9), 3768-3772. (2011).

13. Antiohos, S. K., Papadakis, V. G., & Tsimas, S. Rice husk ash (RHA) effectiveness in cement and concrete as a function of reactive silica and fineness. *Cement and concrete research*, *61*, 20-27. (2014).

14. Xu, W., Lo, Y. T., Ouyang, D., Memon, S. A., Xing, F., Wang, W., & Yuan, X. Effect of rice husk ash fineness on porosity and hydration reaction of blended cement paste. *Construction and Building Materials*, *89*, 90-101. (2015).

15. Anwar, M., Miyagawa, T., & Gaweesh, M. Using rice husk ash as a cement replacement material in concrete. In *Waste Management series* (Vol. 1, pp. 671-684). Elsevier. (2000).

16. Al-Jadiri, R. S. F., Rahma, N. M., & Eweed, K. M. Producing a new type of cement by adding Zirconium Oxide. In *IOP Conference Series: Materials Science and Engineering* (Vol. 454, No. 1, p. 012149). IOP Publishing. (2018, December).

17. Trejo-Arroyo, D. L., Acosta, K. E., Cruz, J. C., Valenzuela-Muñiz, A. M., Vega-Azamar, R. E., & Jiménez, L. F. Influence of ZrO2 nanoparticles on the microstructural development of cement mortars with limestone aggregates. *Applied Sciences*, *9*(3), 598. (2019).

18. Selvaranjan, K., Gamage, J. C. P. H., De Silva, G. I. P., & Navaratnam, S. Development of sustainable mortar using waste rice husk ash from rice mill plant: Physical and thermal properties. *Journal of Building Engineering*, *43*, 102614. (2021).

19. Umarajyadav, M. V. Study of mechanical properties of concrete with nano zirconia. *Int. Res. J. Eng. Technol*, *4*(8), 90-94. (2017).

20. Behnia, B., Anvari, A. A., Safardoust-Hojaghan, H., & Salavati-Niasari, M. Positive effects of novel nano-zirconia on flexural and compressive strength of Portland cement paste. *Polyhedron*, *177*, 114317. (2020).

21. (ASTM C109/ C 109M-02, 2002)*Standard Test Method for Compressive Strength of (Using 2-in Cube Specimens).* ASTM, international, west Conshohocken, PA .

22. ASTM C642. (2001). *"Standard Test Method for Density, Absorption, and voids in hardened conrete.* ASTM, Philadelphia, PA.

ISBN: 978-81-932056-2-4

PARTIAL REPLACEMENT OF CEMENT AND FINE AGGREGATES IN CONCRETE BY SUGARCANE BAGASSE ASH AND GROUNDNUT SHELL ASH

Thoudam Ronaldo Singh[1] and Er. Gagandeep[2]

[1,2] Chandigarh University, Mohali, Punjab, India, 140413

[1] ronaldothoudam324@gmail.com
[2] gagandeep.civil@cumail.com

Abstract. The manufacture of cement contributes to environmental issues including pollution and global warming since it releases a number of dangerous gases. Natural sand is also expensive and difficult to get, thus in order to solve these issues, research is increasingly focusing on exploiting industrial and agricultural waste. Sugarcane Bagasse Ash (SCBA) is a leftover industrial derivative of sugar industry's captive power plant while Agricultural waste known as groundnut shell ash (GSA) that is used to substitute fine aggregates. The purpose of this paper is to observe the possibility of utilizing sizeable quantity of Sugarcane Bagasse Ash and Groundnut Shell Ash here place of cement and fine aggregate in the concrete. In this paper, concrete was batch-produced by weight using M30 mixed ratio. Concrete cubes, concrete cylinders and concrete beams were cast by 5% substitute of cement with sugarcane bagasse ash and fine aggregates by groundnut shell ash in different percentages (5%, 10%, 15%, 20% and 25%). Then concrete was followed via curing in normal water for 7, 28 and 56 days. The reaction mechanism and hydration practice of the produced concrete and paste mixes, Scanning Electron Microscopy (SEM), Energy Dispersive x-ray Spectroscopy (EDS), Ultrasonic Pulse Velocity Test (UPV) and mechanical strength tests were employed. The results showed that 15% replacement demonstrated the highest strength in compression, split tensile and flexural strength.

Keywords: Sugarcane Bagasse Ash, Groundnut Shell Ash, Scanning Electron Microscopy, Energy Dispersive x-ray Spectroscopy, Ultrasonic Pulse Velocity Test.

1 Introduction

Concrete is used deliberately and adapts to environmental conditions, making it appropriate for use in nearly all building and civil engineering structures [1]. The rate of demand in the building sectors, the production rate of the raw materials is insufficient, which is the cause of Portland cement's ongoing price increase [2]. The ability to cast in a range of shapeable and performance in meeting strength criteria, cement is the most commonly used building material. For the purpose of building homes and other types of infrastructure, the construction sector primarily depends on cement [3]. Pozzolanic materials, however, have long proven to be successful in creating high performance concrete (HPC). In many regions of the world, artificial pozzolanas like rice husk ash are now widely used as supplemental cementing materials [4]. Many researchers and engineers are constantly looking for materials that may have pozzolanic properties in building materials and to reduce pollution, energy and carbon dioxide emission to

ISBN: 978-81-932056-2-4

overcome reduction of resources and global pollution [5]. Due to its prominent use in concrete, natural sand is used far too much globally. In emerging nations, there is a significant need for natural sand for infrastructure. However, natural sand is expensive and difficult to get by, thus in order to solve this issue, crushed groundnut shell makes up a minor fraction of the fine aggregate. Various attempts have been made to make use of these shells over the years. Small amounts were incorporated into the animal feed, particularly for the cattle [6]. When combined with Portland cement, these additional cementations materials play a crucial role in strengthening concrete by transforming the pore structure and reducing permeability, which increases the material's water resistant, infiltration, corrosion of the reinforcement and sulphate acid attack. A healthy leguminous crop, groundnut is farmed around the world. Groundnut shells are the byproduct left over when the groundnut seed is removed from the capsule [7]. However, groundnut shells have a number of bioactive and efficient elements that are advantageous for people. It is utilized commercially as a feedstock, food and fillers by carriers for bio-filters as well as fertilizer. However, the majorities of abandoned groundnut shells are burned or dispersed, which causes pollution. Therefore, new methods must be created to achieve zero waste [8].

2 Materials and Method

2.1 Cement

Ordinary Portland cement (43 Grade) obtained from JK supper cement Company of Kharar, Punjab which follows IS: 8112-2013 standard was used in this paper. It was stored in dry area to prevent from hardening. In place where there is no moisture exposure, this cement type is utilized.

2.2 Fine Aggregate

River sand was utilized as fine aggregate. It is independent from silt and clays in addition to natural impurities. Sand passing through IS 4.75mm sieve and in compliance with the specification of IS 383-2016 was utilized and its specific gravity is 2.67.

2.3 Coarse Aggregate

The crushed aggregates were 20 mm in size, angular in shape, and tested in accordance with Indian Standard (IS: 10262, IS: 383). The crushed 20 mm aggregate has a specific gravity of 2.79.

2.4 Sugarcane Bagasse Ash

SCBA is a result of the bagasse burning process in sugar factories. This substance contains amorphous silica, a sign of cementing properties that can lead to strong bonding. It has a specific gravity of 2.24. The ash utilized was obtained from The Morinda Co-operative Sugar Mills Limited, Morinda, Punjab.

ISBN: 978-81-932056-2-4

2.5 Groundnut Shell Ash

GSA is a common waste in every part of the world. The ash was obtained from Nature and Greens, Jamnagar, Gujarat. The shells are air-dried and grinded. The grinded shell was then burned and sieved through 4.75 mm sieve. The product after sieving was replaced as fine aggregates. After performing specific gravity test, the ash has a specific gravity of 2.3.

2.6 Water

PoTable water available in the lab was utilized for the mixing purpose which compliant the requirements of water for concreting and curing as per IS: 456-2000.

3 Experimental work

A total of 135 concrete sample numbers were cast for this experiment. The cube was 150mm x 150mm x 150mm, the cylinder was 150mm x 300mm, and the beam was 100mm x 100mm x 500mm in size. The mix design (process) followed IS: 10262-2019 for M30 grade and the w-c ratio was 0.60. The constant percentage of SCBA, which is 5% replacement by weight of cement, and the various replacement percentages of crushed GSA, which are 5%, 10%, 15%, 20% and 25% substitute by weight of Fine aggregate were estimated based on the component quantities of the mixes. Concrete's components were completely combined to obtain a homogeneous consistency. Machine oil was applied to the interior surfaces of the cast iron moulds prior to casting. Testing of specimens are as follow.

3.1 Ultrasonic Pulse Velocity

The UPV methods, which allow for an investigation of the material homogeneity, can be regarded as one of the most promising NDT techniques for evaluating concrete structures. A structure can be completely controlled by utilizing how its properties change throughout time. The Pulse Velocity = Path Length(L)/Transit Time(T) km/s.

Table 1. Standard for concrete grading quality

Pulse Velocity(km/s)	Grading Quality
> 4.5	Excellent
3.5 - 4.5	Good
3.0 - 3.5	Medium
< 3.0	Doubtful

ISBN: 978-81-932056-2-4

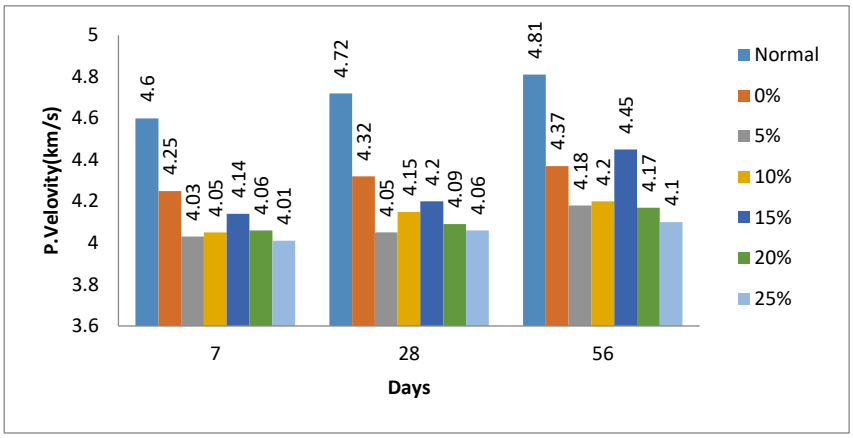

Fig. 1. Comparison between pulse velocity of normal and different percentage of GSA

The chart shows the pulse velocity of different concrete cubes containing various percentages of groundnut shell ash. From the chart it is found that the concrete containing SGBA and GSA for substitute of cement and fine aggregates is good quality. Good quality of this concrete is that the pulse velocity travels from one side of the cube to the parallel side of the cube which falls under 3.5-4.5 Km/s which satisfied the specification to IS: 516-2018.

3.2 Compressive Strength Test

The cube moulds are 150x150x150 mm in size. Specimens were submerged inside water for 7, 28 and 56 days to cure. After curing it was dried for 24 hours and crushed in UTM. The outcome demonstrates the compressive strength of replacement concrete improved up to 15% when GSA was partially replaced for 56 days, giving it the highest strength.

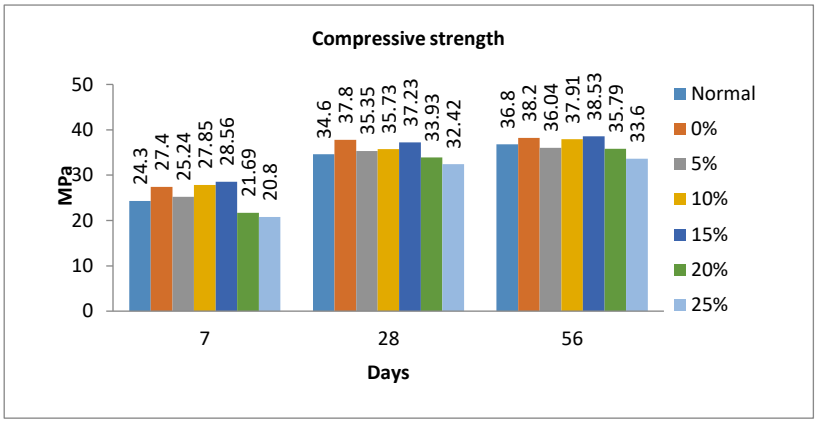

Fig. 2. Comparison between normal and different percentage of GSA

ISBN: 978-81-932056-2-4

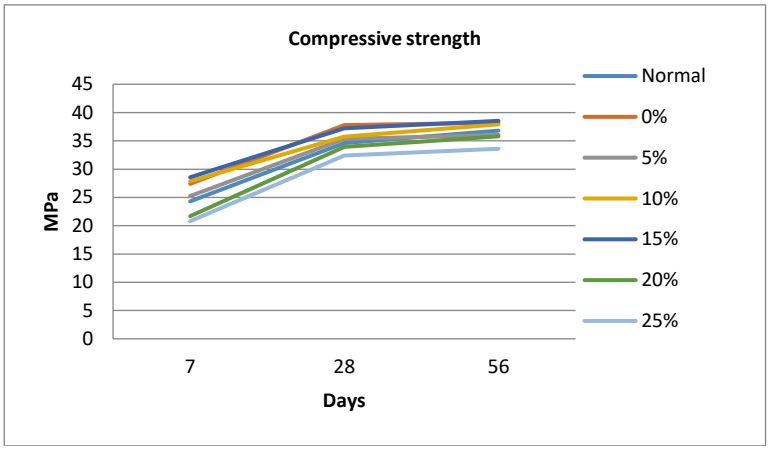

Fig. 3. Comparison between normal and different percentage of GSA in line diagram

3.3 Tensile Strength Test

The cylinder moulds are 150x300mm in size. After curing for 7, 28 and 56 days in water and dried for 24 hours. In a universal testing machine, the samples were evaluated by placing horizontally. The result demonstrates as tensile strength of replacement concrete improved up to 15% when GSA was partially replaced for 56 days, giving it the highest strength by weight of cement

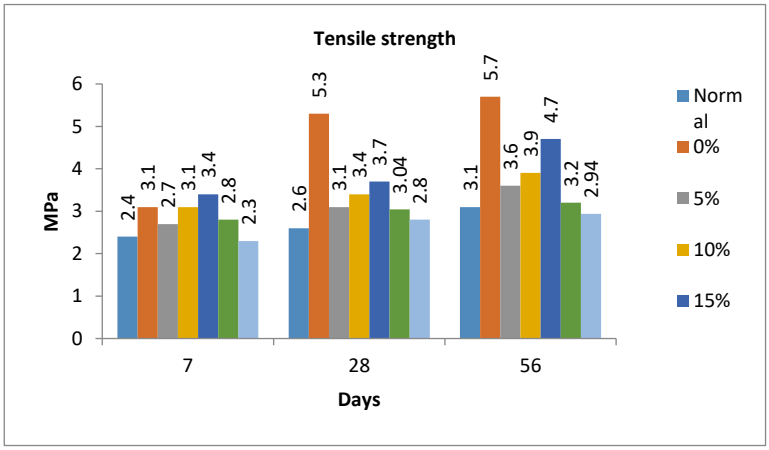

Fig. 4. Comparison between normal and different percentage of GSA

ISBN: 978-81-932056-2-4

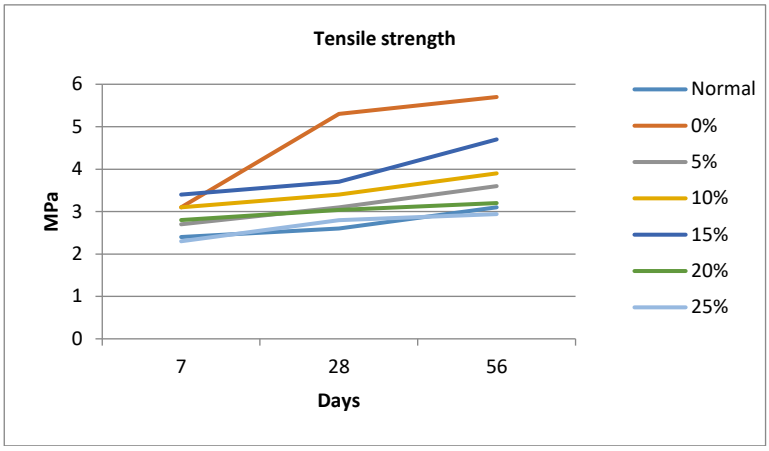

Fig. 5. Comparison between normal and different percentage of GSA in line diagram

3.4 Flexural Strength Test

The beam moulds are 100x100x500mm in size. Specimens were isolated from the water and dried for 24 hours. After curing beams are subjected in four-point bending test. The result demonstrates that flexural strength of replacement concrete increased by up to 15% when GSA was partially replaced for 56 days, giving it the highest strength.

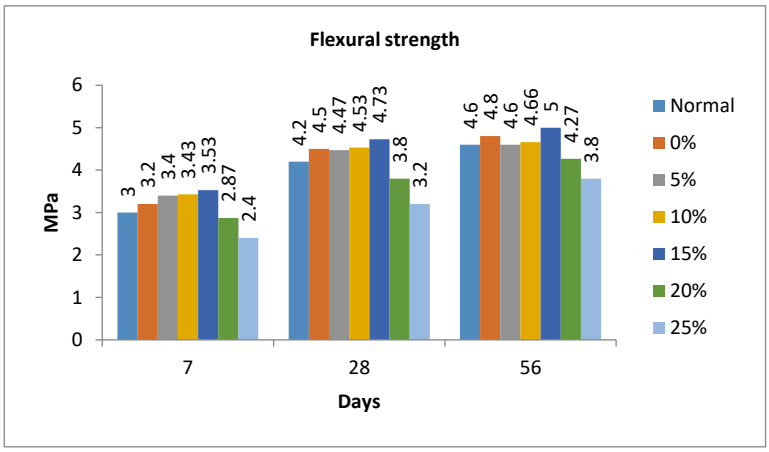

Fig. 6. Comparison between normal and different percentage of GSA

ISBN: 978-81-932056-2-4

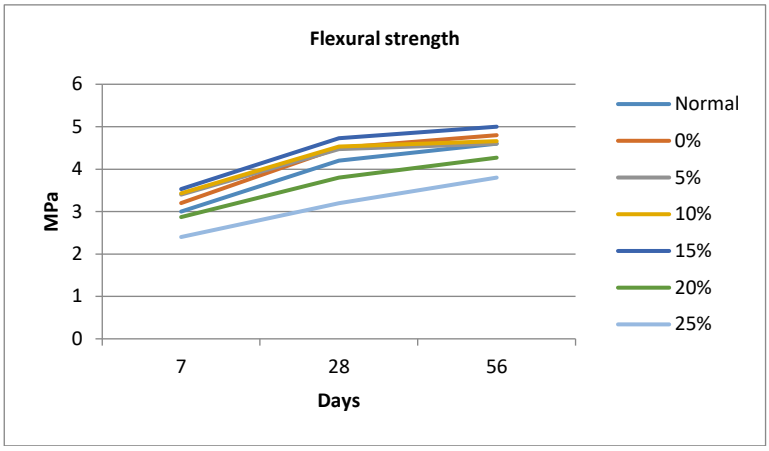

Fig. 7. Comparison between normal and different percentage of GSA in line diagram

3.5 Scanning Electron Microscopy

The analysis was carried out in Chandigarh University's University Centre for Research and Development (UCRD) Laboratory. Figures show SEM secondary electron mode images of hydrated pastes containing 5% SGBA and 15% GSA at 56 days. The structures display the usual surface morphology of thoroughly hydrated concrete, which is defined by a continuous aggregate structure with good particle interlocking. This suggests that suitably hydrated concrete structures will be created when 15% GSA is used in place of fine aggregates in concrete.

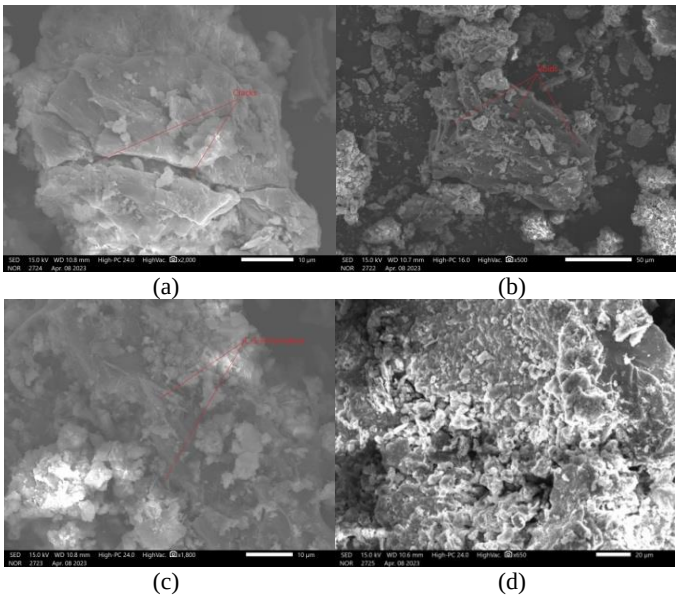

(a) (b)

(c) (d)

Fig.8. SEM pictures (a) SGBA, (b) SGBA with voids, (c) formation of C-S-H and (d) GSA

ISBN: 978-81-932056-2-4

3.6 Energy Dispersive X-Ray Spectroscopy

The analysis was carried out in Chandigarh University's University Centre for Research and Development (UCRD) Laboratory. The test sample was carried out for the best strength, 15% for 56 days of replacement in fine aggregates, as shown in Fig. 8(d). Although it can produce semi-quantitative results, the energy dispersive x-ray spectroscopy (EDS) technique is primarily employed for qualitative analyses of materials. It is used for elemental composition present in the concrete. Different locations were identified during the EDS measurement, and fig. shows the peaks that corresponded to those areas. The Table contained the value expressed as a percentage of weight and atomic mass.

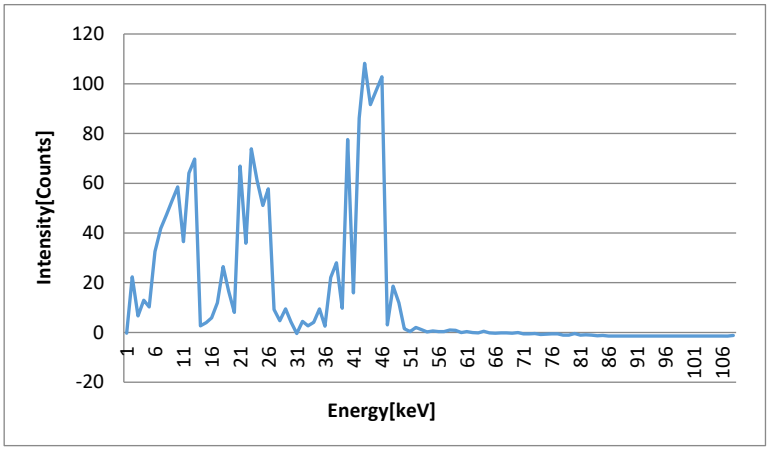

Fig. 9. EDS of Ground Nutshell Ash

Table 2. Elements present in Fig 8(d) SEM image

Element	Line	Mass%	Atom%
O	K	41.60	61.81
Na	K	0.03	0.3
Mg	K	0.93	0.91
Al	K	3.89	3.43
Si	K	10.23	8.66
Ca	K	40.16	23.83
Fe	K	3.16	1.34
Total		100.00	100.00
Fitting ratio 0.268			

4 Conclusions

According to the findings of this study, it can be said that;

- It was found that the concrete had good hydration efficiency and good mechanical interlocking of particles according to SEM pictures.
- It was found that the concrete was of good quality according to UPV testing.

ISBN: 978-81-932056-2-4

- It was found that using GNSA and GSA affects the workability of the concrete because of high water absorption rate.
- The strength of concrete increases up to 15% substitute of fine aggregate with GSA.
- The strength of concrete attained is low which may be due to mixing process, compaction and reactivity of the SCBA and GSA.
- In non-load bearing panels where, structural strength is not a concern, concrete containing SCBA and GSA may be employed.
- In spite of decreasing waste, using SGBA and GSA in concrete will reduce the need for cement and sand.

References

1. Mtallib, M. O. A., & Ibrahim, S. (2009). The effect of delayed placing on the compressive strength of concrete. *Nigerian Journal of Engineering*, *16*(1), 9.
2. Nwofor, T. C., & Sule, S. (2012). Stability of groundnut shell ash (GSA)/ordinary Portland cement (OPC) concrete in Nigeria. *Advances in applied science research*, *3*(4), 2283-2287.
3. Alabadan, B. A., Olutoye, M. A., Abolarin, M. S., & Zakariya, M. (2005). Partial replacement of ordinary Portland cement (OPC) with bambara groundnut shell ash (BGSA) in concrete. *Leonardo Electronic Journal of Practices and Technologies*, *6*, 43-48.
4. Adole, M. A., Dzasu, W. E., Umar, A., & Oraegbune, O. M. (2011). Effects of groundnut husk ash-blended cement on chemical resistance of concrete. *ATBU Journal of Environmental Technology*, *4*(1), 23-32.
5. Nagataki, S. (1994). Mineral admixtures in concrete: state of the art and trends. *ACI Special Publications*, *144*, 447-447.
6. Hill, G. M. (2002). Peanut by-products fed to cattle. *Veterinary Clinics: Food Animal Practice*, *18*(2), 295-315.
7. Zheng, W., Phoungthong, K., Lü, F., Shao, L. M., & He, P. J. (2013). Evaluation of a classification method for biodegradable solid wastes using anaerobic degradation parameters. *Waste management*, *33*(12), 2632-2640.
8. Bhatt, S. M. (2014). Bioethanol production from economical agro waste (groundnut shell) in SSF mode. *Research Journal of Pharmaceutical, Biological and Chemical Sciences*, *5*(6), 1210-1218.
9. Nagarajan, V. K., Devi, S. A., Manohari, S. P., & Santha, M. M. (2014). Experimental study on partial replacement of cement with coconut shell ash in concrete. *International Journal of science and research*, *3*(3), 651-661.

ISBN: 978-81-932056-2-4

10. Sohal, K. S., & Singh, R. (2021). Sustainable use of sugarcane bagasse ash in concrete production. In *Sustainable Development Through Engineering Innovations: Select Proceedings of SDEI 2020* (pp. 397-407). Springer Singapore.

11. Bheel, N., Aluko, O. G., & Khoso, A. R. (2022). Synergistic and sustainable utilization of coconut shell ash and groundnut shell ash in ternary blended concrete. *Environmental Science and Pollution Research*, *29*(18), 27399-27410.

12. Sada, B. H., Amartey, Y. D., & Bakoc, S. (2013). An Investigation into the use of groundnut as fine aggregate replacement. *Nigerian Journal of Technology*, *32*(1), 54-60.

13. Nimityongskul, P., & Daladar, T. U. (1995). Use of coconut husk ash, corn cob ash and peanut shell ash as cement replacement. *Journal of ferrocement*, *25*(1), 35-44.

14. Mahmoud, H., Belel, Z. A., & Nwakaire, C. (2012). Groundnut shell ash as a partial replacement of cement in sandcrete blocks production. *International Journal of Development and sustainability*, *1*(3), 1026-1032.

15. Okpala, D. C. (1987). Rice Husk Ash as Partial replacement in concrete: The Nigeria Society of Engineers. In *Annual conference proceedings, Port Harcourt* (pp. 22-41).

16. Kutshik, J. R., Usman, A. M., & Ali-Dunkrah, U. (2016). Comparative study of protein enrichment of lignocellulose wastes using baker's yeast (Saccharomyces cerevisiae) for Animal Feeds.

17. Sundaram, M. M., & Sivakumar, S. (2012). Use of Indian almond shell waste and groundnut shell waste for the removal of azure a dye from aqueous solution. *Journal of Chemical and Pharmaceutical Research*, *4*(4), 2047-2054.

18. Nwofor, T. C., & Sule, S. (2012). Stability of groundnut shell ash (GSA)/ordinary Portland cement (OPC) concrete in Nigeria. *Advances in applied science research*, *3*(4), 2283-2287.

19. Nyachaka, C. J., Yawas, D. S., & Pam, G. Y. (2013). Production and performance evaluation of bioethanol fuel from groundnuts shell waste. *Am. J. Eng. Res*, *2*(12), 303-312.

20. Prabha, R. T., & Udayashankara, T. H. (2014). Removal of heavy metal from synthetic wastewater using Rice husk and Groundnut shell as adsorbents. *IOSR Journal of Environmental Science, Toxicology and Food Technology*, *8*(7), 26-34.

21. Umoh, A. A., & Olusola, K. O. (2012). Effect of different sulphate types and concentrations on compressive strength of periwinkle shell ash blended cement concrete. *International Journal of Engineering & Technology IJET-IJENS*, *12*(5), 10-17.

22. Adole, M. A., Dzasu, W. E., Umar, A., & Oraegbune, O. M. (2011). Effects of groundnut husk ash-blended cement on chemical resistance of concrete. *ATBU Journal of Environmental Technology*, *4*(1), 23-32.

23. Mehta, P. K. (1994). Rice husk ash--A unique supplementary cementing material. *Advances in concrete technology*, 419-443.

24. Alabadan, B. A., Njoku, C. F., & Yusuf, M. O. (2006). The potentials of groundnut shell ash as concrete admixture. *Agricultural Engineering International: CIGR Journal*.

ISBN: 978-81-932056-2-4

25. Sideris, K. K., & Savva, A. E. (2001). Resistance of fly ash and natural pozzolans blended cement mortars and concrete to carbonation, sulfate attack and chloride ion penetration. *Special Publication*, *199*, 275-294.

26. Sengul, O., Tasdemir, C., & Tasdemir, M. A. (2005). Mechanical properties and rapid chloride permeability of concretes with ground fly ash. *ACI Materials Journal*, *102*(6), 414.

27. Bengtsson, L. P., & Whitaker, J. H. (1986). Farm structures in tropical climates. A textbook for structural engineering and design.

ISBN: 978-81-932056-2-4

COMPARATIVE STUDY OF BRIDGE GIRDERS USING DIFFERENT MATERIALS

Parth D. Patel[1], Arjun M Butala[2], Nirmal S. Mehta[3] and Ankitkumar S. Patel[4]

[1] PG Student, Department of Civil Engineering (U.V.P.C.E.), Ganpat University, Kherva, India.
[2,3,4] Professor, Department of Civil Engineering (U.V.P.C.E.), Ganpat University, Kherva, India.

[1] patelparth2901@gmail.com
[2] amb03@ganpatuniversity.ac.in
[3] nsm01@ganpatuniversity.ac.in

Abstract: The bridges are oldest and important part of infrastructure in this world and their construction evolved over centuries to meet the need of the society. Where the girder is one of component in bridge superstructure that they carry the vehicle load, impact load, carriage way, wearing coat weight and various load. In this present study the several literature papers from diverse journals are reviewed and summarise therefore the further studies requirement indicates that the prestress concrete girder and steel plate girder comparison is visible alternately and plenty of work can be done. This study of work should be done in CSi Bridge software and later the various parameters of girders with change in span length and change in loading condition would be checked for develop stable and effective girder for bridges for change in span length of 20 to 50 m. The conclusion in this study is to compare result of displacement, maximum bending moment at centre, shear at support, and torsion moment at support. The all displacements for all girder are under within a limit.

***Keywords*:** Bending Moment, CSi Bridge, Deflection, PSC Girder, Steel Plate Girder.

1 Introduction

Bridges are the revolutions for the nation. The bridges are one of the oldest and most important pieces of infrastructure in the world. They are also one of the most fascinating, as their design and construction have evolved over the centuries to meet the ever-changing needs of society. Bridges have been built to span everything from small streams to the mightiest of rivers, and their use has expanded from carrying foot traffic to accommodating cars, trains, and even ships.

1.1 Types of Girders

- **Prestress Concrete Girders (PSC):** As the name itself shows, I shape girder bridge is constructed with respected number of girders according to width of the bridge. It is most common type of girder used in small type of bridges.

- **Steel Plate Girders:** Steel could be a solid and tough material, making it perfect for bridges that must be back overwhelming loads. Steel support bridges are for the most part less exorbitant than other bridge sorts, making them an appealing choice for medium to long spans.

ISBN: 978-81-932056-2-4

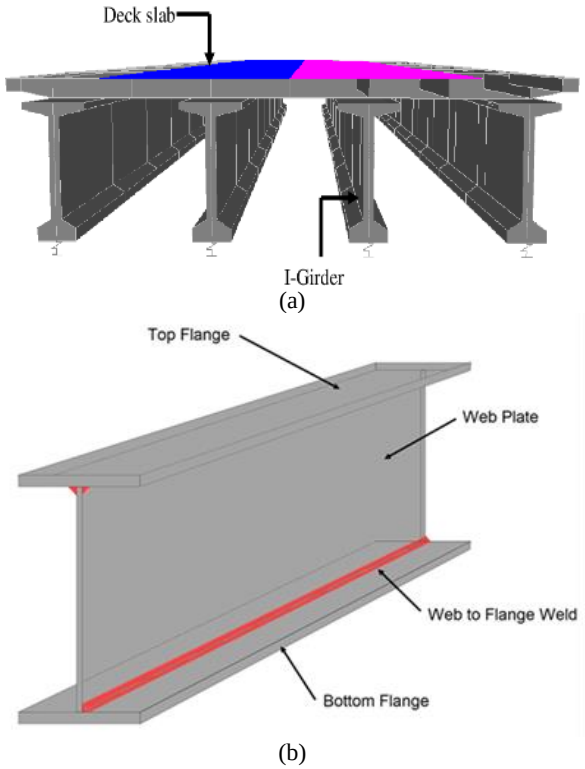

Fig.1. (a) Prestress concrete girder and (b) Steel plate girder

1.2 Literature Review

V. Nazir 2019 has investigated that they made the plan handle helpful for all bridge sorts and has cleared the way to investigate unused concepts and concepts for bigger ventures. Computer application and computer program are presently a fundamentally portion of the bridge lifecycle, right from the conceptual organize to bridge administration. This paper especially focuses on examination of a bridge, which has been planned by Morrice little method, by a program known as CSi Bridge. (Nazir 2019) [1]

B. Sankar and A. Jacob 2013 has investigated that, they have study the deflection of girder and the weight of steel bridge of changing steel-grade, the ratio of panel-aspect, the ratio of web-slenderness on the design result the conclusion is to recognize the performance of the steel plate girder bridge. By use of the Indian standards and the European standards. (Sankar and Jacob 2013) [2]

R. Shreedhar and S. Patil 2016 has investigated that They learning the comparison of the WSM IRC-18(2000) and LSM IRC-112(2011) of the box girder bridge with span to depth ratio 33 and 26. The result from the comparison is the limit state method have

ISBN: 978-81-932056-2-4

preferable for L/D of 33 for span range of 50 to 70 meters and the concrete can be saved from 5 to 12 % in limit state method. (Shreedhar and Patil 2016) [3]

2 Modelling and Methodology

There are many types of girders, including plate girder, box girder, and truss bridges, each with its unique advantages and disadvantages. Choosing the appropriate type of girder bridge for a particular application requires careful consideration of factors such as the span length, traffic volume, site conditions, and budget constraints.

2.1 Design Parameters

For this comparative study, there is three types of bridge girder are selected for modelling work in software.

- Reinforced Concrete Girder
- Prestress Concrete Girder
- Steel Plate Girder

The length of span for girder is varying from 20m to 50m with 10m interval to check the various design criteria such as,[4]

- Deflection at centre
- Maximum Shear at support
- Maximum Bending at centre
- Maximum Torsion

Material Properties for Software Input [5][6]

- Concrete-M50 Grade
- Steel Grade HYSD Fe 550 bars
- High tensile Tension Steel- conforming to IS-1343 (2012)

Table 1. Design Data

Types of girders considered in study	RCC Girder, PSC Girder, and Steel Plate Girder
Bridge span length	20, 30, 40, & 50 meters.
No. of spans	1
Loads acting on structure	Dead, Vehicle live, Moving, Breaking force, seismic loads, Wind load

ISBN: 978-81-932056-2-4

Software	CSI bridge
Grade of concrete	M50
Grade of rebar	HYSD 550
Loading Class	IRC Class A vehicles
Slab thickness	0.22 m
Width of bridge	7.5 m
Number of lanes	2

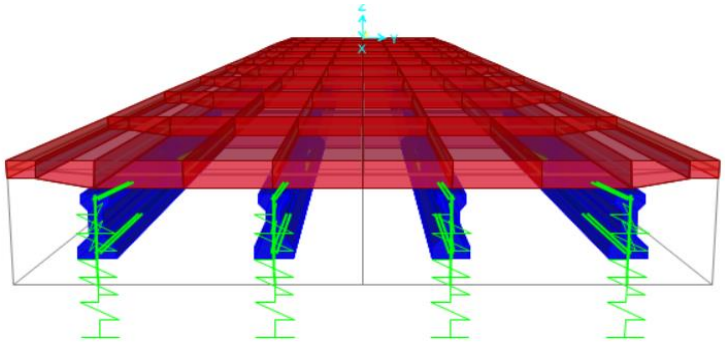

(a)

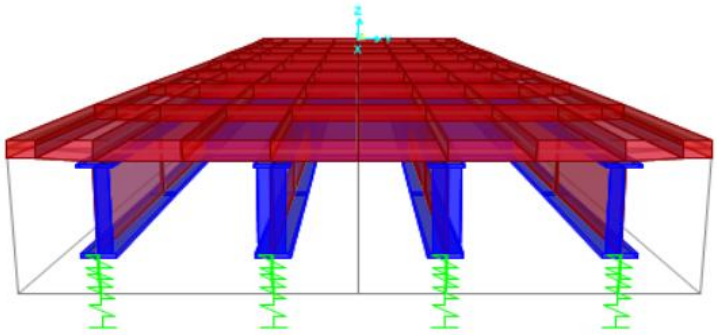

(b)

Fig. 2. (a) PSC girder (b) steel plate girder

The above figure (a) represents the modelling of prestress concrete girder of span length of 20 to 50 m. The figure (b) represents the steel girder of length of span 20 to 50 m.

Table 2. Girder depth

Span Length (m)	RCC (mm)	PSC (mm)	Steel Plate (mm)
20	1650	1300	900
30	1950	1750	1250
40	2400	2100	1650
50	2850	2500	2100

ISBN: 978-81-932056-2-4

3 Result comparison and discussion

The comparison between RCC, PSC and Steel girder is carried out with difference of span length like 20, 30, 40, & 50 meters.

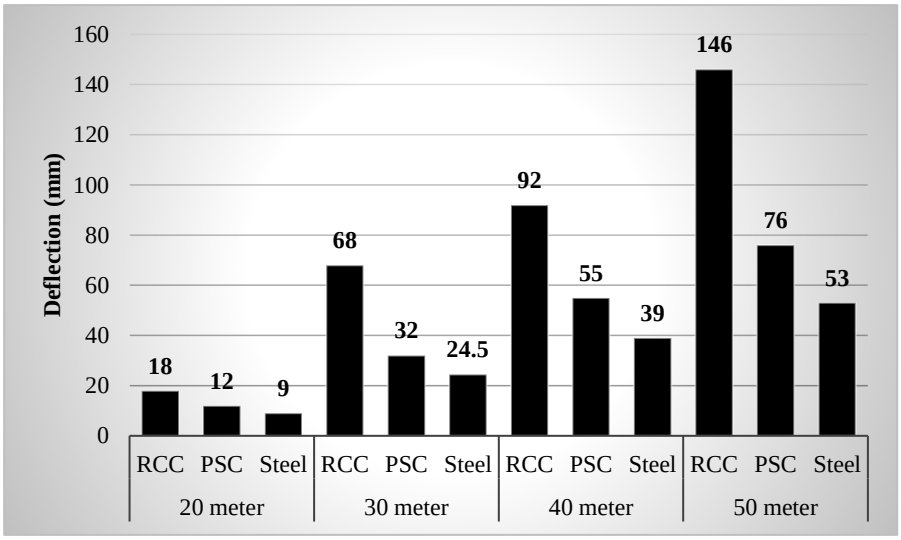

Fig.3. Deflection Results in mm

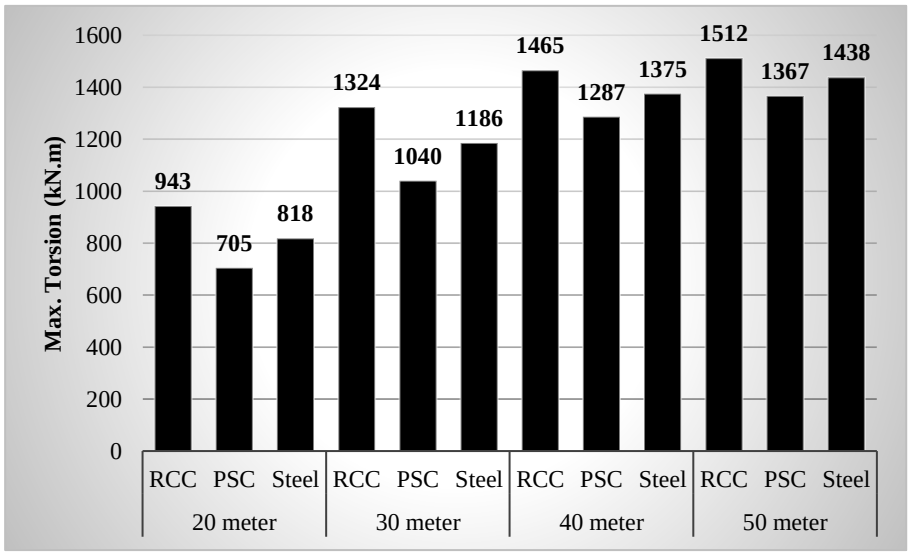

Fig.4. Maximum Torsion Results in kN.m

ISBN: 978-81-932056-2-4

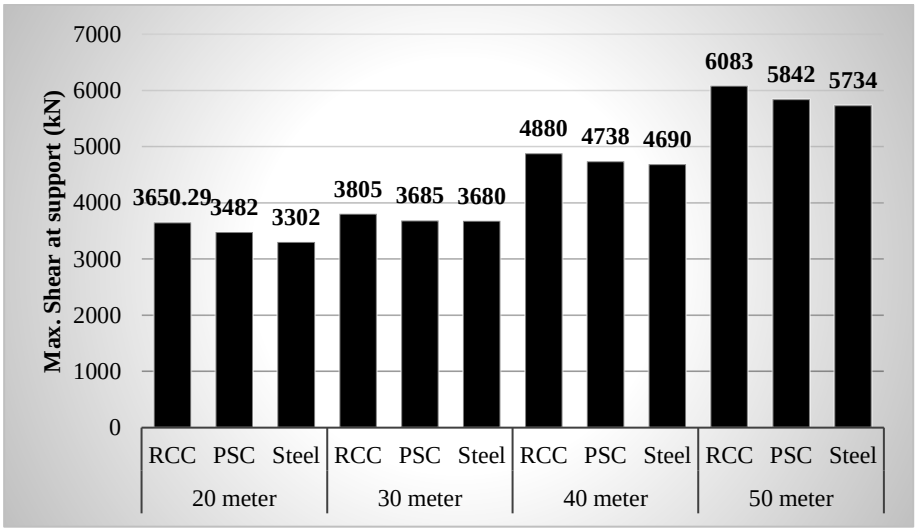

Fig.5. Maximum Shear Force at Support Results in kN

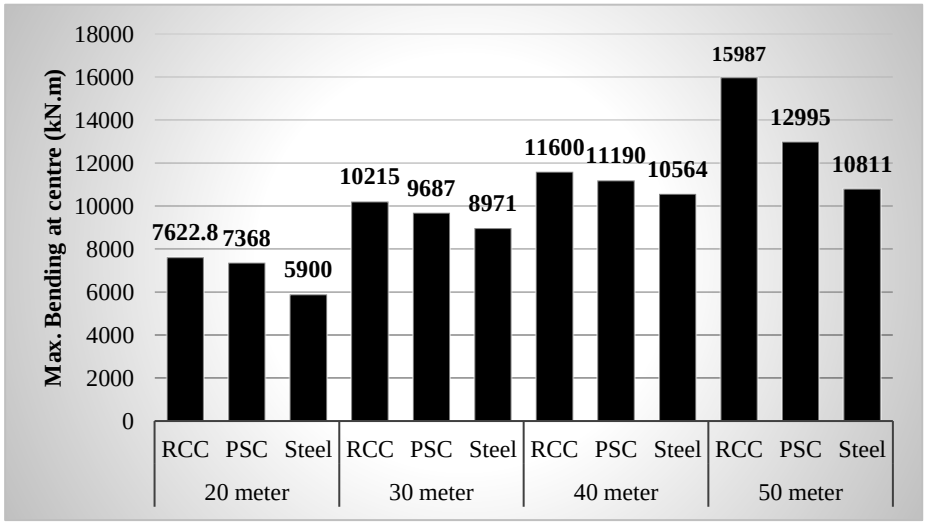

Fig.6. Maximum Bending Moment at Centre Results in kN.m

The obtain results are of 20, 30, 40, & 50 meters span length shows the deflection at centre of span, maximum shear at support, maximum bending moment at centre of span and maximum torsion moment.

4 Conclusions

In the above study, the behaviour of the RCC girders, PSC girders and Steel plate girders are selected for analysis with the change in span length of 20, 30, 40, & 50 meters using the CSI Bridge software. The objective of the study is to check the various design criteria of girders. The results of analysis are in form of vertical deflection at centre,

ISBN: 978-81-932056-2-4

maximum bending moment at centre of span, maximum shear at support section and maximum torsion at support.

Based on the above analysis result, the following conclusion are as follows;

- For vertical displacement of all span length, the RCC girders indicates the most value as compare to PSC and Steel plate girders. The 20 m span, the RCC girder is adopted and for large spans as more than 30 m there should be PSC or Steel plate girders are more superior in design.

- For all span length, the torsion moment is getting high in steel plate girder as compare to other due to its connection with abutments.

- The value of shear is nearly similar in span length of more than 30 m in comparison in PSC and Steel plate girders. For 20 m span approximate 37% variation.

- Relatively RCC girder have highest value in all design criteria for more than 30 m span.

The maximum variation in results of bending moment is for 50m span in PSC and Steel plate girder has difference of nearly 27%.

References

1 Nazir V., & Malhotra S. (2019). Design of PC Bridge and Study by CSi-Bridge. IRJET, 6(9), 1093–1107.

2 Sankar M, & Jacob P.-(2013). Comparison of Steel Railway Bridges. Int. Journal of Engi, 3(2), 1131–1138.

3 Shreedhar R. & Patil S. (2016). Study of P.S.C. -Box Girder Bridge Using-IRC-112(2011). I-Manager's Journal on Structural Engineering, November, 0–7.

4 Kumar, T. P., & Ram, G. P. (2015). Analysis of Super-Structure of the Road and Railway Bridge Crossways River. Int Journal of Scientific Engi and Tech-Research.

5 Ingle V. et.al (2015). Analyze of the Plate-girder-bridge under Class AA Tracked Vehicles Loadings. IJETST, 02(.6), 2423–2444.

6 Kumar, M. H. (2018). Study and Design of Stress Ribbon. Int. Journal of Civil Engi. and Tech., 9(10), 1532–1544.

ISBN: 978-81-932056-2-4

BEHAVIOUR OF TAPERED CHIMNEY WITH VARIATION OF ANGLE

Jay B. Gajjar[1], Nirmal S. Mehta[2], Arjun M. Butala[3] and Jayraj V. Solanki[4]

[1] PG Student,Department of Civil Eng. U.V.P.C.E.,Ganpat University at Kherva,India.
[2,3,4] Professor,Department of Civil Eng. U.V.P.C.E.,Ganpat University at Kherva, India.

[1] gajjar530@gmail.com
[2] nsm01@ganpatuniversity.ac.in,
[3] amb03@ganpatuniversity.ac.in,
[4] jvs01@ganpatuniversity.ac.in

Abstract. In order to vent hot gases from the industrial plant at greater elevation, chimneys are required. The capacity of the plant will influence how the RCC chimney behaves in terms of height to diameter ratio. In the actual practise, choosing the parameter is crucial. To avoid structural issues that could result in the structure collapsing, it is necessary to examine the various loads placed on chimney structures. This study concentrated on three alternatives tapering a ratio for a height of 100 metres: totally, half, and partially half with the aid of software, Moreover, there numerous models are analysed under wind load and seismic load, as a result, the impacts of changing the slope and tapering section of the chimney on various criteria such as base shear, moment, displacement were assessed. Also, the stress pattern checked due to temperature load and it is varying in result with respect to angle of chimney.

Keywords: Bending Moment, Deflection, Shear, Slope gradient.

1 Introduction

As they are known today, chimneys are tall, slender structures that serve a vital purpose. They started off as simple residential vents, but as they became bigger and taller, they started to be called chimneys.

A chimney is a device used to discharge waste gases at a high enough height that, after being diluted by air turbulence, their concentration and that of the solid particles they have entrained are within permissible limits when they reach the ground. A chimney reduces the concentration of several pollutants (SO_2, fly ash, etc.) at the same time and, because it is so reliable, does not need a standby [6].

1.1 Types of Chimneys

The chimney categorises in five parts shows in Fig. 1 named Base on height such as the tall or short chimney, based on number of flues like depended on single flue or multiple flues after that base on Material of construction divided in four parts (Brick, Reinforced Concrete, Steel and FRP). Engineering, Moler and Fire clay included in brick material. Cast in situ Precast and Prestressed categories added in Reinforced concrete in which Cast in Situ has two parts first one is with Tor-steel second one is with mild-steel. Moreover, For Steel chimney has three parts for instance, Mild steel, Stainless Steel and

ISBN: 978-81-932056-2-4

Weathering Steel. Furthermore, Structural Support and lining categories by two parts which is Guyed, Self-Supporting and Lined, Unlined Respectively [6].

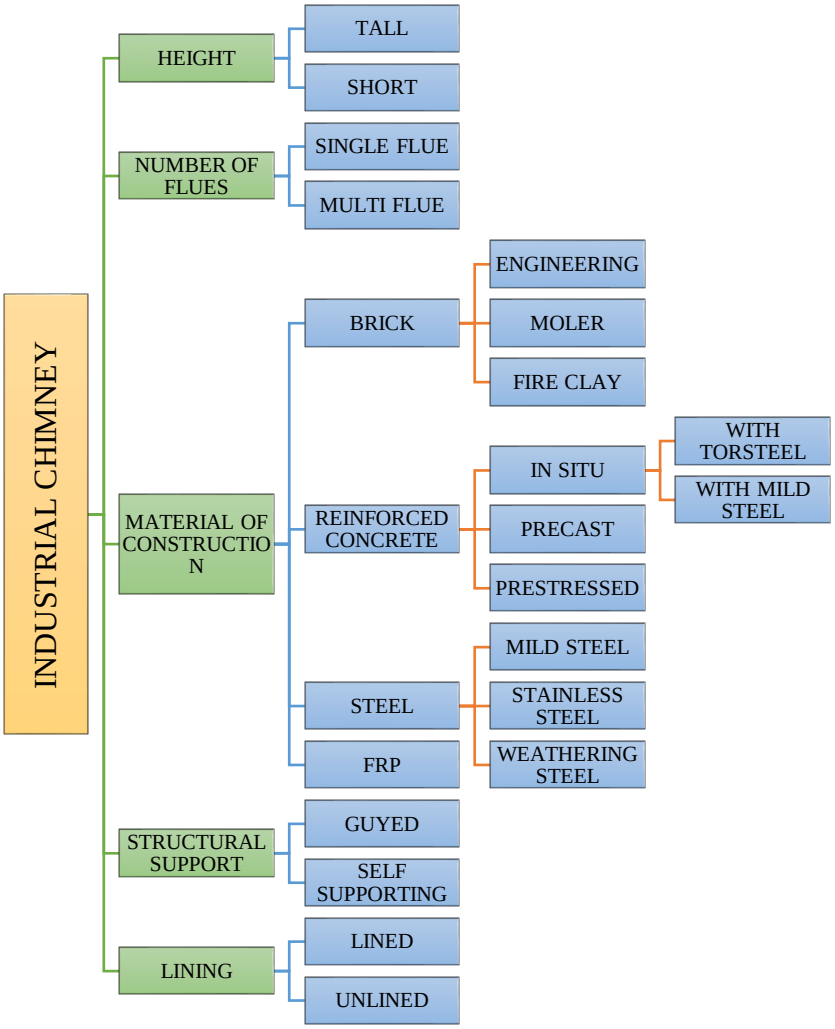

Fig. 1. Types of chimneys

1.2 Function of Chimney

A reinforced concrete chimney typically has a circular shape and their section is shown in Fig. 2, a stiff concrete shell made of a rich concrete mixture of grades M-30 to M-40, and it is reinforced longitudinally vertically and horizontally reinforcement. To lessen the temp. from the internal side of the fire brick lining to the outside side of the concrete wall, a fire brick lining between 100 and 150 mm thick is installed. Moreover, the air gape is kept for maintain pressure.

ISBN: 978-81-932056-2-4

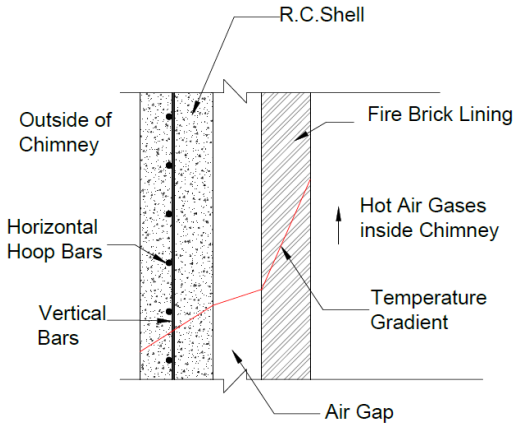

Fig. 2. Parts of RCC chimney

K.R.C. Reddy, O.R. Jaiswal, P.N. Godbole has investigated the loads is calculated as per given in ACI307-98. It has seen that, the seismic zone-5 is slightly close with wind speed is 44 m/s.(Reddy et al., 2011)[4]. Amitha Baiju, Geethu S has found the difference of deflection at top by varying of the height above 275 m. For design author used CED 38:7892 and for the analysis used IS: 4998:1992[part 1] respectively. Along wind and temperature are taken for the research and wind are major impact compared to temperature also found that the lateral deflection at top of chimney increase with the increase in height.(Baiju & Geethu, 2016)[1]. C.V. Siva Rama Prasad, et.al has compared results of wind with earthquake result of a 100m RC chimney. IS:1893(part-4):2005 for Earthquake and CED38(7892):2013 for wind analysis were used. Shear and Bending Moment ascending order with zone factor values also wind force is quite high as compared with the earthquake forces over 100m RCC chimney. In addition, the shape of chimney has to be chosen in order to that the deflection produced at top is well within the permissible limits. (Prasad et al., 2018)[2]. Choppalli Kalyani Ramarao, Patil Yogesh D. has observed stress developed in chimney shell at openings. They had taken two condition without opening and with functional opening and analysis done using STAAD Pro and MS Excel software they found that the stresses in wall with openings have been higher 10 to 16% than without openings.(Ramarao, 2015)[3].

2 Modelling of structure

2.1 Design Parameters

In this study it will be taken different slope ratio of chimney 1in20, 1in35, 1in50 respectively and with three fully, half and partially tapered. The height of chimney is 100m. The height to base ratio remaining constant which is 12 as well as the diameter to thickness ratio also remaining constant 24. Bhuj is the location of the chimney for both loads wind and seismic. Temperature loads are considerable as 150°C. Seismic

ISBN: 978-81-932056-2-4

load as per consideration as per Indian code. Moreover, the Slope ratio, diameter, thickness of wall is mentioned in it.

In results, will be discussed about Base shear, Wind maximum Shear, Wind maximum Moment, Wind maximum Deflection and comparative studies.

Table 1. Design Data

Height of chimney	100 m
Height-to-Diameter Ratio	12
Diameter-to-Thickness Ratio	24
No. platform	2
Grade of Concrete	35
Temperature	150°
Live Load on platform	2 kN/m^2
Seismic Zone value	0.36
Soil	Hard
Location	Bhuj
Reduction Factor	1.5
Importance factor	3
Wind speed	50 m/s
Location	Bhuj
Class	B
Slope	< 3°
Life of structure	100 years
Terrain category	3

3 Modelling

Here modelling using STAAD Pro with different slope ratio of chimney.

Case i: 100M height, 1:20 slope ratio with three different tapered 0%- fully, 50% half and 70%- partially.

ISBN: 978-81-932056-2-4

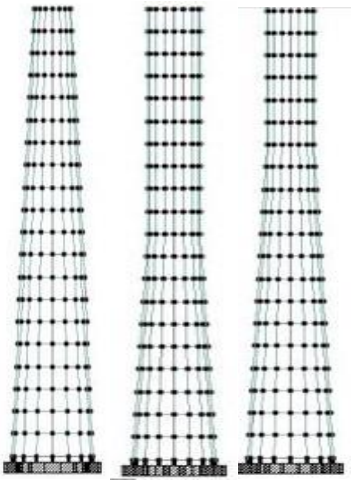

(a) (b) (c)

Fig. 3. 1:20 slope with 0% tapered, 50% tapered and 70% tapered mentioned in (a), (b), (c) respectively.

Case ii: 100M height, 1:35 slope ratio with three different tapered 0%- fully, 50% half and 70%- partially.

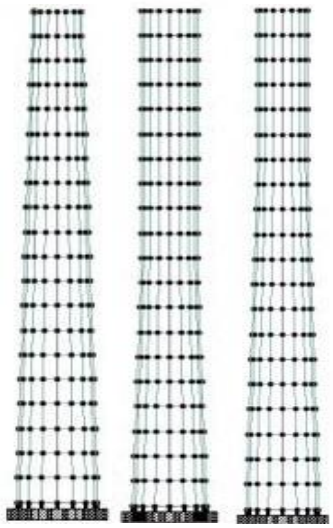

(a) (b) (c)

Fig. 4. 1:35 slope with 0% tapered, 50% tapered and 70% tapered mentioned in (a), (b), (c) respectively.

ISBN: 978-81-932056-2-4

Case iii: 100M height, 1:50 slope ratio with three different tapered 0%- fully, 50% half and 70%- partially.

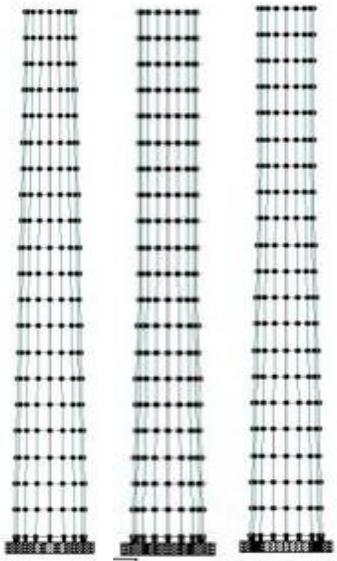

(a) (b) (c)

Fig. 5. 1:50 slope with 0% tapered, 50% tapered and 70% tapered mentioned in (a), (b), (c) respectively

Table 2. Dimensions of chimney

Gradient	Fully Tapered		Tapered	Tapered
	Top	Base	50%	70%
	Diameter (m)	Diameter (m)	Diameter (m)	Diameter (m)
20	8.333	18.333	13.33	15.33
35	8.333	14.048	11.19	12.33
50	8.333	12.333	10.33	11.13

3.1 Result and Discussion

All models are first analysed by for seismic loading to calculate the shear and moments and displacement of all models using STAAD Pro connect edition software. Total 9 models have been analysed and compared.

ISBN: 978-81-932056-2-4

Table 3. Percentage variation individual of chimney

		Seismic Shear Force(kN)	Wind Max. Shear Force(kN)	Wind Max. Moment (kN.m)	Wind Max. Deflection (mm)
	0% and 50%	24.81	31.01	27.75	45.16
1 in 20	**0% and 70%**	16.24	15.59	10.93	37.63
	50% and 70%	11.40	22.36	23.29	5.19
	0% and 50%	13.88	38.43	46.06	34.96
1 in 35	**0% and 70%**	8.37	43.44	48.06	12.20
	50% and 70%	6.40	8.14	3.72	16.87
	0% and 50%	12.48	0.36	4.60	37.40
1 in 50	**0% and 70%**	8.47	9.78	8.96	19.08
	50% and 70%	4.57	9.45	4.57	13.33

Table 4. Percentage of variations

	All slope variation of 1in20, 1in35and 1in 50		
	0% and 50%	**0% and 70%**	**50% and 70%**
Base Shear (kN)	17.06	11.03	7.46
Shear Force (kN)	23.27	22.94	13.31
Moment (kN.m)	26.14	22.65	10.53
Deflection (mm)	39.18	22.97	11.80

1. 100M height, 1:20 slope ratio with three various tapered
2. 100M height, 1:35 slope ratio with three various tapered
3. 100M height, 1:50 slope ratio with three various tapered

ISBN: 978-81-932056-2-4

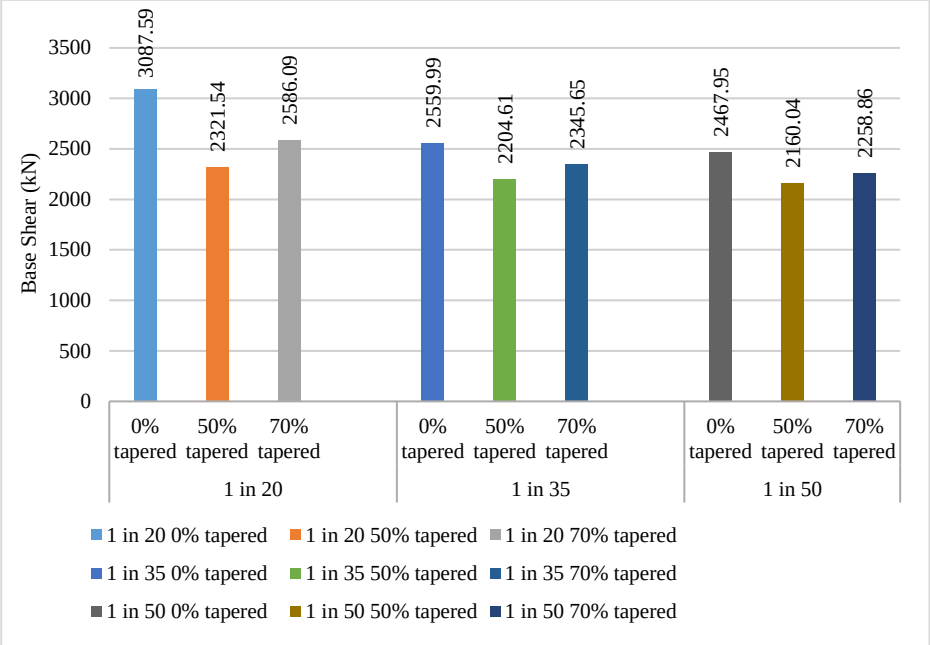

Fig. 6. Comparison of base shear

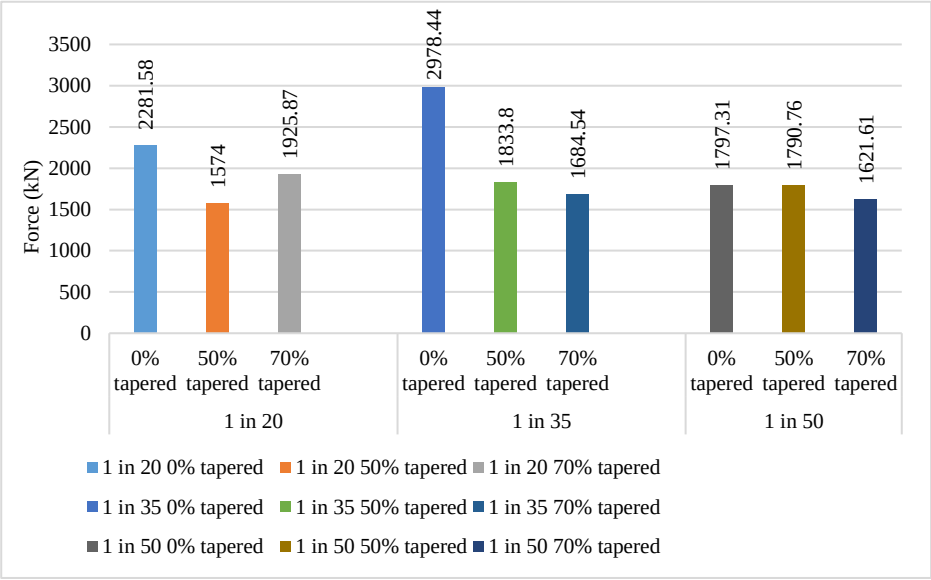

Fig. 7. Comparison of maxi. shear force generated due to wind force

ISBN: 978-81-932056-2-4

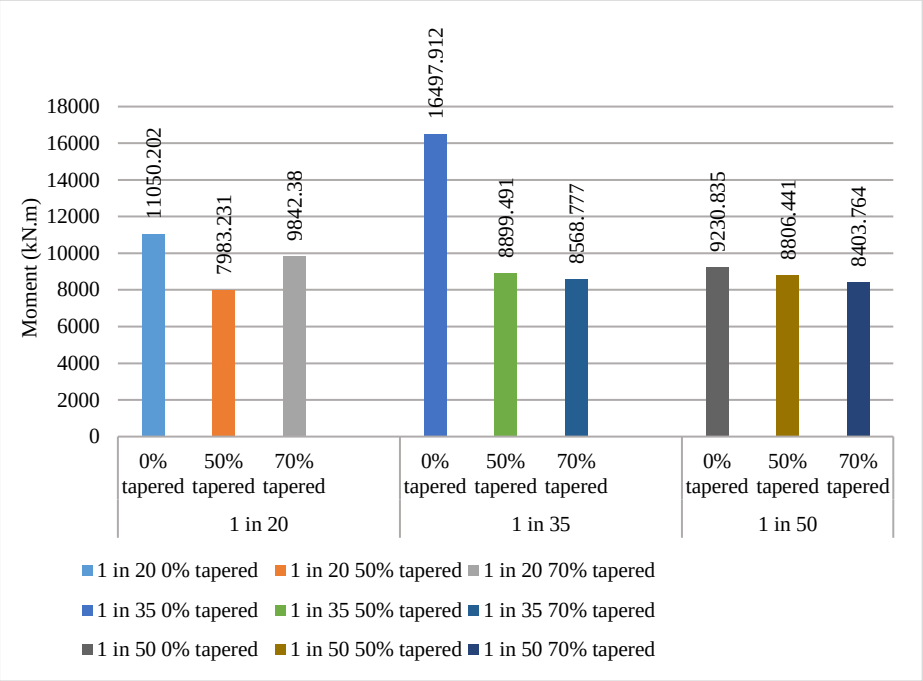

Fig. 8. Comparison of maxi. bending moment generated due to wind force

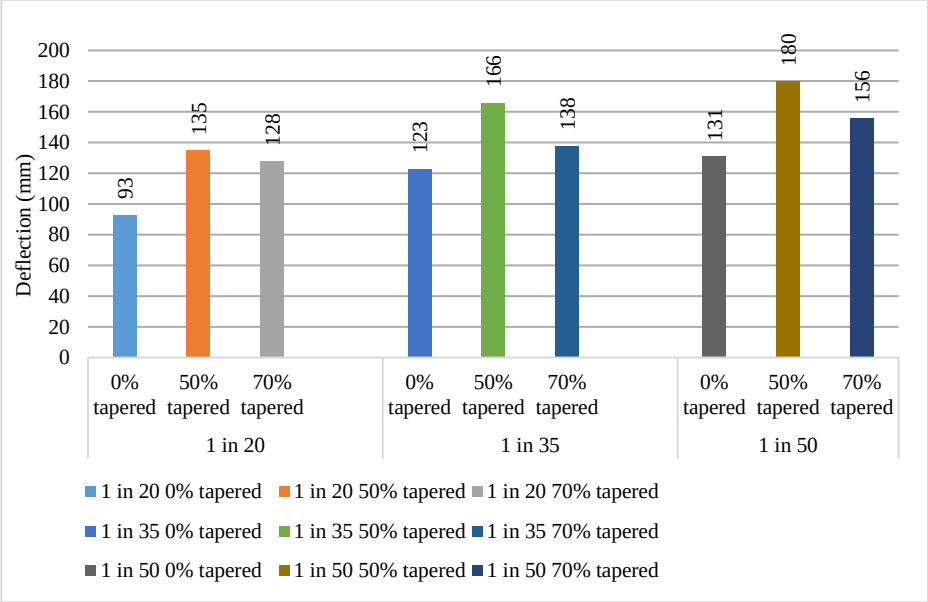

Fig. 9. Comparison of maxi. Deflection

ISBN: 978-81-932056-2-4

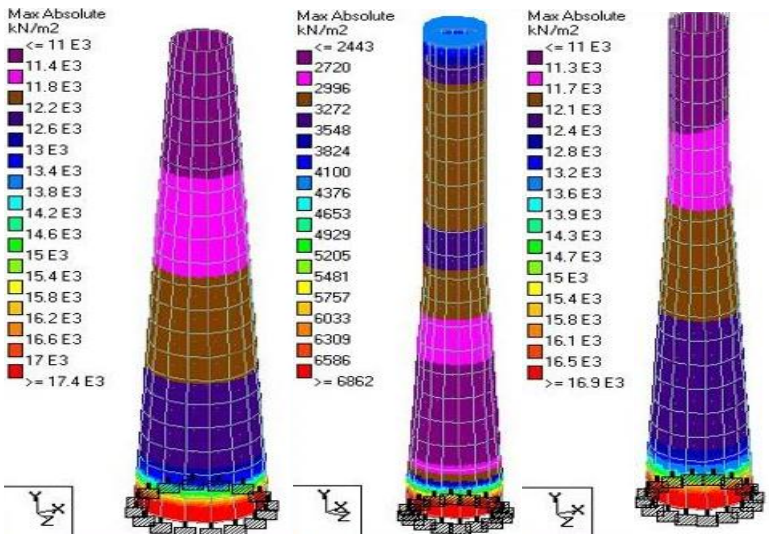

(a) (b) (c)

Fig. 10. Stress diagram of 1:20 slope gradient with 0% (a), 50% (b) and 70% (c) generated due to temperature

4 Conclusions

In this above study, the behaviour of RCC Chimney for analysis with change of slope gradient with different types of tapered using STAAD. Pro CONNECT Edition V22 software. The principal objective is to check various parameters of chimney. The analysed results are in terms of maximum moment and shear due to wind and base shear due to earthquake.

Based on the above analysis result, the conclusion is as following:

- The base shear is consisted higher amount of value in 1:20 with 0% tapered with compare to other fully tapered with slope gradient.
- The maximum amount of deflection is occurred in 50% tapered among the all-slope gradient while the minimum in 0% tapered.
- The maximum shear and moment due to wing is occur in 1:35 with fully tapered. And the moment is reduced significantly in 1:50 slope gradient from 0% to 70% tapered. In 1:20 slope, 0% and 70% tapered is partially difference respectively.
- The stress pattern exits due to temperature load in 1:20 slope. The worst stresses are generated at the bottom and gradually decreasing stresses from bottom to top.
- The percentage of variations of all chimney 1:20, 1:35 and 1:50 their exits in Table .

ISBN: 978-81-932056-2-4

References

1. Baiju A., & Geethu S. (2016). Analysis of RC Chimney as per IS Code. *Int. Journal of Sci. and Research (IJSR)*, *5*(9), 390–394.

2. Rahul K., & D. V. (2018). Analyze of a rcc-chimney 1,2,3. *IJSR.*, *17*(2), 412–415.

3. Rajib, D. S. & S. G. (2015). Seismic Analysis of 275m high RCC Chimney: The Comparison of IS Code Provisions. *Advance in the Structure Eng.: Dynamics, Vol-2, Jan*.

4. Reddy K., & Godbole P. N. (2011) Wind and EQ study of Tall RC Chimneys. *Int. Journal of Earth Sci and Eng*, *04*(06), 20410311.

5. Shaikh M. G., & Khan, H. A. M. I. (2014). Loads for Design of the high-rise RCC Chimney. *Journal of Mech. and Civil Eng.* 12–19.

6. Tall chimney design and construction by S N MANOHAR

7. IS: 875-(2015) part-3- Wind load

8. IS: 1893-(2016) - Earthquake Resistant Design of Structures

9. IS: 4998-Part-1-(1992) - RCC Chimneys

ISBN: 978-81-932056-2-4

PERFORMANCE OF CORNER COLUMN WITH STEEL I BEAM JOINT IN ABAQUS

Divya R. Patel[1], Arjun M Butala[2], Nirmal S. Mehta[3] and Vikram M. Patel[4]

[1] PG Student, Department of Civil Engg (U.V.P.C.E.), Ganpat University, Kherva, India.
[2,3,4] Professor, Department of Civil Engg (U.V.P.C.E.), Ganpat University, Kherva, India.

[1] divyapatel91269@gmail.com
[2] amb03@ganpatuniversity.ac.in
[3] nsm01@ganpatuniversity.ac.in
[4] dean.foet2@ganpatuniversity.ac.in

Abstract: The use of composite construction arises in construction engineering to benefit from both materials. In the last few years, the use of a combination of I steel beam and CFST column is increasing. This study explored the performance of the connection between the CFST corner column and steel beam joint with endplate & bolt using finite element simulation where the variation of endplate thickness (6 mm,8 mm,10 mm,12 mm,14 mm) and loading conditions such as cyclic & monotonic load. As a result, ABAQUS software analyzes load-displacement curves with loading conditions. End plates have a great influence on the strength of beam connections, as they shift the load-displacement curve on the upper side. Loading conditions don't have much effect on the performance of individual beam connections, even when the direction of cyclic load is opposite. The critical stress location is near the joint at a reduced section, providing a safeguard to the connection.

Keywords: CFST-column, End plate, FE-simulation, Load-displacement curve.

1 Introduction

The CFST (concrete-filled steel tube) square is an innovative composite structure that offers several advantages over traditional column systems. It consists of a hollow steel tube section filled with concrete, and it effectively withstands external loads by utilizing the combined strength of steel and concrete, as depicted in Figure 1. This construction technique has gained popularity and has become a new industry standard in recent times. The use of concrete-crammed steel columns in building construction has been revitalized due to its simple construction sequence and the advantages of both steel and concrete frames. It provides structural stiffness and integrity of a cast-on-site concrete building, as well as easy handling and erection. CFST construction is a process of using concrete-filled steel tubes in foreign countries like China, Japan Europe to create composite frame systems. It integrates high stiffness and ductility with alternative load-resisting systems like RCC core tubes or steel shear walls.

ISBN: 978-81-932056-2-4

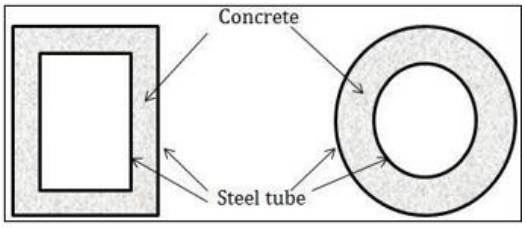

Fig. 1. Concrete Encased CFST Section

1.1 Literature Review

[1] B. R. Niranjana and Eramma H. conducted a study on the response of CFST sections under compressive loads. They compared experimental and analytical results from different design codes (EC-4, ACI-318, and AISC) and found that the experimental results exceeded the analytical results obtained using the codes. This suggests that the existing equations for calculating CFST section strength may not be reliable. (Niranjana 2014)[2]

[2] Burak Evirgen et al. examined the effect of different cross-sectional shapes on the performance of CFST sections under compressive loads. They used various geometries and FEM-based software (ABAQUS) for their analysis. Their findings revealed that the circular cross-section exhibited outstanding performance, indicating that both the steel tube and concrete core in CFST sections are interdependent. (Burak 2014)[3]

[3] Daxu Zhang, Sheng Gao, and Jinghai Gong conducted experiments to investigate the behavior of circular CFST columns subjected to seismic loads. Their study focused on the interaction between CFST columns and I-beams. The results provided insights into the seismic performance of CFST columns in this specific configuration. (Daxu 2017)[4]

[4] Farid Abed et al. studied the response of CFST columns under compressive forces by varying the grade of the inner concrete core and the thickness of the steel tube according to the diameter. They found that reducing the thickness of the steel tube resulted in higher compressive strength, as it offered less confinement. Among different cross-sectional shapes, circular sections exhibited a ductile response and performed exceptionally well. (Farid 2019)[5]

[5] Kumari Beena, Kwatra Naveen, and Sharma Shruti investigated the potential of CFST column and beam connections using experimental and numerical methods. They tested eight specimens with extended end plates and seat angle connections, comparing load-displacement curves. Their findings indicated that the end plate connection outperformed other types of connections. (Beena 2017)[6]

[6] Vishal V. Gore and Popat D. Kumbhar examined the behavior of CFST columns in comparison to regular RCC (reinforced concrete) columns. They highlighted that CFST columns, with their concrete-filled hollow steel tube, offer increased stiffness due to the high modulus of elasticity of the outer steel tube. The confinement provided by the steel

ISBN: 978-81-932056-2-4

tube contributes to the higher compressive strength of CFST sections. Previous works have demonstrated the superior elastic properties and performance of CFST columns. (Vishal 2019) [8]

2 Modelling and Methodology

2.1 Geometry of Building

For our study, we have considered one simple 3-bay building. The plan of the building is 14 m x 10 m. The building is of G+2 type and the height of each floor is 3.0m.the total height of the building taken as is 11.0 m. This Fig 2 Model is prepared for deciding the initial size of connection details using STAAD PRO software.

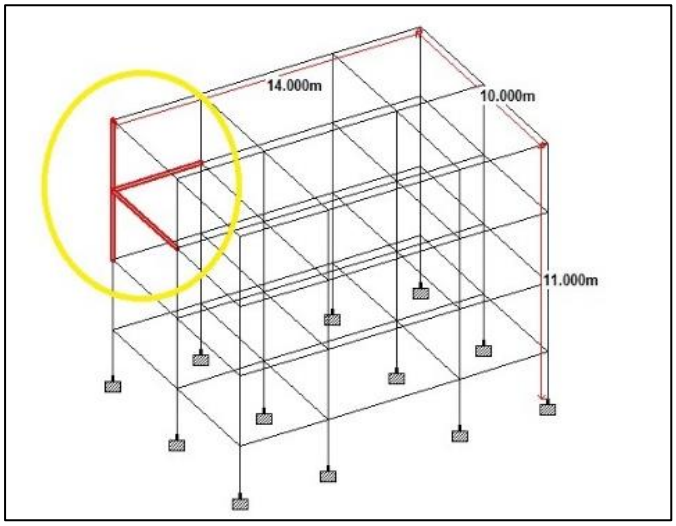

Fig. 2. Corner column the model of STAAD Pro

2.2 Geometry of Connection and Loading Conditions

Parametric study of connection type by changing two parameters to influence design and importance of connection design. Variation of end plate thickness (From 6 mm to 14 mm) Variation of Loading condition (Cyclic and Monotonic).

The model is a corner column connected to two beams, with the same end plate and four-bolt type connection. Different models are prepared to study the behavior of the corner CFST column and beam connection under dynamic loading. Two types of loading are applied at the end of the beam cyclic and monotonic. The standard loading protocol is followed for cyclic loading and monotonic loading using quasi-static cyclic loading history data of the displacement control stage.

Table 1. Summary of loading condition

Loading combination	Loading condition

ISBN: 978-81-932056-2-4

C1C2S	Cyclic Load is applied at both ends of (1&2) and the direction of loading is the same
C1C2O	Cyclic Load is applied at both ends of (1&2) and the direction of loading is opposite
C1M2	Cyclic Load is applied on beam 1 and monotonic load is applied on beam 2
M1C2	Monotonic load is applied on beam 1 and cyclic load is applied on beam 2

Different loading conditions are applied to assembled models, such as bolt load, cyclic load, monotonic and cyclic load, or a combination of both shown in Fig 3. These loading conditions attained the same magnitude of displacement gradually.

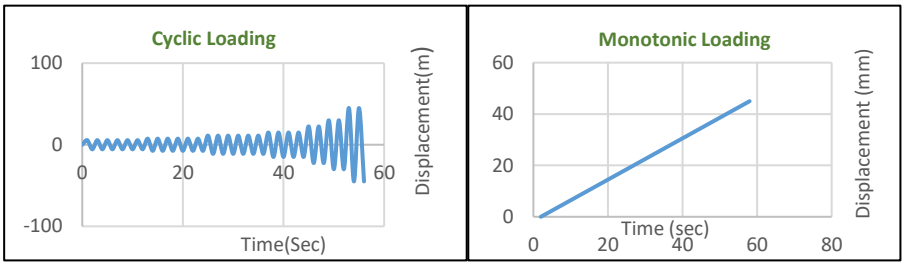

(a) (b)

Fig. 3. (a) Cyclic Loading (b) Monotonic Loading graphical representation

Table 2. Dimension of part of the model

Parts	Dimensions
Beam	ISMB 300 with reduced beam section
Concrete core	Rectangular 500 x 300 mm
Steel tube	10 mm thick
End plate	Plan dimension of 500 x 240 mm

2.3 Material Properties of The Element

The property of a material is important in any analysis, and the Romberg-Osgood coefficient method is used to measure its properties for each element. Steel is used for the outer steel tube, endplate, bolt, and beam, while concrete is used for the inner core to provide the CFST section.

While for the modeling of concrete, a different model is used. As we must consider the nonlinear behaviors of concrete we cannot use the linear curve of the stress-strain of the concrete. We must use a nonlinear curve of the concrete stress-strain. For the analysis concrete damaged plasticity model is used.

3 FE Modeling

ISBN: 978-81-932056-2-4

The model is assembled by assigning elastic and plastic properties to each element. Interactions are provided between different materials and surfaces, such as the beam and endplate, end plate and bolt, and bolt and inner concrete core. The beam and column in the model are subjected to boundary conditions, where the beam is connected to the column through a fixed-end connection, as illustrated in Fig. 4.

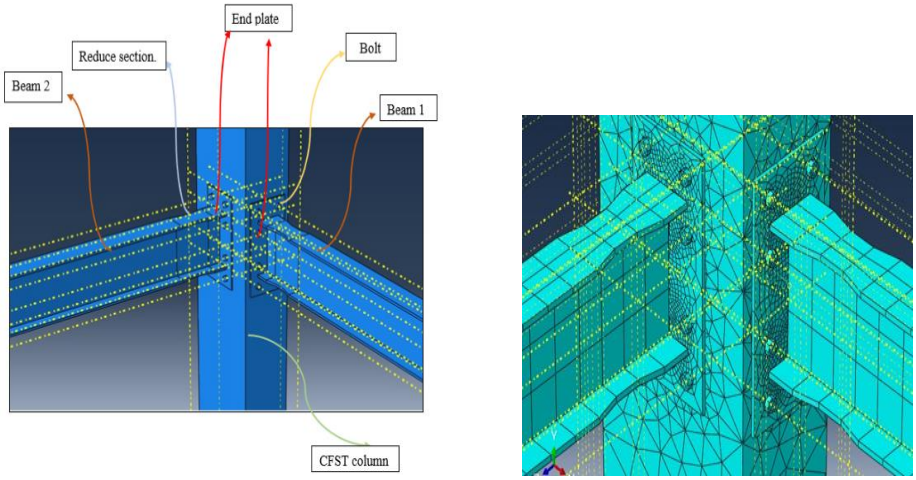

(a) (b)

Fig. 4. (a) Assembly of parts and (b) Meshing of parts

After modeling and applying boundary conditions and loading conditions, the model is run for analysis. The hysteresis plot is taken from the analysis data for each cyclic or monotonic loading case. Various graphs are plotted for different models and conclusions in the graph.

3.1 Comparison of Thickness Results

Under loading Condition C1C2S, cyclic loads are simultaneously applied to both beam 1 and beam 2 in the same direction. In all loading conditions, altering the plate thickness from 6 mm to 8 mm and 10 mm results in an increase in the load-carrying capacity. However, when the plate thickness is further increased to 12 mm and 14 mm, the effect on the load-carrying capacity becomes negligible.

ISBN: 978-81-932056-2-4

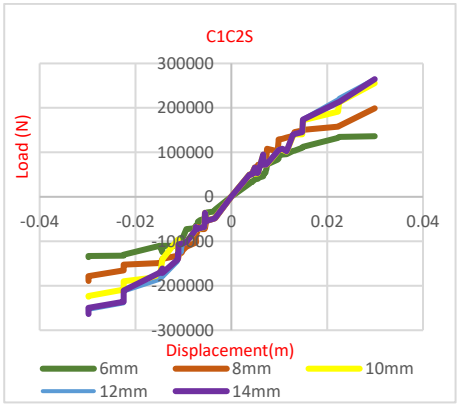

Fig. 5. Loading condition C1C2S

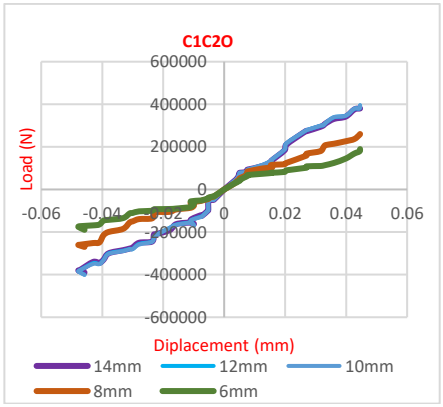

Fig. 6. Loading condition C1C2O

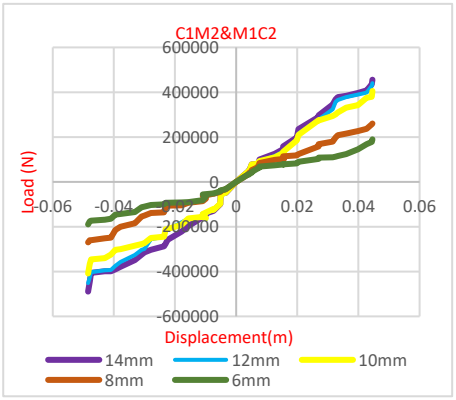

Fig. 7. Loading condition C1M2 & M1C2

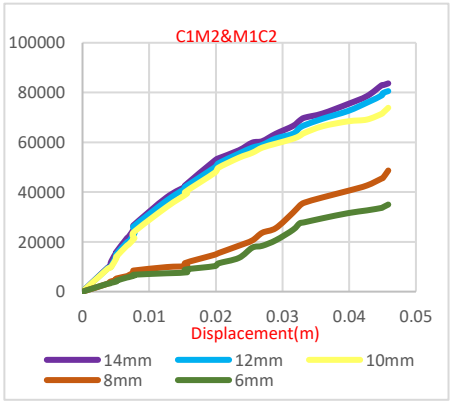

Fig. 8. Loading condition C1M2 & M1C2

3.2 Compression of Thickness Results

In the range of plate thickness from 6 mm to 14 mm, the maximum load carrying capacity is observed for the loading condition C1C2S. For the loading conditions (C1M2 and M1C2), there is a slight decrease in the load carrying capacity. However, the minimum load carrying capacity is seen in the loading condition C1C2O. The variation in capacity is visually represented in the accompanying Fig. 9.

ISBN: 978-81-932056-2-4

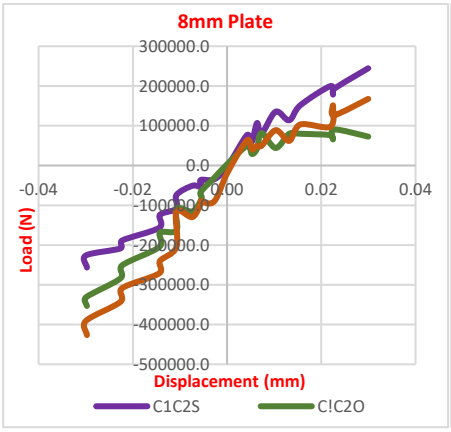

(a) 6 mm plate with various loading

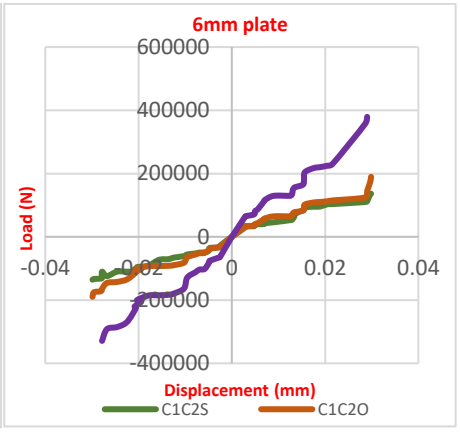

(b) 8 mm plate with various loading

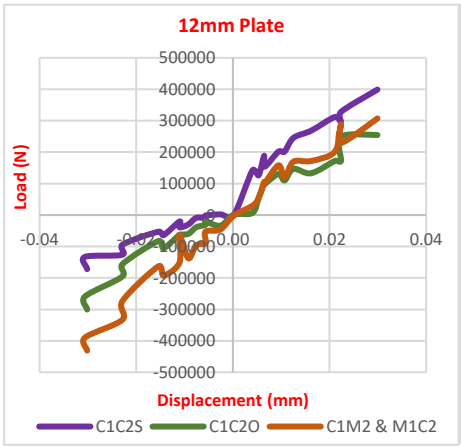

(c) 10 mm plate with various loading

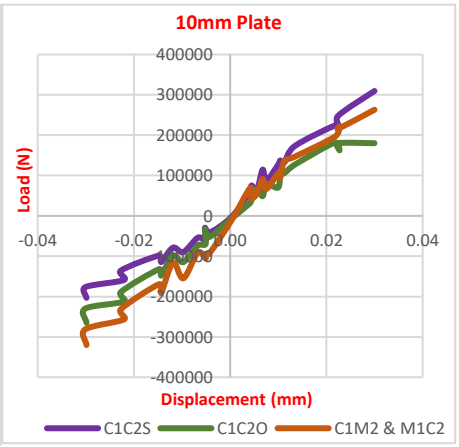

(d) 12 mm plate with various loading

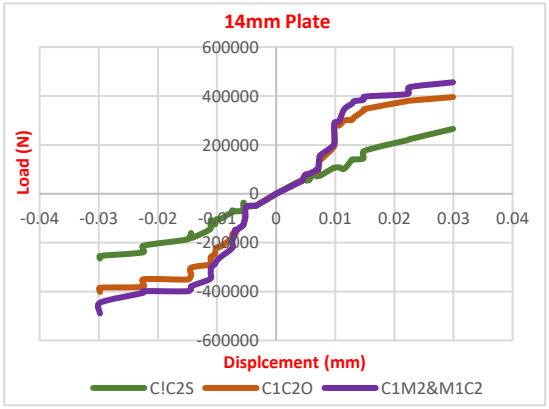

(e) 14 mm plate with various loading

Fig. 9. Load displacement curve for various plate thickness with various loading

ISBN: 978-81-932056-2-4

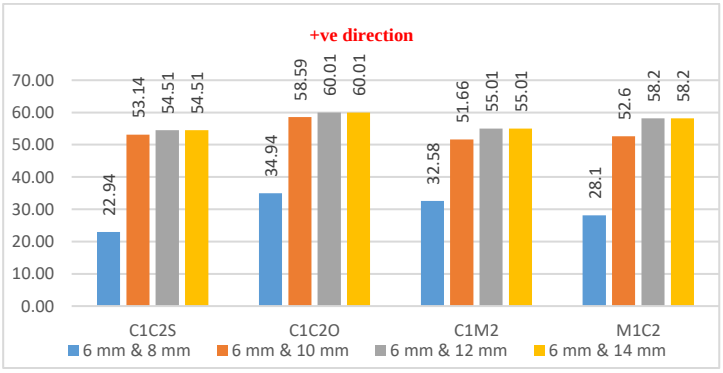

(a)

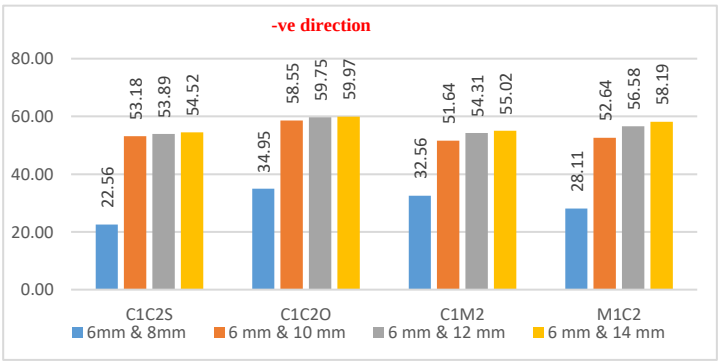

(b)

Fig. 10. (a) +ve direction (b) -ve direction

4 Conclusions

The load-displacement curve and stress distribution of the beam is plotted after analyzing various models in ABAQUS software. Conclusions are drawn after comparing the load-displacement curve and stress distribution of the beam.

- The end plate thickness affects connection strength, with thicker end plates taking more load for the same displacement.

- End plate thickness has a limited influence on connection behavior. As thickness increases from 6 mm to 10 mm, connection capacity increases but not significantly after 12 mm and 14 mm.

- The loading condition has little significant effect on the performance of individual beam connections, as the performance of both beams is similar for each loading condition.

ISBN: 978-81-932056-2-4

- Loading condition 1 (C1C2S) and loading condition 2 (C1C2O) have opposite directions of cyclic load, but their behavior remains similar. Different loading conditions improve connection performance with cyclic load.

- The behavior of the connection is almost unchanged when loading conditions are (C1M2 &M1C2). The critical stress location is located near the reduced section, altered to prevent individual local beam failure before load transfer.

References

1. Akhila Unnikrishan, P Asha Verma Study on CFST column and steel-beam joint under loading. IJRET vol 1 ISSN 2278-0181.

2. B. Niranjan Experimental study on values with different codes of CFST Columns for Concentric Loads American Journal of Eng Research, vol. 3.

3. Burak Evergreen, et.al "Structure behavior of the concrete fill steel-circular element under axial load", vol-80.

4. Daxu Zhang & Shengbin Gao "Seismic study of a steel beam to a circular CFST column with external joint" Journal of the construction steel research 155-166.

5. Farid Abed, Suliman Abdalla, A numerical study on compression of CFST, Journal of the Construction Steel Research, 2013.

6. Kumari beena, Shruti Sharma et.al "Experimental study of a Bolted CFST beam –CFST Column" Springer journal.

7. Md kumara hasan, "FE analysis of CFST column joint with bolts." The Australia Structure Eng 2014 Conference, research gate.

8. Vishal V Gore, Popat D. Kumbha "Function of RCC filled steel-tube column An Examine" IJSR.

ISBN: 978-81-932056-2-4

ANALYSIS AND DESIGN OF GABION WALL USING FINITE ELEMENT METHOD

Manthan R. Rajput[1], Nirmal S. Mehta[2], Arjun M. Butala[3] and Vikki Shah[4]

[1] PG Student,Department of Civil Engineering U.V.P.C.E.,Ganpat University at Kherva,India.
[2] Professor,Department of Civil Engineering U.V.P.C.E.,Ganpat University at Kherva, India.
[3] Professor,Department of Civil Engineering U.V.P.C.E.,Ganpat University at Kherva, India.
[4] Professor,Department of Civil Engineering U.V.P.C.E.,Ganpat University at Kherva, India.

[1] amb03@ganpatuniversity.ac.in
[2] nsm01@ganpatuniversity.ac.in
[3] manthanrajput93@gmail.com
[4] vks01@ganpatuniversity.ac.in

Abstract. The current dissertation's research was primarily concerned with examining the behaviour of the gabions. It's also crucial to note that there is no set standard for the use of gabions as structural components. This form of construction normally does not consider the research of the structural behaviour of these boxes, making it a unique study. This study involves an investigative study of external stability of gabion walls. In this research work the analysis and design of gabion wall is done for various geographical conditions. To check the behaviour of gabion wall for different height to offset ratio are considered. Furthermore, the analysis of gabion wall is carried out using Finite Element Method. The stability of gabion wall is checked for Overturning, Bearing Capacity, and Sliding. It is seen that in the triangular mesh the stress obtained is higher than quadrilateral mesh. The findings of the numerical and analytical research demonstrate that the gabion wall is secure with respect to sliding, overturning, and bearing capacity factors.

Keywords: Gabion wall, Height to offset ratio, Finite Element Modelling, Stability.

1 Introduction

A gabion is nothing more than a stone-filled wire-mesh cage or basket. Gabions are a great tool for construction projects. Examples include lining channels, protecting bridge abutments, and protecting earthen embankments. A gabion is a stone or other suitable material-filled wire mesh cage or basket. Gabions are helpful for protecting river banks and for diverting rivers. The typical gabion basket is made of a single wire mesh piece that can be put together to create a rectangular box with a lid.

If there is a problem with the foundation or seepage, gabion barriers must be installed. These may require some slope movement and significant differential settlement. For high-traffic highways, steep slopes, and terraces, gabion barriers must be taken into consideration. When higher walls are required, these are also appropriate for hill slope angles between 30˚ and 60˚.

Types of gabion wall is categorized into four parts like Gabion Basket, Gabion Mattress, Gabion Sacks, Gabion wire mesh.

ISBN: 978-81-932056-2-4

Peerdawood et al., have conducted research on the analytical investigation of exterior stability variables. The gabion walls' bearing capacity, checking, sliding, and overturning all contribute to their stability. Examining the mechanical behaviour of soil that has been contained by Geo-textiles. numerical analysis of a failed soil gabion wall instance.

Chikute & Sonar, concentrated on flaws and failures found in existing gabion walls. The study takes into account a total of 11 locations with existing gabion wall around the Pune district in India. Investigations are conducted at these locations to find various flaws and potential causes for failures. Also recommended are corrective actions to stop these deflects or failures. Such a study could be helpful in averting failures as well as in laying the groundwork for further research and Gabion wall alterations.

M.Grodecki 2021, has applied water pressure and released from a 4.5 m high wall, and changes in the wall's crest were measured. The results of the experiment simulation using the finite element method were compared to those of the actual experiment. A good correlation between experimentally measured displacements and those predicted by computer simulations was found, particularly during the loading phase. The numerical modelling methodology described here makes it possible to simulate the behaviour of gabion retaining walls in close proximity to reality and may be applied in engineering practise.

Ayyub et al., have studied a 30 m long by 9 m high gabion wall for a residential property in Bahriya-Town Rawalpindi, started to bulge after just one month of construction. In that study, two approaches—analytical and the Finite Element Method with Plaxis-2D software used to assess the structural integrity of the gabion retaining wall. The results of analytical and numerical investigations, with factors of safety (FOS) of 1.19 and 1.07, respectively, show that the gabion retaining wall is only moderately safe. With the maximum strains close to the toe, it was calculated that the displacement at the top was 0.4 m. Finally, it was decided that a practical option would be a stepped-faced gabion wall with 200 mm of concrete at the toe.

Patil et al., studied the behaviour of construction industry which has grown quickly, and different building materials are now used everywhere. In geotechnical engineering, where retaining walls are essential, gabion retaining walls have gained more notoriety. When compared to other retaining walls, gabion walls offer significant advantages in terms of economy, structural stability, and aesthetic appeal. They serve a variety of purposes and have excellent water-draining capabilities. The paper provided an overview of gabion retaining walls, including their types, uses, and stages of construction.

ISBN: 978-81-932056-2-4

2 Modelling

2.1 Design Parameters

Table 1. Parameters for design

Parameters	
Surcharge (*q*)	10 kN/m^2
Backfill Soil	
Density of backfill soil (*γs*)	21 kN/m^3
Backfill soil's internal friction angle (*Ø*)	35˚
Foundation Soil	
Density of foundation soil (*γs*)	20 kN/m^3
Backfill soil's internal friction angle (*Ø*)	36˚
Density of Gabion filling (*γs*)	18 kN/m^3
Slope angle of backfill soil surface (*α*)	10˚
Cohesion (*c*)	5 kN/m^2
Soil Bearing Pressure (*qall*)	140 kN/m^3

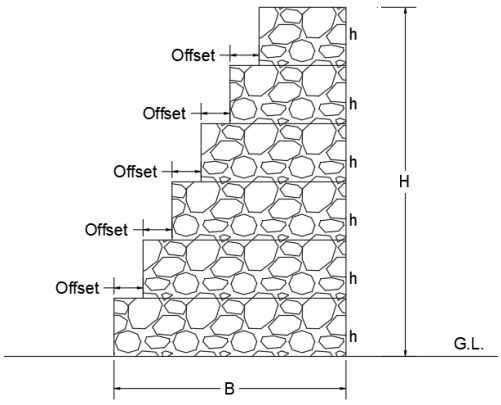

Fig. 1. Cross Section

Table 2. Design Data

Parameters	
Height (*H*)	6m
Base Width (*B*)	4m
height (*h*)	1m, 1.5m
Offset	0.5m , 0.7m ,0.9m

The design parameters are shown in Table-1 which represents the properties that has been used as an input for the design. The data given in Table-1 & 2 are considered after

ISBN: 978-81-932056-2-4

model validation and verified according to the Manual & Codal criteria. Fig. 1 shows the c/s of the gabion wall which was used for designing using STAAD-PRO software.

2.2 Finite Element Modelling

In terms of Finite Element Analysis different models are prepared in STAAD-pro software. Quadrilateral and Triangular meshing is generated in the model. For meshing the plate is divided. for 1m span the plate divided in 10 parts for quadrilateral meshing and for triangular meshing for 1m span the plate divided in 5 parts.

Above Fig. 2 shows the modelling of gabion wall of 0.5m offset and 1m height. the modelling is done in STAAD Pro software. The Fig. 2 (a) shows the quadrilateral meshing the maximum and minimum stress occurred on the face of wall is 4737.88 kN/m^2 and 21125 kN/m^2. The Fig. 2 (b) shows the triangular meshing the maximum and minimum stress generated on the face of wall are 186787 kN/m^2 and 347446 kN/m^2.

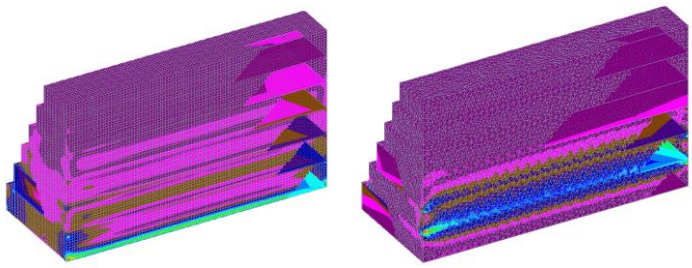

(a) (b)

Fig. 2. Finite Element Model (a) Quadrilateral meshing (b) Triangular meshing (offset 0.5m - height 1m)

Fig. 3 shows the modelling of gabion wall of offset 0.7m and height 1m. The Fig. 3 (a) shows the quadrilateral meshing the maximum and minimum stress occurred on the face of wall is 5859.79 kN/m^2 and 22013.7 kN/m^2. The Fig. 3 (b) shows the triangular meshing the maximum and minimum stress generated on the face of wall are 195246 kN/m^2 and 361130 kN/m^2.

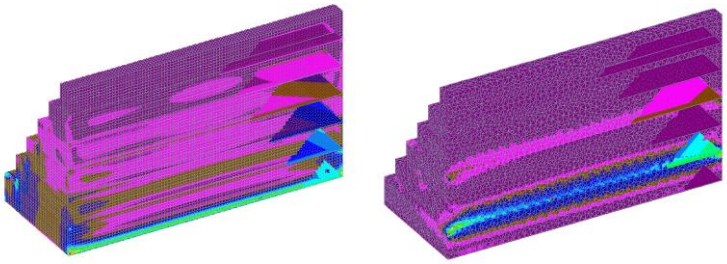

(a) (b)

Fig. 3. Finite Element Model (a) Quadrilateral meshing (b) Triangular meshing (offset 0.7m – height 1m)

ISBN: 978-81-932056-2-4

Fig. 4 displays modelling of gabion wall of offset 0.9m and height 1m. The Fig. 4. (a) shows the quadrilateral meshing the maximum and minimum stress occurred on the face of wall is 4761.49 kN/m^2 and 20807.7 kN/m^2. The Fig. 4. (b) shows the triangular meshing the maximum and minimum stress generated on the face of wall are 177246 kN/m^2 and 335201 kN/m^2.

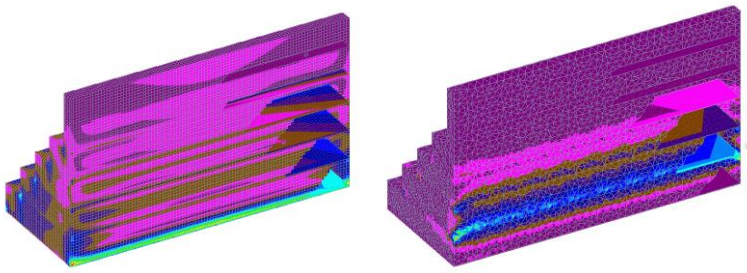

(a) (b)

Fig. 4. Finite Element Model (a) Quadrilateral meshing (b) Triangular meshing (offset 0.9m - height 1m)

Table 3. Abbreviations

Abbreviations	
B	Width of gabion
da	Vertical distance of *Ph* to the toe of the gabion
dg	Horizontal distance of centroid of gabion mass to toe of gabion
dv	Horizontal distance of *Pv* to the toe of the gabion
e	Eccentricity of the vertical resultant *Wv* to centre line of the gabion base
F.S $_{sliding}$	Factor of safety for sliding
F.S $_{over}$	Factor of safety against overturning
F.S $_{bear}$	Factor of safety against bearing capacity
Fr	Resisting forces to sliding
Fs	Sliding forces
H	The wall height
Ka	The coefficient of active soil by coulomb equation
Mo	Over turning moment about toe of gabion
Mr	Resisting moment about toe of gabion
Ø	Backfill soil's internal friction angle
Pa	Total active force on gabion
Ph	Pa's horizontal component
Pv	Pa's Vertical component
q	Surface surcharge pressure
qall	Allowable bearing capacity of soil under gabion
qall	Soil Bearing Pressure

ISBN: 978-81-932056-2-4

Wg	Weight of gabion wall
Wv	Summation of vertical forces
α	Angle of the backfill soil's surface slope
β	Gabion face inclination angle with vertical
γs	Back fill soil density
δ	Angle of wall -soil friction
σmax	Maximum contact stress at base of gabion

2.3 Steps Included in Design

The coefficient of active soil by coulomb equation (Ka)

$$Ka = \frac{Cos^2(\Phi-\beta)}{Cos^2\beta \times cos(\delta+\beta)\left[1+\sqrt{\frac{Sin(\delta+\Phi)\times Sin(\Phi-\alpha)}{cos(\delta+\beta)\times cos(\alpha-\beta)}}\right]^2} \quad (1)$$

Total active force on Gabion (Pa)

$$Pa = \frac{1}{2} x\ ka\ x\ \Upsilon\ x\ H^{\,2} + Ka\ x\ q\ x\ H \quad (2)$$

Horizontal component of *Pa (Ph)*

$$Ph = Pa\ x\ Cos(\delta + \beta) \quad (3)$$

Vertical component of *pa (Pv)*

$$Pv = Pa\ x\ Sin(\delta + \beta) \quad (4)$$

1. Check for Sliding

Factor of safety against sliding $(F.S_{slid})$

$$F.S_{slid} = \frac{Fr}{Fs} \quad (5)$$

Weight of gabion wall (Wg)

$$Wg = g * volume\ of\ wall\ per\ unit\ length$$

Summation of vertical forces (Wv)

$$Wv = Wg + Pv \quad (6)$$

Resisting forces to sliding (Fr)

$$Fr = Wv\ x\ tan\emptyset + c\ x\ B \quad (7)$$

ISBN: 978-81-932056-2-4

$$\boldsymbol{F.S_{slid}} = \frac{\boldsymbol{Fr}}{\boldsymbol{Fs}} > \boldsymbol{1.5\ \ O.K}$$

2. Check for Overturning

Vertical distance of Ph to the toe of the gabion (da)

$$da = \frac{H\,(H+3\ x\ q\ /\ Ys)}{3\,(H+2\ x\ q\ /\ Ys)} + B\ sin\beta \quad (8)$$

Overturning moment about toe of gabion (Mo)

$$Mo = da\ x\ Ph \quad (9)$$

Horizontal distance of centroid of gabion mass to toe of gabion (dg)

$$dg = \frac{\sum Ax}{\sum A} \quad (10)$$

Horizontal distance of Pv to the toe of gabion (dv)

$$dv = Bcos\beta + dasin\beta \quad (11)$$

Resisting moment about toe of gabion (Mr)

$$Mr = Wg\ x\ dg + Pv\ x\ dv \quad (12)$$

Factor of safety against overturning ($F.S_{over}$)

$$\boldsymbol{F.S_{over}} = \frac{\boldsymbol{Mr}}{\boldsymbol{Mo}} \geq \boldsymbol{2\ \ O.K}$$

3. Check for Bearing Capacity

Eccentricity of the vertical resultant Wv to centre line of the gabion base (e)

$$e = \frac{B}{2} - \frac{Mr-Mo}{Wv} \quad (13)$$

$$Check = \frac{6\ x\ e}{B} < 1\ \ O.K$$

Maximum contact stress at base of gabion (σmax)

$$\sigma max = \frac{Wv}{B} x\ 1 + e < qall \quad (14)$$

Factor of safety against bearing capacity($F.S_{bear}$)

ISBN: 978-81-932056-2-4

$$F.S_{bear} = \frac{qall}{\sigma max} > 1 \ O.K$$

Table 4. Results of Sliding, Overturning and Bearing Capacity

	Sliding	Overturning	Bearing Capacity
0.5m offset-1m height	3.09	6.20	1.15
0.7m offset-1m height	2.64	5.46	1.31
0.9m offset-1m height	2.33	4.82	1.57
0.5m offset-1.5m height	3.54	5.39	0.93
0.7m offset-1.5m height	3.27	5.14	1.06
0.9m offset-1.5m height	3	4.81	1.18

Fig. 5 shows the comparison between offset 0.5m – height 1m to offset 0.5m – height 1.5m. The values for sliding (3.09), overturning (6.20) & bearing capacity (1.15) for 0.5m offset – 1m height and the values for sliding (3.54), overturning (5.39) & bearing capacity (0.93) for offset 0.5m – height 1m. It is being observed that both the wall is stable in sliding & overturning but fails to pass the check for bearing capacity in offset 0.5m – height 1.5m. The allowable factor for bearing capacity is 1 and the value for bearing capacity is 0.93.

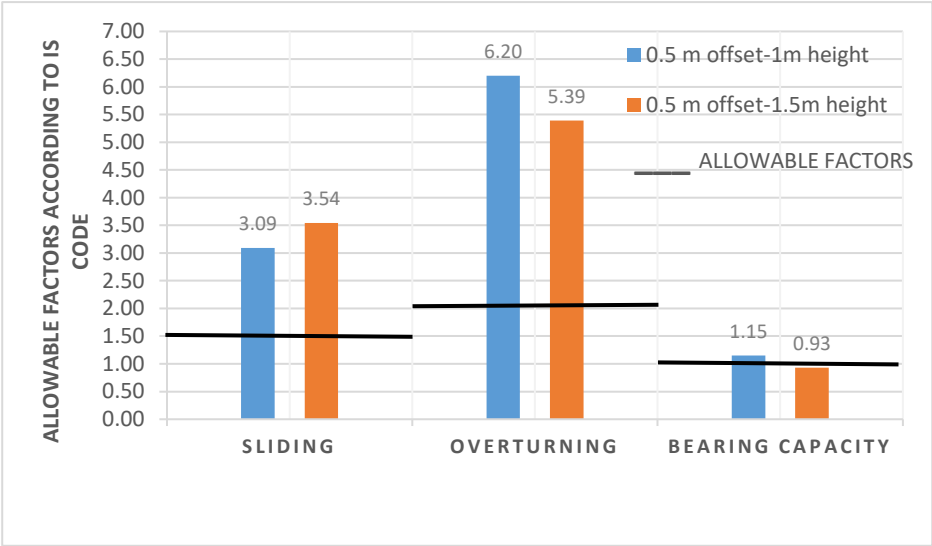

Fig. 5. Comparison of Sliding, Overturning and Bearing Capacity for different height to offset ratio (offset 0.5m - height 1m & offset 0.5m - height 1.5m)

Fig. 6 shows the comparison between 0.7m offset – 1m height to 0.7m offset – 1.5m height. The values for sliding (2.64), overturning (5.46) & bearing capacity (1.31) for 0.7m offset – 1m height and the values for sliding (3.27), overturning (5.14) & bearing

ISBN: 978-81-932056-2-4

capacity (1.06) for 0.7m offset – 1.5m height. It is observed that both the wall is stable in sliding overturning & bearing capacity.

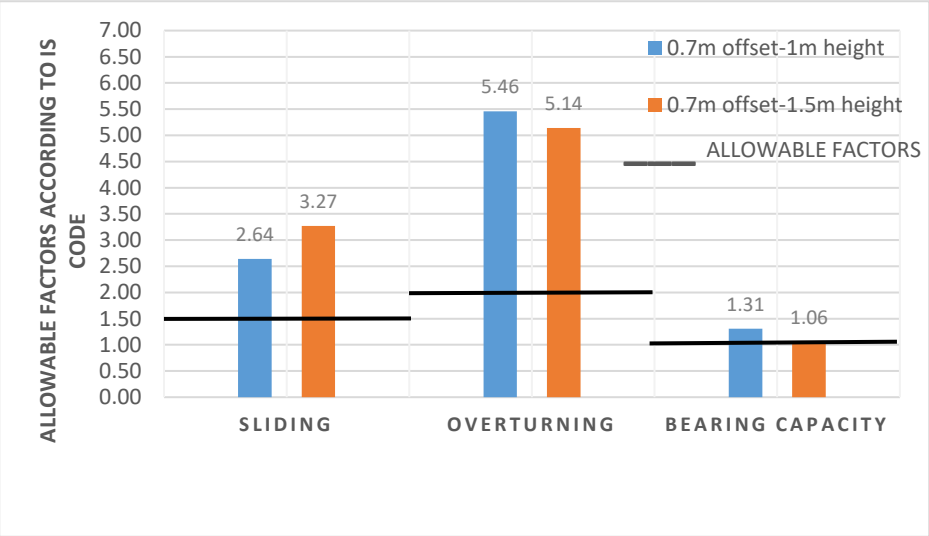

Fig. 6. Comparison of Sliding, Overturning and Bearing Capacity for different height to offset ratio (offset 0.7m - height 1m & offset 0.7m - height 1.5m Results)

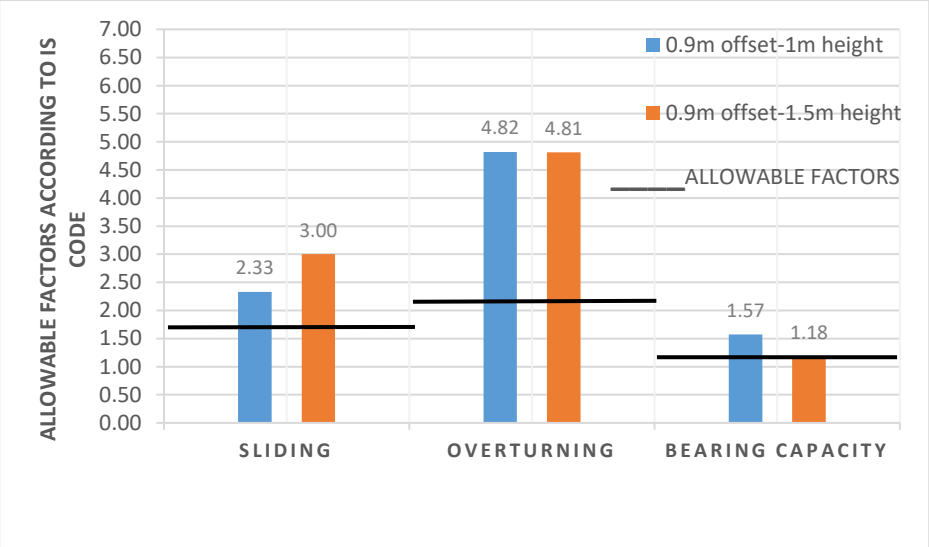

Fig. 7. Comparison of Sliding, Overturning and Bearing Capacity for different height to offset ratio (offset 0.9m - height 1m & offset 0.9m - height 1.5m Results)

Fig. 7 shows the comparison between 0.9m offset – 1m height to 0.9m offset – 1.5m height. The values for sliding (2.33), overturning (4.82) & bearing capacity (1.57) for 0.9m offset – 1m height and the values for sliding (3.00), overturning (4.81) & bearing

ISBN: 978-81-932056-2-4

capacity (1.18) for 0.9m offset – 1.5m height. It is observed that both the wall is stable in sliding overturning & bearing capacity.

Table 5. Finite Element Modelling Software Results

Mesh Type	Model	Minimum Stress (kN/m^2)	Maximum Stress (kN/m^2)
Quadrilateral	0.5m Offset -1m Height	4737.88	21125
Triangular		186787	347446
Quadrilateral	0.7m Offset -1m Height	5859.79	22013.7
Triangular		195246	361130
Quadrilateral	0.9m Offset -1m Height	4761.49	20807.7
Triangular		177246	335201

3 Conclusions

In the study mentioned above, the Gabion wall's behaviour is chosen for analysis with the change in offset to height ratio of offset 0.5m to height 1m, offset 0.7m to height 1m, offset 0.9m to height 1m, offset 0.5m to height 1.5m, offset 0.7m to height 1.5m, and offset 0.9m to height 1.5m using manual calculation. The primary goals of this study are to examine the stability of the gabion walls, including their capacity for bearing weight and susceptibility to sliding and overturning. There is a comparison being made.

The above analysis result, the following conclusion are as follows;

- The comparison between 0.5m offset – 1m height to 0.5m offset – 1.5m height the variation in the value for sliding (14.5%), Overturning (13.06%), & Bearing Capacity (19.13%), it is being observed that the wall is stable in sliding & overturning but fails to pass the check for bearing capacity in 0.5m offset – 1.5m height.

- The comparison between 0.7m offset – 1m height to 0.7m offset – 1.5m height the variation in the value for sliding (23.86%), Overturning (5.86%), & Bearing Capacity (19.08%), the wall is stable in sliding, overturning and bearing capacity.

- The comparison between 0.9m offset – 1m height to 0.9m offset – 1.5m height the variation in the value for sliding (28.76%), Overturning value is somewhat similar in both the cases & Bearing Capacity (24.86%), it is being that the wall is stable in sliding, overturning and bearing capacity.

- For Finite Element analysis it is observed that the stress generated on the face of the wall is higher in the triangular mesh then the quadrilateral mess.

References

1. Ayyub et. Al, "Analysis of the Gabion Retaining Wall by Analytical and Numerical modelling with." UW Journal of Science and Technology, 5, 12–19. (2021).

ISBN: 978-81-932056-2-4

2. Chikute, & Sonar, “Failures of gabion walls”. Int. Journal of Innovative Tech. and Exploring Engineering, 8(11), 1384–1390 (2019).

3. Grodecki, “Numerical modelling of gabion retaining wall under loading and unloading. 2”, 155–164 (2021).

4. Peerdawood, & Mawlood, “Analytical Study for Stability of Gabion Walls”. Journal of Pure and Applied Sciences / Salahaddin University -Hawler, 22(5) (2010).

5. Toprak, B., Sevim, O., & Kalkan, I., “Gabion Walls and Their Uses”. International Journal of Advances in Mech. and Civil Engineering, 3(4), 56–58 (2016).

6. Patil, & Chopade, “A Review Paper on Gabion Wall.” Inter. Research Journal of Engg. and Technology (IRJET), 06(01) (2019).

ISBN: 978-81-932056-2-4

RCC BUILDING ANALYSIS WITH REGARD TO SLOPING GROUND USING SOFTWARE

Dhrumil R Shah[1] Nirmal S Mehta[2] and Chandresh G Patel[3]

[1] PG Student, Ganpat University, Kherva, 384012 Gujarat, India
[2] Assistant Professor, Ganpat University, Kherva, 384012 Gujarat, India
[3] Assistant Professor, Ganpat University, Kherva, 384012 Gujarat, India

[1] dhrumilshah20999@gmail.com
[2] nsm01@gnu.ac.in
[3] cgp01@gnu.ac.in

Abstract. This study presents the G+7 R.C.C. frame structure analysis as per Indian standard codes. Various loads are taken into account when analyzing a structure by Indian national building codes. The software Etabs is used to create the structure's design. ETABS 2019 program is used to analyze the impact of the earthquake load and wind load on the structure at different angles of sloping ground (0°, 10°, 15°, 20°, 25°, 30°, as well as 2 sides 10°). The linear dynamic method is used in conjunction with RSA method to study behavior through top story displacement, story drift, story shear, shear forces induced in the columns at the foundation level, and stiffness of different angles. Decisions are made de- pending on the outcomes of analysis and seismic performance.

Keywords: Sloping Ground, Short column, response spectrum method, Etabs software.

1 Introduction

Buildings on level ground and those in hilly areas are analyzed considerably differently. Due to the site characteristics, buildings on hill slopes have uneven column heights, which causes shorter columns to attract more forces and sustain damage during earthquakes. The RSA method is used in the current study to evaluate two primary types of constructions that are supported by sloping terrain. Building frames with step-backs and step-back-setbacks are taken into consideration, and various criteria like slope and height are analyzed. ETABS v19 was used to analyze each model, and the results were reviewed in terms of storey displacement, storey shear, period, and storey drift. The optimal configuration is then recommended based on the findings and can be used. The lack of available plain land for development is a result of population growth. Without developing & analyzing the model using FEA-based tools, theoretical analysis of the column behavior is highly uncertain. In buildings with this issue, the centres of mass and stiffness don't line up on every floor. Therefore, it is crucial to have reinforced concrete structures in hilly areas, and designing a seismically resistant structure on sloped land is one of the major issues faced by structural engineers. The hilly region is far riskier and harder to work in due to the various types of rock and soil strata.

By comparing sloping terrain with various slopes to plain ground and building using dynamic methods by IS 1893-2016, we performed an analysis using the software. With various sloping ground layouts, the dynamic response and displacement in columns

ISBN: 978-81-932056-2-4

are examined. This study will examine the seismic performance of buildings with both reg- ular and irregular structural layouts. Understanding how buildings react to earthquakes, square roots of summation of squares (SRSS), and wind loads in diverse locations & earthquake zones (4) is the main objective of this research. Using the finite analysis programmed Etabs, they also measured displacement and the maximum force for the building's static and dynamic attributes.

1.1 Literature Review

Paul & Kumar to said that at the foundation level, the building loads are transferred to the hill slope terrain, which could result in failure of the hill slope. In this research, a method to determine the safety factor has been created. The analysis can also take earthquake forces into account. Based on the formulation described in the paper, a com- puter program has been created, and it has been validated by solving a few instances. (Paul & Kumar, 1997).

Birajdar & Nalawade said that the step-back building and the step-back set-back building are the subjects of seismic investigations that produced the results that are given. Using the response spectrum method, a 3-D study that takes into account the torsional impact has been performed. Regarding the feasibility of a building configura- tion on sloping terrain, dynamic response characteristics have been researched, includ- ing basic period, top storey displacement, and base shear action in columns. (B.G. Bi- rajdar, S.S. Nalawade, 2004).

Uttekar & Nayak said that this work examines how RC structures react to sloped terrain. to assess the structure's response through the use of both linear and non-linear analysis. With the aid of instructions based on code I.S. 1893(part I):2002, the analysis will be performed on SAP2000. (Uttekar & Nayak, 2016)

Ghosh & Debbarma said that due to their vertical geometries and mass irregularities, setback constructions are particularly vulnerable to earthquakes, but their susceptibility is increased if they also feature elevational stiffness irregularities. Time history, re- sponse spectrum, and equivalent static force methods are also available. (Ghosh & Deb- barma, 2017).

Mohammad, Baqi, and Arif said framed buildings built on hill slopes exhibit distinct structural behaviour from those built on flat ground because they are inherently asym- metrical, which attracts a lot of shear forces and torsional moments. with the aid of the Response Spectrum Method. Shear pressures created in the columns at the foundation level, fundamental periods, maximum top storey displacements, storey drifts, and sto- rey shear were compared within the analysed configurations of hill constructions. (Mo- hammad et al., 2017).

Raja, Kartheek, and Siva said in order to assess the impact of changing column heights in the ground floor due to sloping terrain, the plan arrangement is kept the same for both structures on the plane and sloping ground. In seismic analysis zone II, the pushover and response spectrum approaches have both been employed to assess the effects of infill during an earthquake. (Raja, Kartheek, Siva, 2017).

ISBN: 978-81-932056-2-4

Mohammed Umar Farooque Patel, A.V. Kulkarni, and Nayeemulla Inamdar said that a 3-D analytical model of eight-story structures for both symmetric and asymmetric building models has been generated in this study. to investigate the impact of the shear wall's effects at various locations during an earthquake and the effect of the ground storey's columns with changing heights due to the slope of the ground. Utilising push- over analysis, seismic analysis has been conducted. (Mohammed Umar Farooque Patel, A.V. Kulkarni, Nayeemulla Inamdar, 2018).

Rajasekhar & Janardhana said that a 21-story RC-framed skyscraper resting on a slope is studied in this research. Buildings built on hill slopes tend to be very asymmet- rical. Buildings located on hill slopes are typically asymmetrical and torsionally linked, making them vulnerable to significant damage from an earthquake's ground motion. reaction spectrum analysis is used to measure the high-rise building's seismic reaction. In this paper, the behaviour of RC-framed buildings resting on sloping ground and flat ground was examined, as well as the effect of infill wall stiffness. (Rajasekhar & Ja- nardhana, 2019).

2 Modelling

2.1 Model Data

Models with 6 bays in the X direction and 4 bays in the Y direction with 5m have been constructed. The wind speed at Darjeeling is 47 m/s, while the seismic zone factor for earthquakes is 4 (0.24).

2.2 Design Parameters

Table 1 depicts design parameters considered in present study.

Table 1. Design Parameters

Ground	0°,10°,15°,20°,25°,30°, 2 side 10°
Floor Height	3 m
Foundation Depth	2.5 m
Slab Thickness	0.125 m
Along Slope	6 bays 5 m
Across Slope	4 bay 5 m
Modulus of Elasticity	25000 N/mm^2
Reinforcement	500 MPa
Earthquake Zone	4
Response Spectrum	5
Building Type	SMRF/Residential Building
Soil Type	Medium soil
Column Size	0.5 × 0.5 m
Beam Size	0.3 × 0.6 m

ISBN: 978-81-932056-2-4

Dead Load + Floor Finish Load On Slab	5 kN/m^2
Live Load On Slab	2 kN/m^2
Load On Beam	7 kN/m
Wind Speed (Vb) m/s	47
Risk Coefficient (k1Factor) m/s	1
Terrain, Height Factor (k2 Factor)	Category 4
Topography (k3 Factor)	0°, 10°, 15°, 20°, 25°, 30°, 2 S 10° 1, 1.14, 1.28, 1.36, 1.36, 1.36, 1.36
Importance Factor for Cyclonic Region (k4)	1

3 Results

Fig. 1 to Figure 12 shows a graph of displacement, drift, stiffness, and shear of all models. And Table 2 to 5 discuss the results of different models with % variation comparision.

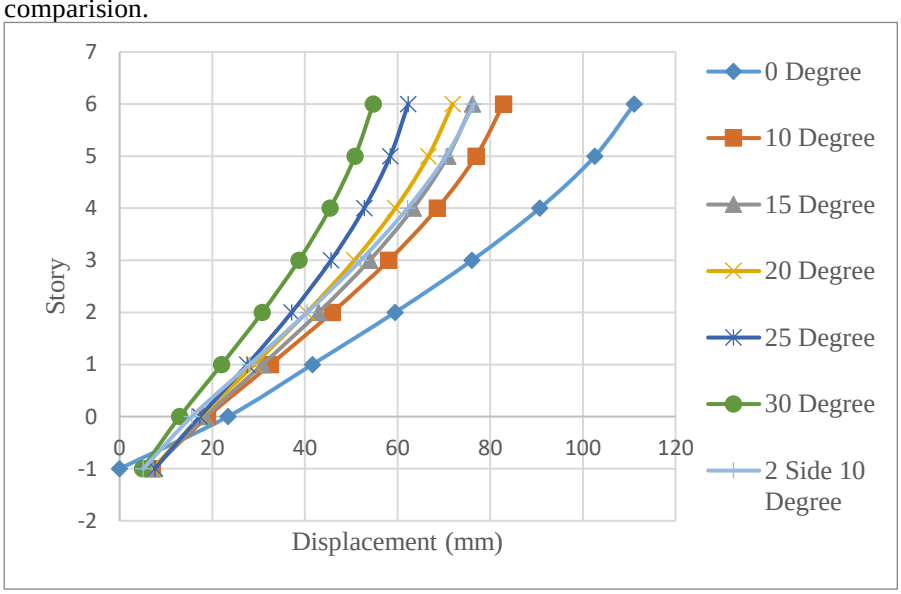

Fig. 1. Eq X displacement in X direction for all model

ISBN: 978-81-932056-2-4

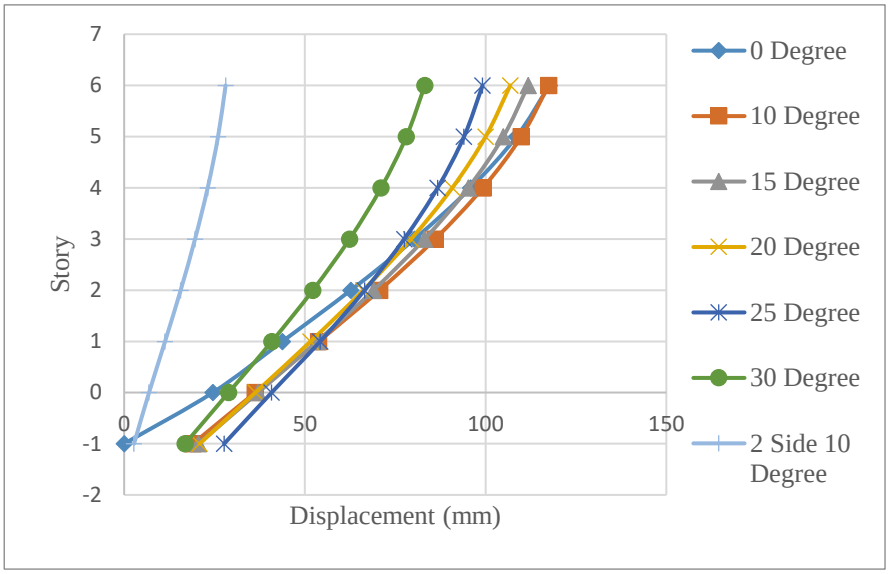

Fig. 2. Eq Y displacement in Y direction for all model

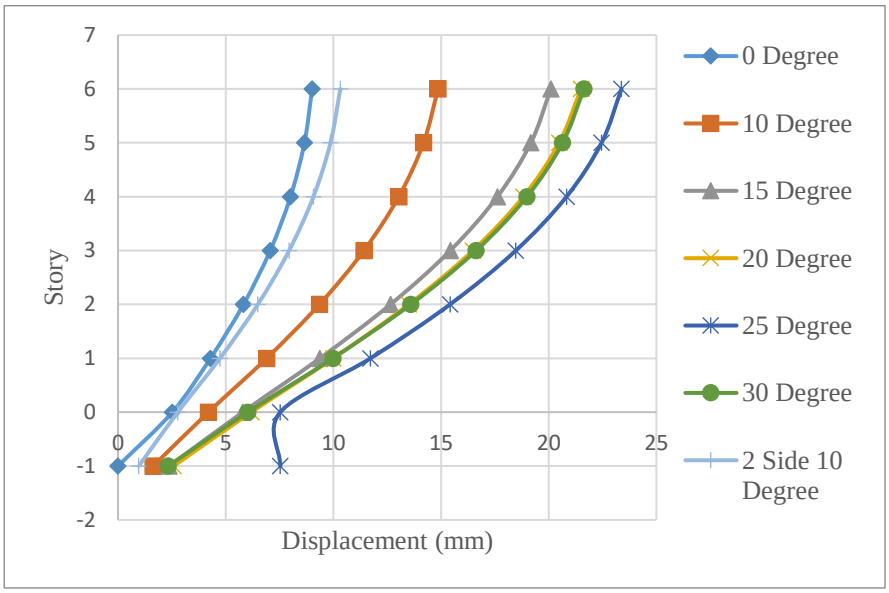

Fig. 3. WL X displacement in X direction for all model

ISBN: 978-81-932056-2-4

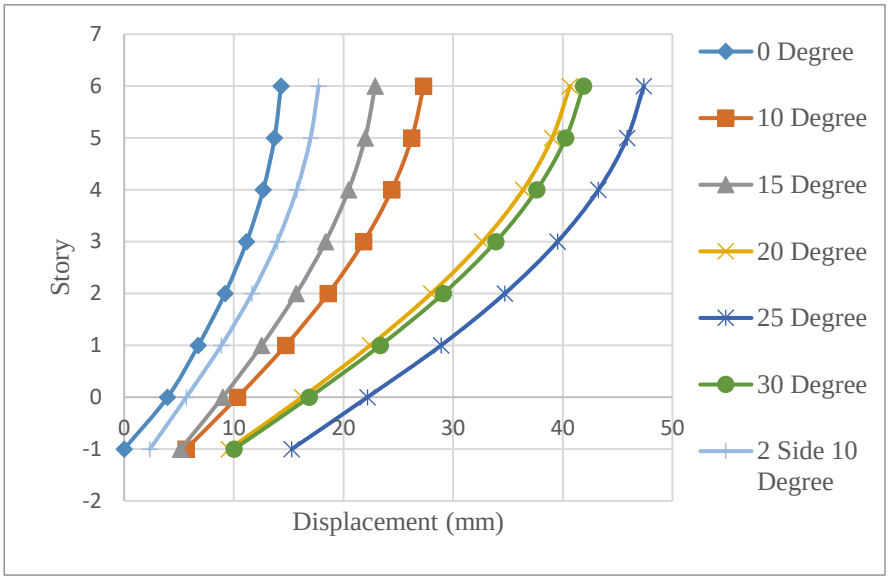

Fig. 4. WL Y displacement in Y direction for all model

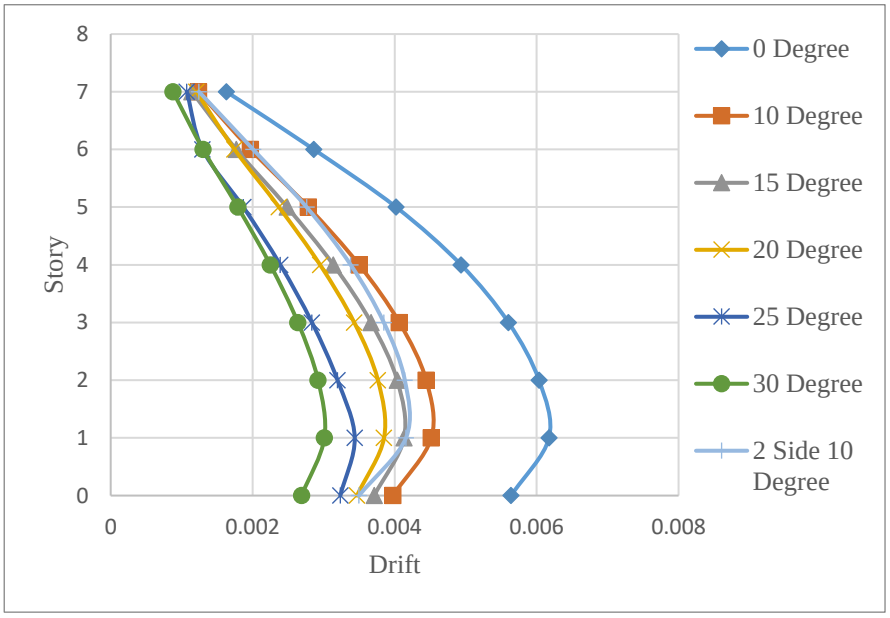

Fig. 5. Eq X story drift in X direction for all model

ISBN: 978-81-932056-2-4

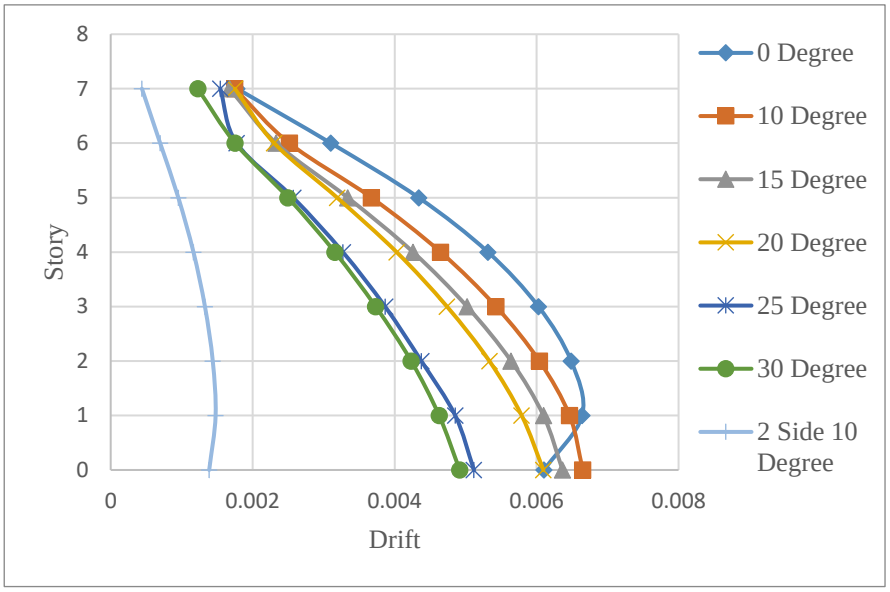

Fig. 6. Eq Y story drift in Y direction for all model

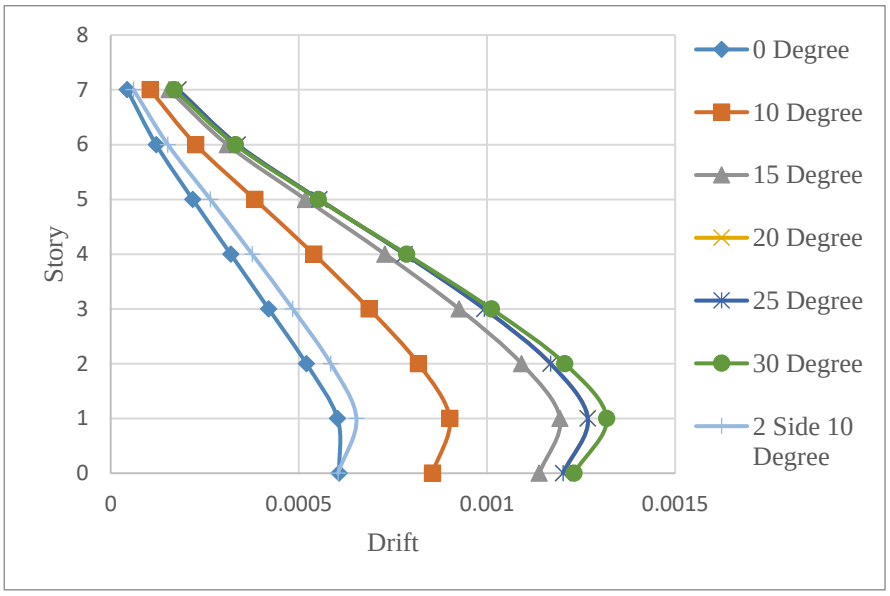

Fig. 7. WL X story drift in X direction for all model

ISBN: 978-81-932056-2-4

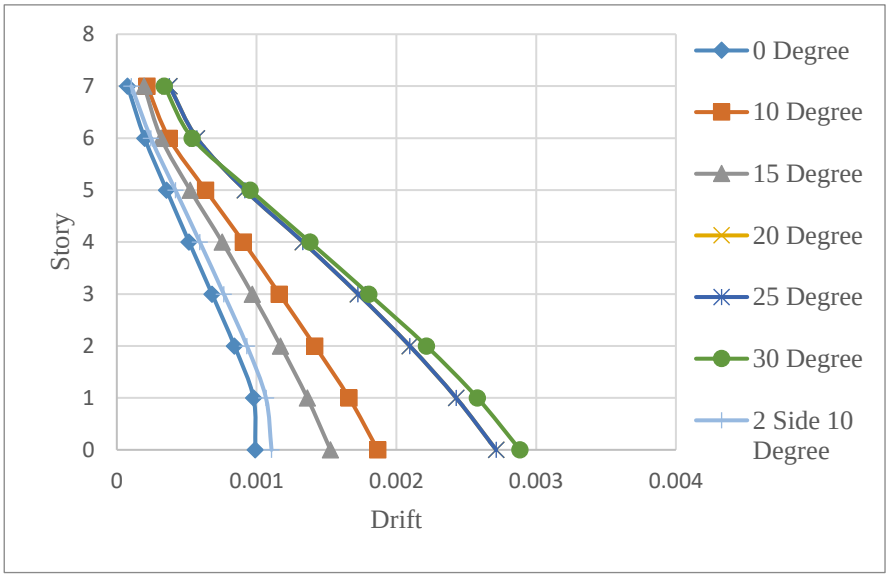

Fig. 8. WL Y story drift in Y direction for all model

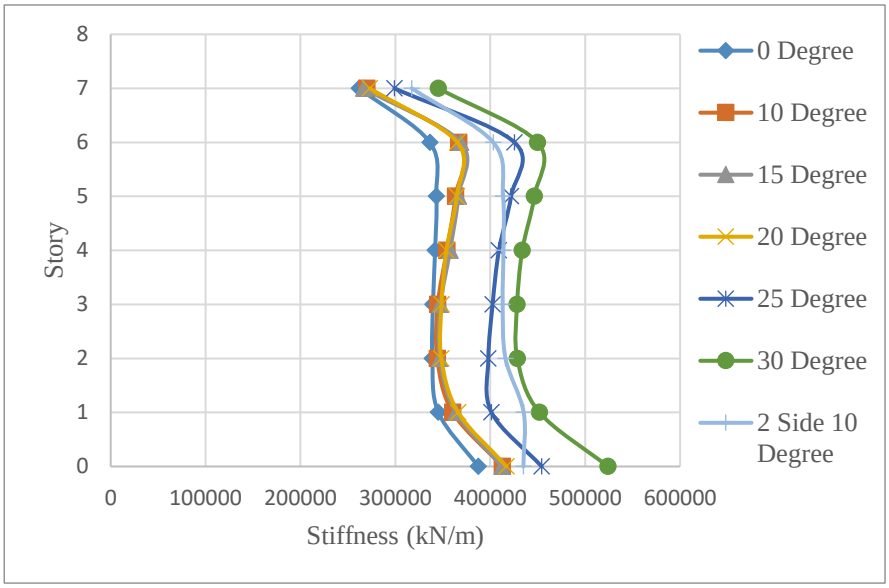

Fig. 9. SRSS X story stiffness in X direction for all model

ISBN: 978-81-932056-2-4

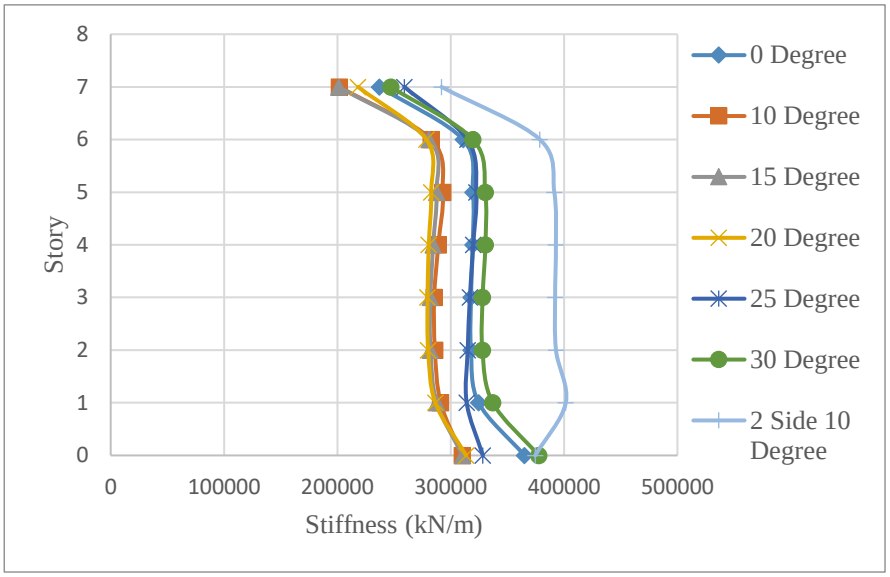

Fig. 10. SRSS Y story stiffness in Y direction for all model

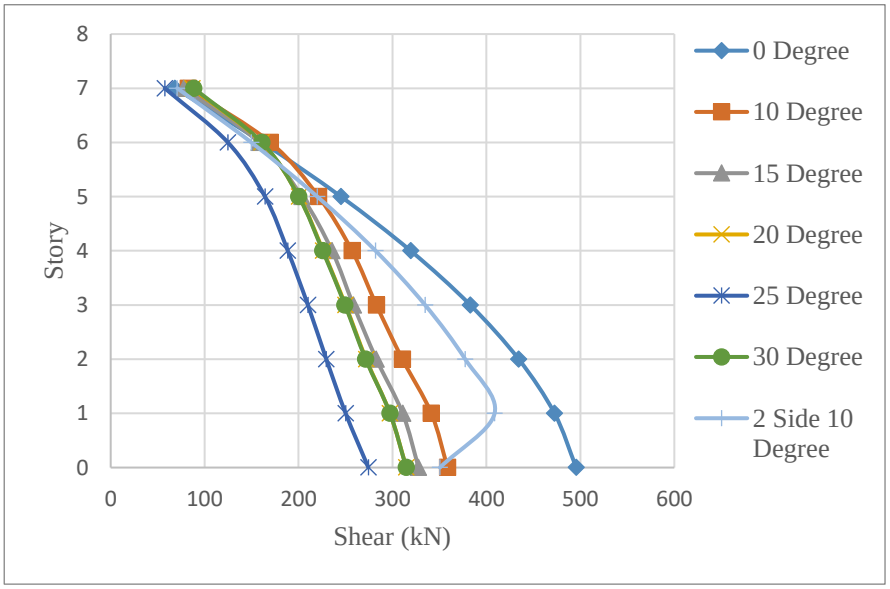

Fig. 11. SRSS X story shear in X direction for all model

ISBN: 978-81-932056-2-4

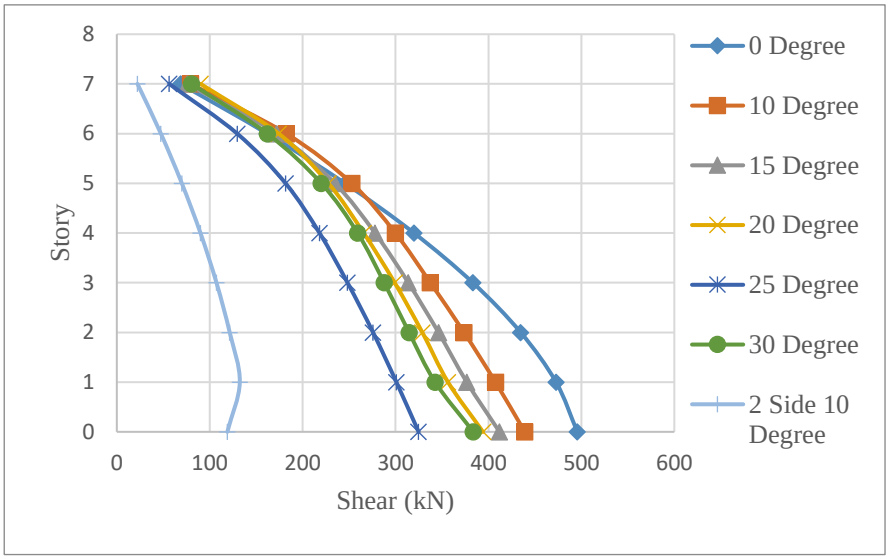

Fig. 12. SRSS Y story shear in Y direction for all model

Table 2. Base Reaction Fz (kN)

Model Name	Output Case	Case Type	Fz kN	%
0°	1.5(DL+LL)	Combination	126640.2805	-
10°	1.5(DL+LL)	Combination	144698.0368	14
15°	1.5(DL+LL)	Combination	148230.6828	17
20°	1.5(DL+LL)	Combination	152961.0133	21
25°	1.5(DL+LL)	Combination	163832.4598	29
30°	1.5(DL+LL)	Combination	174268.0667	38
2 side 10°	1.5(DL+LL)	Combination	157940.9807	25

Table 3. Moment X (kN-m)

Model Name	Output Case	Case Type	Mx kN-m	%
0°	1.5(DL+EQ X)	Combination	1073787.989	-
10°	1.5(DL+EQ X)	Combination	1455950.837	36
15°	1.5(DL+EQ X)	Combination	1503077.447	40
20°	1.5(DL+EQ X)	Combination	1563271.312	46
25°	1.5(DL+EQ X)	Combination	1692761.826	58
30°	1.5(DL+EQ X)	Combination	1817788.786	69
2 side 10°	1.5(DL+EQ X)	Combination	1402571.806	31

ISBN: 978-81-932056-2-4

Table 4. Moment Y(Anticlockwise) (kN-m)

Model Name	Output Case	Case Type	My kN-m	%
0°	1.5(DL+LL)	Combination	1913467	-
10°	1.5(DL+LL)	Combination	2174337	14
15°	1.5(DL+LL)	Combination	2216296	16
20°	1.5(DL+LL)	Combination	2280346	19
25°	1.5(DL+LL)	Combination	2400790	25
30°	1.5(DL+LL)	Combination	2565090	34
2 side 10°	1.5(DL+LL)	Combination	2369498	24

Table 5. Moment Z (kN-m)

Model Name	Output Case	Case Type	Mz kN-m	%
0°	1.5 (DL-EQ X)	Combination	144110.5934	-
10°	1.5 (DL-EQ X)	Combination	138906.7173	-4
15°	1.5 (DL-EQ X)	Combination	133608.9586	-7
20°	1.5 (DL-EQ X)	Combination	127883.5752	-11
25°	1.5 (DL-EQ X)	Combination	126744.156	- 12
30°	1.5 (DL-EQ X)	Combination	127796.2725	- 11
2 side 10°	1.5 (DL-EQ X)	Combination	83510.9639	- 42

4 Conclusions

- The maximum base reaction obtained in model 30° among others increases with 38% variation.
- The maximum moment X is obtained in model 30° among others increases with 69% variation.
- The maximum moment Y (anticlockwise) is obtained in model 30° among others increasing with 34% variation.
- The maximum moment Z is obtained in model 2 side 10° among others increase with 42% variation.
- Modal 0° for Eq force in X & Y direction shows maximum story displacement from all models.
- Model 25° for wind load in X & Y direction shows maximum story displacement from all models.
- Modal 0° in an earthquake in X & Y direction shows maximum story drift from all models.

ISBN: 978-81-932056-2-4

- The largest tale drift from all models is shown by models with wind loads of 25° in the X direction and 20° in the Y direction.
- Modal 30° in X direction shows maximum story stiffness from all models.
- Model 2 side 10° in Y direction shows maximum story stiffness from all models.
- Modal 30° in X direction shows maximum story shear from all models.
- Model 20° in the Y direction shows maximum story shear from all models.

References

1 Paul, D. K., & Kumar, S. (1997). Analysis of slope stability under buildng loads. Engineering for Soil Dynamics and Seismic events, 16(6), 395–405.

2 Uttekar, S. D., & Nayak, C. R. (2016). An evaluation of the RC building's reactivity to earthquakes on sloped terrain. Journal of Engineering Research International, 5(10), 701–704.

3 Ghosh, R., & Debbarma, R. (2017). Performance assessment and failure mitigation of setback buildings with an open ground level on the plain and sloping ground. International Journal of Advanced Structural Engineering, 9(2), 97–110.

4 Mohammad, Z., Baqi, A., & Arif, M. (2017). RC Framed Buildings Resting on Hill Slopes' Seismic Response. In Procedia Engineering (Vol. 173, pp. 1792–1799).

5 Raja, C. N., Babu, K. K., & Rao, N. S. P. (2017). RC Building Study with Shear In Irregular Form. 2(20), 154–162.

6 Umar, M., Patel, F., Kulkarni, A. V, & Inamdar, N. (2018). An analysis of the seismic performance of structures with RC frames on slopes. IOSR Journal of Mechanical and Civil Engineering, 2014(February), 51–58.

ISBN: 978-81-932056-2-4

COMPARATIVE STUDY OF MULTI- STOREY BUILDING WITH MASS AND VERTICAL GEOMETRIC IRREGULARITY USING LINEAR STATIC AND LINEAR DYNAMIC METHOD

Ritesh H. Halai[1], Nirmal S. Mehta[2] and Arjun M. Butala[3]

[1] PG Student,Department of Civil Engineering U.V.P.C.E.,Ganpat University at Kherva,India.
[2,3] Professor,Department of Civil Engineering U.V.P.C.E.,Ganpat University at Kherva, India.

[1] parelritu858@gmail.com
[2] nsm01@gnu.ac.in
[3] amb03@gnu.ac.in

Abstract. The primary objective of this paper is to analyse the performance of multi-storey structures with vertical irregularities using linear static and linear dynamic method. The analysis involves the application of equivalent static method and response spectrum method. The structures located in Zone III with medium soil conditions based on earthquake load specifications (IS 1893 Part 1:2016). Models have been considered for residential buildings with a G+10 storey of mass irregularity and a G+15 storey for vertical geometric irregularity. Analysis is conducted using STAAD.Pro software, comparing various parameters including shear force, bending moment, storey drift, and base shear. A total of 10 models with mass irregularities, along with one regular model, and 3 models with vertical geometric irregularities, along with one regular model, are considered for evaluation. Also in this study we compare all parameters between linear static and linear dynamic method. The analysis shows that the base shear of mass irregularity structure is more than the regular structure and in case of vertical geometric irregularity base shear results are vice- versa.

Keywords: Base Shear, Bending Moment, Shear Force, Storey Drift.

1. Introduction

The circumstance that an earthquake happened in a multi-story building demonstrates what happens when structures are not properly planned and built with sufficient strength they completely collapse. Building behavior during earthquakes is influenced by its overall size, geometry, and shape. One of the challenging tasks in structural engineering is calculating the impact of earthquakes on the structure. There is a lot of study being done in this area to suggest straightforward approaches that may predict results very accurately. Seismic analysis of structures is a crucial component of civil engineering and is essential for determining how buildings and other structures respond to earthquake forces. In order to ensure the safety and resiliency of structures, it involves knowing how they behave during earthquake. Seismic analysis includes a variety of techniques, each providing a unique perspective on the structural response.

There are several variables that affect how a structure will respond to an earthquake, including the buildings ductility, type of foundation, importance of building, damping factor and natural frequency of the structure. New seismic design rules demand that structural engineers do both static and dynamic analysis for the design of the structure

ISBN: 978-81-932056-2-4

of multi-storey buildings as around the world progresses towards the fulfillment of performance-based engineering principles in seismic design of structures engineering.

However, after doing static and dynamic analysis, we are still unsure if the building is secure against local failure caused by the unexpected loss of a column, abnormal stress, such as cylinder blasts, or terrorist attacks. Due to this, it is essential to check structural design decisions on seismic analysis using the appropriate techniques.

1.1 Equivalent Static Method (ESM)

In the subject of structural engineering, analysing complicated structures is a key component in assuring their stability and safety. The Equivalent Static Method, leading to converts the dynamic behaviour of a structure under seismic loads into an equivalent static analysis, is one frequently utilised technique for analysing structures. With the help of the Equivalent Static Method, engineers may more easily understand the complex dynamic behaviour of structures that are subject to seismic forces. This approach makes it possible to develop effective and useful design solutions, assuring the stability and safety of buildings in earthquake-prone areas by reducing the issue to a comparable static analysis.

1.2 Response Spectrum Method (RSM)

In structural engineering, this method is a commonly used method for studying the dynamic response of structures to earthquakes. It provides an effective way to determine the seismic performance of buildings. The approaches based on the idea of a response spectrum, which is a visual representation of a structures highest response to a range of fundamental excitations at various frequencies. In terms of acceleration, velocity, or displacement, depending on the scale used, the response spectrum shows the structural response. Standard seismic design techniques or ground motion data are often used to calculate the response spectrum. Engineers may use it to better understand how a structure might react to various ground motion frequency components since it represents the characteristics of the earthquake ground motion. The response spectrum approach facilitates engineers to rapidly evaluate the seismic performance of structures without carrying out sufficient time-history evaluations for every possible earthquake scenario.

1.3 Mass Irregularity (MI)

Mass irregularities are described as occurring when any storey's effective mass exceeds 150 percent that of the level below. Fig.1. displays the masses of three different stories as Wi, Wi+1, and Wi-1.

ISBN: 978-81-932056-2-4

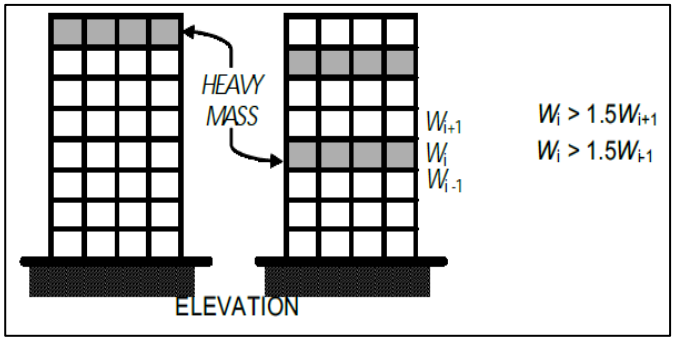

Fig. 1. Mass irregularity

1.4 Vertical Geometric Irregularity (VI)

Vertical geometric irregularity is taken into consideration when the horizontal dimension of the lateral force-resisting system in any storey is larger than 125 percent of that in an adjacent storey. The vertical geometric irregularity is seen in Fig.2.

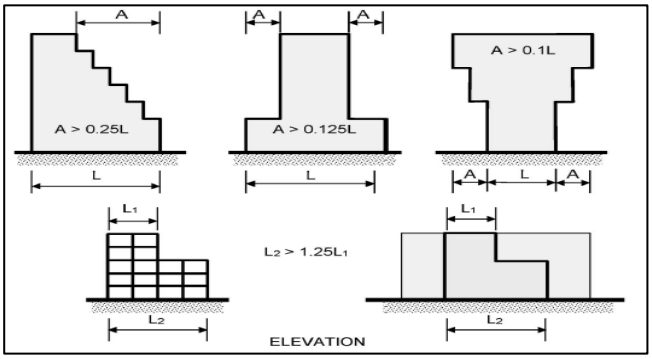

Fig. 2. Vertical geometric irregularity

1.5 Literature Review

Gupta and Pendharkar (2020) have done in this paper analysing multi-storey buildings with and without floating columns in this paper. A multi-storey RCC frame containing G+4, G+10, and G+20 in seismic zone III with and without floating columns was analysed by the equivalent static method. ETABS software is used to carry out the analysis. When comparing the displacement variations between cases 1 and 6 in the X direction, we found that the displacement values are lower than those obtained when comparing case 1 to all other cases, including cases 2, case 3, 4, and 6.(Gupta & Pendharkar, 2020)

Moharana and Mouli (2019) have done Static, dynamic, and progressive collapse analysis of multi-story (G+10) residential buildings by ETABS software In this study, G+10 multi-storey residential buildings are analysed with static, dynamic, and

ISBN: 978-81-932056-2-4

progressive collapse analyses using ETABS. The structure of the G+10 RC frame is analysed both statically and dynamically, along with the study of progressive collapse. Results for zone 2 (case 1), zone 3 (case 2), zone 4 (case 3), and zone 5 (case 4) with medium soil type are compared between static and dynamic results.(Moharana & Mouli, 2019)

Namdev and Singh (2021) have done response spectrum analysis of base-isolated regular and vertical irregular buildings in different types of soil. They create a model of a G+10-story structure with a variety of vertical irregularities. That is located in zone IV and is analysed under various loading conditions. These building models with a fixed base and base isolation devices passed through response spectrum analyses. For the isolated building at the base, the displacement in the response spectrum sharply increases at the upper levels.(Namdev & Singh, 2021)

Jain and Rai (2017) have done in this paper a comparison of the static and dynamic analyses of an irregular, multi-storey structure with an adjustable shear wall position. This paper covers the seismic analysis of a multi-storey irregular structure for both static and dynamic analysis. The ESM and RSM were used as the method for analysis. The data must be used to determine which building would work better in zone III with medium soil quality. For the seismic study, they took into consideration the G+11 storey residential building in zone III analysis in STAAD.Pro software. Three models one without a shear wall, one with a shear wall at the inside, and one with a shear wall at the boundary are taken into consideration for research. (Jain & Rai, 2017)

2. Modelling and Methodology

In this study models have been considered with vertical irregularity. For mass irregularity taken 10 numbers of G+10 storey building models and for the vertical geometric irregularity taken 3 numbers G+15 storey building models with its regular models have been considered. M1, M2, M3, M4, M5, M6, M7, M8, M9 & M10 are mass irregular building models with its regular model M. V1, V2 & V3 are vertical geometric irregular building models with its regular model V. Seismic loading considered as per Indian standard code. For all model design of beams and columns are safe and also they are design optimally.

Table 1. Types of multi-storey models to be prepared for mass irregularity

Type of model	Model Notation
Model with regular structure	M
MI on 3rd floor	M1
MI on 6th floor	M2
MI on 9th floor	M3
MI on 4th and 8th floor	M4
MI on 5th and 9th floor	M5
MI on 6th and 10th floor	M6
MI on 3rd, 6th and 9th floor	M7

ISBN: 978-81-932056-2-4

MI on 4th, 6th and 8th floor	M8
MI on 5th, 7th and 9th floor	M9
MI on 6th, 8th and 10th floor	M10

2.1 Design Parameters

Table 2. Design data for mass irregular building models with its regular model

Grade of concrete	M30
Column size for foundation	0.60 m×0.60 m
Column size above ground floor	0.55 m×0.55 m
Beam size	0.23 m×0.45 m
Unit weight of RCC	25 KN/m^3
Unit weight of Masonry	20 KN/m^3
Poisson's ratio	0.17
Depth of foundation	3
Height of each floor	3
Slab thickness	0.15 m
Self weight of slab	3.75 kN/m^2
Floor finishing	1.5 kN/m^2
Total slab load	5.25 kN/m^2
Masonry external wall	0.23 m
Masonry external wall load	13.8 kN/m
Masonry internal wall	0.115 m
Masonry internal wall load	6.9 kN/m
Parapet wall	0.23 m
Parapet wall load	4.6 kN/m
Live load	4 kN/m^2
Live load for earthquake calculation	2 kN/m^2
Seismic zone	III
Importance factor	5
Response reduction factor	1.2
Damping	5%
Soil type	Medium soil
Period in X direction (PX)	0.66 Second
Period in Z direction (PZ)	0.66 Second

ISBN: 978-81-932056-2-4

Table 3. Design data for vertical geometric irregular building models with its regular model

Grade of concrete	M30
Column size for ground floor to 4th floor	0.60 m×0.60 m
Column size for 5th floor to 12th floor	0.55 m×0.55 m
Column size for 13th floor to 15th floor	0.47 m×0.47 m
Beam size	0.23 m×0.60 m
Unit weight of RCC	25 KN/m^3
Unit weight of Masonry	20 KN/m^3
Poisson's ratio	0.17
Depth of foundation	3
Height of each floor	3
Slab thickness	0.15 m
Self weight of slab	3.75 kN/m^2
Floor finishing	1.5 kN/m^2
Total slab load	5.25 kN/m^2
Masonry external wall	0.23 m
Masonry external wall load	13.8 kN/m
Masonry internal wall	0.115 m
Masonry internal wall load	6.9 kN/m
Parapet wall	0.23 m
Parapet wall load	4.6 kN/m
Live load	4 kN/m^2
Live load for earthquake calculation	2 kN/m^2
Seismic zone	III
Importance factor	1.2
Response reduction factor	5
Damping	5%
Soil type	Medium soil
Period in X direction (PX)	0.72 Second
Period in Z direction (PZ)	0.72 Second

ISBN: 978-81-932056-2-4

2.2 Load Combinations

1. EQX+
2. EQZ+
3. EQX-
4. EQZ-
5. DL
6. LL
7. WX+
8. WX-
9. WZ+
10. WZ-
11. RSX
12. RSZ
13. 1.5 (DL+LL)
14. 1.5 (DL+EQX+)
15. 1.5 (DL+EQX-)
16. 1.5 (DL+EQZ+)
17. 1.5 (DL+EQZ-)
18. 1.2 (DL+LL+EQX+)
19. 1.2 (DL+LL+EQX-)
20. 1.2 (DL+LL+EQZ+)
21. 1.2 (DL+LL+EQZ-)
22. 0.9 DL+1.5 EQX+
23. 0.9 DL+1.5 EQX-
24. 0.9 DL+1.5 EQZ+
25. 0.9 DL+1.5 EQZ-
26. 1.5 (DL+WX+)
27. 1.5 (DL+WX-)
28. 1.5 (DL+WZ+)
29. 1.5 (DL+WZ-)
30. 1.2 (DL+LL+WX+)
31. 1.2 (DL+LL+WX-)
32. 1.2 (DL+LL+WZ+)
33. 1.2 (DL+L+WZ-)
34. 0.9 DL+1.5 WX+
35. 0.9 DL+1.5 WX-
36. 0.9 DL+1.5 WZ+
37. 0.9 DL+1.5 WZ-
38. (DL+LL+RSX)*1.2+0.36*RSZ
39. (DL+LL+RSX)*1.2−0.36*RSZ
40. (DL+LL−RSX)*1.2−0.36*RSZ
41. (DL+LL−RSX)*1.2+0.36*RSZ
42. (DL+LL+RSZ)*1.2+0.36*RSX
43. (DL+LL+RSZ)*1.2−0.36*RSX
44. (DL+LL- RSZ)*1.2−0.36*RSX
45. (DL+LL−RSZ)*1.2+0.36*RSX
46. (DL+RSX)*1.5+0.45*RSZ
47. (DL+RSX)*1.5−0.45*RSZ
48. (DL−RSX)*1.5−0.45*RSZ
49. (DL−RSX)*1.5+0.45*RSZ
50. (DL+RSZ)*1.5+0.45*RSX
51. (DL+RSZ)*1.5−0.45*RSX
52. (DL−RSZ)*1.5−0.45*RSX
53. (DL−RSZ)*1.5+0.45*RSX
54. (0.9*DL+1.5*RSX)+0.45*RSZ
55. (0.9*DL+1.5*RSX) −0.45*RSZ
56. (0.9*DL−1.5*RSX) −0.45*RSZ
57. (0.9*DL−1.5*RSX)+0.45*RSZ
58. (0.9*DL+1.5*RSZ)+0.45*RSX
59. (0.9*DL+1.5*RSZ) −0.45*RSX
60. (0.9*DL−1.5*RSZ) −0.45*RSX
61. (0.9*DL−1.5*RSZ) +0.45*RSX

For linear static analysis load combinations 1 to 37 are considered and for linear dynamic analysis all above mentioned load combinations are considered.

ISBN: 978-81-932056-2-4

2.3 Modelling

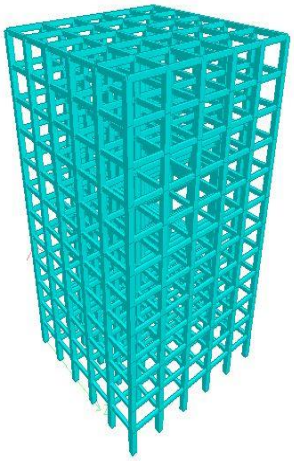

Fig. 3. 3D view of all Mass irregular models

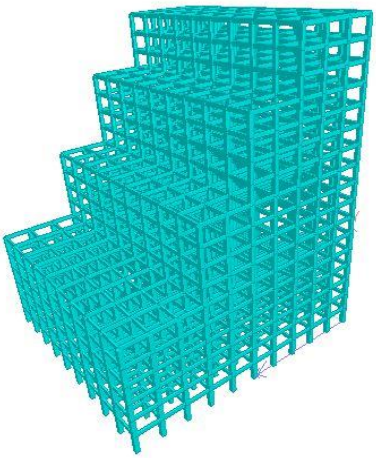

Fig. 4. 3D view of model V1

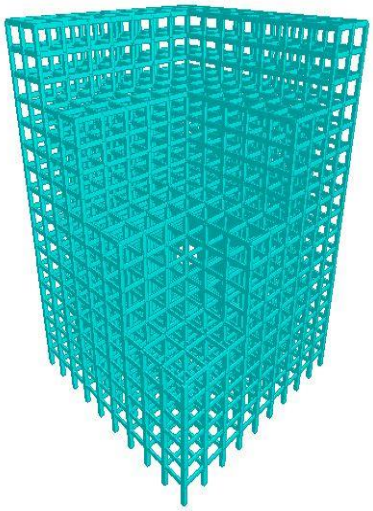

Fig. 5. 3D view of model V2

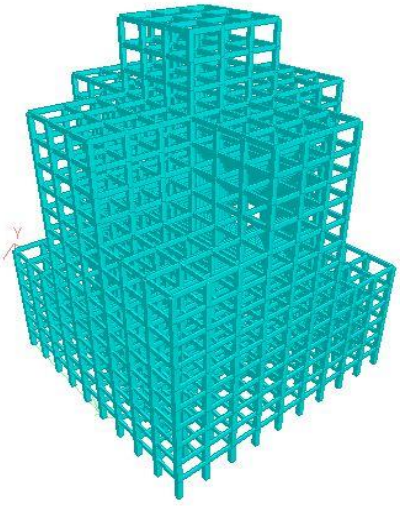

Fig. 6. 3D view of model V3

ISBN: 978-81-932056-2-4

2.4 Result Comparison and Discussion

Result comparison between ESM & RSM for mass irregular building models

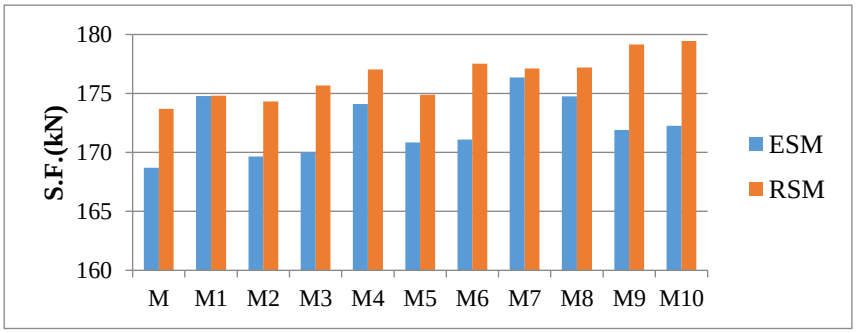

Fig. 7. Comparison of all models maximum shear force for beam

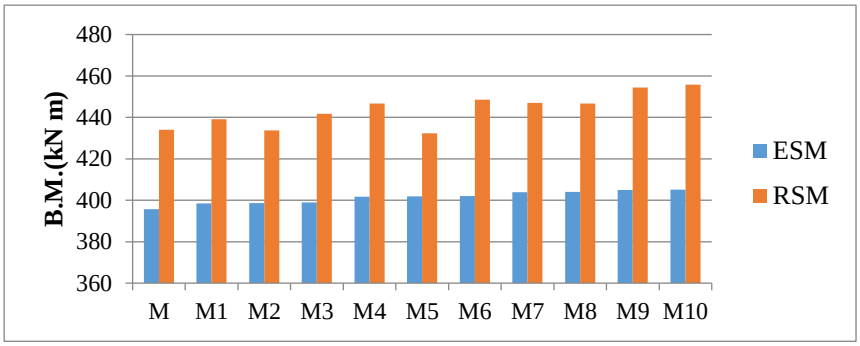

Fig. 8. Comparison of all models maximum bending moment for beam

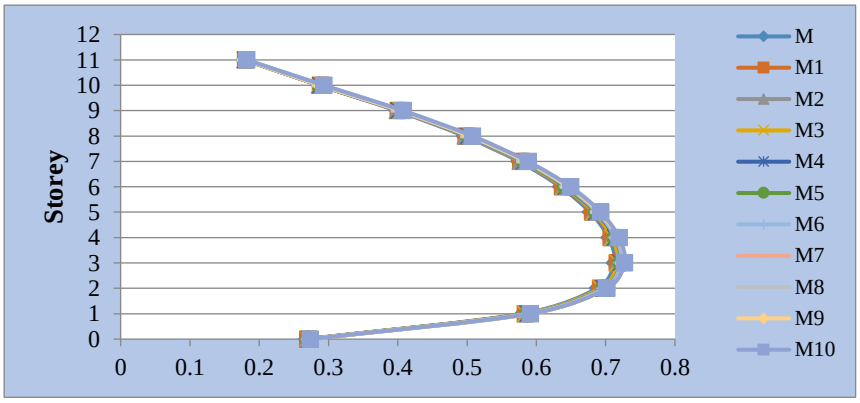

Fig. 9. Comparison of all models storey drift for ESM

ISBN: 978-81-932056-2-4

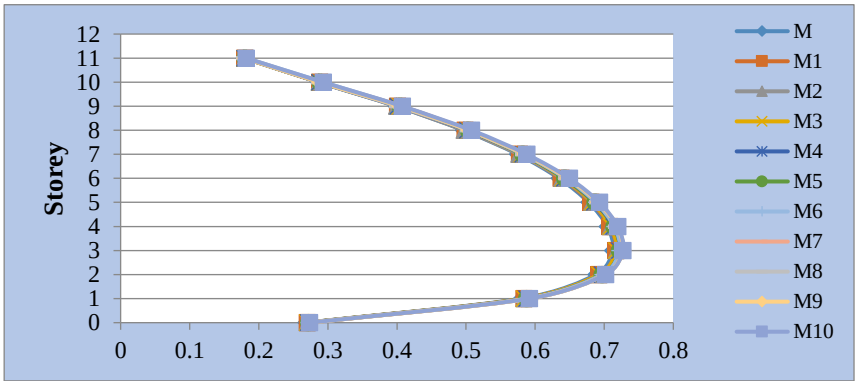

Fig. 10. Comparison of all models storey drift for RSM

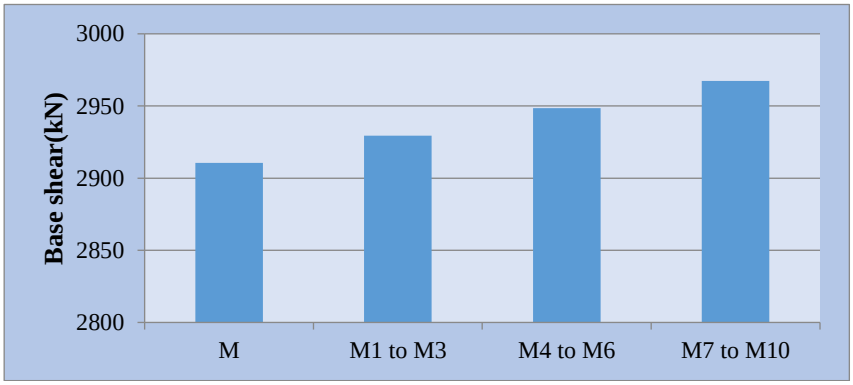

Fig. 11. Comparison of all models base shear

Result comparison between ESM & RSM for vertical geometric irregular models

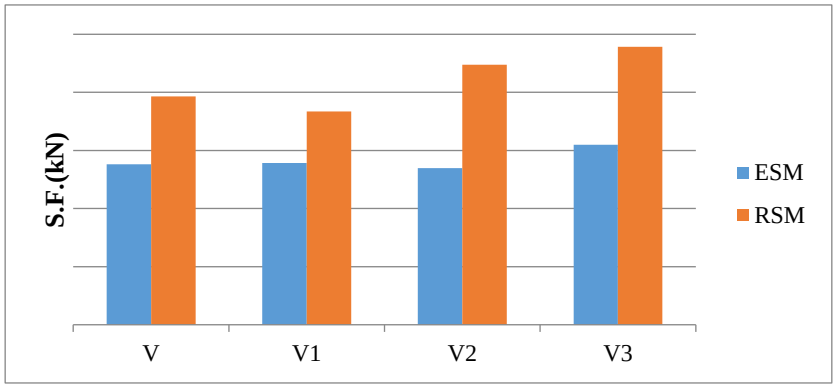

Fig. 12. Comparison of all models maximum shear force for beam

ISBN: 978-81-932056-2-4

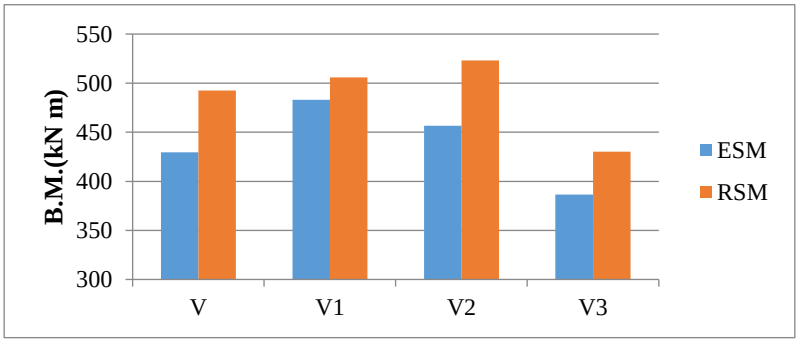

Fig. 13. Comparison of all models maximum bending moment for beam

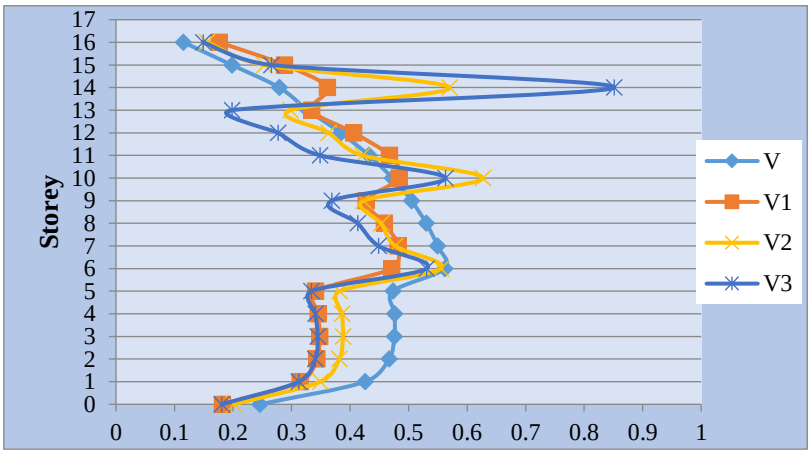

Fig. 14. Comparison of all models storey drift for ESM

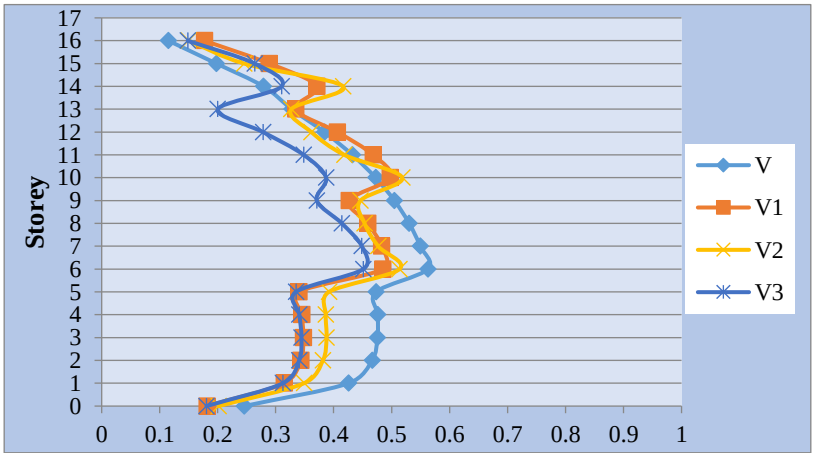

Fig. 15. Comparison of all models storey drift for RSM

ISBN: 978-81-932056-2-4

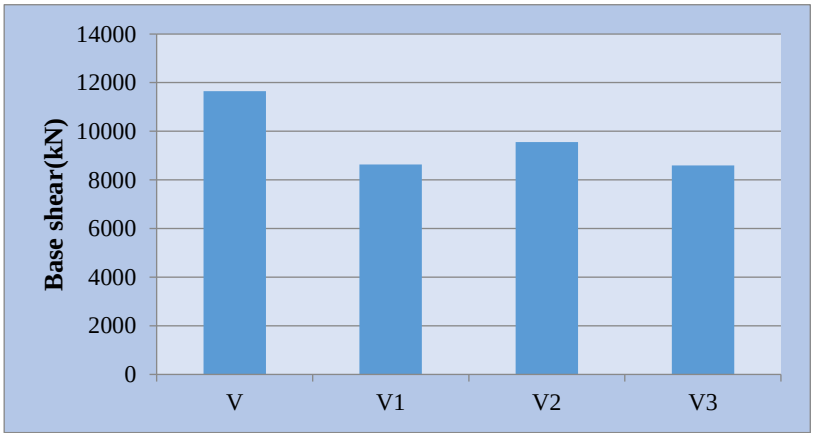

Fig. 16. Comparison of all models base shear

3. Conclusions

For high rise structures having mass and vertical geometric irregularities, linear static and linear dynamic analysis was performed to analyze the behaviour of the structures. The results of analysis like shear force, bending moment, storey drift and base shear. While irregularities have increased with increasing height for both analytical methods, the drift in upper stories is significantly more vulnerable. When comparing vertical irregularity structure to a normal structure, it has been shown that there are significant structural displacements.

The conclusions are as follows based on the findings of the analysis specified above:

- For both irregularities shear force and bending moment of RSM is more than ESM. The variation of maximum shear force is 0.02% to 4.21% and 3.90% to 7.85% for mass and vertical geometric irregular structures respectively. Also, the variation of maximum bending moment is 7.59% to 12.53% and 4.78% to 14.58% for mass and vertical geometric irregular structures respectively.

- Storey drift results for mass irregular structures are comparable for both methods, meanwhile results for vertical geometric irregular structures vary model to model but in model V3 there is huge difference between ESM and RSM results.

- The analysis shows that the base shear of mass irregularity structure is more than the regular structure and in case of vertical geometric irregularity base Shear results are vice- versa.

ISBN: 978-81-932056-2-4

References

1. Gupta & Pendharkar-(2020). "Multi storey Building with and Without Floating Column". Inter. Journal of Innovative Tech. and Exploring Engineering, 9(4), 2143–2146.

2. Jain & Rai. (2017). “Comparative Study by Static and Dynamic Analysis of an Irregular-Multistory Building for Different Location of Shear Wall.”

3. Moharana & Mouli. (2019). "Static, &Dynamic with Pogressive Collapse Analysis of Multi-Storied (G+10) Residential Building by ETABS Software." International Journal of Innovative Technology and Exploring Engineering, 9(2S3), 566–574.

4. Namdev & Singh. (2021). "Response Spectrum Analysis(RSA) of the Base-Isolated Regular and Vertical Irregular Building. International Jour.of Research in Applied Science and Engineering Technology, 9(10), 1095–1103.

5. Chaudhary et al., (2021). "Response analysis of irregular shape of high rise buildings with combined effect of plan and vertical irregularity using Etabs. IOP Conference Series: Environmental Science, 889(1).

6. Kangle et al., (2020). "Response-Spectrum Analysis of a Regular Multistory building in Seismic Zone III. Inter. Journal of Engineering& Research, Vol-9, 478–483.

ISBN: 978-81-932056-2-4

DYNAMIC ANALYSIS RESPONSE OF CLADDING SANDWICH PANELS WITH VARIANTS OF HONEYCOMB

Aby Sandrine Albertine Pime[1], Dr. Vijaykumar R. Panchal[2] and Nirpex A. Patel[3]

[1] PG Student, M. S. Patel Department of Civil engineering, Chandubhai S. Patel Institute of Technology, Faculty of Technology & Engineering, Charotar University of Science and Technology (CHARUSAT), CHARUSAT campus, Changa 388421, India.
[2] Assistant Professor, M. S. Patel Department of Civil engineering, Chandubhai S. Patel Institute of Technology, Faculty of Technology & Engineering, Charotar University of Science and Technology (CHARUSAT), CHARUSAT campus, Changa 388421, India.
[3] Assistant Professor, M. S. Patel Department of Civil engineering, Chandubhai S. Patel Institute of Technology, Faculty of Technology & Engineering, Charotar University of Science and Technology (CHARUSAT), CHARUSAT campus, Changa 388421, India.

[1] 21pgcl003@charusat.edu.in,
[2] nirpexpatel.cv@charusat.ac.in
[3] vijaypanchal.cv@charusat.ac.in

Abstract. This research aims to investigate the performance of honeycomb sandwich panels under cyclic loads, to identify the most suitable configuration for specific applications. The study involves material characterization, finite element modeling, dynamic analysis, and design optimization to assess the stiffness, strength, and vibration-damping properties of cladding sandwich panels (14mm overall wall thickness) with different types of honeycomb cores. The considered variants of honeycomb cores like hexagonal, circular, and triangular cells with various cell sizes (10mm, 20mm, and 30mm) and cell thicknesses (0.6mm, 0.8mm, and 1mm) were tied within two skin plates of the same size (220mm×220mm×2mm) and the assemble panels were mounted within a steel frame sized 220mm×220mm×10mm. Steel materials were assigned to the honeycombs and the plates. The findings of this study could help create better lightweight and energy-efficient structures in the construction sector. The study shows that the thickness of the panel's core cells has a significant impact on the behavior of panels with triangular and hexagonal cores, while the one with the circular core; the effect of variant cells thicknesses is minor. Overall, the study demonstrates that varying the height, diameter, and thickness of such panels has a significant impact on their behavior. The findings of this study provide an important overview of the design and optimization of cladding sandwich panels with honeycomb cores for dynamic loading applications.

Keywords: Composite, Honeycomb Cladding panels, Dynamic Analysis, Abaqus, Hysteresis Graph.

ISBN: 978-81-932056-2-4

1 Introduction

Cladding panels are typically used to affect how aesthetically pleasing a structure appears, enhance thermal insulation, and provide weather protection. The design and optimisation of lightweight and energy-efficient building components have drawn a lot of attention recently in the field of structural engineering. Sandwich panels for cladding that are made of a core material and two outer skin plates have great potential to improve the performance and sturdiness of structures exposed to dynamic loading conditions [1,2] and [3–7]. In a bid to dissipate impact energy through plastic deformation, Wang Chenga, et al.[1] proposed an empty welled aluminium 6063-T6 and mild-carbon steel C45E4 tubes with an outer diameter of 38 mm, two plates of DOMEX 700 Steel with size (220 × 220 × 2) mm for the front, and mild steel with size (300 × 300 × 2) mm were used as blast mitigates. A modified version of the cladding sandwich panel with the empty tubular cores filled with aluminium foam to increase the energy-resistant performance of the sandwich panels was evaluated by Jingyi Lu, et al.[2] using LS-DYNA software. A dynamic wind load analysis of an aluminium wall cladding panel with the dimensions (120 mm × 2440 mm × 4 mm) of an existing 15-story structure with a total height of 48.8 m was proposed by Okafor Chinedum Vincent, et al.[4]. By examining three design criteria specified in the standard ISO 22502:2020 isostatic, integrated, and dissipative Marco Lamperti Tornaghi et al.[8] concentrated on the practical connections for the horizontal cladding panel. Previous research has extensively studied various core materials, such as tubular structures, aluminum foam, and composite sandwich panels, to enhance the energy absorption and impact resistance properties of cladding sandwich panels [3,9]. However, there has been limited research on the use of honeycomb cores for these applications. Therefore, this study aims to investigate the performance of cladding sandwich panels with different types of honeycomb cores, specifically hexagonal, circular, and triangular cell configurations, considering various cell sizes and thicknesses[10]. The impact of these honeycomb cores on the overall behavior of the panels under cyclic loads will be comprehensively analyzed using Abaqus/CAE 6.11, a numerical research approach. The experimental setup involves placing the honeycomb cores between two steel skin plates, each measuring (220 x 220 x 2) mm [1-2]. The panels with honeycomb cores are set inside a (220 x 16 x 10) mm steel frame to imitate realistic structural conditions. This setup aims to objectively represent real-world scenarios. The research intends to provide a helpful understanding of the behavior of sandwich panels with honeycomb cores when subjected to cyclic loads through dynamic loading experiments [11].

2 Analytical Study

2.1 Modeling

Abaqus/CAE 6.11 was utilised to model and analyse the behaviour of sandwich cladding panels with variants of honeycomb cores Fig. 1 in conjunction with a frame. Such honeycomb plates are practically feasible to manufacture. The modelling

ISBN: 978-81-932056-2-4

procedure involved assembling the plate, honeycomb, and frame components within the Abaqus Assembly module while ensuring proper global coordinate alignment [1–3,7]. Several significant steps were implemented to ensure accurate results. To capture the intended system behaviour, appropriate boundary conditions were assigned, taking into account interactions between the panels and the frame. To accurately simulate bearing conditions and structural response, step-by-step procedures were implemented. The geometry was discretized using meshing techniques after materials were designated to the respective components. In the model, the frame was modelled as a 3D rigid element, while the plate and honeycomb were represented as 3D deformable elements. Utilising the Abaqus Interaction module, surface constraints between the plates and honeycomb as well as plate edge constraints with the frame were established. Using rigid body (Tie) constraints, reference points and frame components were joined to form an integrated frame structure. Wires were used to establish connections between the reference points and frame components, and the Join+Rotation connection type was assigned. To accurately represent loading and support conditions, the Abaqus Load module applied various boundary condition categories to the frame, such as Displacement/Rotation, Symmetric/Antisymmetric, and Encastre. The analysis was conducted using a static general-step procedure, which allowed for the investigation of the system's response to various applied stresses. This research project intended to provide valuable insights into the behaviour and performance of cladding sandwich panels integrated into a frame by meticulously following these modelling and analysis steps.

Skills Utilized:

- Abaqus/CAE 6.11 for modeling and analysis
- Assembly module for instance assembly using global coordinates
- Interaction module for surface constraints and rigid body connections
- Load module for applying boundary conditions
- Static general step procedure for the analysis

In Table 1, the diameter represents the inner diameter (d_i) of the circular honeycomb cells and the height represents the inner height (h_i) of the triangular as well as hexagonal honeycomb cells.

ISBN: 978-81-932056-2-4

Table 3. Series of analysis conducted

Configuration's Name	Cell Inner Diameters (d_i) / Heights (h_i) (mm)	Cell Thickness (t) (mm)
Circular honeycomb	10	0.6
	20	0.8
	30	1
Triangular honeycomb	10	0.6
	20	0.8
	30	1
Hexagonal honeycomb	10	0.6
	20	0.8
	30	1

2.2 Material and Geometry Properties

In the properties module of Abaqus/CAE, a single material was created and assigned to both the honeycomb and plate components. The material, named "steel" was characterized by its general, mechanical behaviors, and nonlinearproperty which are detailed in Table 2 and Table 3. The geometry properties of each part are illustrated in Fig. 1.

Table 4. Mechanical Behaviors

Parts	Material	Density (tonne/mm^3)	Young's Modulus (MPa)	Poison's Ratio
Plate Honeycomb Frame	Steel	7.85E-09	2.10E+05	0.3

Table 5. Nonlinear property

Element	Yield Stress (MPa)	Yield Strain
Steel Plate	272	0
	384	0.002
Steel Frame	250	0
	256	0.001
	300	0.002

ISBN: 978-81-932056-2-4

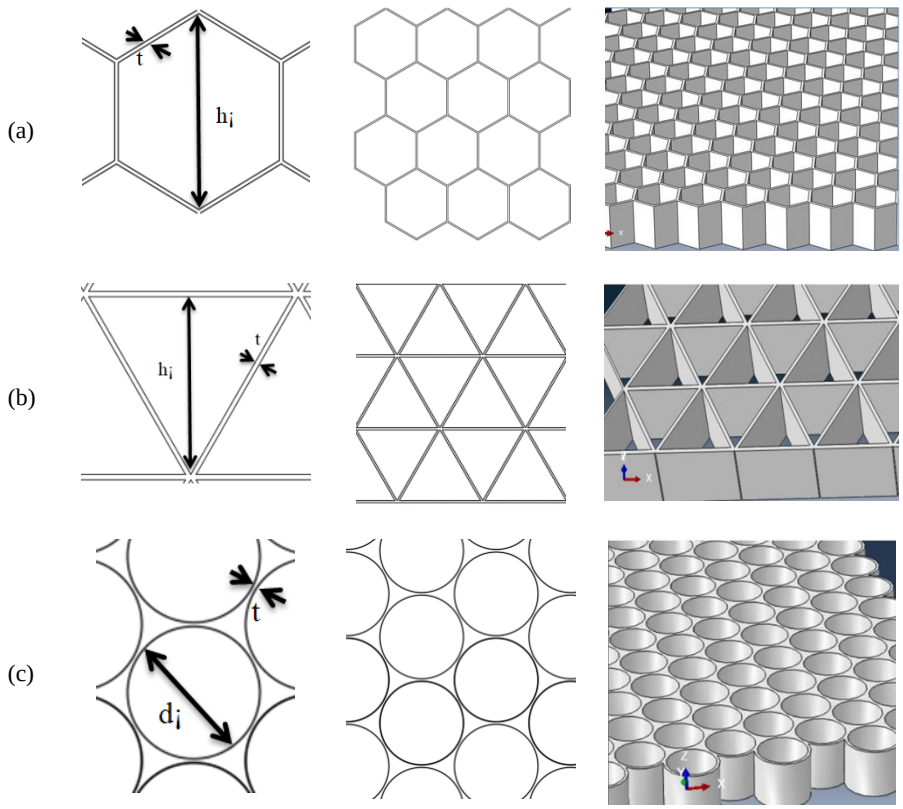

Fig. 1. Honeycomb structure configuration: (a) hexagonal (b) triangular (c) circular

2.3 Meshing

No mesh sensitivity analysis was carried out to finalize size of mesh. The mesh size for the plate, frame, and honeycomb components was carefully chosen to achieve precise results depending on the unique model requirements. Depending on the type of honeycomb panel under consideration, the mesh sizes vary. A global mesh size of 4.2mm was assigned to the honeycomb component of the spherical honeycomb panels whereas a mesh size of 5mm was assigned to the frame. A uniform mesh size of 11mm was used for both the honeycomb and frame components in the case of the triangular and hexagonal honeycomb composite panels. The plate component was given a constant mesh size of 5mm throughout the whole series of models run. The mesh sizes had to be carefully adjusted to the unique panel geometry and modeling in order to produce accurate and reliable outcomes for the analysis.

ISBN: 978-81-932056-2-4

2.4 Loading

A time history as shown below was applied to the whole honeycomb cladding panel models. The displacement magnitudes gradually increase with a range of 5 to 10mm.

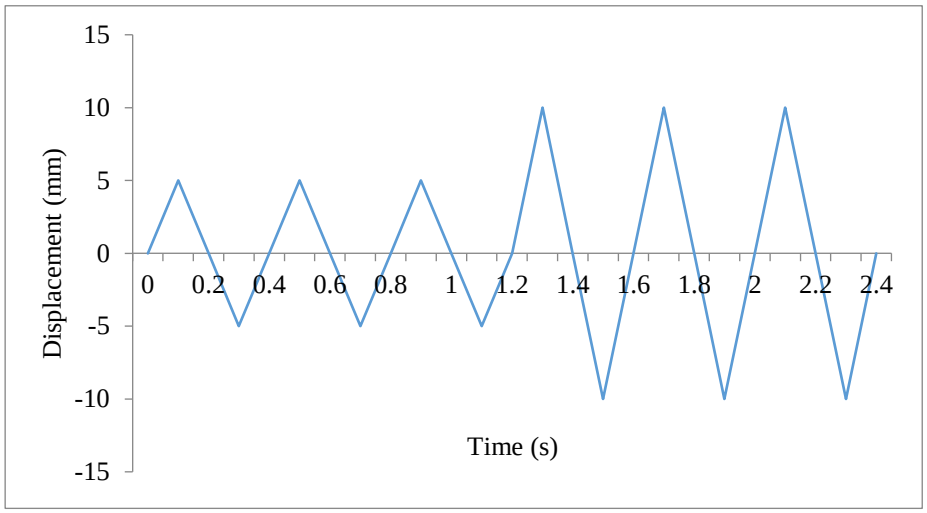

Fig. 2. Displacement vs. Time

3 Results

3.1 Comparative Study

A report of the outcomes achieved through the simulations conducted on cladding panels subjected to cyclic loading.

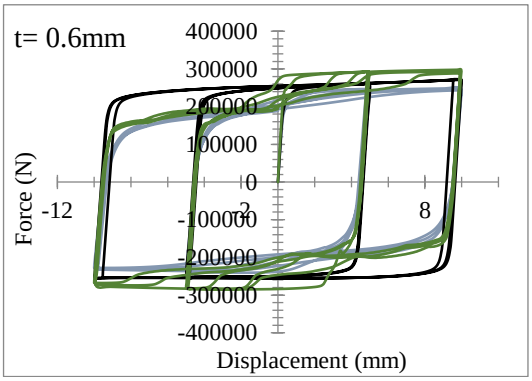

a) Honeycombs with d/h= 10mm

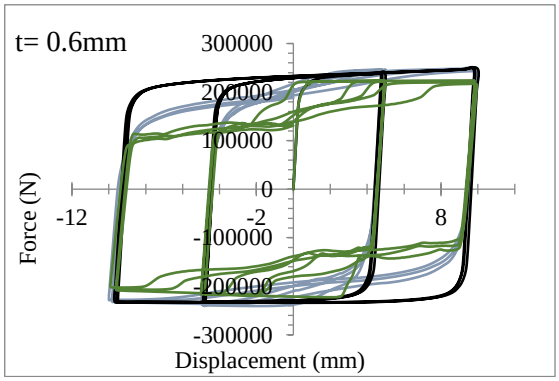

b) Honeycombs with d/h=20mm

ISBN: 978-81-932056-2-4

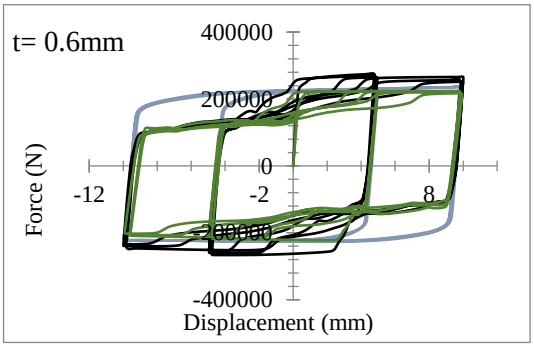

c) Honeycombs with d/h= 30mm

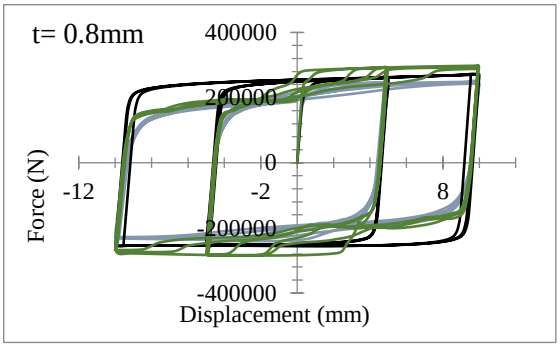

d) Honeycombs with d/h=10mm

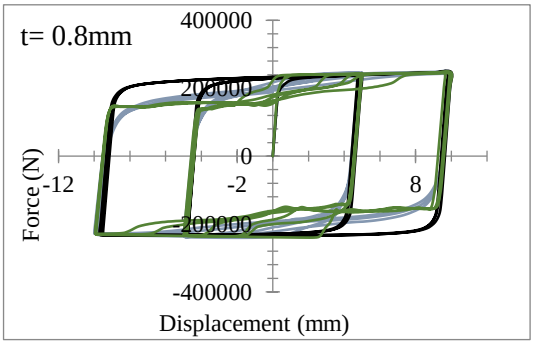

e) Honeycombs with d/h=20mm

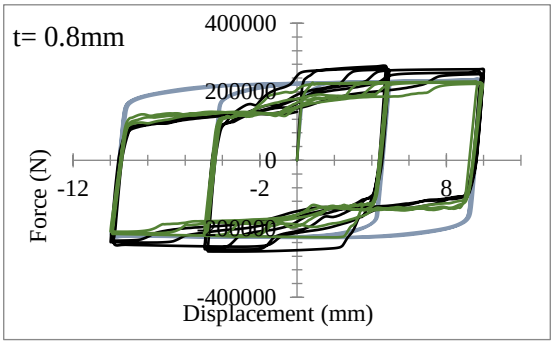

f) Honeycombs with d/h=30mm

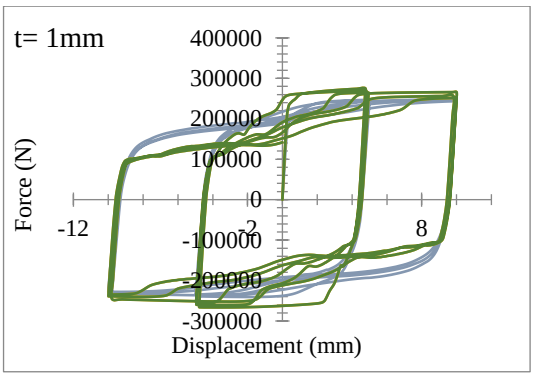

g) Honeycombs with d/h=10mm

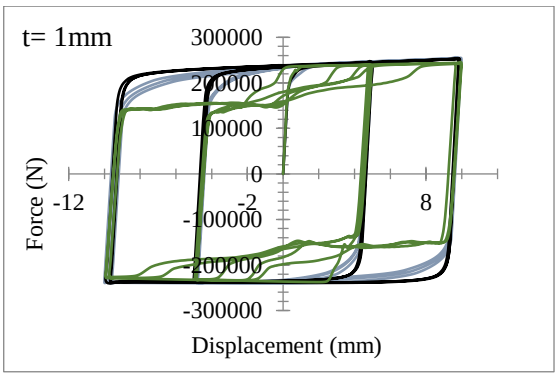

h) Honeycombs with d/h=20mm

ISBN: 978-81-932056-2-4

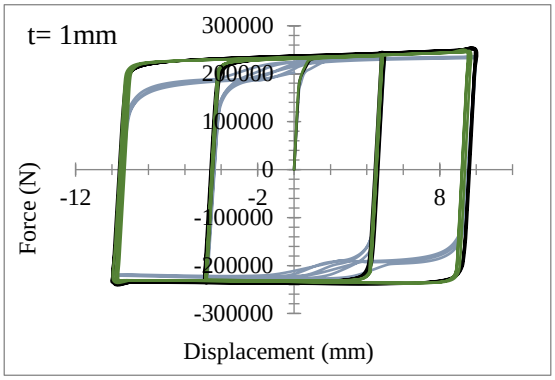

i) Honeycombs with d/h=30mm

Fig. 3. Hysteresis analysis of triangular, hexagonal, and circular honeycomb composite panels

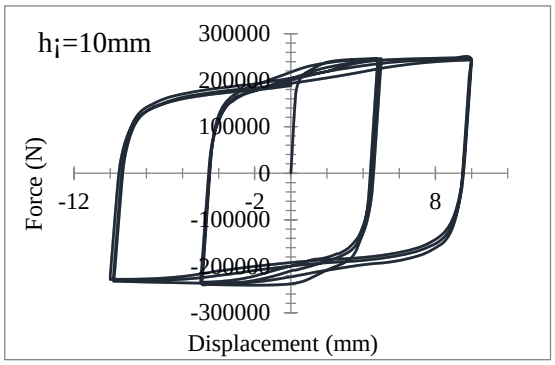

a) Triangular honeycomb with t= 0.6; 0.8 and 1mm

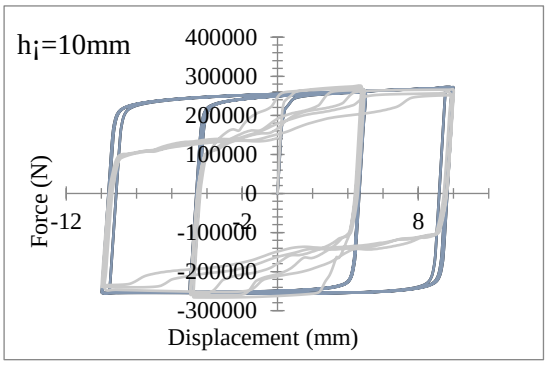

b) Hexagonal honeycomb with t= 0.6; 0.8 and 1mm

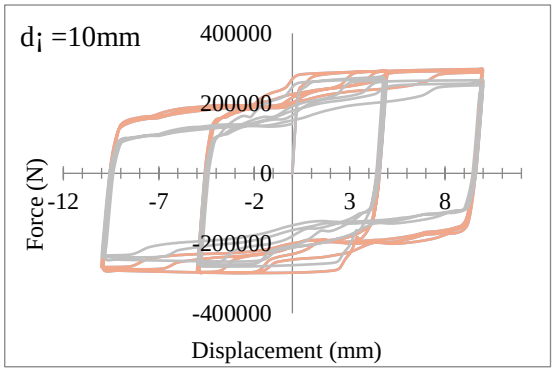

c) Circular honeycomb with t= 0.6; 0.8 and 1mm

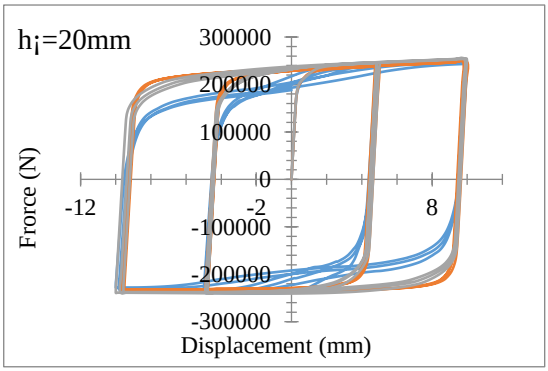

d) Triangular honeycomb with t= 0.6; 0.8 and 1mm

ISBN: 978-81-932056-2-4

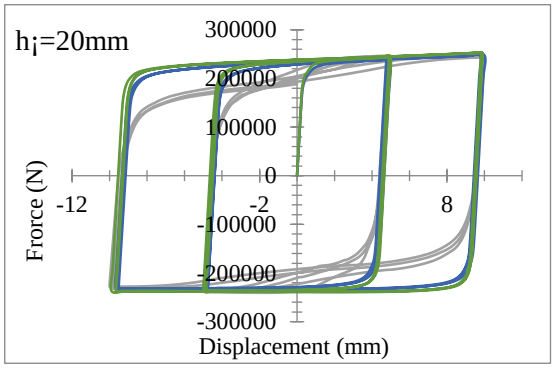

e) Hexagonal honeycomb with t= 0.6; 0.8 and 1mm

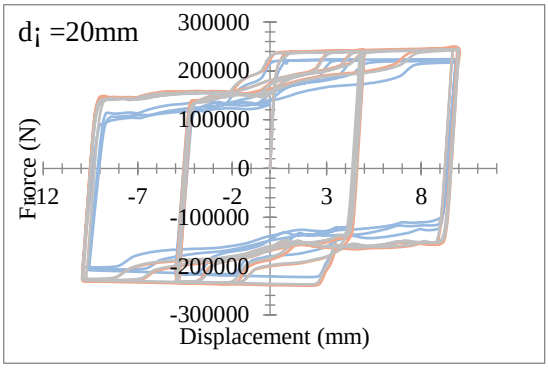

f) circular honeycomb with t= 0.6; 0.8 and 1mm

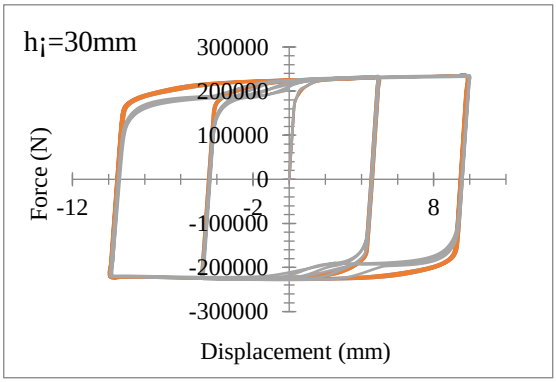

g) Triangular honeycomb with t= 0.6; 0.8 and 1mm

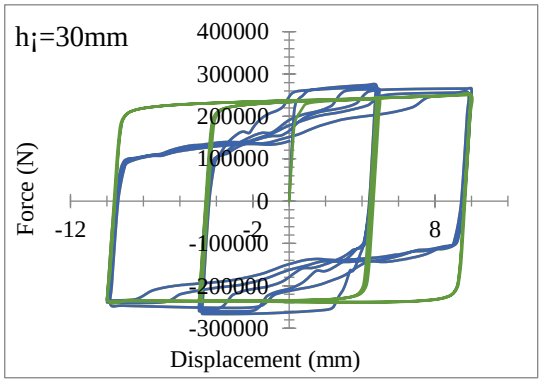

h) Hexagonal honeycomb with t= 0.6; 0.8 and 1mm

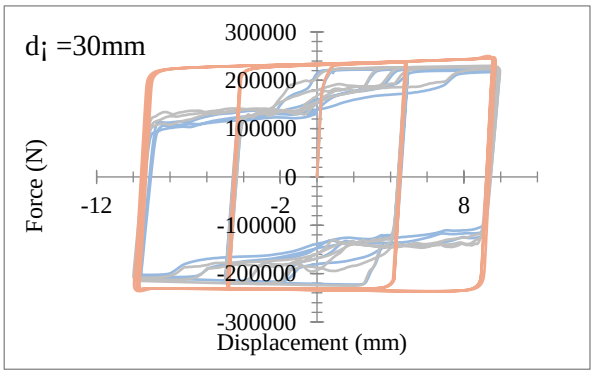

i) Circular honeycomb with t= 0.6; 0.8 and 1mm

Fig. 4. Hysteresis analysis of the impact of cell thickness variation on each honeycomb

ISBN: 978-81-932056-2-4

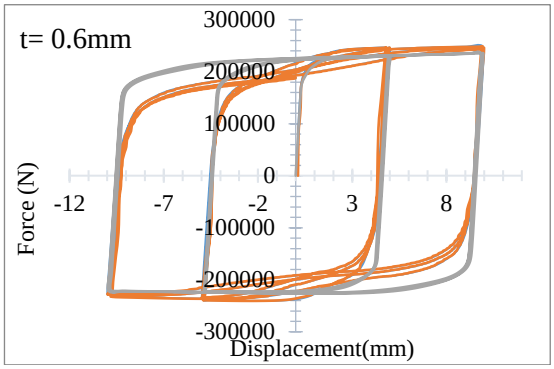

a) Triangular honeycomb with h= 10; 20, and 30mm

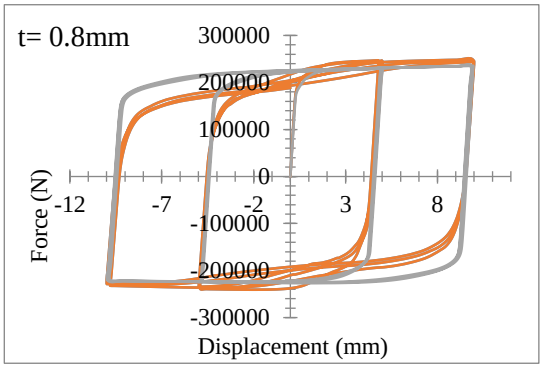

b) Triangular honeycomb with h= 10; 20, and 30mm

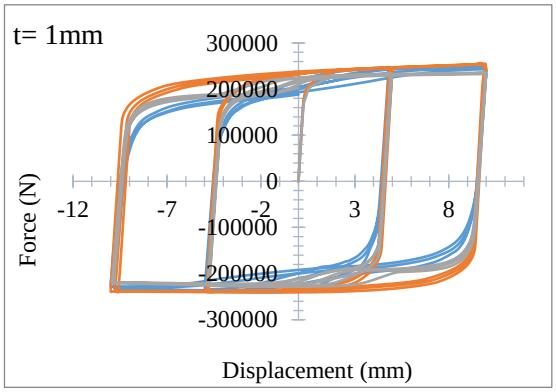

c) Triangular honeycomb with h= 10; 20, and 30mm

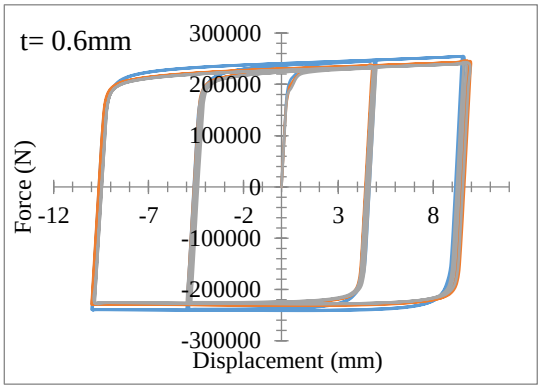

d) Hexagonal honeycomb with h= 10; 20, and 30mm

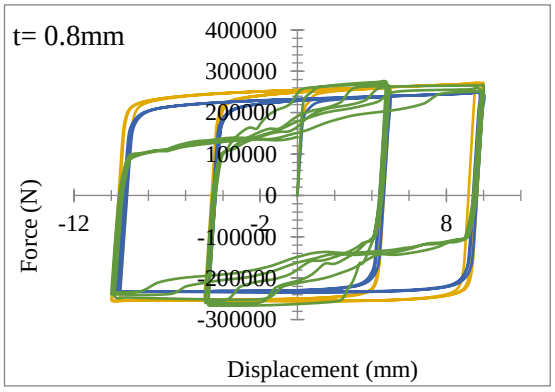

e) Hexagonal honeycomb with h= 10; 20, and 30mm

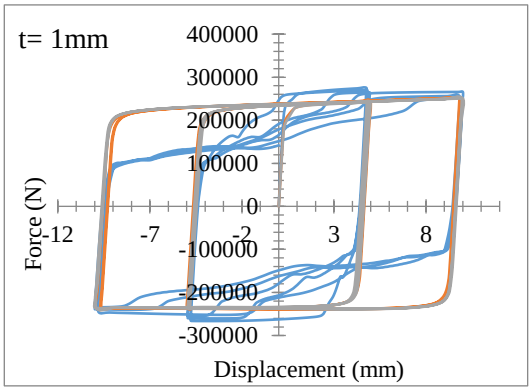

f) Hexagonal honeycomb with h= 10; 20, and 30mm

ISBN: 978-81-932056-2-4

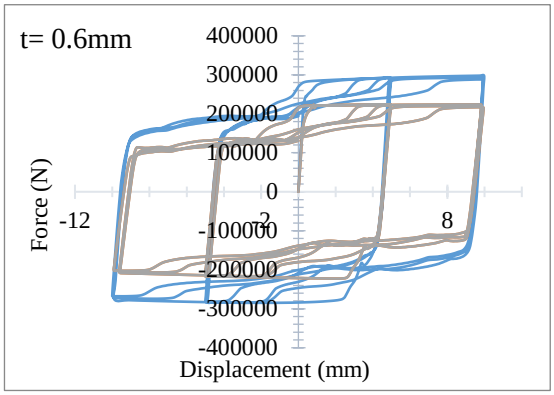

g) Circular honeycomb with h= 10; 20, and 30mm

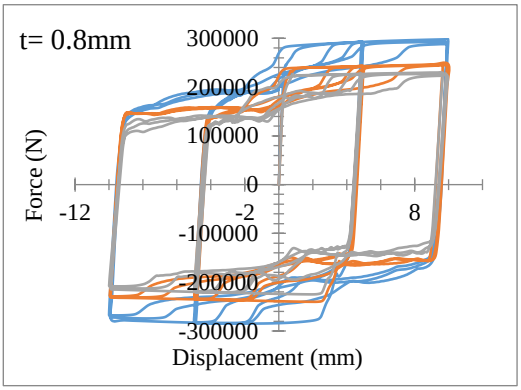

h) Circular honeycomb with h= 10; 20, and 30mm

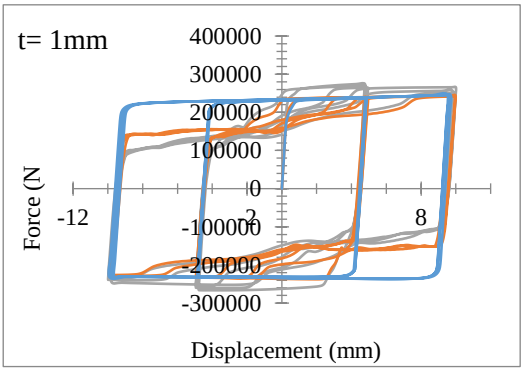

i) Circular honeycomb with h= 10; 20, and 30mm

Fig. 5. Hysteresis analysis of honeycombs with varied Cell inner diameter or height

Table 4. Area under Hysteresis (N.mm)

Configuration's Name	Diameter/Height (mm)	Thickness (mm)	Area under Hysteresis (N.mm)
Triangular honeycomb composite panels	10	0.6	8437501
	20		8437501
	30		8852772
Hexagonal honeycomb composite panels	10		8185384
	20		9265915
	30		911712
Circular honeycomb composite panels	10		27660488
	20		24004187
	30		1218260

ISBN: 978-81-932056-2-4

Triangular honeycomb composite panels	10	0.8	8437501
	20		8437501
	30		8852772
Hexagonal honeycomb composite panels	10		374613
	20		8007868
	30		27660488
Circular honeycomb composite panels	10		9112419
	20		15761058
	30		127157
Triangular honeycomb composite panels	10	1	8437501
	20		8098275
	30		8098275
Hexagonal honeycomb composite panels	10		27660488
	20		251004
	30		12046365
Circular honeycomb composite panels	10		27660488
	20		24004187
	30		1218260

4 Conclusions

Different core shapes, including triangular, hexagonal, and circular Fig 1, were analyzed under cyclic load Fig 2 and the comparison of hysteresis loops for the honeycomb panels with varying geometry parameters according to the Table 1 and Fig. 1 shows that the panels' thickness, height, diameter, and core shapes have a significant impact on their behavior. The effect of varying thicknesses on panel behavior is dependent on the specific panel geometry and thickness. For triangular panels with a height of 10mm (Fig. 3), changing the thickness does not affect their behavior. However, for hexagonal honeycomb composite panels with a 1mm thick core and the same height (Fig. 3), a smaller hysteresis loop area corresponds to less energy dissipation. Circular honeycomb composite panels with different cell thicknesses (0.6mm, 0.8mm, and 1mm) and a diameter of 10mm (Fig. 4) exhibit similar hysteresis loop areas, but the panel with a 1mm thickness shows lower energy dissipation. Considering larger core sizes (heights of 20mm and 30mm), varying thicknesses have a significant impact on panel behavior. Thinner triangular panels with these heights (Figs. 4) and thinner hexagonal honeycomb composite panels (Figs. 4) demonstrate reduced energy dissipation. However, the impact of thickness variation on circular honeycomb composite panels with diameters of 20mm and 30mm is relatively small (Figs. 5). The hysteresis graphs (Figs. 5) further confirm that the thickness, height, and diameter of the panels are significant factors

ISBN: 978-81-932056-2-4

influencing their behavior. The observed differences in energy dissipation indicate that modifying these parameters has a considerable effect on the panels' performance. It was found in Table 4 that circular cores tend to have smaller hysteresis loop areas with values ranging from 1218260 N.mm to 27660488 N.mm and lower energy dissipation compared to hexagonal and triangular cores providing high levels of damping or shock absorption. Varying the thickness, height, or diameter of the panels also had a significant impact on their behavior. Overall, the triangular honeycomb composite panels exhibit consistent hysteresis area with values ranging from 8437501 N.mm to 8852772 N.mm across different dimensions and thicknesses, while the hexagonal honeycomb composite panels offer more flexibility in adjusting its damping properties, with the hysteresis area values ranging from 8185384 N.mm to 9265915 N.mm. Therefore, it is important to take carefully into consideration these parameters when designing and analyzing the behavior of such structures. Overall, the findings of this analysis can be useful for designing more efficient structures with better energy dissipation characteristics.

References

1. W. Cheng, X. Bin, and S. C. Kim, “International Journal of Impact Engineering Numerical analysis of cladding sandwich panels with tubular cores subjected to uniform blast load,” vol. 133, no. June, 2019, doi: 10.1016/j.ijimpeng.2019.103345.

2. J. Lu, Y. Wang, X. Zhai, X. Zhi, and H. Zhou, “Impact behavior of a cladding sandwich panel with aluminum foam-filled tubular cores,” *Thin-Walled Struct.*, vol. 169, Dec. 2021, doi: 10.1016/j.tws.2021.108459.

3. M. Latour, M. D. Aniello, R. Landolfo, and G. Rizzano, “Thin-Walled Structures Experimental and numerical study of double-skin aluminium foam sandwich panels in bending,” *Thin-Walled Struct.*, vol. 164, no. May, p. 107894, 2021, doi: 10.1016/j.tws.2021.107894.

4. O. C. Vincent, M. E. Cyril, K. C. Okolie, and D. A. Obodoh, “Finite Element Modeling for Wind Response of Aluminum Wall Cladding in Tall Building,” vol. 2, no. 4, pp. 165–172, 2017.

5. E. Pantoli and T. Hutchinson, “Seismic accelerations in architectural precast concrete cladding,” *Eng. Struct.*, vol. 180, no. September 2018, pp. 742–749, 2019, doi: 10.1016/j.engstruct.2018.11.062.

6. C. Balocco, G. Grazzini, and A. Cavalera, “Transient analysis of an external building cladding,” vol. 40, pp. 1273–1277, 2008, doi: 10.1016/j.enbuild.2007.11.008.

7. A. Raj, D. Sathyan, K. Balaji, and K. M. Mini, “Materials Today : Proceedings Heat transfer simulation across a building insulated with foam concrete wall cladding,” *Mater. Today Proc.*, vol. 42, pp. 1442–1446, 2021, doi: 10.1016/j.matpr.2021.01.242.

8. M. Lamperti Tornaghi, A. Scalbi, and P. Negro, “Precast RC buildings: What is wrong with

ISBN: 978-81-932056-2-4

horizontal cladding panels?," *Eng. Struct.*, vol. 266, no. May, 2022, doi: 10.1016/j.engstruct.2022.114456.

9. T. Sharaf and A. Fam, "Analysis of large scale cladding sandwich panels composed of GFRP skins and ribs and polyurethane foam core," *Thin-Walled Struct.*, vol. 71, pp. 91–101, 2013, doi: 10.1016/j.tws.2013.05.006.

10. Y. L. Yap and W. Y. Yeong, "Shape recovery effect of 3D printed polymeric honeycomb Shape recovery effect of 3D printed polymeric honeycomb This paper studies the elastic behaviour of different honeycomb structures produced by PolyJet technology," vol. 2759, no. September, 2015, doi: 10.1080/17452759.2015.1060350.

11. L. S. Jangid, V. R. Panchal, and N. A. Patel, "FE Analysis of High Pressure Laminate Panel for High Rise Building," vol. 11, pp. 1–8, 2022.

ISBN: 978-81-932056-2-4

SEISMIC PARAMETER EVALUATION OF FLAT SLAB BUILDING WITH SHEAR WALL AND BRACING SUBJECTED TO GRAVITY AND EARTHQUAKE LOAD

Ruchita Morkhande[1], S. G. Hirekhan[2], Dr. V. P. Dehadrai[3] and A. A. Yadav[4]

[1] PG Student, Department of Civil Engineering, Yeshwantrao Chavan College of Engineering, Nagpur, India
[2 & 4] Assis. Professor, Department of Civil Engineering, Yeshwantrao Chavan College of Engineering, Nagpur, India·
[3] Aquades Structural Consultant Nagpur, India

[1] morkhande12@gmail.com
[2] sghirekhan@ycce.in
[3] aquades@rediffmail.com
[4] amruta_capricorn@yahoo.co.in

Abstract. In modern construction world the main objectives of civil engineering are to design tall buildings which can resist the horizontal forces. Flat slab is RCC slab constructed without beam, also known as beamless slab. The slab directly rest on columns and load transfer directly slab to the columns. Flat slab can reduce floor to floor height of the building and give aesthetical appearance. Drop and columns head provide to raise the shear strength of slab increase punching resistance and reduce the negative moment in the slab. shear wall and bracing system designed to counteract horizontal forces acting on structure. In the present work, five different type building are taken into account; flat slab building, flat slab with a shear wall surrounding it, flat slab with bracing at periphery, shear wall and bracing are with flat slabs at their corners. Using the ETABs20 analysis tool, the Response spectrum analysis i.e. static linear analysis is carried out. The realized outcomes are correlated in term of storey deracination, storey drift, Storey stiffness, Time period. This research's goal was to examine how flat slab buildings with shear wall and bracing performed during an earthquake in seismic zone IV according to Indian standard code.

Keywords: Shear wall, flat Slab, Bracing, Lateral Load ETABs.

1 Introduction

Seismic activity is one of nature's most destructive events, and its occurrence is frequently unforeseen. Seismic behavior is a matter of concern in high rise building. Flat slab system can reduce the height of building. In flat slab building more number of floor can be constructed. Near to supporting columns to boost the shear strength and negative moment capacity, drop and column heads are used. [7] IS 456: 2000 use for design and analysis flat slab building. High rise buildings use a variety of lateral load resisting devices to lessen lateral displacement. Lateral loads exerted on a structure can be mitigated by a shear wall and bracing system. moment resistant frame that has been

ISBN: 978-81-932056-2-4

particularly specified to produce ductile behavior and to meet the [10] IS 13920: 2016. Good result can be obtained by the combining of flat slab structures with some lateral load resisting system. It is crucial to analyses a flat slab with a wall shear and bracing in order to examine how the structure responds to various forces occurring on it. The analysis can be done with a variety of software programs, including Staad pro, Sap, Etabs, etc.

Etabs software use for G+20 narrative analysis and design with five different models of the flat building with shear wall and bracing. storey deracination, drift storey, stiffness Time Period, result obtain by analysis. By using the response spectrum approach, three distinct models of structure with bare frame, structure with flat slab and wall shear, and structure with flat slab and bracing were evaluated against seismic force as per Indian standard codes at v zone. Their work is a valuable source of information on the parameters deracination, drift, and shear at base. According to Md. Shahzar, Md. Tasleem (2021) [1] flat slab buildings with lateral load resting systems offer good outcomes, however shear wall systems are better appropriate to withstand the lateral load.

Twelve unique models of structures of variable height, shear wall, and bracing at the periphery with flat slab were evaluated against seismic force as per Indian standard codes in the II zone using the response spectrum technique. This study offers numerous information on the factors deracination, stiffness, drift, shear base deracination increase with increasing storey of building. Deracination decreases after providing shear wall. According to Ms. Nail Ashwini Shankarrao, Dr. P.B. Ullagaddi (2021) [2] shear wall performance is superior when compared to flat slab bracing. Etabs was used to calculate the six- and ten-storey buildings base shear ratios, period of vibration, and displacement. All models were tested with different shear wall positions, and they discovered a suitable finite element model of shear wall dominating flat slab RC structures that can be utilized to analyses its dynamic behavior. According to Mohamed Abdel-Basset Abdo (2012) [3] presented a flat slab without and with walls shear, the walls shear with flat slab help to lowering the even axial force in the column in the central frame zone. According to Fayazuddin Ahmed Syed, et.al (2012) [4] When wind blows on other building frames, the column axial force decreases similarly.

Several factors have been examined for the commercial multistorey structure with flat slab and conventional slab. It has been studied how both constructions function and behave in India's seismic zones II and V. The displacement of industrial and commercial structures built utilizing the flat slab technology is greater than the regular slab system used traditionally. Here, it is possible to state that a flat slab with a shear wall provides better displacement resistance. Displacement also continues to rise as a structure's height does. According to Dr. K Naresh (2019) [5] A comparison between the two methods has been done in order to determine which earthquake-resistant construction is more appropriate for a building with shear wall and bracing in seismic zone V. The programmer ETABS has carried out a Response Spectrum Analysis. Compared to the bare frame model, the shear walls and braced models offer superior resilience to

ISBN: 978-81-932056-2-4

earthquake forces. shear wall model from the obtained results provides the least displacement values. According to Nandona Goswami (2022) [6] The study's purpose is to assess the impact of structures with flat slab and wall shear and lateral load bracing to learn more about how flat-slab structures operate. to look at how a shear wall affects a flat slab structure. to look at the behavior of braced flat slab structures. Comparison of results movement, drift, stiffness, and time are all elements in a storey.

1.1 Structural Data

- Building Dimension = 30×30m
- Slab Depth = 200mm
- Size of Column = 300×500mm
- Height from Floor to Floor = 3m
- Building Height = 60m
- Shear wall thickness = 230mm
- X Bracing = ISMC 175
- Concrete Grade = M-30
- Rebar Grade = Fe550 & Fe250
- Zone = 4
- Basic Speed of Wind = 44 m/sec
- Factor Zone = 0.24
- Response reduction Factor (SMRF) = 5
- Soil = Type II

2 Summarize Procedure

According to the Indian standard code, a G+20 storey building is developed in this paper to withstand seismic forces. Its structure is thought to be in zone IV according to [9] IS 1893: 2016. The loads used to the model for model verification are specified by the [8] IS 875: 2015. Flat slab structures with lateral load resistance systems are simulated for various combinations of static loads as per India standard code. As opposed to RCC conventional structures, flat slabs are used to build multiple floors. The flat slab building without any lateral load resisting systems was analyzed using Etabs software. All structural elements have been verified to be safe. To improve stability of building against lateral loads system use to resist the lateral loads like bracing and shear wall. These systems are placed at different location separately in four different model and perform analysis to compare the behavior of models.

ISBN: 978-81-932056-2-4

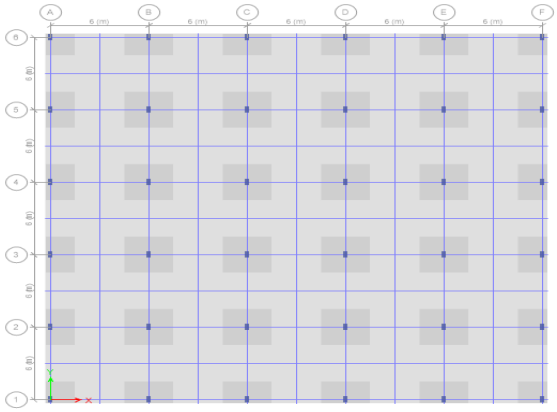

Fig. 1. Building plan with a flat slab

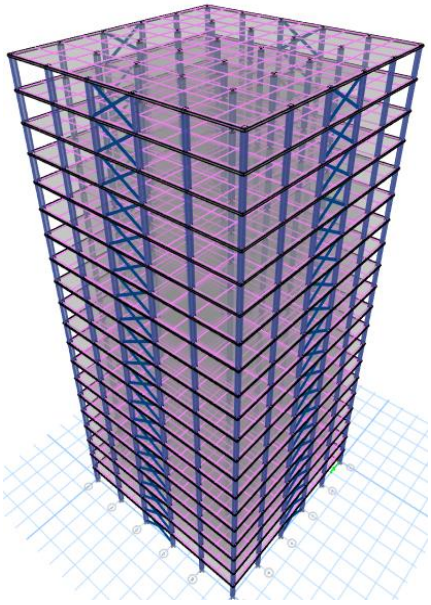

Fig. 2. Three-dimension model of a structure with flat slab and bracing at periphery

ISBN: 978-81-932056-2-4

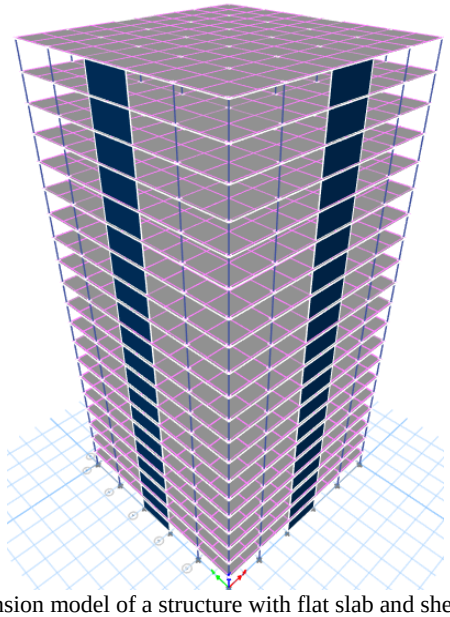

Fig. 3. Three-dimension model of a structure with flat slab and shear wall at periphery

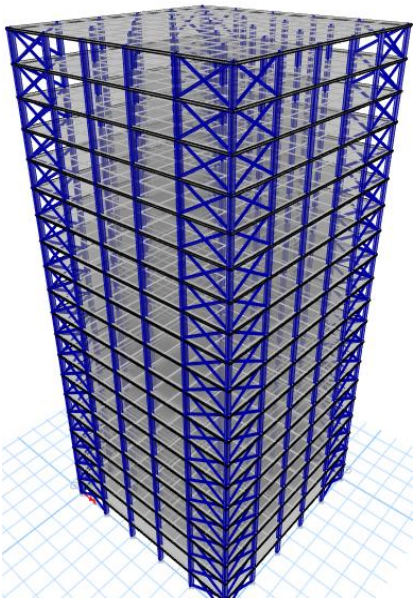

Fig. 4. Three-dimension model of a structure with flat slab and bracing at corner

ISBN: 978-81-932056-2-4

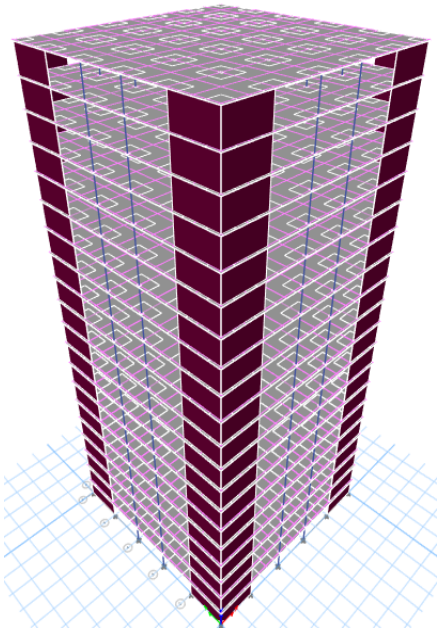

Fig. 5. Three-dimension model of a structure with flat slab and shear wall at corner

3 Results

The analysis of a structure with a flat slab, shear wall, and bracing. This analysis was used in the context of narrative selection, drift tale, stiffness, and period time.

Where,

FSB = Flat Slab Building.

FSB+BR I= Flat Slab Building with Bracing at Periphery.

FSB+BR L= Flat Slab Building with Bracing at Corner.

FSB+SW I= Building with a flat slab and shear wall at Periphery.

FSB+SW L= Building with a flat slab and L-shaped shear wall at Corner.

ISBN: 978-81-932056-2-4

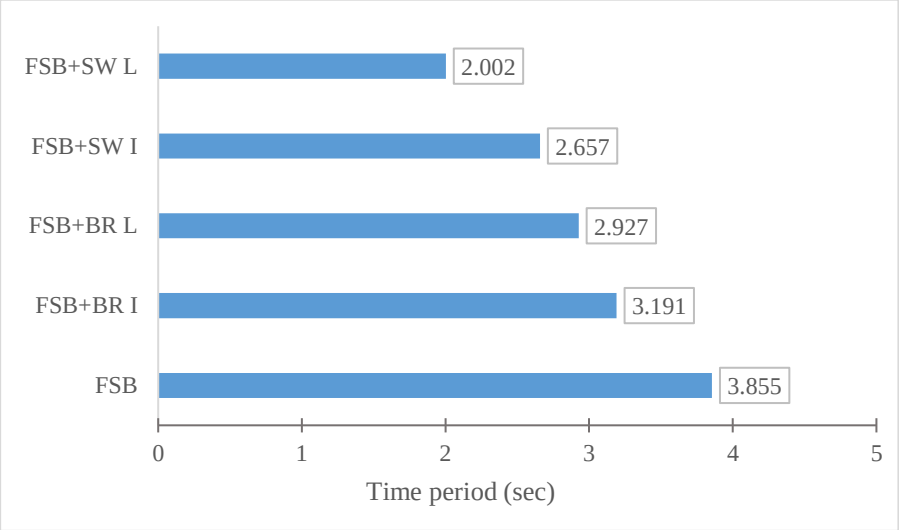

Fig. 6. Time period of various models

The above Figure 6 show that value of Natural time period shorter in L-shaped flat slab buildings of shear wall as compare to the flat slab structure and structure with flat slab and bracing. The difference between a flat slab structure maximum value 3.855Sec and a structure with flat slab and a L type shear wall's maximum value is 2.002Sec.

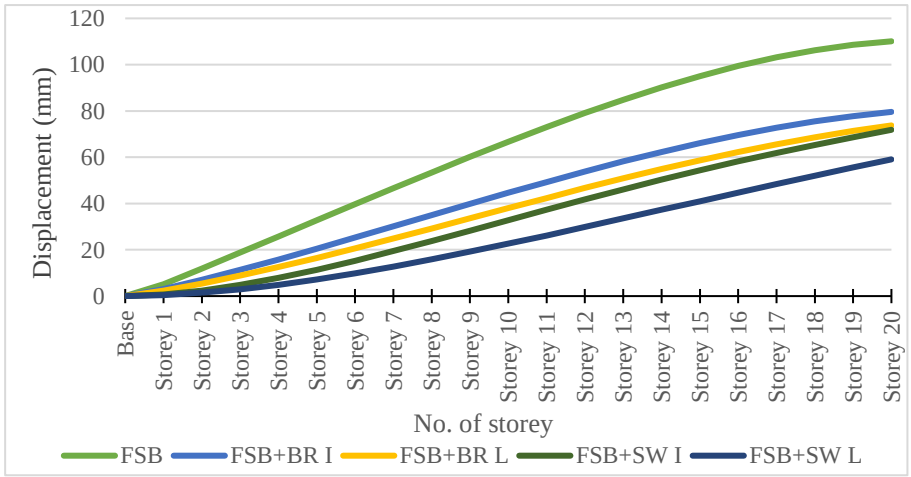

Fig. 7. Displacement in x direction

ISBN: 978-81-932056-2-4

The above Figure 7 show that displacement x direction is shorter in flat slab building with L type shear wall at corner as compare to the flat slab structure and structure with flat slab and bracing. Difference in the maximum value of flat slab structure 110.088mm and maximum value of structure with flat slab and L type shear wall 59.063mm.

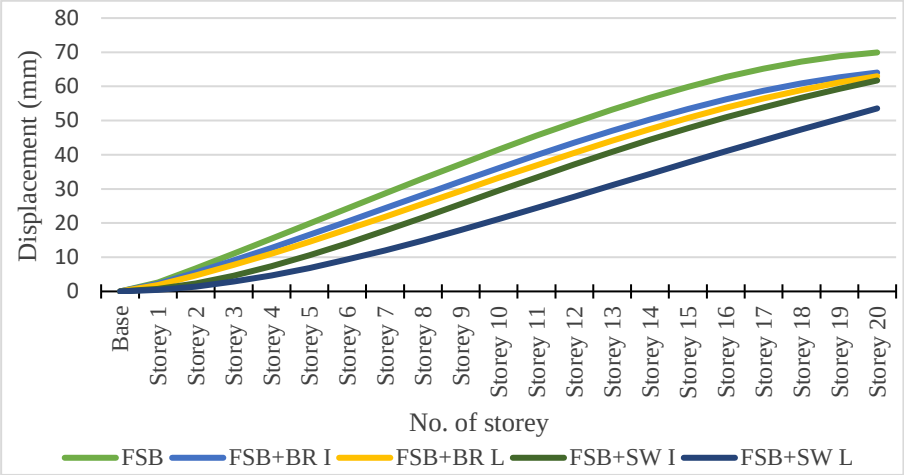

Fig. 8. Displacement in y direction

The above Figure 8 show that displacement y direction is shorter in flat slab structure with L type shear wall at corner as compare to the structure with flat slab and structure with flat slab and bracing. Difference in the maximum value of flat slab structure 69.936mm and maximum value of structure with flat slab and L type shear wall 53.556mm.

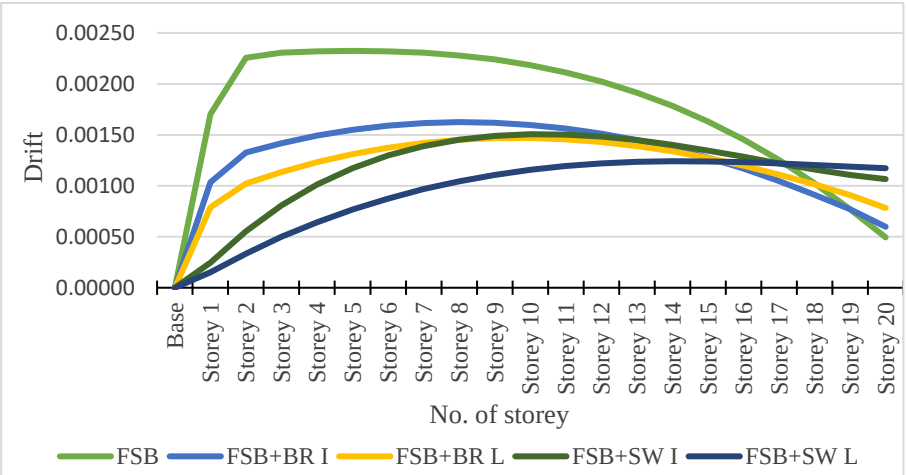

Fig. 9. Drifts x direction

ISBN: 978-81-932056-2-4

The above Figure 9 show that drifts in x direction value found to be within permissible limit according to is 1893:2016 code. Difference in the maximum value of flat slab structure with 0.002324 and maximum value of structure with flat slab and L type shear wall 0.001241.

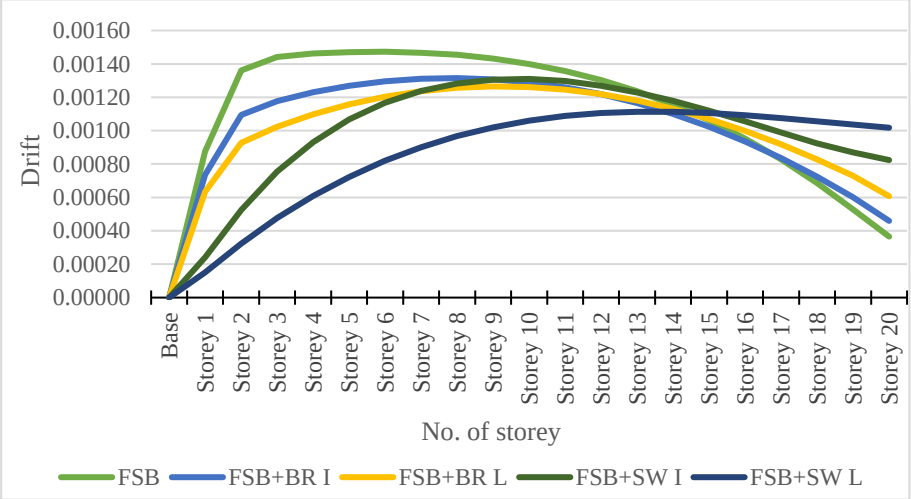

Fig. 10. Drifts y direction

The above Figure 10 show that drifts in y direction value found to be within permissible limit according to is 1893:2016 code. Difference in the maximum value of flat slab structure 0.001473 and maximum value of structure with flat slab and L type shear wall 0.001113.

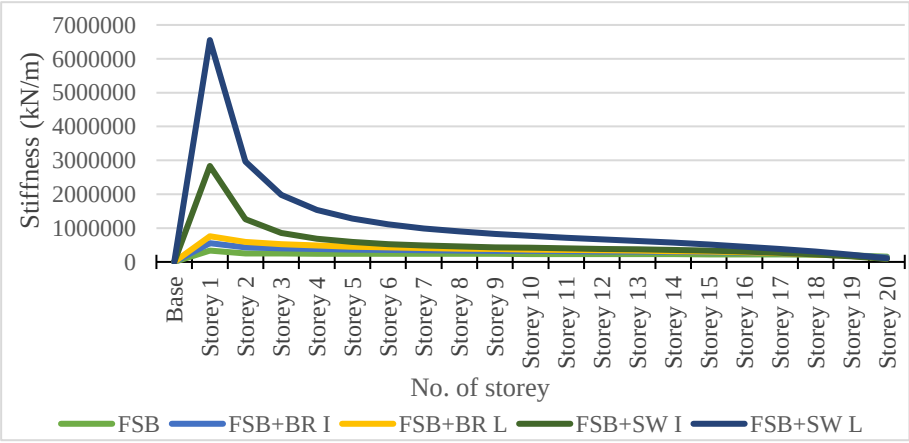

Fig. 11. Stiffness x direction

ISBN: 978-81-932056-2-4

The above Figure 11 show that stiffness in x direction value is maximum at storey 1 in flat slab with L type shear wall as compare to the flat slab structure and structure flat slab and bracing. Difference in the maximum value of flat slab building 334789.143 kN/m and maximum value of flat slab building with L type shear wall 6553441.269 kN/m.

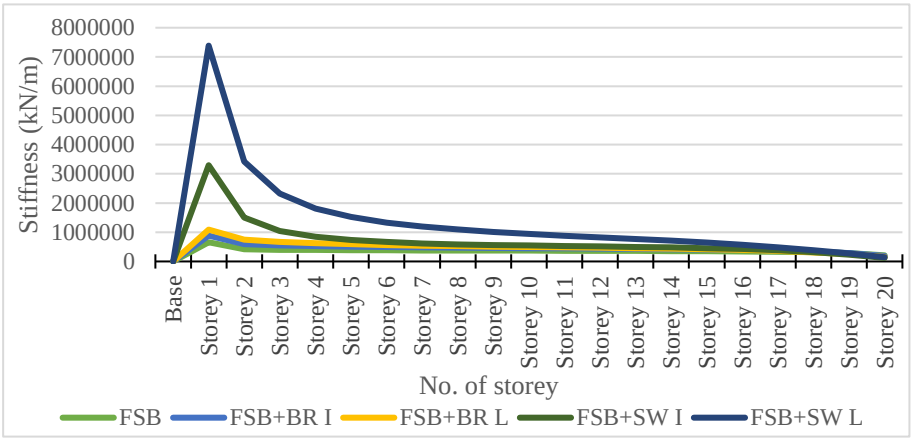

Fig. 12. Stiffness y direction

The above Figure 12 show that stiffness in y direction value is maximum at storey 1 in flat slab with L type shear wall as compare to the structure flat slab and structure flat slab with bracing. Difference in the maximum value of flat slab building 656237.251 kN/m and maximum value of flat slab building with L type shear wall 7386981.538 kN/m.

4 Conclusions

- A structure with a flat slab and shear wall has the lowest displacement value compared to a structure with a flat slab and bracing.
- The drift value was found to be within the permitted limit according to IS 1893:2016.
- The natural time period of a structure with a flat slab and shear wall is less than that of a flat slab structure and a flat slab structure with bracing.
- The storey stiffness performs well in a structure with a flat slab and an L-type shear wall.
- The obtained outcomes are more in the direction of x than y since of the column size.

ISBN: 978-81-932056-2-4

- The entire performance of all five buildings was studied using various parameters. It was discovered that the flat slab structure with an L-type share wall at the corner could improve the later stability of the structure.

References

1. Md. Shahzar md. Md. Tasleem.: Comparative study of flat slab building with shear wall and bracing, International journal of advances in engineering and management vol. 03, (2021).

2. Ms. Nail ashwini shankarrao, Dr. P.B. Ullagaddi: Comparative assessment of flat slab with shear wall and bracing system for different building heights, International research journal of engineering and technology vol. 08, (2021).

3. Mohamed Abdel-Basset Abdo.: Modeling of shear-wall dominant symmetrical flat-plate reinforced concrete buildings, International Journal of Advanced Structural Engineering (2012).

4. Fayazuddin Ahmed Syed, et al.: Comparative Analysis of Flat Plate Multistoried Frames with and Without Shear walls under Wind Loads, International Journal of Engineering and Advanced Technology vol. 02, (2012).

5. Dr. K Naresh.: Comparative Study of Flat Slab and Conventional Slab Structure with and without shear walls using ETABS, International Research Journal of Engineering and Technology, Vol. 06 (2019).

6. Nandona Goswami.: Comparative Study On the Effects of Shear wall and Bracing On Multistoried Building, International Journal of Engineering Applied Sciences and Technology, Vol. 07 (2022).

7. IS 456 (2000).: Plain and Reinforced concrete code of practices, bureau of Indian standards.

8. IS 875 (2015).: Code of practice for design loads for buildings and structures.

9. IS 1893 (2016).: Criteria for earthquake resistant design of structures, general provisions and buildings, bureau of Indian standards.

10. IS 13920 (2016).: Ductile design and detailing of reinforced concrete structures subjected to seismic force.

ISBN: 978-81-932056-2-4

REVIEW AND APPLICABILITY OF IS 3370 (2021) FOR MONOLITHIC PRECAST RCC TANKS

Shree Patel[1] and Vishesh Mistry [2]

[1] CEPT university, Ahmedabad, Gujarat,
[2] Adani university, Ahmedabad, Gujarat

[1] shree.ug180577@cept.ac.in
[2] visheshmistry.im22@adaniuni.ac.in

Abstract. This paper provides a comprehensive review of IS 3370 (2021) and its applicability for monolithic precast RCC tanks. The study captures the salient features of IS 3370 (2021) requirements for RCC Tanks. The authors also compare the provisions of IS 3370 (2021) with international standards to identify areas of major differences. Through their analysis, the authors conclude that IS 3370 (2021) is a valuable resource for designers and engineers working on water tank projects, however its utilization for precast monolithic RCC tanks has some shortfalls. Overall, this paper contributes to the ongoing development of precast structures and best practices in water tank design and construction.

Keywords: RCC water tank, Indian standards, international standards, Structural design, Coefficient method

1 Introduction

Precast concrete is a popular choice for water tanks and other structures due to its combination of strength, durability, customization, and sustainability. It is cost-effective, speed of construction, quality control, and versatility, making it a popular choice in international markets. Many organizations are using this technology at international and national levels.

Monolithic precast RCC tanks are used in various industries for storing liquids. They are designed to be watertight and resistant to corrosion and damage from hazardous chemicals. They can be customized to meet specific requirements and are durable, easy to maintain, and cost-effective. They are also used in the oil and gas industry, wastewater treatment plants, and food and beverage industry. Overall, monolithic precast RCC tanks are a versatile and reliable option for storing liquids.

The most important details are the different types of water tanks available, such as elevated water tanks, ground-level water tanks, and porTable water tanks. Elevated water tanks are typically located at higher elevations to utilize gravity for water pressure and distribution, while ground-level tanks are installed at or below ground level and are used in rural areas. PorTable water tanks are designed for temporary water storage or transportation and are used in emergency situations, construction sites, and outdoor

ISBN: 978-81-932056-2-4

events. Efficient water tank design and management contribute to the sustainability and reliability of water supply systems. For our study we had considered a tank size of 2 m x 2m and height of 3m.

This article discus the salient aspects of 1S 3370 (2021) in design and construction of water tanks. Further this article also presents a comparative study of tanks provisions in international standards.

2 General Requirements as Per IS 3370 (Part -1)

2.1 Materials

The materials used in the construction of liquid retaining concrete structures must comply with IS 456 and IS 1343 standards. Reinforcement must be free from rust and have sufficient bond strength, and pre-stressed concrete must conform to IS 1343. Aggregates must be strong, durable, and free of impurities. Admixtures must conform to IS 456 and IS 9103 to improve concrete properties.

2.2 Exposure Conditions and Durability

IS 456 requires reinforced concrete to have a minimum grade of M30 and a maximum water-cement ratio of 0.45, with a cement content of 320 kg/m3 and a cover thickness of 40-50 mm.

The most important details are the provisions for durability in plain and reinforced concrete structures. For severe exposure conditions, the minimum cement content is 300 kg/m3 and the maximum water-cement ratio is 0.45. For pre-stressed concrete structures, the minimum cement content is 400 kg/m3 and the maximum water-cement ratio is 0.40.

The minimum nominal cover requirements for reinforcement in concrete structures depend on the level of exposure, with 20 mm for mild steel reinforcement and 15 mm for high-yield strength deformed bars for mild, 30 mm for moderate, 40 mm for severe, and 45 mm for very severe and extreme.

2.3 Site Conditions

The physical and geological features of the soil and supporting foundations should be considered when designing a liquid retaining structure. The structures are to be designed to resist water pressure and precautions to prevent floating (uplift) and ensure stable equilibrium under all conditions of internal and external loads need to be taken.

Checking the structure's stability is necessary. 1.25 of safety factor is to be considered for uplifting. When an unsymmetrical structure is subjected to an uplift force, tilting or

ISBN: 978-81-932056-2-4

rotation may result in a loss of stability. In this situation, the safety factor should be at least 1.4 against rotational stability.

2.4 Causes and Control of Cracking

Applied loads, temperature gradients, and retaining liquids at higher temperatures can cause cracking in concrete. Temperature and moisture effects can be controlled by reinforcement and movement joints. Cracking usually occurs when the concrete is still weak.

IS 3370 recommends some methods of crack control. Plain concrete liquid retaining structures with direct tension and reinforcement can be designed. Cracking can be controlled by avoiding or reducing temperature and moisture, curing, covering the surface, and adding structural fibers. Use of deformed bars, tightly spaced bars, and small-size bars, along with proper placement of reinforcing bars, all contribute to better binding in the total reinforcement. Therefore, scattered dispersion of cracks is preferable.

Structural fibers can be added to concrete to improve performance, but it must be tested based on experimental research to ensure improvement in performance.

2.5 Stability

For sloped terrain, the resistance to sliding is crucial in conjunction with earthquake-induced pressures. The restoring moment must be greater than the sum of 1.4 times the maximum overturning moment due to dead and applied loads and 1.2 times the maximum overturning moment due to wind/seismic action to maintain stability.

Probabilistic changes in dead weight, liquid load, and ground pressure must be considered during construction, repair, or other temporary actions to ensure stability at all times.

2.6 Construction

The provisions of IS 456 and IS 1343 shall apply to the building of reinforced concrete and pre-stressed concrete, unless otherwise indicated in this standard. Tank should not be kept empty for more than 3 days and filled with water/liquid of minimum 300 mm depth to avoid drying shrinkage cracks. After liquid-tightness test, tank should be cleaned and disinfected before normal use.

Typically, walls with a thickness of 200 mm or greater are advised. For small tanks with a height under 2 meters, the minimum wall thickness is permitted to be 160 mm. If single layer bar mesh is necessary, the walls of channels and canals in treatment facilities may be 125 mm thick.

ISBN: 978-81-932056-2-4

2.7 Lining of Tanks

The type of liquid to be stored should be considered in relation to the possibility of corrosion of the steel or attack on the concrete. An impermeable protective lining should be provided for resistance to the effects of corrosive liquids. In certain cases, sulphate resisting Portland cement, pozzolana cement, and slag cement may be advantageous. Poly-aluminum chloride tanks and alum solution tanks should be provided with acid resistance coating or lining.

2.8 Testing of Structures

The structure should be cleaned and filled to the normal maximum level with the required liquid at a uniform rate of no more than 2 m per 24 hours at first. When first filled, the liquid level should be stabilized by adding more liquid for a period while absorption and autogenous healing occur. The stabilizing period may be 7 days for a maximum design crack width of 0.1 mm or 21 days for a maximum design crack width of 0.2 mm or more. Following the stabilizing period, the level of the liquid surface must be measured at 24-hour intervals during a 7-day test period. After allowance for evaporation and rainfall, the total allowable reduction in level during this 7-day test period should not exceed 1/500th of the average water depth of the complete tank and 10 mm, or another specific number mutually agreed upon by the contracting parties.

In the event of underground tanks with a covered top, the total allowable decline in surface level over a 7-day period shall not exceed 20 mm.

3 Review of requirements as per IS 3370 (Part -2)

3.1 Loads

All structures required to retain liquids should be designed to withstand the loads they would be subjected to during their service life, such as dead load, imposed load, earthquake load, wind load, earth pressure, snow load, and liquid load.

Liquid Load (FL) is the effect of mass or pressure of the liquid to be considered in the design. It should account for the actual density of the liquid retained and the weight due to deposited silt, grit, accumulated sludge, lime, etc. It should be calculated at zero, partial and full condition to achieve the most critical load combination. Free board of 150-300 mm may be considered for large horizontal tanks.

In the calculation of liquid load, the quantity of liquid must be assumed up to the following levels: Full Supply Level (FSL) Including Dead Storage, Level Under Maximum Overflow Rate or Maximum Top Level (MTL).

ISBN: 978-81-932056-2-4

3.2 Limit State Design

Every section's resistance to bending, shear, torsion, and axial stresses must meet the required value for that section. Section created utilizing the relevant partial safety factors and the most likely adverse load and structural combination. The load combinations and partial safety factor considered are shown in Table 1.

Table 1. Partial Safety Factors and Load Combinations, γ_f for Loads

Load Case	Limit State of Collapse					Limit State of Serviceability				
	DL	***IL***	***EP***	***FL***	***WL/EL***	***DL***	***IL***	***EP***	***FL***	***WL/EL***
1	1.5	1.5	1.5	1.5	–	1.0	1.0	1.0	1.0	–
2	1.2	–	1.0	1.2	1.4	1.0	–	0.7	1.0	0.3
3	0.9	–	1.0	1.0	1.4					
4	1.4	–	1.0	–	1.4					
5	1.2	1.2	1.2	1.2	1.2					

NOTES
Wind and earthquake loads should be considered one at a time and not simultaneously.
For any load combination, the partial safety factor for liquid load (*FL*) may be further reduced if it is expected to give more critical design action at a section of a member. In a combination, liquid load can range from zero (empty tank) to 1.5. The same can be said for earth pressure in load combinations.
Earthquake base shear must be calculated for a load combination of 1 DL + 1 FL + 1 ILs + 0.7 ILp, where ILs is the storage-imposed load and ILp is the provisional imposed load induced by equipment load. The determined earthquake base shear (or force action) must be multiplied by the load factor shown in Table 1 before being combined with additional loads.

Shear strength of a member subjected to direct tension in combination with bending moment The design shear strength of concrete given in Table 19 of IS 456 shall be multiplied by the following factor: $\delta = 1 - 8 \times Pu/ (Ag\ f_{ck})$. Crack widths due to temperature and moisture effects must be calculated in accordance with IS 3370-2021 (Part-2) Annex A for immature concrete and Annex B for mature concrete. Details of maximum stresses in plain round mild steel bars are shown in Table 2 as per IS 456 and when crack width calculations are not done permissible stress are applicable from IS:3370 (Part II).

Table 2. Maximum Stresses in Plain Round Mild Steel Bars (SLS)

Sr. No.	Limiting Crack Width (mm)	Maximum Stresses (N/mm²)	
		Plain Round MildSteel Bars	High Strength Deformed Bars
1	0.1	85	100
2	0.2	115	130

ISBN: 978-81-932056-2-4

Table 3 shows the specifications of Maximum Tensile Stress in Steel Reinforcement for Crack Control in Walls and Slabs.

Table 3. Steel Reinforcement Maximum Tensile Stress for Crack Control in Walls and Slabs (SLS)

Sr. No	Diameterof Steel Reinforcement (mm)	Centre-to-centre Spacing of Reinforcement, *Max* (mm)	Maximum Stress, *Max* (N/mm^2)
1	10 or 12	75	155
2	12 or 16	100	150
3	16 or 20	125	148
4	20 or 25	150	145
5	20 or 25	175	142
6	25 or 28	200	140
7	32	200	135

Table 4 shows different tightness class with respect to the limiting crack width and requirement for leakage.

Table 4. Classification of Tightness

Sr. No.	Tightness Class	Limiting crack width (mm)	Requirements for Leakage
1	1	Full thickness of the section (that is, no compression block) be limited to 0.2 mm.	Leakage will be kept to a minimum. Surface stains or damp patches are Acceptable.
2	2	0.2 mm and cracks expected to extend through the entire thickness of the section are avoided unless appropriate measures such as liners or water bars are used. Alternatively, limiting crack width shall be 0.1 mm.	Leakage to be minimal. The appearance should not be harmed by staining.
3	3	Limiting crack width shall be 0.1 mm.	No leakage permitted. Special measures such as Prestressing or liner required.

The limiting crack width values as given in 4.4.3.3 may be exceeded by 0.05 mm, if H/t ratio is 20 or less. However, the limiting crack width shall not exceed 0.2 mm, in any case.

3.3 Detailing

ISBN: 978-81-932056-2-4

The reinforcement provided for design of the precast RCC tank is not less than that specified in Table 5.

Table 5. Minimum Percentage of Reinforcement

Sr. No.	Grade of Reinforcement	Elevated Tankwith Length		Ground supported Tankwith Length	
		≤ 14 m	≥ 28 m	≤ 14 m	≥ 22 m
1	Fe 250	0.44 Percent	0.66 Percent	0.40 Percent	0.60 Percent
2	Fe 415 or Fe 500	0.28 Percent	0.42 Percent	0.24 Percent	0.36 Percent

The minimum reinforcement for walls having thickness less than 160 mm or slabs having thickness less than 180 mm should be placed in one face. For ground slabs having thickness less than 300 mm, the reinforcement should be placed wholly in top surface with cover not exceeding 50 mm. For ground slabs having thickness more than 300 mm, the reinforcement should be calculated separately for top and surface zone and placed accordingly with cover not exceeding 50 mm.

4 Design Practice for RCC Precast Monolithic Tank as Per IS 3370 -2021(Part:4)

4.1 Introduction

The code proposes a co-efficient method for identification of defects and shear and moment calculation in tanks at various locations. Part-04, section :2 gives design Tables for rectangular tanks. The scope covers single cell and multi-cell rectangular tanks. The factors considered for developing various cases and the nature of load (triangular/rectangular), boundary conditions, such as fixed tops and base of tank and aspects ratio. The tank dimensions are divided into 10 parts, vertically and horizontally and co-efficient for deflection, shear, moment is provided for various cases.

4.2 Methodology for Structural Design of RCC Water Tanks as Per IS 3370

The structural design of a precast water tank using IS 3370 (2021) coefficient method includes determining the design load, selecting the appropriate coefficient, calculating the minimum wall thickness, determining the concrete grade and cover, calculating the total tension force, determining the reinforcement, calculating the minimum area of reinforcement required, determining the number and size of reinforcement bars required, and determining the spacing of the reinforcement bars required to meet the minimum area of reinforcement.

ISBN: 978-81-932056-2-4

5 Steps for Designing a Rectangular Precast RCC Water Tank.

1. The IS 3370: 2021 code is referred for designing the water tank.
2. Input of material grades such as concrete and steel grades.
3. Required tank size input (height, width, and length)
4. Input of parameters such as site conditions such as subterranean or above ground.
5. Modulus of elasticity Ec, Poisson's ratio input
6. Identifying the boundary condition at the tank's base and top (free, hinged, or fixed)
7. Identification of load combinations with suitable safety factors.
   (a) Water inside, no earth outside
   (b) Earth outside, no water inside
   (c) Surcharge outside, no water inside
   (d) No water inside, Earth and surcharge outside
8. Identification of appropriate case (based on BC & loading)
9. Extraction of deflection coefficient for appropriate case.
10. Calculation of deflection:

    $\delta = 12\ \delta_c\ q\ a^4\ (1-\mu^2) / (1000\ E_c\ t^3)$

11. Identification of moment coefficient for applicable case.
12. Calculation of moments

    Moment per unit width, in N-m/m is given by the following equations:

    $M_x = M_{xc}\ q\ a^2/1000$

    $M_y = M_{yc}\ q\ a^2/1000$

    $M_z = M_{zc}\ q\ a^2/1000$

ISBN: 978-81-932056-2-4

$M_{xy} = M_{xyc}\, q\, a^2/1000$

$M_{yz} = M_{yzc}\, q\, a^2/1000$

13. Calculation of area of steel (A_{st}) required based on moments.
14. Selection of bar diameter and spacing based on area of steel (A_{st}). Planning of standardized reinforcement cage.
15. Identify of shear coefficient for applicable case as per IS3370 Part 4 section 1.
16. Calculation of shear.
17. Provision of shear reinforcement if required.
18. Calculation of crack width and adjustment of cover and reinforcement to comply to crack width requirement.
19. Identification of cover, location of lifting embedment's etc.
20. Detailing of precast tank as per requirement.

6 Comparative Analysis with International Standards

This study includes comparative analysis of important aspects such as minimum wall thickness, cover blocks, concrete grade, and performance testing for watertightness of Indian standards with international standards such as National Precast Concrete Association (NPCA), American Society for Testing and Materials (ASTM) C1127, and American Concrete Institute (ACI) 350. Table 6 shows the comparison between the minimum wall thickness required as per different standards.

Table 6. Minimum wall thickness

Standards	Tank type	Wall Thickness
NPCA	Precast concrete tank	76.2 mm
ACI 350	Precast concrete tank	102 mm
IS 3370 (Part 1): 2021	Construction of Walls	200 mm or more, and minimum 160 mm for tank height of 2 m

Table 7 shows the cover block requirements as per all the listed international standards.

Table 7. Cover blocks comparison

ISBN: 978-81-932056-2-4

Standards	Environment condition	Specified cover (mm)
American concrete institute ACI 318.2M-14	Exposed to weather or in contact with ground	30 – 40
	Not exposed to weather or in contact with ground	20 – 10
ASTM C 1227 - 09	Reinforcing Steel Placement	>25
IS 456 2000	Mild Exposure	20
	Moderate	30
	Severe	45
	Very severe	50
	Extreme	75
IS 3370 (Part 2): 2021	Not specified	50

In the Table 8, minimum concrete grade required for Precast RCC tanks is shown as per IS code and international standard.

Table 8. Concrete grade comparison

Standards	Compressive strength	Compressive Strength (MPa)
American concrete institute ACI 318-11	Minimum compressive strength	18
ASTM C1227 - 09	Minimum compressive strength	28
IS 3370 (Part 1): 2021	Minimum compressive strength	30

Different performance testing of water tightness is shown in Table 9 as per the international standards.

Table 9. Performance Testing for Water tightness

Standards	Test type	Description
ASTM C1227 – 13	Vacuum Testing	Apply a vacuum to 4" of mercury and seal the empty tank. If the tank can maintain 100% vacuum for two minutes, it is approved. Apply a minimum vacuum of 4" mercury and seal the tank.
NPCA Best Practices Manual	Vacuum Testing	Depending on a number of circumstances, the vacuum may need some time to stabilize (it is okay to keep vacuuming until it is steady at 4"). Turn the hoover pump off. If there is no pressure loss for five minutes, the tank is certified. If the tank fails the test, it may be repaired and retested.
IS 3370 Part 2: 2021	Leakage Testing	Tightness class 1: Leakage will be kept to a minimum. Surface stains or moist areas are Acceptable. Tightness class 2: Leakage should be kept to a minimum. The appearance should not be harmed by stains. Tightness class 3: No leaking allowed. Prestressing or a liner are necessary as special measures.

ISBN: 978-81-932056-2-4

7 Conclusions

The research article refers to IS 3370 (2021) for possible use in monolithic rectangular precast RCC tanks. The study identifies that the code is a good reference document for water tank design and has simplified the method of design by coefficient method. Further, the code has divided the tank proportions in $1/10^{th}$ of the dimension to be able to optimize on the stresses and therefore, the reinforcement. However, it's suitability of use for precast RCC tanks is limited because of the following aspects:

- Monolithic precast tanks are limited to comparatively smaller sizes and therefore the optimization benefit provided by the coefficients for 1/10th the tank dimension is not utilized. Due to smaller possibility of sizes, standardization of precast reinforcement cage and minimum crack control spacing, it is generally prudent to design for the maximum moments.

- The thickness, cover and reinforcement requirements of IS 3370 (2021) are much conservative for precast structures. Similar codes for precast septic tanks and international codes exist that give much benefit in terms of material saving.

In a nutshell, the article concludes that there is need to address the precast RCC water tanks with value engineering principles and propose alternate limits for precast structures as compared to cast in situ structures in design.

References

1. Concrete Structures for Retaining Aqueous Liquids - Code of Practice: Part 1 General Requirements. (2021). Bureau of Indian Standards.

2. https://www.services.bis.gov.in/php/BIS_2.0/bisconnect/standard_review/Standard_review/Isdetails?ID=MjU2OTc%3D

3. Concrete Structures for Retaining Aqueous Liquids - Code of Practice: Part 2 Plain and Reinforced Concrete Structures. (2021). Bureau of Indian Standards. https://www.services.bis.gov.in/php/BIS_2.0/bisconnect/standard_review/Standard_review/Isdetails?ID=MjU2OTg%3D

4. Concrete Structures for Retaining Aqueous Liquids - Code of Practice - Part 4 Design Tables - Section 2 Rectangular tanks. (2021). Bureau of Indian Standards. https://infostore.saiglobal.com/en-au/standards/is-3370-part-4-sec-2-2021-1221971_saig_bis_bis_2967021/

5. IS 456: 2000 Indian Standard PLAIN AND REINFORCED CONCRETE - CODE OF PRACTICE. (2000). https://www.academia.edu/6262807/IS_456_2000_Indian_Standard_PLAIN_AND_REINFORCED_CONCRETE_CODE_OF_PRACTICE_Fourth_Revision

ISBN: 978-81-932056-2-4

6. Building Code Requirements for Structural Concrete (ACI 318-19). (2020). Retrieved May 30, 2023, from https://www.usb.ac.ir/FileStaff/5526_2020-1-25-11-12-7.pdf

7. Standard Specification for Precast Concrete Septic Tanks. (2013). Retrieved May 30, 2023, from https://www.fortaferro.com/pdfs/internal%20documents/ASTM%20Reports/ASTM%201227-00b.pdf

8. (2015). BEST PRACTICES MANUAL. Retrieved May 30, 2023, from https://precast.org/wp-content/uploads/2015/02/Precast-concrete-on-site-wastewater-tank-best-practices-manual.pdf

ISBN: 978-81-932056-2-4

INVESTIGATIVE STUDY ON EFFECT OF BASALT FIBERS AND GGBS ON DURABILITY ASPECT OF ULTRA HIGH STRENGTH CONCRETE USING RAPID CHLORINE PENETRATION TEST AND MERCURY POROSITY TEST

Gaurav P. Gohil[1], Prof. Indrajit N. Patel[2], Prof. Amit D. Raval[3] and Prof. Jagruti Shah[4]

[1] Government Polytechnic, Vyara, Gujarat, India
[2] BVM Engineering College, Vallabh Vidyanagar, Gujarat, India
[3] B & B Institute of Technology, Vallabh Vidyanagar, Gujarat, India
[4] BVM Engineering College, Vallabh Vidyanagar, Gujarat, India

[1] gohilgaurav534@gmail.com
[2] inpatel34@gmail.com
[3] adraval@bbit.ac.in
[4] jagruti.shah@bvmengineering.ac.in

Abstract. In present era of the field of advance concrete technology, uses of an Ultra High strength concrete (UHSC) increase due to the higher demand of strength and long-term serviceability, modulus of elasticity, thermal expansion, shrinkage, and durability. For any structural element durability play a vital role which is decide the life span. In present study, especially influence on durability incorporating 1% and 2% of Basalt Fibres in various mixes of UHSC has been investigated. Ground Granulated Blast Furnace Slag (GGBS) has been also added in UHSC as replacement of cement to enhance the concrete properties in proportion of 10%, 12% and 15% at very low water cement ratio. In this paper, durability of UHSC investigated by conducting Mercury Porosity test (MPT) and Rapid Chlorine Penetration Test (RCPT) at 91 days of age with conventional curing technique. As per the guideline of ASTM C 1202, the amount of resist of chloride ion penetration result was found negligible at normal curing condition of curing. While resistant against mercury penetration in MPT also give an excellent result among penetration of mercury.

Keywords: Basalt Fibres, Durability, GGBS, MPT and RCPT.

1 Introduction

To define durability of any concrete, very important and essential terms considered as a “pore” which must be considered while calculating the life span of concrete structure. Generally, the pore is nothing but the internal structure which may be developed by many ways. These pores play a very important role while the performance of any structure comes into the picture. The pores in the structure of concrete might be either air, capillary, or gel pores. Concrete is characterized as heterogeneous which converted to homogenous by optimized microstructure by removing the course materials and

ISBN: 978-81-932056-2-4

introduced a new innovative finer material for precise gradation of all the particles in the mix to yield maximum density [1]. Generally, Fibres in reinforced concrete used when the element is expected to wear and tear; and increase the substantial benefits including enhancing the durability, impact, Fatigue, Flexural strength, toughness and tensile strength, ductility as well shrinkage cracking control [2,4].

Basalt Fibres are newly developed, revolutionary fiber with exceptional mechanical attributes especially in the engineering, thermal and Mechanical properties. Innovation Deserving Exploratory Analysis (IDEA) had used it kind of fiber in high construction and the use of doses was found in the range of 0.1% to maximum 0.5% of the volume of cement. While mixing the concrete it is found that basalt Fibre easily disperse without any segregation and lose their shape. the main reason was due to flexibility. unlike comparing with other fibers which really cause very difficult in handling and mixes with cement this basalt fiber has tendency to user-friendly application like other solid material. Basalt Fibres also encouraging the effect of concrete strength and cracking resistance.

It is essential to have sufficient knowledge of material used in the development of concrete and performance of concrete. The parameter of material which is likely to be used in concrete has great impact on long term durability and performance of structural element. The basic ranges of use of supplementary material and along with fiber develop significant role to resist against the forces like compressive, tensile, developing the internal movement in terms of thermal expansion and contraction etc. To overcome and justify the challenges, in the experimental work the authors have used high amount of Basalt fibre in the range of minimum 1% to maximum 2% ranges in various proportional concrete matrix to identify the effect on mainly durability of UHSc.

2 Materials and Experimental Investigation

2.1 Cement – OPC 53 Grade

OPC of 53 grades available in local market is used in the investigation. The basic test on cement was performed and it was found satisfactory as per IS 4031-1988 and conforming to the IS 12269-1987.

2.2 Fine Aggregate

Fine aggregate used was confirmed to zone-II and obtained from river. The sp. gravity and Fineness modulus were found respectively 2.6 and 2.86.

ISBN: 978-81-932056-2-4

2.3 Silica Fume

Silica fume (D 990 Grade) was obtained from Elcom India Pvt. Ltd with major part 93.87% SiO_2 conforming the IS 15388-2003 and Oil and Natural Gas Corporation of India (ONGC) specifications.

2.4 Quartz Sand

Quartz Sand of size 300 micron was used in this experimental investigation with river sand.

2.5 GGBS

The GGBS was acquired from a local corporation. GGBS is ground to less than 45 microns and has a glassy structure. There are between 350 and 450 m^2/kg of surface.

Table 6. Chemical content of Cement, Silica Fume and GGBS [8]

	OPC-53 Grade	**Silica Fume**	**GGBS**
Specific Surface (m^2/g)	2.95	16.4	3.3
Loss of Ignition (%)	-	1.9	1.41
Average Size of particle (Micron)	-	-	2.4 – 3.6
SiO_2 %	21.82	93.3	-
Al_2O_3 %	2.21	0.08	14.42
CaO %	71.34	1.0	37.34
MgO %	1.58	0.8	8.71
SO_3 %	2.25	-	-
MnO %	0.16	0.05	0.02
Na_2O_3 %	0.23	0.4	-
SiO_2 %	-	-	37.73
K_2O %	0.26	2.43	-
TiO_2 %	0.15	0.04	-
MnO %	0.16	-	-
Fe_2O_3 %	-	-	1.11

2.6 Basalt Fibres

Chopped Basalt Fibres of size 0.2 x 25 and Specific Gravity of 2.63 – 2.78 was used. The following Table 2 and 3 shows the amount of chemical composition along with its physical properties of Basalt fiber.

ISBN: 978-81-932056-2-4

Table 7. Amount of Chemical ingredients founds in Basalt Fibres

Chemical proportion of Basalt Fibres (%)							
SiO_2	Al_2O_3	CaO	MgO	FeO + Fe_2O_3	TiO_2	Na_2O + K_2O	Others
54-60	15 – 18	6 – 7	3.2 – 5	9.0 – 14	0.8 – 2.25	0.75 – 2.0	0.08 – 0.14

Table 8. Properties of Basalt Fibres [9]

Fibre Type	Shape	Size (mm)	Tensile Strength	Modulus of Elasticity	Specific Gravity	Elongation %
Chopped	Rectangular	0.2 x 25	4100 – 4820 MPa	93.1 – 1.2 GPa	2.63 – 2.78	2.9

2.7 Super Plasticizer

Super plasticizer of Gellinium series was used in this investigation study. The dosage was decided by mash cone test.

2.8 Water

Locally available potable water is used, and it conforms to the BIS 456-2000.

3 Specimens

For experimental investigation the following size of cube and sample were used.

1. For RCPT, cylinder of size 100mm diameter and 50mm height were cast and left for curing 91 days as per ASTM C1202.

2. For mercury penetration test, the sample was taken approximately by 2gm, and it was obtained from the cube of 28 days curing specimen.

3.1 Design Mix

Based on literature study, references, and practical repetition with trial mixes; six trial mixtures were prepared for targeted strength 120MPa. Final design mixtures with replacement and without replacement are shown in Table 4.

Table 9. Mix Design of UHSc.

Series	Sample	Cement (kg/m^3)	Addition (kg/m^3)		FA (kg/m^3)		BF (%) of Cement	Water	W/C	SP.
			Silica Fume	GGBS	River Sand	Quartz				
A	M1	930	291	0	1172	146	0 %	186	0.2	17.67
	M2						1 %			

ISBN: 978-81-932056-2-4

	M3						2 %			
	N1						0 %			
B	N2	837	291	93	1172	146	1 %	167.4	0.2	15.9
	N3						2 %			
	O1						0 %			
C	O2	819	291	98.3	1172	146	1 %	163.8	0.2	15.56
	O3						2 %			
	P1						0 %			
D	P2	790	291	139.5	1172	146	1 %	158	0.2	15.01
	P3						2 %			

Series A

Mix 1 with GGBS content 0% GGBS + 0% Basalt Fibres at w/c ratio 0.2
Mix 2 with GGBS content 0% GGBS + 1% Basalt Fibres at w/c ratio 0.2
Mix 3 with GGBS content 0% GGBS + 2% Basalt Fibres at w/c ratio 0.2

Series B

Mix 1 with GGBS content 10% GGBS + 0% Basalt Fibres at w/c ratio 0.2
Mix 2 with GGBS content 10% GGBS + 1% Basalt Fibres at w/c ratio 0.2
Mix 3 with GGBS content 10% GGBS + 2% Basalt Fibres at w/c ratio 0.2

Series C

Mix 1 with GGBS content 12% GGBS + 0% Basalt Fibres at w/c ratio 0.2
Mix 2 with GGBS content 12% GGBS + 1% Basalt Fibres at w/c ratio 0.2
Mix 3 with GGBS content 12% GGBS + 2% Basalt Fibres at w/c ratio 0.2

Series D

Mix 1 with GGBS content 15% GGBS + 0% Basalt Fibres at w/c ratio 0.2
Mix 2 with GGBS content 15% GGBS + 1% Basalt Fibres at w/c ratio 0.2
Mix 3 with GGBS content 15% GGBS + 2% Basalt Fibres at w/c ratio 0.2

4 Test of UHSc and Discussion

4.1 Rapid Chlorine Penetration Test

RCPT results with various proportions of GGBS and Basalt Fibres are shown in Table 5 and Fig. 1 at the age of 91 days. RCPT results show negligible amount penetration of iron comparing to normal mix design as per ASTM C1202.

ISBN: 978-81-932056-2-4

Table 10. RCPT test Results at 91 days age

Series	Sample	BF	% of GGBS	Chloride ion Penetration
A	M1	0 %	0%	70
	M2	1 %		73
	M3	2 %		75
B	N1	0 %	10%	71
	N2	1 %		75
	N3	2 %		78
C	O1	0 %	12%	72
	O2	1 %		74
	O3	2 %		71
D	P1	0 %	15%	80
	P2	1 %		81
	P3	2 %		74

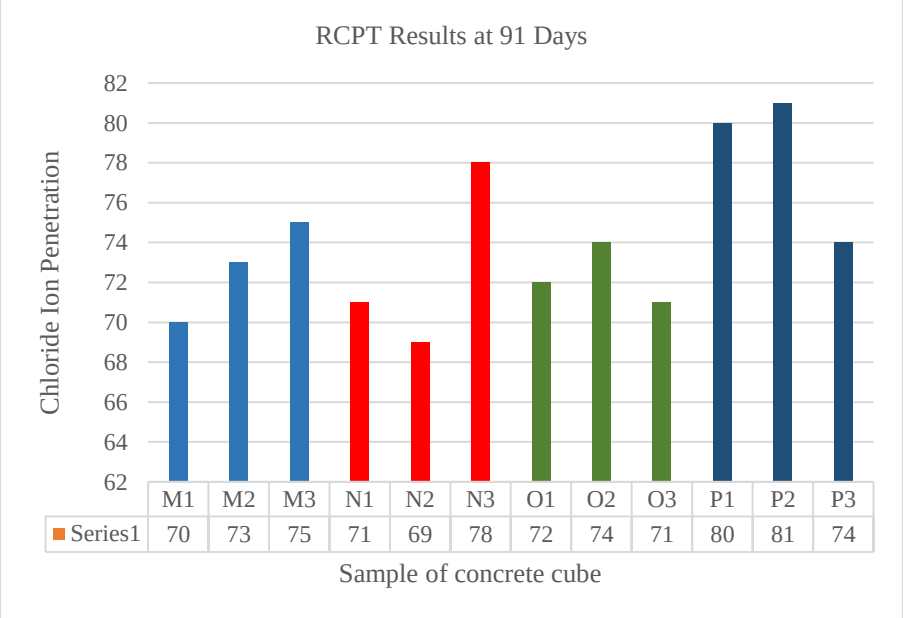

Fig. 1. RCPT test results at 91 days

From Table 5 and Fig.1, it is observed,

- In UHSc samples without any incorporation of SCM, it is observed that average RCPT values at 91 days are 70, 73 and 75. After adding 10 % GGBS, chloride

ISBN: 978-81-932056-2-4

penetration value increases and it is further decrease while adding more GGBS up to 12% and it is again increasing the penetration value while adding 15%.

- Measurement of passing of current for six hours in all samples at an interval of 15 min found that the value to be almost constant which reflects uniform dense mix and lower permeability in the concrete.

- All samples with and without Fibre inclusion show negligible permeability as per ASTM C1202 and show excellent quality concrete.

4.2 Mercury Penetration Test

MPT results with various proportions of GGBS and Basalt Fibre are shown in Table 6 and Table 7 which implies the improvement in resisting against the penetration of mercury at age of 91 days which reflects denser texture.

Table 6. Mercury Penetration Test input data

Sample mass (gm)	1.642
Density of Sample in Gram(g)	1
Height of Mercury (mm)	27.666
Volume of mercury at run (mm^3)	471
Dilatometer weight + mercury + sample (g)	232.051
Capillary mercury height (mm)	0.666

Table 7. Mercury Porosity Test output data

Gross cumulative Volume (cc/g)	0.059
Total specific surface area (m^2/g)	9.404
Avg. pore diameter (micron)	0.028
Gross porosity (%)	8.672
Bulk density (g/cm^3)	1.450
Apparent density (g/cm^3)	1.587
Sample volume correction	0.923

ISBN: 978-81-932056-2-4

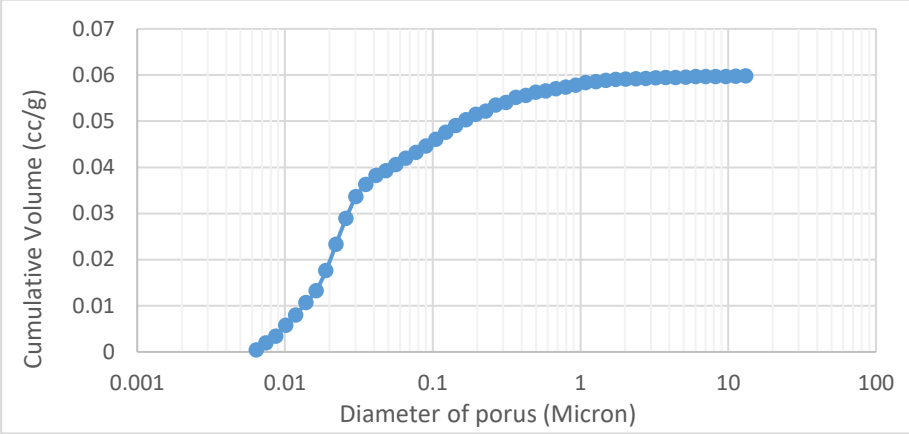

Fig. 2. Cumulative Volume v/s Dia of pores

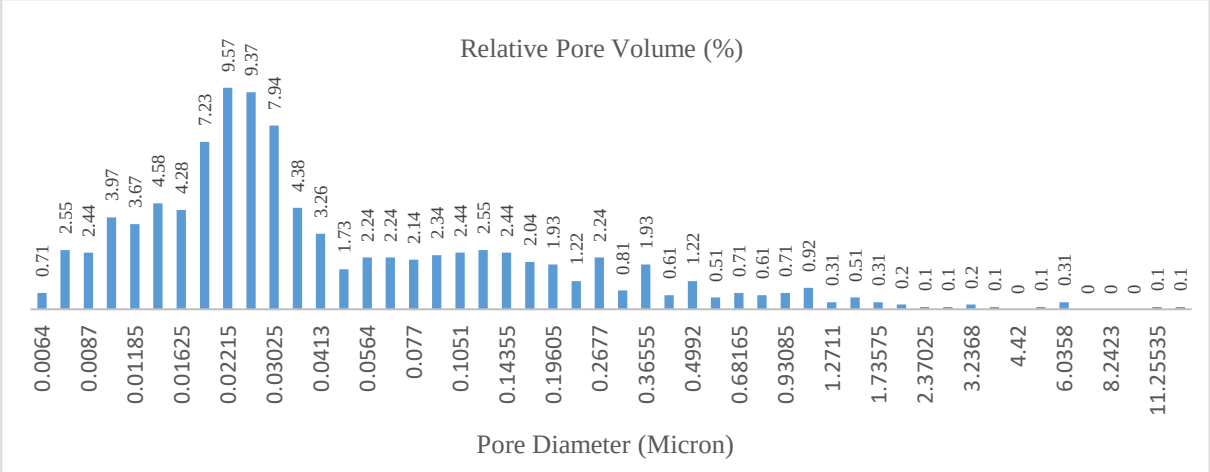

Fig. 3. Relative pore volume (%) v/s Pore Diameter

From Table 6 and 7 and Fig. 2 and 3, it is observed,

- From Fig. 2, pore size distribution shows the arrangement of uniformly well graded particles which indicated the good packing matrix of mixes. For same Fig. 3 shows the relative pore volume per defined pore diameter ranges. In which as the size of diameter of pore increases, relative pore volume increases and further decreases as diameter increases.

- Due to the well graded uniformly distributed particles, a high degree of packing density was achieved and that is the main result to sustain against the deteriorations.

ISBN: 978-81-932056-2-4

5 Conclusions

The following results have been obtained as the outcome of the experimental work, analysis, and comparative investigations.

In the current investigation, it was found that the application of UHSC to substitute some of the cement with mineral admixtures helped concrete's durability attributes. From the Mercury porosity test, the porosity is less due to dense texture of concrete which shows very good durability of concrete. Because of high degree of packing density and uniform pore size distribution, penetration of Chlorine ion negligible range as per ASTM C1202[7] which shows good durability of concrete.

References

1. Artemenko S., Polymer composite materials made from carbon, Basalt, and glass Fibres. Structure and properties. Fibre Chemistry 35(3), p. 226 (2003)

2. Brown, R., Shukla, A., & Natarajan, K. R. 2002. Fibre reinforcement of concrete structures. Technical Report (URITC Project No. 536101) for University of Rhode Island Transportation Centre.

3. Brik, V., Ramakrishnan, V., Tolmare, N. Performance evaluation of 3-D Basalt Fibres reinforced concrete & Basalt rod reinforced concrete. IDEA Program Final Report, Contract No. NCHRP-45 (1998).

4. Gaurav Gohil, Indrajit patel et.al, "Experimental Study, used of SCMs on Engineering Properties of RPC – A Review". Journal of civil engineering and Environment technology, vol 3, p. 75 – 77.(2016).

5. Sivakumar, A., Santhanam, M. Mechanical properties of high strength concrete reinforced with metallic and non-metallic Fibres. Cement and Concrete Composites 29 (8), p. 603.(2017).

6. Shen, L.J., Xu, J.Y., Li, W.M., Fan, F.L., Yang, J. Y. Experimental investigation on the static and dynamic behavior of Basalt Fibres reinforced concrete. Concrete 4:026.(2008).

7. Handbook for Rapid Chloride Penetration Test Guidelines ASTM C 1202

8. Elecom 201 and JSW Cement Ltd data sheet.

9. Arrow Technical Textile Private Ltd data sheet.

ISBN: 978-81-932056-2-4

EFFECT OF BASALT FIBRES ON ENGINEERING AND RHEOLOGICAL PROPERTIES OF ULTRA HIGH STRENGTH CONCRETE

Gaurav P. Gohil[1], Prof. Indrajit N. Patel[2], Prof. Amit D. Raval[3] and Prof. Jagruti Shah[4]

[1] Government Polytechnic, Vyara, Gujarat, India
[2] BVM Engineering College, Vallabh Vidyanagar, Gujarat, India
[3] B & B Institute of Technology, Vallabh Vidyanagar, Gujarat, India
[4] BVM Engineering College, Vallabh Vidyanagar, Gujarat, India

[1] gohilgaurav534@gmail.com
[2] inpatel34@gmail.com
[3] adraval@bbit.ac.in
[4] jagruti.shah@bvmengineering.ac.in

Abstract. Objective: In the following study, an experimental work was carried out to investigate the effect on compressive strength and rheological properties of Ultra-High Strength Concrete (UHSC) by using various proportion of chopped Basalt Fibres (BF) and Ground Granulated Blast Furnace Slag (GGBS). **Methods**: In this study, Chopped BF were added into the UHSC by percentage of cement weight fraction of 0%, 1% and 2% with GGBS of 0%, 10%, 12% and 15% weight of cement and casted a controlled concrete mix for 0.2 W/C ratio. **Findings**: In order to find the effective use of GGBS and BF on the rheological and engineering properties of UHSC, slump test and compressive strength test were carried out to find out workability of fresh concrete and comp. strength at age of 7, 28 and 91 days. To find out compressive strength, the specimens were tested under universal compressive testing machine with loading capacity of 200 tonne. The test results Shows that increment of BF up to 1% and GGBS up to 12% in UHSC leads to increase both rheological as well as compressive strength parameter.

Keywords: Basalt Fibre, Engineering Properties, Ultra-High Strength Concrete

1 Introduction

Many experimental research work on high strength concrete has been conducted over many years which strives to a develop Ultra High Strength Concrete (UHSC). The UHSC itself considered as a special type of concrete in which the microstructure of the concrete is been optimized by accurately selected materials gradation until to get maximum density which help for enhancing in homogeneity and microstructural properties. In the field, UHSC is been one of the primary advances in concrete and it gives many reasonable solutions on problem regarding to concrete. UHSC having high potential against the static dynamic strength, higher fraction capacity, shrinkage, and durability under the very severe atmosphere conditions. The basic improvements in

ISBN: 978-81-932056-2-4

strength parameter of UHSC is only due to uniform particle size distribution, homogeneity in concrete matrix, less porosity and improvement in microstructures. The generalized failure mechanism in ordinary concrete under compressive load is due to create a weaker zone between coarse aggregate and cement paste. For that reason, coarse aggregate eliminates from the UHSC. The Compressive Strength properties can be achieved in range between 100 – 800 MPa, Energy during fracture of the concrete ranges between 1200 and 40,000 J/m^2 at the strain value of 1% of ultimate tensile strength [2]. UHSC is significantly used where required some special architectural consideration in which less weight and high load carrying configuration needed. However, as a property of UHSC in which subjected to sustained loads tends to be brittle failure. That is main drawback to use in earth quake sensitive region. In addition to Fibres in concrete beneficial to convert the brittle failure in to ductile failure, improve tensile strength, increase in toughness, flexural strength, and ductility. In this research paper, the rheological and mechanical properties of UHSC through slump and compression test by using Basalt Fibres and GGBS at 0.2 W/C ratio has been analyzed.

2 Experimental Program

2.1 Properties of Materials

For the experimental work, cement used in UHSC mixes was OPC 53 grade conforming to codal provision of IS 12269- 1987. Local river sand used as a fine aggregate having with specific gravity of 2.40. As Ultrafine material, densified normal silica fume with spherical particles sizes less than 1 μm in diameter was used. For improvement of workability of fresh concrete, water reducer (super plasticizer) Master Gelenium 51 has been used. In additional to increase the packing density, quartz powder used in concrete matrix. The detailed properties of Basalt fibre and Silica fume shown as in Table 1. After conducting various trial mixes, the final mix design has been given in Table 2

Table 1. Engineering Properties of Basalt Fibres and Silica Fume (SF)

Properties	Basalt Fibres	Silica Fume
Length/Dia. (Average)	25 mm	-
Shape	Chopped	Spherical
Size/Diameter	2mm x 25 mm	0.09 – 0.12 μm
Density (kg/m^3)	2300 - 2650	270 – 310
Specific Gravity	1.2-1.4	2.25
Tensile Strength (MPa)	4100 – 4850	-
Modulus of Elasticity (MPa)	93 - 110	-

Table 2. UHSC mix proportion

w/c Ratio	Cement	River Sand	Silica Fume	Quartz Sand	Chemical Admixture

ISBN: 978-81-932056-2-4

-	Kg/m^3	Kg/m^3	Kg/m^3	Kg/m^3	-
0.20	930.0	1100.0	230.0	150.0	1.4 %

2.2 Test Specimens details

To analyze the rheological properties of UHSC, slump cone with top dia. 100 mm, bottom dia. 200 mm along with height 300mm were used. To find the compressive strength, 100 x 100 x 100 mm cubical mould were used. In the preparation of concrete mix, all the finer materials, fine aggregate and cement initially mixed in dry state. In second stage Basalt Fibers were added in dry mix through uniformly mixing operations. 50% water added in the first stage, 50% super plasticizer is added afterwards. After mixing them, rest of water and super plasticizer are been added in to the concrete matrix. The specimens were kept in to the dry place for 24 hours and after it will be allowed to demolded the cube and put the specimen in to the water up to next testing date. The various proportion of mixes presented in Table 3.

Table 3. Mix matrix for trail

Mix Type	Replacement of GGBS	Basalt Fibres
M1	0%	0% 1% 2%
M2	10%	0% 1% 2%
M3	12%	0% 1% 2%
M4	15%	0% 1% 2%

3 Test Results and Discussion

3.1 Fresh Concrete Properties

Rheological properties of fresh concrete have been analyzed by slump test, the experimental results are as shown in Figure 1. It was found that slump is ranging between 110 - 122 mm for water cement ratio 0.2. from the result is has been observed that slump value increased as percentage of Basalt Fibre and GGBS increase up to 1% and 12% and further decreases. Up to 15% GGBS, it does not affect the initial setting time of concrete and mixing operation. Up to 10% GGBS, required amount of water reducer was 1.4% but it increase up to 0. 4% as % of GGBS increases.

ISBN: 978-81-932056-2-4

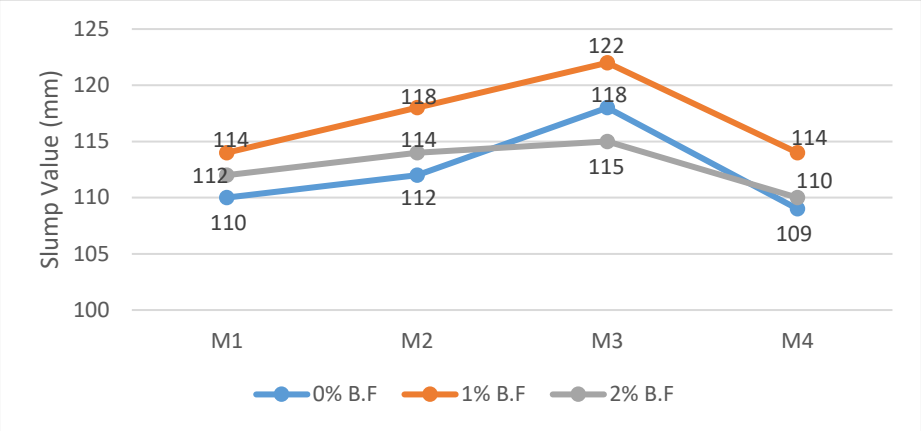

Fig. 1. Slump test result data

3.2 Compressive Strength

The compressive strength test was performing on a universal testing machine (UTM) of 200 tonne capacity. The test was carried out on 7th, 28th and 91th day of curing. After 7 days, the maximum strength was achieved in specimen M3 with 1% BF of 72.29 N/mm^2 which was higher than the other Control Mix as in Figure 2. Average compressive strength at 28 days of M3 with 1% BF was 127.1 N/mm^2 compared to the normal control mix M1 with 0% BF, this was 8.65% higher as shown in Figure 3. M3 yielded a 129.0 N/mm^2 with 1% BF which was 8.89% higher than the control mix M1 with 0% BF at 91 days as shown in Figure 4. It has been observed that as increases in percentage of GGBS up to 12% and BF up to 1%, compressive strength of UHSC increases up to 8 - 9 % and further it decreases as increase percentage of GGBS and BF.

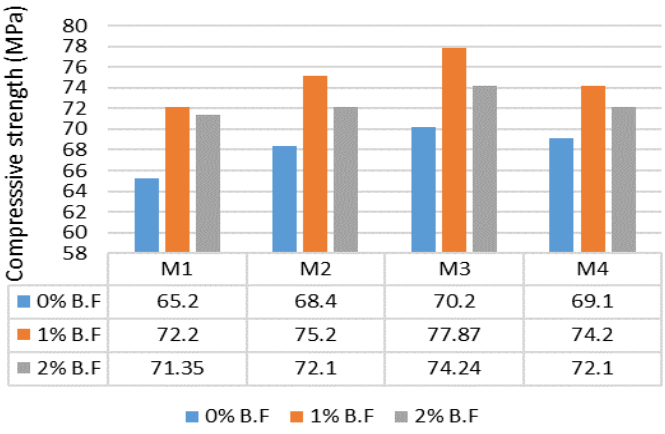

Fig. 2. Compressive strength tests at 7 days age result data

ISBN: 978-81-932056-2-4

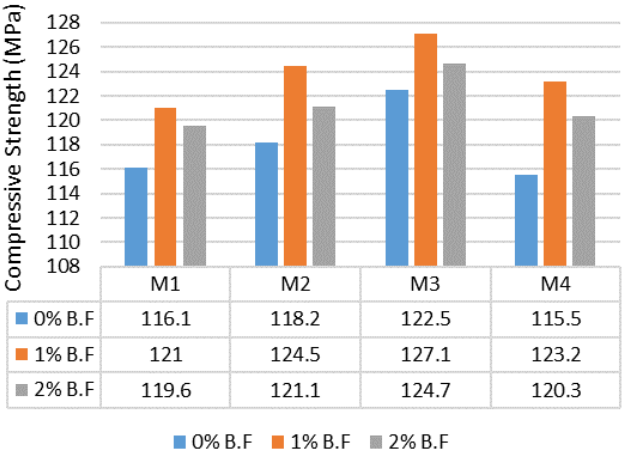

	M1	M2	M3	M4
0% B.F	116.1	118.2	122.5	115.5
1% B.F	121	124.5	127.1	123.2
2% B.F	119.6	121.1	124.7	120.3

Fig. 3. Compressive strength tests at 28 days age result data

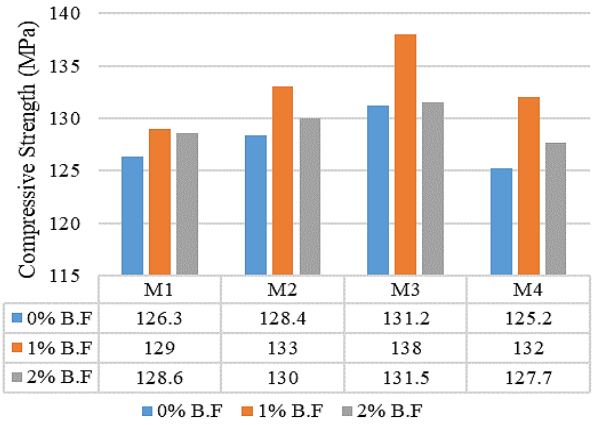

	M1	M2	M3	M4
0% B.F	126.3	128.4	131.2	125.2
1% B.F	129	133	138	132
2% B.F	128.6	130	131.5	127.7

Fig. 4. Compressive strength test at 91 days age result data

4 Conclusions

- Slump Value ranges from 110 to 120 mm average which shows good workability and suitability for UHSC. Slump is gradually settled due to self-weight no collapse found.

- Overusing basalt fibres, above 1% of cement, has a deleterious effect on both the slump and setting time of cement. Additional dosages of super plasticizer, up to a dosage of 0.2 to 0.3%, were required to restore the original characteristics of concrete.

ISBN: 978-81-932056-2-4

- By experiments it was observed that up to 15% used of GGBS not affect the setting time basically initially of concrete.
- Cement partially replaced by amount of GGBS was improves the workability due to fineness of GGBS.
- Compression failure does not reflect sudden crushing but it is gradual from surface to core. This may be due to well dispersed of Basalt Fibres.
- The high strength is achieved due to uniform distribution of all courser and finer materials with high degree of packing density.
- Compressive Strength is increased by 5 – 8% by incorporating GGBS and Basalt Fibres.

References

1. Yin-Wen Chan*, Shu-Hsien Chu Effect of silica fume on steel fiber bond characteristics in reactive powder concrete, Cement and Concrete Research 34 1167–1172 (2004)
2. M.M. Reda, N.G. Shrive, J.E. Gillott, Microstructural investigation of innovative UHPC, Cem. Concr. Res. 29 323– 329 (1999)
3. N. Roux, t C. Andrade,z and M. A. Sanjuan, "Experimental study of durability of Reactive Powder Concretes". Journal of materials in civil engineering / February 1996 /1.
4. Assem Abdelalim, Mohamed Ramadan, Tarek Bahaa and Wael Halawa. "Performance of Reactive Powder Concrete Produced using Local Materials". HBRC Journal VOL. 4 No. 3 December (2008)
5. Halit Yazıcı, Mert Yucel Yardımcı, Serdar Aydın, Anıl S. Karabulut. "Mechanical Properties of Reactive Powder Concrete Containing Mineral Admixtures under Different Curing Regimes". Construction and Building Materials 1223–1231 (2009)

ISBN: 978-81-932056-2-4

EXPLORATORY REVIEW ON COMPOSITE SLABS WITH PROFILE DECKING IN STATE OF ART BUILDING CONSTRUCTION

Pinal Patel[1] and Dr. Vijaykumar R. Panchal[2]

[1] Assistant Professor, M. S. Patel Department of Civil engineering, Chandubhai S. Patel Institute of Technology, Faculty of Technology & Engineering, Charotar University of Science and Technology (CHARUSAT), CHARUSAT campus, Changa 388421, India.
[2] Professor, M. S. Patel Department of Civil engineering, Chandubhai S. Patel Institute of Technology, Faculty of Technology & Engineering, Charotar University of Science and Technology (CHARUSAT), CHARUSAT campus, Changa 388421, India.

[1]pinalpatel.cv@charusat.ac.in
[2]vijaypanchal.cv@charusat.ac.in

Abstract. Now a day, the structural steel and reinforced concrete composite are widely preferred now a days in mixed building systems. This is because of the availability of new rolled and cold formed section, skilled labour, and advancement in anticorrosive paints. This review paper presents an exploratory overview of recent developments in composite slabs with profile decking. The review begins with idea of composite slabs with profile decking and highlights the main characteristics, benefits, and uses. Further the paper explores the behaviour of structural and performance characteristics of composite slabs, with a focus on load-carrying capacities and long-term durability. The highlights of research in different kinds of mechanical steel-concrete connections and types of profile decking used in composite slabs with steel profile decking system is provided. The paper assesses individual advantages, drawbacks, and suitability for various construction demands of these systems. The review also looks into the various factors that affect the overall structural effectiveness and performance of composite slabs with profile decking. In addition, the paper analyses several experimental, analytical, and design approaches used in composite slab systems. The findings of this exploratory review add expansion of knowledge on composite slabs with profile decking and provide researchers, engineers, and building construction industry professionals with useful information. The current best practices and innovations in this field is covered for further development and encouraging the use of effective and environmentally friendly building techniques in contemporary construction projects.

Keywords: Composite slab with steel profile decking, steel – concrete connection, longitudinal shear behavior, Ultimate load carrying capability.

1 Background

Slab is an important structural component of all type of building construction. In traditional construction techniques basically two types of slabs, traditional Flat slab and Reinforced Concrete (RC) slab are used. The RC slab or Beam slab construction is

ISBN: 978-81-932056-2-4

conventional reinforced concrete slab. The slab rests on a set of beams spread out at regular spacing at right angles. The beams are supported by columns. Load transfer mechanism in such type of system is slab to beams which act as primary load carrying members and beam to columns. The characteristics of a conventional slab include increased stiffness, increased load carrying capability, safety, and affordability. The current free ceiling elevation is lowered owing to the depth of the beams. In order to increase ceiling height, slabs are occasionally supported directly on columns rather than on beams. This is called beamless or flat slab. Eddy and Turner were the first to give description on flat slabs [9]. Load transfer mechanism such type of system is slab load transferred directly to columns which act as a primary load carrying members. The usage of flat slab buildings has many benefits over traditional RC frame buildings. This includes lower floor-to-floor heights, more architectural flexibility, improved weight drop, efficient space usage, simpler formwork, as well as quicker time of construction. On other side the major disadvantages of flat slab are higher deflections and potential need for additional reinforcement against punching shear [1, 8]. In the present scenario composite construction is picking up significance throughout the world due to quicker and lighter construction when compared to traditional construction techniques. When two or more than two materials are integrally connected and analysed together to act as a single unit for their use in different purpose or events it is referred as composite. In general, it can be concrete/timber, steel/concrete, or steel/timber etc. Reinforced concrete is cast over profile steel decking, which serves as temporary formwork during construction, to create composite slabs. Fig. 1 displays a detailed outlook of a composite slab using profiled steel decking and additional reinforcement [1, 8]. The composite slab with profile decking is designed in accordance with the various codes for composite steel and concrete buildings.

- According to IS 11384 (1985), a composite construction combines in-situ concrete with prefabricated structural components such steel beams, precast reinforced or prestressed concrete beams. To function as a single structural unit, the construction should guarantee monolithic action between the prefabricated and in-situ components.

- A composite slab is, in the words of ASCE (1992), "a slab system composed of light weight or normal weight structural concrete placed permanently over cold formed steel decks, where the steel deck serves as both a form for the concrete during construction and a source of positive reinforcement for the slab during service."

- A structural member that complies with Euro code 4 (2004) has structural or cold-formed steel and concrete components that are joined together by shear connections to avoid longitudinal slip among the concrete and steel causing separation of the components. Additionally, there is a slab where profiled steel sheets are originally employed as permeant shuttering before structurally joining with the hardened section of concrete to serve as reinforcement resisting tensile forces in the floor.

ISBN: 978-81-932056-2-4

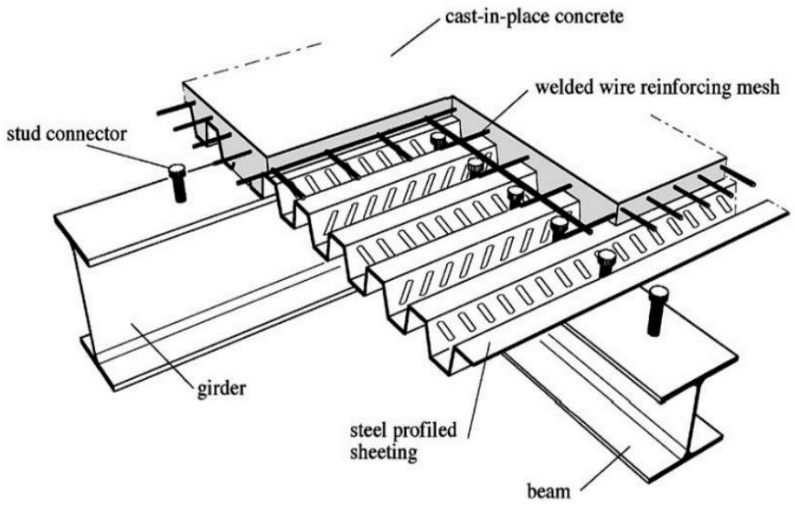

Fig. 1. Composite slab with profiled steel decking reinforced [1]

1.1 Types of Profile Deck

The deck, which is created by interconnecting the steel profile member and reinforced concrete slab, serves as a positive moment support. Furthermore, the deck serves to give concrete shape and provides foundation. The profile sheet is designed as formwork during construction and as a central tensile reinforcement after construction for the composite slab with profile decking. Decking profiles are produced by manufactures. The precise size and form depend on the manufacturers. Two prominent types of deck profiles, Trapezoidal profile steel deck shown in Fig. 2a, and Re-entrant (or Dovetail) profile deck shown in Fig. 2b [4].

(a)

ISBN: 978-81-932056-2-4

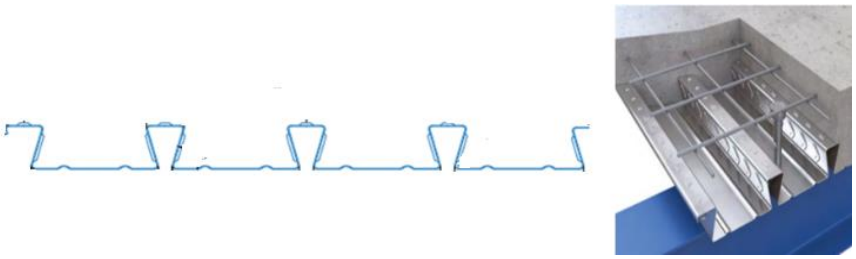

(b)

Fig. 2. (a) Trapezoidal Profile Steel Decking [4] and (b) Re-entrant (or Dovetail) Profile Steel Decking [4]

1.2 Steel - Concrete Connection

With the aim of to generate the composite action among steel deck and concrete, the steel deck should withstand vertical separation and longitudinal. Here it is important to mention that concrete and steel's adhesive is insufficient to provide a good composite motion. As shown in fig. 3 an efficient connection can be achieved by providing four different mechanisms. The first mechanism includes mechanical interlocking in form of embossments. The second mechanism is by providing frictional interlock in Re-entrant trough profile. The third mechanism uses welded studs for end anchorage and the fourth mechanism applies by distorting the ribs at the termination of the sheeting for end anchorage. [3]

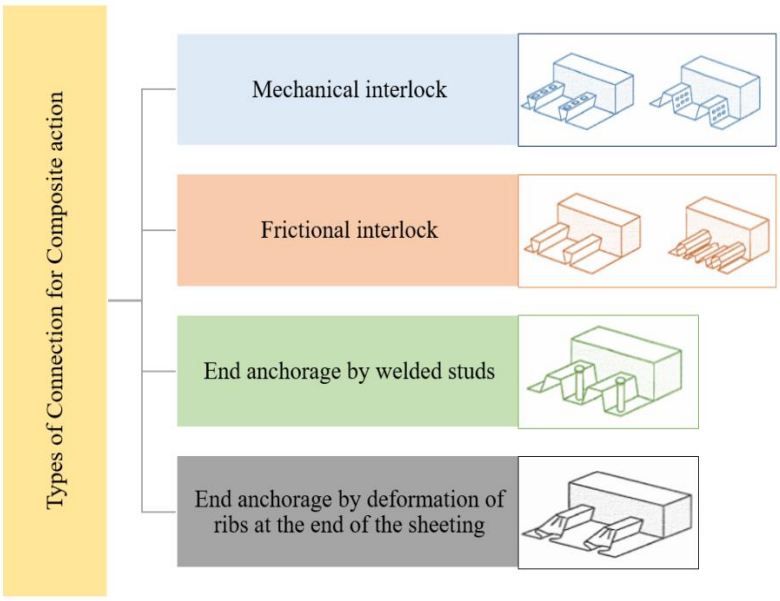

Fig. 3. Types of Connection for Composite action between Composite slab and profile deck

ISBN: 978-81-932056-2-4

1.3 Advantages of Composite Slab with Profile Decking

The construction industry embraces the system of composite slab with profile decking with open arms because of its numerous advantages over the other types of floor systems [5,6]. Constructions using the method in steel-framed building systems are easier, quicker, lighter, and more affordable than those using other types of floor systems. Figure 4 illustrates the benefits of a composite slab with a profile decking system in a schematic way. Composite slab has many advantages like: [7].

- Rapid and simple construction and construction time is reduced
- Act as a safe working platform and elimination of formwork
- Steel building is a sustainable approach since it can be recycled or reused
- Reduced dead load to the foundation and saving in weight
- Reduction in labour cost
- Significant reduction in tensile reinforcement
- Profiled sheeting acts as formwork for casting of concrete
- Profiled sheeting acts a tensile reinforcement which reduces heavy reinforcement
- Effective utilization of material

Fig. 4. Advantages of composite slab with profile decking system in construction industry

ISBN: 978-81-932056-2-4

2 Exploratory Review

Experimental, Numerical and Analytical works were taken up by researcher for parametric studies of the composite slab with profile decking. Many full-scale experiments conducted in the past by researchers to determine the mode of failure and the load carrying capability of composite slabs with profile decking. This section attempts to outline the investigations commenced in the area of composite slab with profile decking system.

To investigation on the ultimate load capability of composite slab, Wright et al. [1987] performed the tests by taking variables as types of profile sheet (trapezoidal and re-entrant) and depth of embossment, concrete strength, and application of cyclic loading. The findings revealed that although the strength of concrete and the application of cyclic load had only a minor effect, the depth of the embossment had significant effect on the ultimate load capability of composite slab.

To analyse the longitudinal shear behavior of composite slabs, Makelainen and Sun [1999] considered thickness of profile sheets as well as the embossment's thickness, size, and position as variable. According to the experiment, it is concluded that the embossment depth had a greater impact on the longitudinal shear behavior than its length or form. This study concluded that the profile sheet's stiffness significantly influences by the sheeting's thickness.

Burnet et al [2001], performed the test on composite slab with trapezoidal profile deck and dovetail profile deck with chemical bond and mechanical bond by rib shear connectors. This study concluded that the mechanical bonding by embossment substantial enhances shear strength in trapezoidal shape rather than in re-entrant shape. The effect of chemical bonding mainly very with geometry.

The longitudinal shear strength among steel and concrete deck is diagnostically assessed by Partial Shear Connection (PSC) method and m-k method suggested in Euro code 4 (2004) and IS11384 (1985). Both these approaches rely on data from experiments using practical samples. The performance of slab may be labelled as ductile or brittle depending on the test findings. A new, simplified method to forecast composite slab behavior was put out by Crisinel and Marimon [2004]. Findings of the study support the notion that the suggested approach may be used for both brittle and ductile slab. Based on experimental full-size test and analytical study. Abdullah & Easterling [2011], suggested enhanced PSC design process. This method was compared with the m-k technique and found to be equivalent.

Finite element technique for the composite slab using nonlinear contact notation was confirmed and approved by Chen & Shi [2011]. The pull-out test and bending test results for the composite slabs are compared. The results verified and validated nonlinear contact theory-based FE approach for composite slabs.

ISBN: 978-81-932056-2-4

Rehman et al. [2016], conducted an experimental investigation using push-off tests to determine the stiffness, ductility, and shear strength of demounTable bolted shear connectors in the composite slabs with steel decking. Different concrete strengths, connector counts, and connector diameters were taken into consideration. Similar shear capacities and behaviors between welded shear studs and demounTable shear connectors is observed in test results. According to experimental findings, a mixture of Euro code 3 and 4 can be used to accurately forecast the shear strength of demounTable shear connectors. The shear capability of demounTable shear connections for connector failure mechanisms can be assessed with the ACI and AISC codes.

Hicks [2018] used the interface contact model in Finite Element (FE) analysis. The results shows that finite element analysis accurately estimate function and weight carrying capability of composite slab. Longitudinal shear bond failure is observed in all composite slabs in this study.

Bonilla et al (2019), used finite element method to investigate slip behavior and shear capability of headed steel stud. FE model positively predicted shear connection the resistance and load slip behavior of headed steel stud. It is observed that failure mode for open deck profile with perpendicular orientation, closed deck profile with parallel and perpendicular orientation was same under monotonic loading. Dovetailed deck profile failure under monotonic loading was concrete pull out and under cyclic loading rib shearing combined with stud shearing failure was observed. Closed profile deck achieved similar strength for monotonically and cyclic loaded specimen. They also observed that specimens loaded monotonically shows better ductility compare with specimens loaded cyclically. ‘C’ shape bending stud deformation was observed in open profile deck, ‘S’ shape double curvature stud deformation was observed in dovetailed profile deck and ‘Opposite C’ shape deformation of stud was closed in dovetailed profile deck. [17] It is determined from a comparison of experimental strength to that computed using design codes that specimens with the failure mechanism of concrete pull out may have overestimated strength, whilst specimens with closed profile deck may have underestimated strength. [16,17]

To analytical assessment of the shear strength in longitudinal direction among the steel and concrete deck without adding extra reinforcement, standard codes (Euro code, Brazilian standards, Australian/New Zealand standards, American standards) suggested PSC method and m-k method. Both approaches rely on data from experiments using practical samples. Grossi et al. [2020] conducted an experimental as well as analytical examination of composite slabs having profile steel decking and providing extra reinforcement bars. The analysis resulted in an analytical model to assess the longitudinal shear capability of composite slabs with additional reinforcement. The findings demonstrated that the calculation m-k method in EC4 is not applicable to composite slabs with added bars of reinforcement. Additionally, it is found that compared to equivalent specimens without additional reinforcement bars, composite slabs with added bars of reinforcement displays better load capability and ductility.

ISBN: 978-81-932056-2-4

Avudaiappan et al [2021] conducted experiments using composite slab samples with various profiles, including dovetail, rectangular, and trapezoidal, for analysing several factors, such as ultimate capability of load carrying in relation to deflection, load in relation to slip, ductility ratio, strain energy, and causes of failure. According to the test results, dovetailed profiled composite slabs perform better than the rectangular, and trapezoidal profiled composite slabs in terms of resistance.

Vellaichamy et al. [2022] undertook an experimental analysis to examine the performance of composite slab with profile decking specimens connected with headed stud connectors for a range of shear spans and profile heights. In this work, the longitudinal shear bond strength of the composite slab is assessed for two distinct steel deck sheets profiles. It is determined that the longitudinal shear bond failure between the composite slab and profile decking causes the most frequent failure of all studied specimens. Empirical methodologies are employed to assess the shear binding mechanism between the composite slab and profile deck since longitudinal shear is a complex event.

3 Conclusion/Synthesis and Reflection

- The literature review makes it abundantly evident that the interfacial shear interaction has the greatest impact on the composite slab's ability to support loads. The interfacial shear is impacted by several factors, including concrete strength, the kind, height, and thickness of the profile sheet, the type of loading, and the height, pattern, and orientation of the embossment.

- A series of practical experiments and linear regression analysis are required for the variables that affect the shear-bond capability.

- The capability of horizontal shear transmission among the steel deck and concrete slab influences the composite deck's strength. It has been discovered that embossment patterns affect the interface shear strength. Even a small modification in the geometry necessitates separate performance evaluation tests because of the distinctive nature of these embossment patterns.

- The flexure causes vertical separation among the steel and concrete in addition to the interfacial shear forces, and any changes to the current embossments need a number of tests. This complicates the analysis of composite slab with profile decking.

- The PSC and m-k method, suggested in the codes, could be used to find out the longitudinal shear strength of simply supported composite slabs with profile decking without extra reinforcement. Grossi et al. [2020] gave an analytical model for the m-k method for composite slabs with extra reinforcement which could be

ISBN: 978-81-932056-2-4

used for simply supported composite slabs with extra reinforcement to determine longitudinal shear strength.

References

1. Crisinel, M., Marimon, F.: A new simplified method for the design of composite slabs. Journal of Constructional Steel Research 60(3-5), 481-491 (2004).

2. IS 11384-1985: Code of Practice for Composite Construction in Structural Steel and Concrete, https://www.cracindia.in/admin/uploads/IS-11384.pdf

3. Eurocode 4 (2004): Design of composite steel and concrete structures, https://www.phd.eng.br/wp-content/uploads/2015/12/en.1994.1.1.2004.pdf

4. TATA STEEL: ComFlor Manual for Composite floor decking design and technical information, https://www.tatasteeleurope.com/sites/default/files/ComFlor%20manual.pdf

5. De Andrade, S.A.L., Vellasco, P.C.D.S., da Silva, J.G.S., Takey, T.H.: Standardized composite slab systems for building constructions. Journal of Constructional Steel Research 60(3-5), 493-524 (2004).

6. Mäkeläinen, P., Sun, Y.: The longitudinal shear behaviour of a new steel sheeting profile for composite floor slabs. Journal of Constructional Steel Research 49(2), 117-128 (1999).

7. Hedaoo, N.A., Gupta, L.M., Ronghe, G.N.: Design of composite slabs with profiled steel decking: a comparison between experimental and analytical studies. International Journal of Advanced Structural Engineering, 4, 1-15 (2012).

8. Lv, J., Zhou, T., Wu, H., Sang, L., He, Z., Li, G., Li, K.: A New Composite Slab Using Crushed Waste Tires as Fine Aggregate in Self-Compacting Lightweight Aggregate Concrete. Materials 13(11), 2551 (2020).

9. Manu, K.V., Naveen Kumar, B.M., Priyanka, S.: Comparative Study of Flat Slabs and Conventional RC Slabs in High Seismic Zone. International Research Journal of Engineering and Technology 2(6), 29-34 (2015).

10. Wright, H.D., Evans, H.R., Harding P.W.: The use of profiled steel sheeting in floor construction. Journal of Constructional Steel Research 7(4), 279-295 (1987).

11. Burnet, M.J., Oehlers, D.J.: Rib shear connectors in composite profiled slabs. Journal of Constructional Steel Research 57(12), 1267-1287 (2001).

12. Abdullah, R., Easterling, W.S.: Elemental Bending Test and Modeling of Shear Bond in Composite Slabs. In: Proceedings of the Sixth International Conference on Composite Construction in Steel and Concrete, pp. 138-150. American Society of Civil Engineers, Tabernash, Colorado (2011).

ISBN: 978-81-932056-2-4

13. Chen, S., Shi, X.: Shear bond mechanism of composite slabs - A universal FE approach. Journal of constructional steel research 67(10), 1475-1484 (2011).

14. Rehman, N., Lam, D., Dai, X., Ashour, A.F.: Experimental study on demounTable shear connectors in composite slabs with profiled decking. Journal of Constructional Steel Research 122, 178-189 (2016).

15. Hicks, S.: Strength and ductility of headed stud connectors welded in modern profiled steel sheeting. Structural Engineering International 19(4), 415-419 (2009).

16. Bonilla, J., Bezerra, L.M., Mirambell, E.: Resistance of stud shear connectors in composite beams using profiled steel sheeting. Engineering Structures 187, 478-489 (2019).

17. Sun, Q., Nie, X., Denavit, M.D., Fan, J., Liu, W.: Monotonic and cyclic behavior of headed steel stud anchors welded 42 through profiled steel deck. Journal of Constructional Steel Research 157, 121-131 (2019).

18. Grossi, L.G.F., Santos, C.F.R., Malite, M.: Longitudinal shear strength prediction for steel-concrete composite slabs with additional reinforcement bars. Journal of Constructional Steel Research, 166, 105908 (2020).

19. Avudaiappan, S., Flores, E.I.S., Letelier, G.A., Thomas, W.J., Raman, S.N., Murali, G., Amran, M., Karelina, M., Fediuk, R., Vatin, N.: Experimental investigation on composite deck slab made of cold-formed profiled steel sheeting. Metals 11(2), 229 (2021).

20. Vellaichamy, P., Veerasamy, S. and Mangottiri, V.: Shear bond characteristics of steel concrete composite deck slab. Građevinar, 74(5), 393-401 (2022).

ISBN: 978-81-932056-2-4

AICTE Sponsored Online International Conference on

ADVANCEMENTS IN STRUCTURAL ENGINEERING

ASE'2023

Indian Concrete Institute (ICI)
Students Chapter
CHARUSAT

Indian Association of Structural
Engineers (IAStructE)
Student Chapter
CHARUSAT

NAAC GRADE A+

CENTER OF EXCELLENCE
GOVT. OF GUJARAT

CHAROTAR UNIVERSITY OF SCIENCE AND TECHNOLOGY

CHANDUBHAI S. PATEL
INSTITUTE OF TECHNOLOGY